

Determining effects of geometry on energy efficiency of medium-sized solar buildings

A PhD research conducted by:

Abbas Rahmani

Supervisor: Prof. Dr.-Ing. R. Wagner

Second consultant: Prof. Dr.-Ing. M. Pfeifer

Institut Entwerfen und Bautechnik (IEB)
Fachgebiet Bautechnologie (FGB)

(2023)

Determining effects of geometry
on energy efficiency of medium-sized solar buildings

Zur Erlangung des akademischen Grades
eines Doktors der Ingenieurwissenschaften (Dr.-Ing.)
von der KIT-Fakultät für Architektur des
Karlsruher Instituts für Technologie (KIT)
genehmigte Dissertation

von

Abbas Rahmani

Hauptreferent: Prof. Dr.-Ing. Rosemarie Wagner

Korreferent: Prof. Dr.-Ing. Matthias Pfeifer

Tag der mündlichen Prüfung: 12.01.2023

Acknowledgements

I would like to express my deepest gratitude to all the individuals who have supported me throughout this thesis:

Prof. Dr.-Ing. Rosemarie Wagner for her invaluable and candid supervision and guidance.

Prof. Dr.-Ing. Matthias Pfeifer for his effective and unwavering support.

Prof. Dipl.-Ing. Andreas Wagner for his valuable guidance.

Dr. Tilmann E. Kuhn for his kind encouragement in developing the core of this investigation.

Prof. Dr. Wolfgang Streicher for his candid recommendations.

I would also like to extend my appreciation to my colleagues in my lovely department: Stefan Sander, Bernd Sum, Kai Heinlein, and Arnold Mager.

A special thanks goes to my wife, Hana, for coordinating our life within the framework of my work, and, last but not least, to my delightful daughter, Niha, for being a constant source of motivation throughout this journey.

Abbas Rahmani

Abstract

This work initially aims to determine the effects of the overall geometry of a building on thermal performance and electricity generation quantities. The primary goal of the developed method in this work is to streamline the complex process of 'energy simulation' for medium-sized buildings during the initial design phases. The complexity of existing simulation tools largely stems from the 'lack of available parameters in the early stages' and the 'lengthy simulation times' they require. Therefore, the new approach employed in the developed estimation tool in this work seeks to provide more usability in the early design stages, with reduced simulation time for 'energy demand estimation,' making it more accessible to the majority of building designers.

In this context, both opaque and transparent components representing walls, roofs, and windows have been initially considered, along with the possibility of integrating PVs through different configurations resulting in BIPV, BAPV, and PV glazing. The method simultaneously calculates the thermal performance and electricity generation of combinations of these five components on the building's envelope. It employs a steady-state heat transfer method across different levels of building geometry, including individual components, the composition of different components on a building's facade, and finally, the entire building's geometry. In this process, the method estimates the heating and cooling demands of building components. At a higher level of geometry, it estimates the holistic energy demand of the entire external geometry of the building, which comprises various components with specific areas. Real weather data from Stuttgart, including hourly, monthly, and annual data on temperature, irradiation, wind and cloudiness is integrated into the calculations. The initial calibration of the developed method involves comparing the elementary calculated indexes with 'DesignBuilder,' and the acceptable deviations demonstrate the precise utilization of the integrated method.

In the next chapter of this work, the calculation of building 'energy efficiency indicators,' namely 'self-sufficiency' and 'self-consumption,' takes into account the simultaneous consideration of PV efficiency under different operating temperatures and the varying heat flows that can either increase or decrease the energy demand of the building. These calculations pertain to different configurations arising from various geometrical setups, resulting in different proportions of 'self-generated electricity' compared to the covered and uncovered energy demands of the building. In the process of the second calibration of the integrated method developed in this work, the energy demand of a constructed and monitored building (conducted by ZukunftBAU) is considered. The same material assembly for this building's envelope and its PV integration is applied, resulting in an acceptable deviation in terms of the final 'electricity generation' and the 'total energy demand of the building.' The final chapter of this work demonstrates the effects of the building envelope's geometry in altering the 'energy efficiency indicators.' It confirms that the range of changes in the two indexes, 'self-sufficiency' and 'self-consumption,' is consistently linked to the building's external geometry when the construction setup and PV configuration remain the same. The developed method is easily integrable into the initial stages of architectural building design, as it primarily enables the exploration of energy efficiency differences among various geometrical setups. The application of this method can prove highly beneficial for different geographical locations, material combinations, and PV configurations in conjunction with opaque and transparent components.

Content

Acknowledgements	I
Abstract	II
Content	III
Nomenclature	1
1. Introduction	2
2. Necessity of work	2
2.1 Role of geometry	2
2.2 Definitions	4
2.2.1 Energy efficiency	4
2.2.2 Solar buildings	4
2.2.3 Geometry modification	5
2.2.4 Solar panels	5
2.2.5 Electrical power and thermal performance	5
2.3 State of the art	6
2.3.1 Energy demand and envelope parameters	6
2.3.2 Energy demand and exterior geometry	9
2.3.3 Envelope PV installations and geometrical setups	...	12
2.3.4 Geographical location and optimization of geometry	...	13
2.3.5 Further development	14
2.3.6 Approaches of energy estimation tools	15
3. Goal setting	16
3.1 Research questions	16
3.2 Hypothesis	16
3.3 Flowchart of work	17
4. Method	20
4.1 Heat flow	20
4.1.1 Effective phenomena	20
4.1.2 Thermal performance of components	21
4.1.3 Electrical power of components	21
4.2 Boundary condition	21
4.2.1 Inside comfort temperature	21
4.2.2 Inside convection heat coefficient	22
4.2.3 Irradiation	23
4.2.3.1 Reflection in opaque component	24
4.2.3.2 Reflection in transparent component	25
4.2.4 Outside convection heat coefficient	27
4.2.5 Sky emissivity	29
4.2.6 Sky temperature	30
4.3 Component emissivity	30
4.4 Sol-air temperature	30
4.5 Surface temperatures and heat flow	31
4.6 Value of heat flow	32
4.6.1 Heating demand	32
4.6.2 Cooling demand	33
4.6.3 Heating auxiliary	33
4.6.4 Cooling auxiliary	33
4.6.5 Energy demand of combination of components	...	34
4.7 Dividing effect of convection and emission	35

4.7.1	Net radiation loss	36
4.8	Geometrical configuration	36
4.9	Components	37
4.9.1	Opaque component	38
4.9.1.1	Physical characteristics	38
4.9.1.2	Conduction heat transfer coefficient	39
4.9.1.3	Heat transfer algorithm	40
4.9.2	Transparent component	40
4.9.2.1	Physical characteristics	40
4.9.3	BIPV (building integrated photovoltaic system)	42
4.9.3.1	Physical characteristics	42
4.9.3.2	Heat transfer algorithm	42
4.9.4	BAPV (building-applied photovoltaics)	43
4.9.4.1	Physical characteristics	44
4.9.4.2	Thermal resistance	44
4.9.4.3	Heat transfer algorithm	45
4.9.5	PV glazing	45
4.9.5.1	Thermal resistance	46
4.9.5.2	Heat transfer algorithm	47
4.9.5.3	Surface temperatures and heat flow	47
4.9.5.4	Assembly of PV glazing	48
4.10	Power Balance Model	48
4.10.1	Power input	50
4.10.3	Electrical power	51
4.10.4	Thermal dissipation	51
5.	Simulation	52
5.1	Geographical location	52
5.2	Weather data	52
5.2.1	Dry-bulb temperature	52
5.2.2	Outside dew-point temperature	52
5.2.3	Wind velocity and direction	53
5.2.4	Solar altitude and azimuth	53
5.2.5	Direct normal and diffuse horizontal irradiation	53
5.3	Intervals of calculation	53
5.4	Simulated variants	53
5.4.1	Geometrical configuration	55
5.4.2	Boundary condition	55
5.4.3	Components	55
5.4.4	Representative date	55
5.5	Opaque component	56
5.5.1	Daily performance - Summer day	57
5.5.2	Daily performance - Winter day	60
5.5.3	Monthly performance	62
5.5.4	Orientation	65
5.5.5	Inclination	66
5.5.6	Inside air temperature	66
5.6	Calibration of calculated surface temperature	69
5.6.1	Winter day	70
5.6.2	Summer day	71
5.6.3	Deviation	72

5.7	Transparent component	74
5.7.1	Daily performance - Summer day	74
5.7.2	Daily performance - Winter day	77
5.7.3	Monthly performance	79
5.7.4	Orientation	81
5.7.5	Inclination	82
5.7.6	Inside air temperature	83
5.8	BIPV	86
5.8.1	Daily performance - Summer day	87
5.8.2	Daily performance - Winter day	89
5.8.3	Monthly performance	90
5.8.4	Orientation	91
5.8.5	Inclination	92
5.9	BAPV	93
5.9.1	Daily performance - Summer day	94
5.9.2	Monthly performance	96
5.9.3	Inclination and orientation	96
5.10	PV glazing	98
5.10.1	Daily performance - Summer day	98
5.10.2	Monthly performance	101
5.10.3	Inclination and orientation	101
5.11	Comparing 5 components	102
5.12	Proportion of outside convection and emission (BIPV) ...	103
6.	Self-sufficiency – self consumption	105
6.1	Energy demand through building’s envelope	106
6.2	Calibration of self-sufficiency and self-consumption ...	108
6.2.1	Energy concept	109
6.2.2	Boundary condition	110
6.2.3	Energy performance of components	111
6.2.3.1	Walls	111
6.2.3.2	Windows	111
6.2.3.3	Floor and door	112
6.2.3.4	Roof	113
6.2.4	Energy demands – Electricity generation	113
6.2.5	Flat rate of energy	114
6.2.6	Electricity demand for heating and cooling	115
6.2.7	Deviation	116
6.2.8	Daily and annual self-consumption – self-efficiency ...	117
7.	Demonstration of effects of geometry	118
7.1	Sample building	118
7.2	WWR	119
7.3	One storey building	120
7.4	Proportion	120
7.5	Orientation	121
7.6	Distribution of PV	121
7.7	PV on ‘Dachgeschoss’	122
7.8	PV on ‘Sloping roof’	123
7.9	PV on ‘Sloping wall’	125
7.10	Domain of influence of geometry	125
8.	Geometry setups and indicative of energy efficiency	126

8.1	Proportions	128
8.2	Orientation	129
	8.2.1 BAPV on flat roof	129
	8.2.2 BAPV on sloping roof	130
	8.2.3 BIPV and BAPV on wall	131
	8.2.4 PV glazing on wall	134
8.3	Inclination	135
	8.3.1 Wall with low WWR	135
	8.3.2 Wall with high WWR	136
	8.3.3 Wall holding BIPV	137
	8.3.4 Wall holding BAPV	138
	8.3.5 Sloping roof holding BAPV	140
	8.3.5.1 Geometry of sloping roof	141
8.4	WWR	143
	8.4.1 Wall	143
	8.4.2 Sloping roof in 'Dachgeschoss'	144
8.5	Roof type	146
8.6	Building expansion	147
	8.6.1 Vertical expansion	147
	8.6.2 Horizontal expansion	149
8.7	Distribution of PV	150
	8.7.1 BAPV on sloping roof with different inclinations	150
	8.7.2 Symmetric and asymmetric distribution of BAPV	153
8.8	Proportion + Orientation + WWR	155
8.9	Inclination + Orientation + WWR	157
8.10	Priority of integration	159
	8.10.1 Flat roof	159
	8.10.2 Sloping roof (Inc. 30° - south-north)	160
	8.10.3 Sloping roof (Inc. 30° - east-west)	162
	8.10.4 Sloping roof (Inc. 60° - south-north)	163
	8.10.5 Sloping roof (Inc. 60° - east-west)	165
	8.10.6 Dachgeschoss (Inc. 60° - south-north)	166
	8.10.7 Dachgeschoss (Inc. 60° - east-west)	168
9.	Conclusion	170
10.	References	177
	Appendix 1 - Extended explanation of sol-air temperature	182
	Appendix 2 - Description of energy demands of the selected building	189
	Appendix 3 - Numerical calculation of energy demands	202

Nomenclature

Symbol	Variable	Unit
$T_{(in)}$	inside comfort temperature	$^{\circ}\text{K}$
$T_{(out)}$	outside ambient temperature	$^{\circ}\text{K}$
h_i	inside convection coefficient	$\text{W}/\text{m}^2.\text{K}$
h_o	outside convection coefficient	$\text{W}/\text{m}^2.\text{K}$
$G_{Tt}(I)$	total solar radiation density incident	W/m^2
G_B	direct beam	W/m^2
G_D	diffuse light	W/m^2
θ	angle of incidence of the sun rays on the tilted plane	$^{\circ}$
ρ	foreground's albedo	-
φ	declination of sun	$^{\circ}$
ϕ	latitude of the considered location	$^{\circ}$
γ	surface azimuth angle	$^{\circ}$
β	angle between the normal of the surface and normal of earth	$^{\circ}$
ω	hour angle	$^{\circ}$
$r_B(\omega)$	reduction coefficients of direct light	-
$r_D(\omega)$	reduction coefficients of diffuse light	-
ε'	exponent of reduction in radiation transmittance of glass	-
ε_{sky}	Sky emissivity	-
N	Opaque sky cover	-
$T_{dewpoint}$	dew-point temperature	$^{\circ}\text{K}$
T_{sky}	sky temperature	$^{\circ}\text{K}$
ε	component emissivity	-
$T_{(Sol-air)}$	sol-air temperature	$^{\circ}\text{K}$
a_s	Solar absorptivity	-
σ	Stefan–Boltzmann constant	$5670400 \times 10^{-8} \text{ W}/\text{m}^2\text{K}^4$
T_{s-out}	Outside surface temperature	$^{\circ}\text{K}$
T_{s-in}	inside surface temperature	$^{\circ}\text{K}$
CT	comfort temperature setpoint	$^{\circ}\text{K}$
$\sum R_I$	thermal resistance excluding outside air film resistance	$\text{m}^2.\text{K}/\text{W}$
$\sum R_{II}$	thermal resistance excluding inside & outside air film resistance	$\text{m}^2.\text{K}/\text{W}$
q	heat transfer	W/m^2
G^+	heating auxiliary	W/m^2
L^-	heating demand	W/m^2
L^+	cooling auxiliary	W/m^2
G^-	cooling demand	W/m^2
q_{tr}	transmitted irradiation through transmission	W/m^2
q_{em}	emission from the outside surface of component	W/m^2
R	thermal resistance of material	$\text{m}^2.\text{K}/\text{W}$
d	thickness of material	m
λ	heat conductivity	$\text{W}/\text{m}.\text{K}$
U	U-value	$\text{W}/\text{m}^2.\text{K}$
γ_f	reflection factor	-
α_f	absorption factor	-
τ_f	transmission factor	-
η	PV efficiency	%
α_{coeff}	temperature co-efficiency of PV	%/K
T_M	operation temperature of PV	$^{\circ}\text{K}$
T_{STC}	temperature of module at STC	$^{\circ}\text{K}$
q_e	electricity generation	W/m^2
A	area of component	m^2
TFA	treated floor area	m^2
WWR	Window to wall ratio	%
SS	self-sufficiency	-
SC	self-consumption	-

Tab. 03. variables, sequences based on priority of integration in procedure of calculation

1. Introduction

Medium-sized buildings, as the primary constituents of the residential sector, are major energy consumers. With drops in feed-in tariffs and increasing electricity prices, there is a growing interest in achieving more demand-based electricity generation in both existing and new buildings by integrating photovoltaic (PV) systems.

The interaction between electrical power and the thermal performance of all components in a building's envelope, which can be partially covered by PVs, depends primarily on the geometrical setups of these components (inclination and orientation) and, secondarily, on the holistic geometry of the building. Making the right decisions regarding the proportions and properties of these components, coordinated with their geometrical installation, is a complex task. Despite many research efforts aimed at addressing the advantages of specific geometrical setups that enhance the coverage of electricity generation to meet energy demands, the emergence of a holistic, universally applicable criteria has not yet been feasible due to the significant impact of changing weather conditions in different geographical locations on the effects of geometry. While using existing simulation tools can facilitate achieving the goal, they are generally not easily modifiable to change their calculation methods, and integrating new parameters is typically only feasible for software developers. Indeed, the ultimate objective of this work is to develop a parametric assessment of building components, both with and without PVs, in order to determine the effects of different building geometries on the final energy performance of the building. For this purpose, the determination of two critical indexes, self-consumption and self-efficiency, in relation to the geometrical configurations of individual components as well as the entire building, is the primary focus of this work.

2. Necessity of work

2.1 Role of geometry

The energy demand of each building is the result of an interaction between its energy gains and energy losses [1]. With the reduction in "feed-in tariffs," buildings equipped with photovoltaic (PV) systems now prioritize two critical indexes to determine their level of "energy efficiency" [01]. The first index, "self-consumption," refers to the ratio of self-consumed electricity to total production, while the latter describes the "ratio of self-consumed electricity to total demand" [02]. Economically, considering the costs of solar panels, only a limited area of a building's envelope is allocated to PVs [03]. Consequently, different components of buildings can be chosen for this "limited PV installation." Various decisions regarding the selection of the "building component holding PVs," in addition to considerations of proportional geometry, orientation, and inclination of the building and its components, can significantly alter levels of self-consumption and self-sufficiency [03]. This influence primarily arises from two fundamental factors:

a. Electrical power: The output power of PVs with the same area varies depending on different configurations.

b. Thermal performance: The energy demand of a building differs based on various variations in the "thermal conductivity" of the building's envelope, whether they are covered by PVs or remain uncovered. In fact, the intervals and quantities of demand are not consistent throughout

the year. A diverse area coverage of the building's envelope by PVs results in different thermal behaviors that can either help reduce the monthly and annual energy demand of the building or have the opposite effect.

As a result, different geometrical setups of buildings that can provide adequate component area to cover electricity demand will yield varying levels of 'self-sufficiency' and 'self-consumption'. This project aims to develop a fundamental-based method for predicting the energy performance of a building's envelope when it is partially covered by PVs in different configurations. The goal is to determine which geometric proportion of the building offers higher energy efficiency concerning both the 'electricity generation performance of PVs' and 'reducing seasonal and annual energy demand of the building' due to 'thermal conductivity changes of components covered by PVs.' All components comprising the building's envelope influence the energy performance of the building based on the specific thermal behavior of their materials. When considering the total amount of irradiation hitting a certain area of each component of the building during a specific period, the total related energy will be divided into different proportions through three main phenomena: absorption, reflection, and transmission [04]. When treating a PV as a layer covering a component, the division of fractions of energy becomes more complex and exhibits more variable proportions, primarily for two reasons:

a. A specific portion of absorption (within a component covered by PVs) is allocated to electricity generation, while another portion of absorption that generates heat affects the proportions of transmitted energy through conduction, convection, and radiation simultaneously. This second fraction of absorption, in the form of heating, also influences the rate of electricity generation since the efficiency of PVs is partly affected by their operating temperature [05]. The proposed method in this work aims to estimate the impact of variables that alter electrical power and thermal performance of components composed of specific layers and covered by PVs. Ultimately, this work seeks to evaluate the energy performance of a building resulting from the thermal behavior of its envelope based on the fundamentals that underpin this phenomenon.

b. A component covered by PV will exhibit different thermal conductivities under varying thermal conditions [06]. Until now, when calculating the thermal behavior of buildings partially covered by PVs, the thermal conductivity of PVs has been derived from the manufacturer's datasheet, typically based on Standard Test Conditions (STC) with specified values for a cell temperature of 25°C and an irradiance of 1000 W/m². However, in real PV usage, both "outside temperature" and "irradiance" constantly change. Relying solely on a constant value for the "thermal conductivity" of PVs leads to inaccurate results [06]. Palencia et al. observed this inaccuracy to be as high as 35% under different irradiation conditions. This inaccuracy arises from not considering the variations in thermal boundary conditions throughout the year.

As a result, this work aims to develop a geometry-based method for determining the energy performance of buildings, whether they lack PVs entirely or allocate a specific area of their components to be covered by PVs. The final results will clarify which geometric configuration of a building yields higher energy efficiency. The primary scientific objective of this work will be to include the 'changing of parameters' of a building's envelope under different thermal and wind conditions, which, so far, have either been largely ignored or integrated through much more complex procedures in related software. In this work, the following aspects will primarily be taken into account (as they are rarely considered all together in the state of the art of the topic):

1. By examining the datasheets of numerous Zero Energy Buildings (ZEBs), a positive annual "Surplus of electricity" has primarily been regarded as an index for justifying the efficiency level of a building in achieving ZEB status. However, changes in "Feed-in Tariffs" have shifted this priority, emphasizing higher "self-consumption" as a means to reduce annual electricity bills, even if it leads to a lower annual "Surplus of electricity" [07]. Consequently, "self-consumption" and "self-sufficiency" will now be considered as the main indexes in final comparisons, rather than the annual "Surplus of electricity".

2. Any temperature other than the "Standard Test Condition" (STC) will have varying effects on the rate of electricity production from PV [05]. Changes in outside temperature can result from either the "normal ambient temperature" or different inclination setups of PVs, leading to different convection heat transfers. The electrical power output of differently tilted PVs in various configurations (such as BIPV, PV without an air gap, PV with an air gap with/without air ventilation) has been primarily calculated in some recent research [08]. However, there hasn't been a consistent consideration of the effects of the combination of components shaping the building's envelope and the potential of the building's inclinations and orientations to deliver the optimal amount and configuration of required PV through a simple estimation tool.

3. By considering different efficiencies of PVs in various geometry setups of components, primarily resulting from orientation and inclination, the components of a building can be prioritized for PV coverage to achieve higher "self-consumption" in terms of electricity generation and greater "self-sufficiency" concerning energy demand. When contemplating different versions of buildings with the same Total Floor Area (TFA) but different geometric proportions, these buildings can also be assessed based on their potential for increased self-consumption and self-efficiency. In the process of building design, numerous solutions and related parameters can be incorporated, and calculating the energy efficiency of a building by taking all these parameters into account requires a substantial number of simulations [09].

2.2 Definitions

2.2.1 Energy efficiency

Self-consumption and self-sufficiency are the main selected indexes in this work to assess level of energy efficiency of building. Self-consumption (SC), referred to as a load matching index can be defined as is the self-consumed part relative to the total production [01]. It is inversely related to the amount of PV (or other sources) power exported to the grid. Self-sufficiency (SS), describes the proportion of a building's final energy demand that is supplied through self-generated photovoltaic electricity [01].

2.2.2 Solar buildings

The term 'solar building' in this work refers to normal-sized residential buildings that are suitable for the integration of solar panels (BIPV, BAPV, and PV glazing in this work) to enhance irradiance absorption during peak demand intervals related to electrical power. Additionally, the thermal performance of individual building components and the overall geometry of a solar building should contribute to reducing daily and seasonal energy demands associated with the building's envelope. In a solar building, a portion of the energy demand is

intended to be offset by self-generated electricity from PV components, aiming to align periods of electricity generation as closely as possible with electricity demand.

2.2.3 Geometry modification

In this work, various versions of buildings with the same TFA (Treated Floor Area) will be developed and compared. Since the roof is typically the first component of the building considered for PV installation, we have taken into account the most common roof types in Germany and their corresponding inclinations while ensuring that the total roof area remains constant (achieved by multiplying length by width). In this context, a range of different roof forms based on their primary inclinations can be considered, such as Flachdach (inclination: 0°), Satteldach (inclination: 10° to 50°), and Mansardendach (inclination: 60° to 80°). A similar condition for comparing the usable area provided by walls will also be considered. Additionally, the presence of windows will be accounted for by inputting the window-to-wall ratio (WWR). The primary constraint applied throughout these geometric modifications is to maintain the same TFA to ensure a fair comparison of energy performance. In this work, besides the entire external surfaces of the building, the roof and walls are the primary components suitable for mounting solar panels. The surface area of windows can also be allocated to PV glazing.

2.2.4 Solar panels

This phrase refers to the integration of PVs that precisely adhere to the geometry and dimensional properties of the building. The photovoltaics are parallel and directly attached to the building's surface without any intermediary infrastructure that would alter the tilt, orientation, or the area of a portion of the building's envelope. With this method, the primary form of the building remains unaltered by the mounting of solar panels, and the total potential integration area does not exceed the building's envelope. Additional structures such as canopies, shades, and other extensions for solar panel mounting are also excluded.

2.2.5 Electrical power and thermal performance

Since the primary focus of this work is on the energy efficiency of a 'solar building,' the fundamental basis of the developed method involves the simultaneous calculation of the ratio of momentary and annual self-generated electricity to energy demand. In this context, the term 'electrical power' pertains to the quantities of self-generated electricity produced by the installed PVs on a building's envelope. In this work, this term is defined for each of the three installation setups: BIPV, BAPV, or PV glazing. In contrast, the term 'thermal performance' encompasses all five components defined in this work and fundamentally considers the resulting heat flow through the envelope's components. Depending on different boundary conditions, the quantities of heat flow during various intervals are considered either as heating demand, cooling demand, or their respective auxiliaries. The interaction of these demands and auxiliary components of heating and cooling through each component shaping all faces of the building indicates the thermal performance of the building. In this work, at a building scale, the interaction of the individual thermal performance of all five defined components that shape the envelope of a specific building estimates the overall thermal performance of that building.

2.3 State of the art

The researches introduced in the state of the art primarily align with the three main defined objectives of this PhD as well. The first objective is explored by research that focuses on how to 'estimate' a building's energy demand based on its envelope's geometrical configurations in relation to external material properties. The second objective is addressed by research that demonstrates how external geometry, in relation to the proportion of external components, 'modifies' the energy demand of a building. The third objective is investigated by research that illustrates how different PV installations, through varying geometrical configurations, concurrently influence 'electrical power' and the 'thermal performance' of the entire building's envelope.

Since this PhD encompasses all three objectives, after introducing each research, its developed method and related integrated parameters will be briefly discussed to what extent the parameters used align with the integrated parameters in this PhD. Additionally, it will be indicated how this work complements or refines each of the previous research efforts. In this context, the main emphasis will be placed on identifying the effective parameters that have been overlooked or utilized differently in prior research. Similarities between each investigation regarding the defined objectives, employed parameters, and developed methods will also be briefly explained to illustrate the logical progression of this PhD as an advancement of previous works.

2.3.1 Energy demand and envelope parameters

A considerable amount of previous research has been conducted to estimate the energy demand of buildings in relation to the energy performance of their envelopes. The need for developing these 'estimation tools' alongside 'accurate simulation tools' arises from the fact that, in the initial stages of building planning, designers require simple tools to assess the average energy performance of a building for various design variations. These tools should be user-friendly enough to be accessible to the majority of designers while also reducing the time required compared to dynamic simulation tools. In pursuit of this objective, different methods have been developed to estimate the annual heating and cooling demand of a building based on the characteristics of its envelope. In each of these research endeavors, a comparison between the final estimated 'envelope-related energy demand' and the results of 'comprehensive dynamic simulations' has demonstrated that the deviations remain within acceptable ranges.

Different prediction models have been proposed by various researchers during the years, including Fourier series models [10], regression models [11–12-13] and neural network (NN) models [14]. Similarly, there are simplified methods commonly used for quick predicting of building heating demand that are based on degree-days or degree- hours [15]. These methods estimate the heating demand (can be used for cooling demand as well) using as inputs the difference between the base temperature and the outdoor temperature or an equivalent outdoor temperature which employs the effect of solar radiation.

Among them Catalina et al. (2008) [16] validated polynomial regression models to forecast heating energy demand in dwellings for temperate climates. He performed his simplified estimations and compared it with extended database obtained by dynamic simulations for 16 major cities of France. The inputs of his regression models are the building shape factor, the building envelope U-value, the window to floor area ratio, the building time constant and the climate which is defined as function of the sol-air temperature and heating set-

point. He concluded that the obtained energy estimations can do predictions quite well, as a maximum deviation between prediction and the simulation is noticed to be 5.1%, with an average error of 2%. His final comparisons revealed that the simplified energy equations obtained on his study could be used by architects and engineers during the early design stage of their projects, instead of using complicated and time-consuming simulation software.

Evaluation: The parameters he utilized are nearly identical to the parameters in this PhD. In his work, the 'building shape factor' is recognized by other research as a critical parameter that can lead to inaccurate energy estimation. Furthermore, the interaction between the sol-air temperature as an external weather parameter and the heating set-point as the primary internal parameter is also employed similarly in this PhD. However, the possibility of investigating the effects of different inclinations and orientations is largely overlooked in his work.

Jaffal et al. (2009) [17] developed an alternative evaluation method obtained from simple polynomial functions which estimates the annual energy demand as a function of building envelope parameters. Similar to other simplification methods he clarified that output of the models is annual energy demand, but the choice of the most significant parameters to include in the model should be referred to sequence of effectiveness of parameters. From geometrical point of view, he considered an optimal selection of the envelope components that in his work are walls, floors, roofs, windows and doors of a building and his integrated parameters are given shape, orientation and location. He analysed eleven selected parameters in the selected components by the fact that they may approximate complicated functions of dynamic simulation. The eleven integrated parameters of the polynomial functions in his work are; thermal transmission through vertical walls, floor, roof, thermal bridges and windows plus solar radiative flow through north, east, south and west windows and as the last two parameters thermal flow by infiltration and ventilation. Despite that he mentioned that some of these integrated parameters are not independent but interrelated, he showed effect of changing of each of these eleven parameters in annual heating demand of considered prototypes in three different locations in France. He compared 'prediction of building heating demand as a function of the 11 selected parameters' with 'results of dynamic simulation of TRNSYS'. After identifying minimum and maximum absolute errors he concluded that since the computational time of polynomial functions is very low and the results cover all selected parameter levels, these models may be used to evaluate the annual heating demand in a rational multicriteria choice of solutions for low energy buildings. He mentioned that the method may also be extended for estimation of cooling demand.

Evaluation: Among his eleven building envelope parameters, the primary geometrical parameters are precisely integrated into this PhD. However, the last two parameters, infiltration and ventilation, will not initially be incorporated in this PhD, as the primary focus is on considering the effects of geometry. In his work, the application of orientation effects is only feasible through the main four geographical directions, with the effects of inclination being disregarded

Granadeiro et al. (2013) [18] developed a method to give a design indicator of energy performance of residential buildings that determines relation of energy demand to envelope. He clearly indicates that the architectural variables which mostly influence the energy performance of a building are envelope materials, shape and window area. He divided the investigated geometries to eight groups regarding different WWRs in four main envelopes of north, south east and west and the types of window, wall and roof regarding heat conduction and heat transmission. To address logical relation between envelope and energy demand he clearly identified that employing shape factor for energy demand estimation fails for a good correlation

in the presence of important solar gains that is a direct result of considering effects of envelope energy performance. He presented a new design indicator of energy performance for residential buildings, the Envelope-Related Energy Demand (ERED), which aims to overcome the shortcomings of the shape factor while maintaining a reasonable simplicity of use. He investigated on the same envelope components as Jaffal et al. [17] investigation and included areas of envelope elements as floor, walls, roofs and windows in inputs of ERED. He also integrated U-values of envelope materials, solar heat gain coefficients (SHGC) of windows and site related parameters, concerning temperature and solar irradiation. He explained that ERED should be geometrically considered rather than shape factor in estimations because the shape factor only accounts for heat transfers by thermal transmission, between indoor and outdoor environments, though with some imprecisions. The first imprecision is type of surface, in terms of thermal conductivity, which is not distinguished in the shape factor. In general, walls transfer a lot less heat than windows, but a building with no windows and the same building with large windows have the same shape factor. A second imprecision is floor area, which is not accounted in the shape factor. His logical definition for the periods of heating demand was the difference between the thermostat temperature setpoint and the average outdoor temperature multiplied by its length, in days. Similar logical definition is also defined in definition of cooling and heating demand in this PhD. ERED was validated against detailed simulation results of 8000 hypothetical residential buildings, varying in envelope shape, window areas and materials as the validation tests were performed to check its correlation with heating and cooling energy demand, separately. Results showed that there is a strong correlation between ERED and simulated energy demand and confirmed the adequacy of ERED to assist design decisions in early stages of the design process. Final conclusion of his investigation indicates an illustration as correlation between ERED and total energy demand and proves that the results of ERED and total simulated energy demand are fairly close. Therefore, for all eight investigated groups of buildings and under the validation tests conditions, the absolute value of ERED is indicative of total energy demand. He clearly identified that the architectural design variables which most influence the energy performance of a building are related to the envelope design. ERED was developed based on the hypothesis that heat transfers by thermal transmission through the building envelope and solar gains concentrate most of the envelope-related influence on the thermal balance in residential buildings. These results confirm the hypothesis in the origin of ERED and its adequacy to assist design decisions in early stages of the design process.

Evaluation: The envelope materials, shape, and window area represent the exact combination of geometrical setups and component properties that are also employed in this PhD. In his work, 'ERED' as the developed index attempts to refine the shortcomings of the shape factor, but it is developed based on only eight groups of buildings with limited types of geometrical setups. This limitation does not allow for considering all types of geometrical setups for energy estimation. Another missing aspect in his work is the lack of a clear solution to define different variants of window-to-wall ratio (WWR) in each building's envelope. Consequently, feasible investigations can only be performed on buildings with specific WWR ratios that provide limited variations, neglecting all possible variants arising from different WWRs in each envelope. Furthermore, his work lacks the incorporation of intermediate orientations or the consideration of the effects of different inclinations that can alter the energy performance of each component. In the developed method of this PhD, all possible proportions of transparent components into opaque components through each favorable orientation or inclination are considered. Additionally, in his developed method to define periods of heating demand, he employed the formula 'difference between the thermostat temperature setpoint and the average outdoor temperature multiplied by its length.' In this PhD, a similar logic has been used to define both 'heating demand' and 'cooling demand,' which is the 'direction of heat flow regarding temperature differences between the outside and inside.'

Koo et al. (2014) [19] introduced an estimation model for the heating and cooling demand of a residential building with a different envelope design using the finite element method. His work was conducted in three steps: (i) selection of building envelope design elements affecting the heating and cooling demand of a multi-family housing unit, (ii) establishment of a standard database for the heating and cooling demand by building envelope design through energy simulation and (iii) implementation of the finite element method for estimating the heating and cooling demand by building envelope design. The unique part of his work is that in definition of variables he separated them as independent and dependent variables as building envelope design elements. In his division the independent variables were architectural-design elements and the window design elements. He put final heating demand and cooling demand as dependent variables. The other variables that he took into accounts are orientation and WWR in interval of 45° and 20%, respectively. In integrating finite element method seven variables affecting the heating and cooling demand by building envelope design were defined. Five of these variables; region, household size, household location, glazing type, and awning type are in the nominal scale, and the other two variables; orientation and WWR are in the ratio scale. He determined that relation between the heating and cooling demand and the orientation and window-to-wall ratio is nonlinear. The proposed model was validated compared to the simulation results and the actual data. Regarding the comparison with the simulation results, the average error rate for the heating and cooling demand was determined to be 1.09% and 6.61%, respectively. So, the proposed model could accurately estimate the heating and cooling demand of a residential building with envelope design in the early design phase.

Evaluation: Similar to the scope of this PhD, in his developed method, fundamental geometry parameters and the conduction and transmission properties of opaque and transparent components can be integrated. Furthermore, the applicability of his work in various geographical locations is enhanced compared to previous research, given the inclusion of region as the first variable. However, the flexibility of his work regarding geometrical modifications and component proportions is still a critical consideration, as inclination is not yet integrated, and the adjustment of window-to-wall ratio (WWR) is only possible in intervals of 20°.

2.3.2 Energy demand and exterior geometry

A significant number of previous research studies have also been conducted to estimate the energy demand of buildings in relation to their exterior geometry and the proportion of external components. This group of investigations utilizes the primary external dimensions of a building with respect to its shape, the ratio of windows to walls, and the roof area, in addition to their thermal properties, to assess the impact of exterior geometrical parameters on the energy performance of the building.

Ourghi et al. (2007) [20] introduced a simplified analysis tool to assess impact of building shape on total annual energy use for office buildings. He selected certain prototypical building models and by doing parametric analysis developed his simplified ‘energy demand estimation method’. His analysis indicates that relative compactness of entire geometry beside type and percentage of glazing are mainly found to affect building total energy use. He introduced a simplified calculation method for estimation of annual total energy use for a building relative to a reference building (with the same volume and all with cubical form) as a function of the relative compactness, WWR and the glazing solar heat gain coefficient.

Evaluation: His applied constraint was 'the same volume and cubical form,' and as a result, his developed method is not suitable for conducting extensive comparisons of buildings with varying geometrical proportions. However, through the development of the tool introduced in this PhD, it will be possible to assess not only cubical forms but also various other types of geometries.

Granadeiro et al. (2011) [21] presented a methodology to assist design decisions regarding the 'building envelope shape' implications on the energy performance of the building. The methodology is based on establishing a direct link between early design generation, mainly the envelope shape and energy demand resulted from individual simulations. In his main diagrams he divided different geometrical forms to simple foursquare shapes, and as the next steps he considered which faces of these simplified shapes are either interior or exterior envelopes and finally estimated outcome of energy performance of these combined faces. Indeed, his method is not an independent method from simulations as he indicates that to discuss energy efficiency relation to envelope shape, values from energy simulation have to be available in early design stages. He clearly indicated that between exterior faces and interior partitions of building, interior shape namely partitioning has much less impacts on energy performance. So, a quick estimation of the quantity of the energy consumption by adopting simplified models on external envelopes of building results reliable estimations. To integrate a regulation for geometrical division he employed 'grammar for Frank Lloyd Wright's prairie houses' [22] as a design system that considers main elements of building regarding their shape, size and location. His integrated geometry division was based on the logic that shape of every block is set by a parametric rule, in which the quotient between its length and width may vary between 1 and 4. To consider contribution of different variants of proportions of windows in wall he supposed placing a window at the center of every external wall, with an area value determined by certain WWR.

Evaluation: Although the primary procedure of his estimation is based on the resulting energy performance of the combination of the exterior and interior envelopes, he acknowledged in his final comparisons that the energy performance of the exterior envelope could serve as a good indicator of the entire building. The accuracy of his method depends on the simulation software used, as he divided the entire volume of the building into simpler parts and simulated them separately. He applied fixed values for the building's components, such as the heat transfer coefficient for both opaque and transparent components. This limitation means that his results may not be applicable to the same geometrical variants if the basic material properties change. Additionally, in 'grammar for Frank Lloyd Wright's prairie houses,' the possibility of employing different inclinations of external components is missing.

Hachem et al. (2011) [23] also investigated on effects of geometric form on solar potential of housing units. In her study she mainly considered two-storey single-family housing units, located in mid-latitude climate and compared solar potential of seven plan geometries as; square, rectangle, trapezoid, L, U, H and T shapes. She compared effect of these shapes on two major response variables; solar radiation incident on equatorial-facing facades and transmitted by the fenestration of such facades, and electricity production potential of building integrated photovoltaic (BIPV) covering roof surfaces with optimal solar exposure. She also considered variations of roof design consist of modifications to the tilt and side angles of hip roofs. Her work indicated that manipulation of unit shapes and window location (in the case of self-shading level) can lead to optimization of solar radiation and its utilization for electricity generation and thermal performance. In her study she employed EnergyPlus building simulation program and the final results are followed by a comparative analysis to assess the effect of shape parameters on the solar potential, relative to a reference case. The unique point

of her investigation compared to previous ones is that she also indicates differences of solar potential of envelopes in each seven plan geometries if they partly receive shading resulted from the building's geometry itself or not. As her second unique consideration she assessed potential benefits and penalties associated with different plan layouts and roof shapes in comparison with the reference rectangular shape. At her final comparison results she pointed to different amounts of 'solar transmission', 'electricity generation per unit area by the BIPV system' and 'shifting the time of peak generation' in relation to investigated shapes. Later on, Hachem et al. (2012) [24] in her extensive dissertation discussed about effectiveness of geometrical parameters as aspect ratio, orientation, WWR, roof design as well as neighborhoods. She confesses that all the effects studied are specific to the climatic conditions of mid- latitude northern climate.

Evaluation: The applicability of her work is limited, as she exclusively conducted her research in the specific location of Montreal, Canada. Therefore, her conclusions can only be confidently applied in locations with the same latitudes and similar weather patterns.

Granadeiro et al. (2013) [25] based on his previous researches developed a methodology to generate alternative envelope shape designs to calculate energy demand of each design (rather than a certain geometry). In his latter developed method he divided holistic geometry of building into living and service zones with certain different energy demands and both following certain proportional dimensions as foursquare connected shapes. He discussed on possible external borders that can be outcome of different attachments and considered certain potential energy performance for each variant.

Evaluation: The consideration of external borders as the primary potential energy performance factor in his research aligns with the scope of this PhD. However, similar to the omission of 'weather condition input' in other research studies, his work is exclusively based on the energy performance of geometries in the weather conditions of Lisbon, Portugal.

Košir et al. (2017) [26] studied on influence of envelope geometrical characteristics on building energy performance in central European climatic conditions. He considered interconnectedness of building form, orientation and window area in regard to energy consumption for heating and cooling of a generic building and proved that in some cases buildings that are not compact are more energy efficient compared to cubic compact buildings with the same volume. His investigations indicated that in heating demand period the best building proportion is different from the ideal geometrical proportion in cooling demand period. He clearly indicated that in majority of European countries elementary steps of architectural designs are mainly focused on reducing heat losses and neglecting optimisation of demands (regarding cooling demand) often results more total energy demand. In his methodology he compared different geometrical proportions having the same volume but different proportions and WWRs. He applied fixed amount of U-values to opaque components and detected changing of energy demand when WWR and orientation of building changes. He considered fixed heating and cooling set-points in summer and winter and assumed existence of a constant natural ventilation and excluded influence of internal heat gains from occupants and electrical appliances. His final results are parametric discussions in matrixes that are combination of different orientations, geometry proportions and WWRs. In each variant he specified heating and cooling demand and their annual sum. His comparisons showed that the cases with the lowest heating energy use also exhibit the highest cooling energy consumption. His final comparisons mainly indicated four main conclusions. Firstly, less compact building form does not cause any significant increase in energy consumption. Secondly, bringing windows to building envelope (to an absolute opaque component) results in the decrease of energy

consumption but is not linear and increasing the window area to extremes does not result in lower heating energy demand. Thirdly, in regard to the cooling energy consumption increase of glazed area results in the increase of cooling energy demand. Fourthly, effect of different WWRs are much higher during heating demands compared to cooling demands that in some orientations is even identical.

Evaluation: While his integrated parameters are also incorporated into this PhD, his results are solely based on comparisons of a limited set of geometries. Furthermore, the absence of the possibility to modify weather data renders the algorithm not applicable when considering other proportions of geometry or when the geographical location changes.

2.3.3 Envelope PV installations and geometrical setups

There are a number of research studies that exclusively aim to demonstrate the different effects of PV installation configurations on the energy performance of the façade while also considering variations in electrical power. Some of these research studies also indicate how PV performance is influenced by different orientations and inclinations through various installation setups, and to what extent the thermal performance of the combined component differs from that of a simple component.

Wang et al. (2006) [27] concluded that the optimum configuration of PV is with ventilated air-gap because this integration leads to a high PV conversion efficiency and low cooling load. In winter, the appropriate integration building of PV is the non-ventilated (closed) air duct BIPV because of the combination of the low heating-load and the high PV electrical power. He mentioned non-ventilated air-gap BIPV, slightly decreases the heat-gain and peak cooling-load in contrast with the conventional roof. Also, cooling load for these roofs is reduced significantly because of the PV shading and natural convection of air in the gap.

Evaluation: A method to quantify the changes in the energy performance of the considered PV configurations based on different geometrical setups is still lacking.

Beringer et al. (2011) [28] illustrated that maximum power of PVs in winter are achievable in tilts of 50° to 70° whereas in summer tilts of 0° to 30° will result the maximum power. Also, sensibility of electrical power to different inclinations in winter is higher than summer. The difference between maximum and minimum values of power in winter months is 10 to 20% while in summer months is 5 to 10%.

Evaluation: Although he exclusively illustrated the effect of inclination on the electrical power of PVs, his numerical comparisons are only applicable in his specific geographical location. Furthermore, changes in the thermal performance of components holding PVs are ignored in his results.

A research performed at Fraunhofer IWES by Misara (2012) [29] showed relation of changing total u-value of PV installation to constructive materials of component. Furthermore, Siwanand Misara (2014) [30] in her dissertation introduced a temperature model with power balance concept based on steady heat transfer equations, taking into accounts the different configurations and installation possibilities of the module that are free- standing (only a layer of PV), variable gap (a distance of 5 to 10 cm between PV and backside insulation) and full-integrated configuration (PV attached to backside insulation or BIPV). Regarding geometrical setups, she considered inclinations of 0°, 45° and 90° as three main applicable inclinations. Her

unique conclusion is that she derived changes of u-value of a simple component or when it is covered by PV with or without backside distance in her explained inclinations.

Evaluation: The primary index investigated in her work is the 'heat transmission coefficient,' which results in 'heat flow' for limited defined inclinations. Her work does not allow for the integration of orientation, as both her measurements and calculations are based on constant quantities of irradiation in laboratory conditions. Similarly, the effects of wind are not considered in her work.

Through investigation of Hartner et al. (2015) [31], the optimum PV orientation in Germany considering electricity generation is discussed. As instance, he indicated that an optimal azimuth of 165° could bring more profitability compared to an absolute south orientation and this optimum orientation depends on if optimization is only based on maximum annual generation or level of self-sufficiency. Similarly, some studies also clarified specific orientations and its advantages compared with conventional orientation of "south". A Swedish study pointed that PV self-consumption of apartments and detached houses in Sweden can be increased by respectively 2% and 3% through optimizing the PV orientation through an east–west orientation. (Nyholm et al., 2016) [32]. Some studies also revealed that there is not an absolute optimized orientation or inclination for building components. A German study proved that for rooftops oriented towards east/west it is possible to benefit from the high self-consumption of the east orientation and the high degree of self-sufficiency of the west orientation. It showed two opposite impacts that depend on orientation when switching from a tilt angle of 30° to 45° . For a south orientation, self-sufficiency is increased, while for west and east orientations, self-consumption increases (Lahnaoui et al., 2017) [33]. Some of researches are also exclusively performed to examine thermal performance and electrical power of building's envelop, when PVs is applied through different configurations. As instance, Toledo et al. (2016) [34] mentioned that BIPV panels used in his study reduces heating loads in low ambient temperatures and increases cooling loads in warm climates.

Evaluation: All three mentioned works were conducted in similar geographical locations with comparable levels of momentary and cumulative irradiation. It is common for the effects of local wind to be disregarded in the calculation process.

2.3.4 Geographical location and optimization of geometry

A European research tried to determine optimal design of a building shell based on the optimization of its solar exposure (Fokaides et al., 2017) [35]. The calculations were performed for two European cities (Athens and London) to see whether the guideline of geometrical optimization is the same in different latitudes. The results revealed that the different cumulative irradiation of Athens and London have a significant impact on the optimal geometry of the investigated subject. The case of Athens suggests that the maximization of the south exposed surface resulting to a quasi-rectangular instead of a convex quadrilateral shape maximizes the solar gains of the building shell, whereas the optimal shape in London is an isosceles trapezoid.

Evaluation: The results of the mentioned work provide a clear emphasis on the integration of weather data in the calculation procedure and the upcoming method. Parts of the developed method aim to address the effects of different dimensional proportions on the energy performance of buildings.

2.3.5 Further development

Based on the research conducted and individual evaluations of each study, the scientific objective of this PhD is to provide feasible solutions for the issues that remain unresolved in the existing body of work. These upcoming challenges can be viewed as problems that have not yet been fully addressed. The scientific direction of this work and the developed method in this PhD aim to either overcome these challenges or facilitate further advancements in future research:

1. In the design of simulation tools, the precise detailing of the external layout of a building is essential to make it usable in the calculation process. This requirement arises from the need for complete numerical and dimensional data of the building's envelope and the related comprehensive material properties. Without this information, running the software would be impossible. This issue presents a clear limitation on the flexible and efficient design of various architectural variants. Typically, the elementary architectural layout does not provide the necessary parameters for simulation software. Consequently, a significant barrier exists when attempting to compare the energy performance of basic geometric variants. Running the simulation for each variant consumes a considerable amount of time. The time limitation at this early stage of building design prevents comprehensive comparisons of each variant based on their energy performance simulations. As a result, the testing of energy performance for further geometric variants is often ignored due to the time-consuming nature of the simulation process, which involves a vast number of parameters as software inputs.

2. Working with simulation software requires in-depth professional knowledge to handle it effectively, and it demands a significant investment of time for education and training. While it is possible to learn these simulation tools through participation in workshops and by studying instructor guides, the consequence is that within a design team, there are planners who do not personally simulate the energy performance of their ideas. Moreover, the simulation experts are typically not designers and are often removed from the architectural design process. This situation contributes to the complexity of developing elementary architectural designs because, to test the energy performance of each idea, it must be conveyed to a 'simulation expert team.' Consequently, the communication between the 'architectural team' and the 'simulation experts' becomes much more time-consuming compared to a simpler scenario where both architectural design and simulation are performed by the same person or group of experts.

3. There are several technical parameters that are not readily available for software input during the early phases of design, such as the precise definition of thermal properties of materials. Additionally, the integration of heating and cooling devices is typically decided in the final phases of design, while energy simulation ideally should be performed in the early stages of design. This situation means that there are consistently unavailable geometrical and technical parameters, which often postpone the simulation process to the last phase of design.

4. Calculating the energy performance of the combination of PVs with building components such as walls, windows, and roofs is possible through various existing software programs. However, this consideration requires extremely accurate data as software input, and sometimes, integrating PVs on the desired component is not feasible within the predefined capabilities of the software. Furthermore, the ability to manipulate the software to account for different installation setups of PVs, which can result in varying thermal and electricity production performance, is not always included in these software solutions.

2.3.6 Approaches of energy estimation tools

Taking into account the state of the art in the performed works and research, as well as individual evaluations and the existing unsolved issues in using the majority of simulation tools, the goals and approaches of this work are outlined in the upcoming diagram (Figure 2.1).

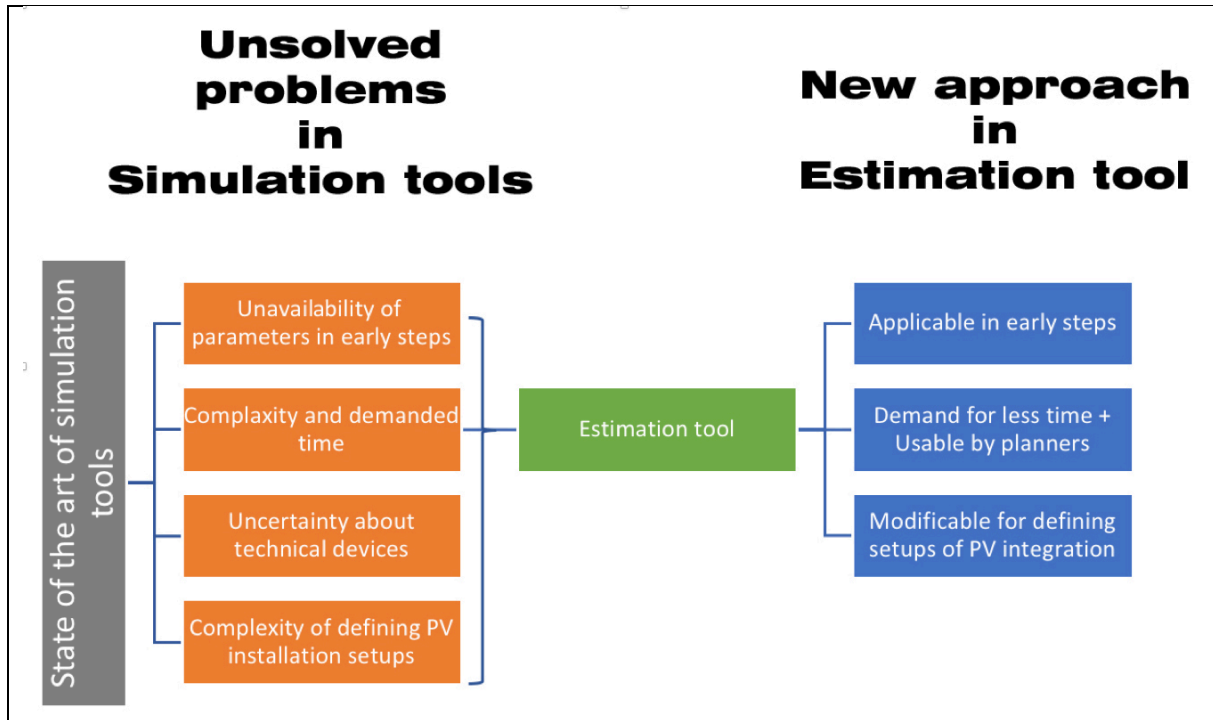


Fig. 2.1 Approaches of energy estimation tools compared to unsolved problems in simulation tools

3. Goal setting

3.1 Research questions

1. Is it possible to estimate energy demand of a building based on average energy performance of its envelope?
2. What is advantage and disadvantages of integration PV on facades and roofs in different geometrical setups regarding final energy performance of building?
3. How it could be feasible to employ effects of conduction, transmission and emission together through a method to estimate energy demand of building?
4. How energy efficiency of buildings can be estimated regarding its envelope geometrical properties?

3.2 Hypothesis

Definition of hypothesis of this work is basically considering the defined research questions. So, upcoming hypotheses are predicted and defined;

1. Energy balance of a building's face can be estimated by calculating of energy performance of one square meter of each component that the face is consisted of them regarding each component's area and interaction of their individual energy performances. In this scaling up, compensation of heat flow resulting from convection, conduction, emission, reflection and transmission of combination of opaque and transparent components in a building's face with or without PVs should be simultaneously calculated.
2. Energy demand of a building can be estimated by calculating outcome of energy performance of all faces shaping envelope of building. In this scaling up, area of each face and its momentary heat flow regarding boundary condition indicate energy demand of building.
3. By simultaneous calculation of 'energy demand' and 'self-generated electrical power' of building considering interaction of 'electrical and thermal' performance of PVs in different configurations, indicative of self-sufficiency and self-consumption of building can be estimated.
4. Estimating indicative of energy efficiency is calculated by outcome of energy performance of all faces shaping envelope of building. Considering initial integrated geometrical parameters, changes of energy efficiency can be interpreted regarding effectiveness of each 'geometrical parameter'. *

* **Constraints:** In this procedure thermal properties of all components shaping building's envelope as well as thermal properties and energy efficiency of PVs should be set on fixed quantities. Configuration of PVs should remain the same. Similarly, weather data should be representative of a specific geographical location. Comparison of different geometrical variants to indicate effectiveness of each geometrical parameter should be done between variants with 'the same quantities of integrated PVs and TFA' or 'the same ratio of integrated PVs into TFA'.

3.3 Flowchart of work

The integration of geometrical parameters at different levels, weather data, material properties, and components for developing the proposed method and assessing the final indexes are illustrated in Figure 3.1.

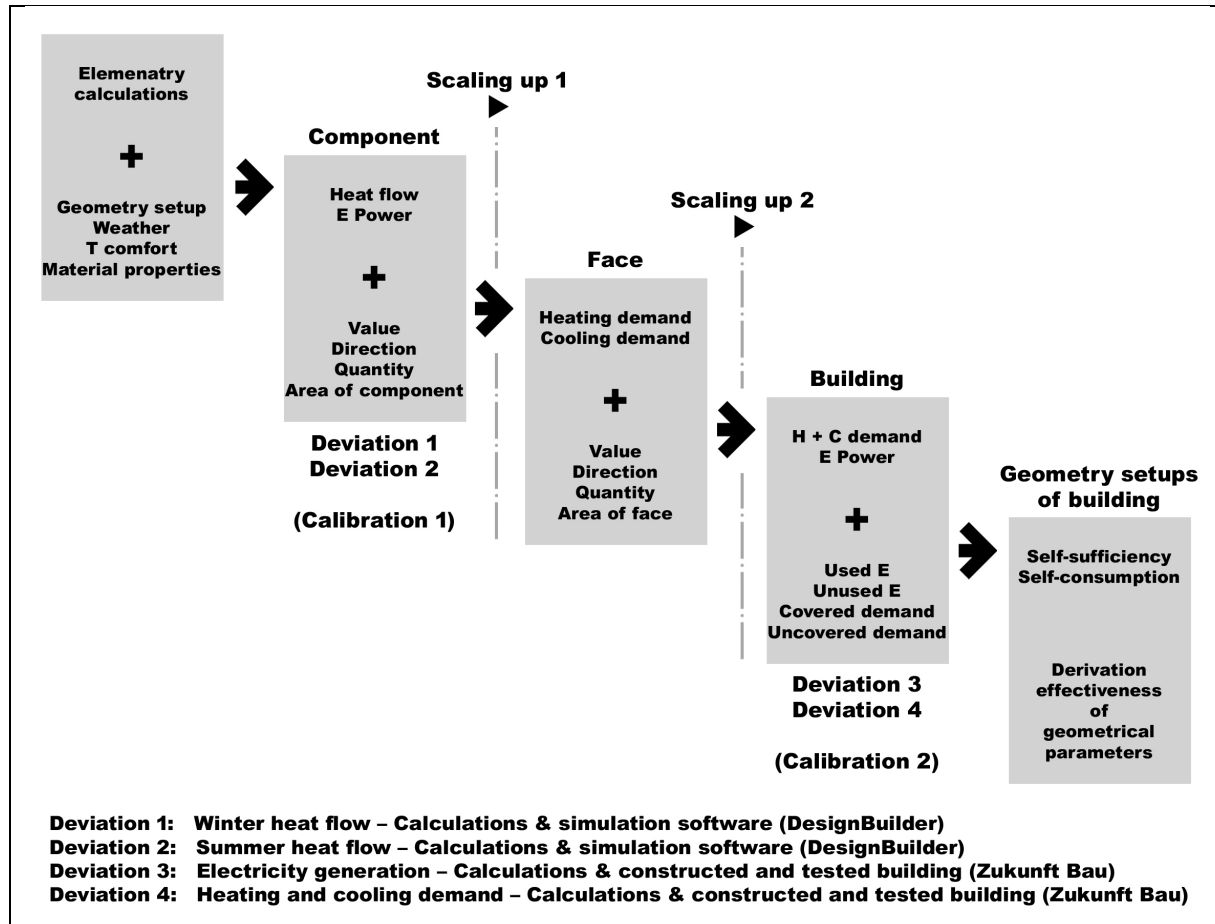


Fig. 3.1 Flowchart of work – Calculated indexes in different geometry levels + Calibrations phases

The presented procedure demonstrates that achieving the planned indexes involves scaling up calculations to higher geometry levels in different phases. This process begins by integrating initial parameters, primarily comprising geometry setups, weather data, thermal comfort criteria, and material thermal properties. These initial calculations yield heat flow at the component level. At this stage, two initial calibrations are conducted to compare the calculated heat flow for winter and summer with the results obtained from simulation software (DesignBuilder) [36]. By utilizing the heat flow values, considering their direction, quantity, and the differences between outside air and inside comfort temperatures, heating and cooling demands are calculated. In the next phase, taking into account the areas of components within a face, the calculated heat flow can be scaled up to the higher geometry level of the face. Here, heating and cooling demands, characterized by heat flows, their values, and the area of each face comprising the building envelope, are scaled up to the higher geometry level of the building itself. In this same phase, using the calculated electricity generation of components that hold PVs through BIPV, BAPV, or PV glazing setups, the feasibility of calculating used electricity, unused electricity, covered demand, and uncovered demand—the four main components required for calculating the target indexes of self-sufficiency and self-consumption—is determined. Two additional calibrations are performed at this level to compare the calculated

electricity generation and heating and cooling demand with those obtained using an integrated method with a constructed and tested building (Zukunft Bau) [37]. Finally, in the last phase of the work, the effectiveness of different geometrical parameters is evaluated by comparing changes in the two indexes of 'self-sufficiency' and 'self-consumption,' which serve as indicators of energy efficiency.

The accuracy of the four developed hypotheses is assessed throughout the work, encompassing all initial calculations and subsequent calculated indexes. Figure 3.2 illustrates the sequence of hypotheses and calculated indexes across different geometrical levels, including components, faces, and the building as a whole. Subdivisions of geometrical indexes at each level indicate the potential for calculating complex geometrical indexes. For example, initial parameters such as orientation and inclination at the 'component level' are scaled up to the 'face level.' This enables the comparison of energy demand for a face under different proportions and combinations with other components (e.g., WWR or any other combination of the five defined components). After scaling up heating and cooling demands to the building level, it becomes possible to discuss the effectiveness of various combinations of geometrical parameters. This includes assessing the effectiveness of proportion, orientation, inclination, WWR, and more when more than one geometrical parameter changes. The holistic approach of this work offers the opportunity to compare the magnitudes of changes in energy efficiency and the effectiveness of each geometrical parameter in altering the 'indicative of energy efficiency.'

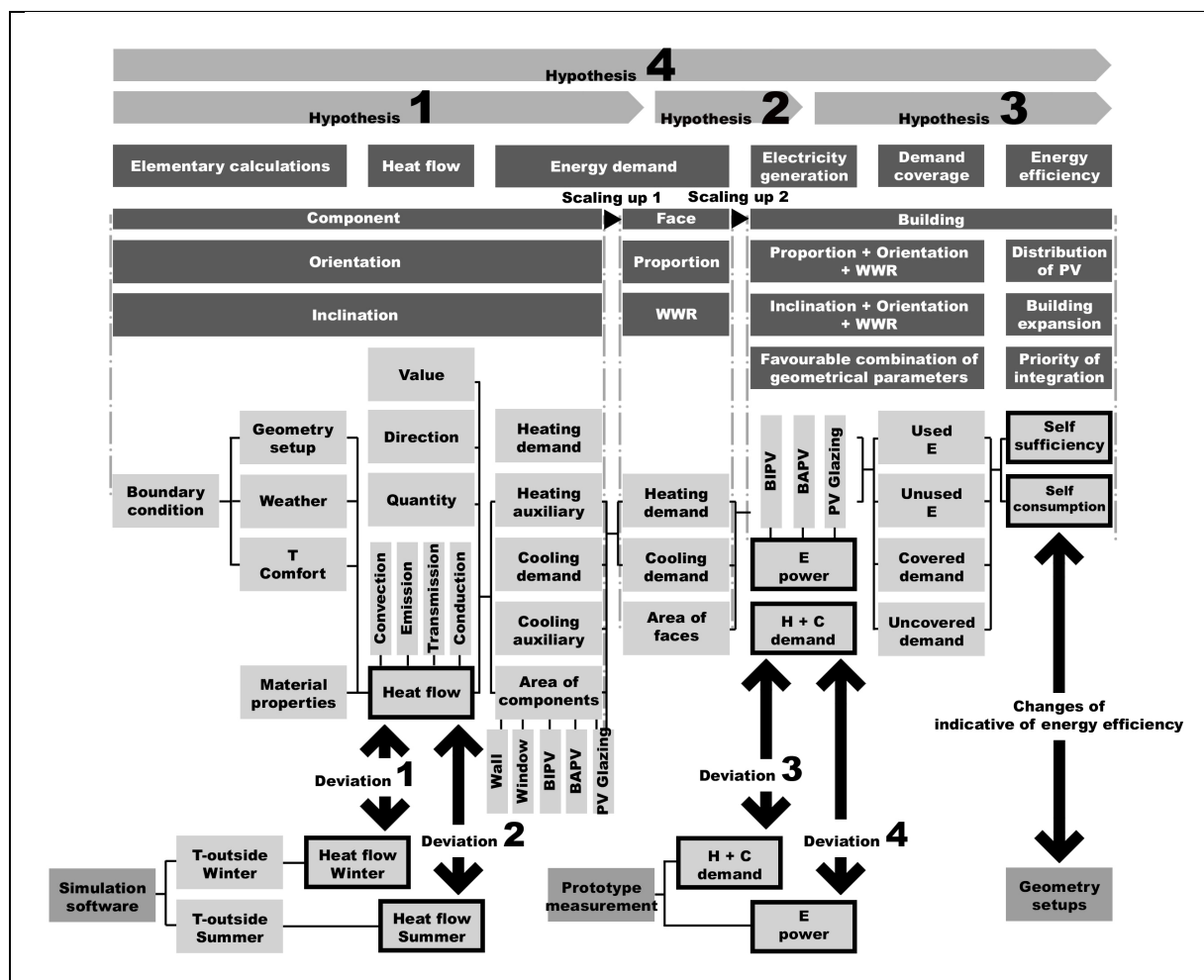


Fig. 3.2 Flowchart of work – Hypotheses, sub-divisions of geometrical parameters, process of calculation + Deviations

A schematic illustrating the interaction of weather parameters, comfort temperature, material properties of the building envelope, and two initial geometrical parameters, inclination and orientation, is presented in Figure 3.4.

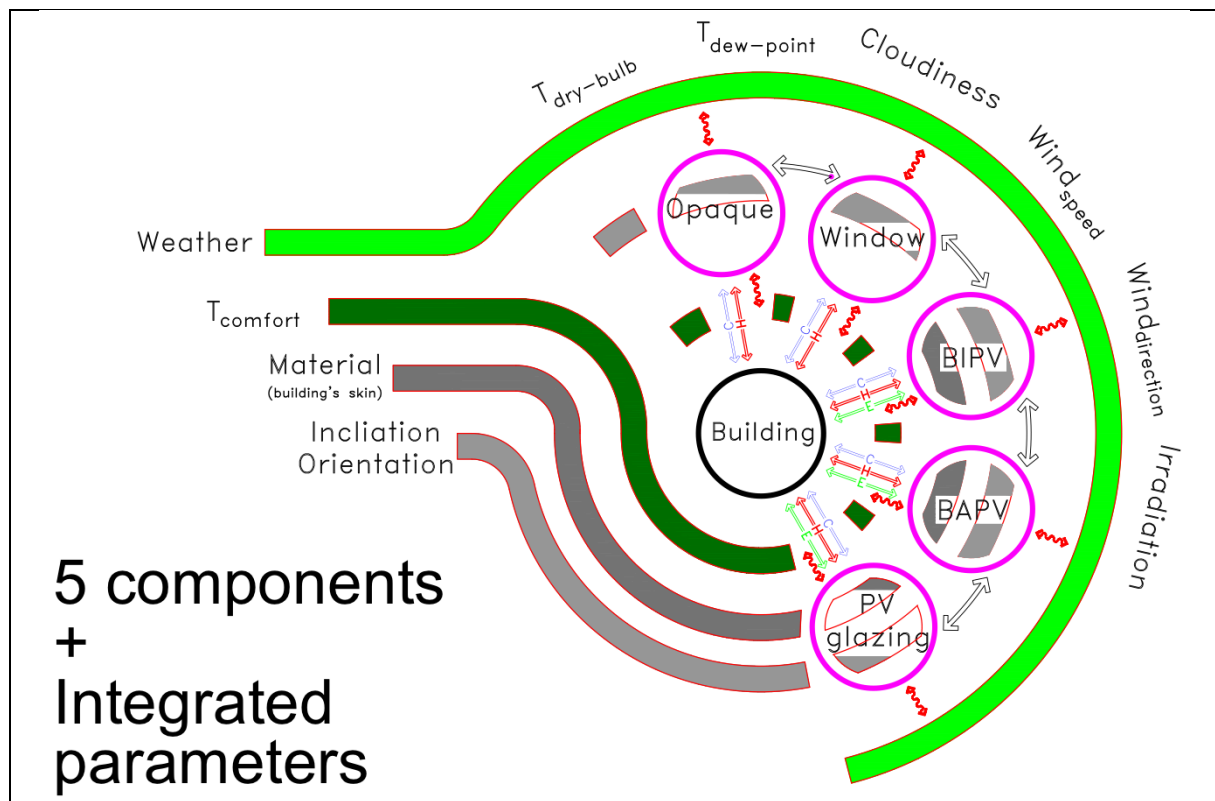


Fig. 3.3 Interaction of weather parameters, comfort temperature, material properties and geometrical setup on buildings energy performance – Initial heat flows and resulted heating and cooling demand

The initial weather parameters, which primarily include dry-bulb temperature, dew-point temperature, cloudiness, wind velocity, wind direction, and irradiation, result in heat flow through the components of the building's envelope. These components consist of the opaque component, transparent component, and three PV integration setups: BIPV, BAPV, and PV glazing. The interaction of the thermal performance of each combination of these five components, considering the compensation of demand among them when assembled in one face, is calculated. This calculation yields individual heating and cooling demands for each component within the building, which can be considered as the energy performance of a face.

In this phase, the differences in thermal performance of components generating electricity are also calculated, parallel to the differences in electricity generation for different installation setups. The building itself, as the core of the outcome of this interaction, is influenced by the performance of its envelope's faces in terms of electricity generation and thermal performance. Therefore, this phase estimates the energy performance of the building based on its envelope.

It's important to note that additional energy demand of the building, such as lighting, household appliances, cooking, etc., is not included in this diagram. Instead, it is assumed that these energy demands are fixed at a flat rate, considering referenced sample prototypes in the same weather conditions for buildings of the same size.

4. Method

4.1 Heat flow

To measure the heat flow passing through the investigated components, different methods including static, quasi-static, and dynamic methods were considered, and the "quasi-static" method was employed. In this context, the changes in boundary conditions are quantitatively affected by variations in irradiation, temperature, wind velocity and direction, emissivity of the sky, and other factors. Taking into account the rates of change in these parameters based on the available weather data, as well as the resolution of the calculations (which are based on 1-hour intervals), it can be concluded that the fluctuations in these parameters are not highly significant. As a result, the target index, which is mainly the "heat flow," stabilizes within each hour, making the quasi-static method with a relatively high resolution (24 points in each day) a reliable choice for this analysis.

4.1.1 Effective phenomena

The basic calculation aims to integrate the varying amounts of heat flow passing through the main structural components of the building. These components include opaque elements representing walls and roofs, as well as transparent components like windows, each with their specific thermal characteristics. Additionally, three alternative configurations involving the integration of photovoltaics (PVs) with both opaque and transparent components have been examined: Building-Integrated Photovoltaics (BIPV), Building-Attached Photovoltaics (BAPV), and PV Glazing. These configurations, with their selective thermal and electrical efficiency characteristics, act as components that not only influence the thermal performance of the building but also generate electricity, thereby impacting the building's energy performance from an electrical power perspective. All five components considered in this study are assumed to be integrated into the building's surrounding envelope. Therefore, their outside temperature is simultaneously influenced by boundary conditions from both the interior and exterior of the component, as well as the effects of irradiation, convection, and emission, which are the three main phenomena under investigation. These phenomena are quantitatively dependent on angular configurations, such as the angle between the direction of momentary irradiation, temperature, wind, percentage of cloud cover, and more. Consequently, the parameters of weather continuously change, resulting in variable boundary conditions used in this work. The quantity of heat transfer has been examined in terms of conduction, reflection, and transmission (Figure 4.1). [38]

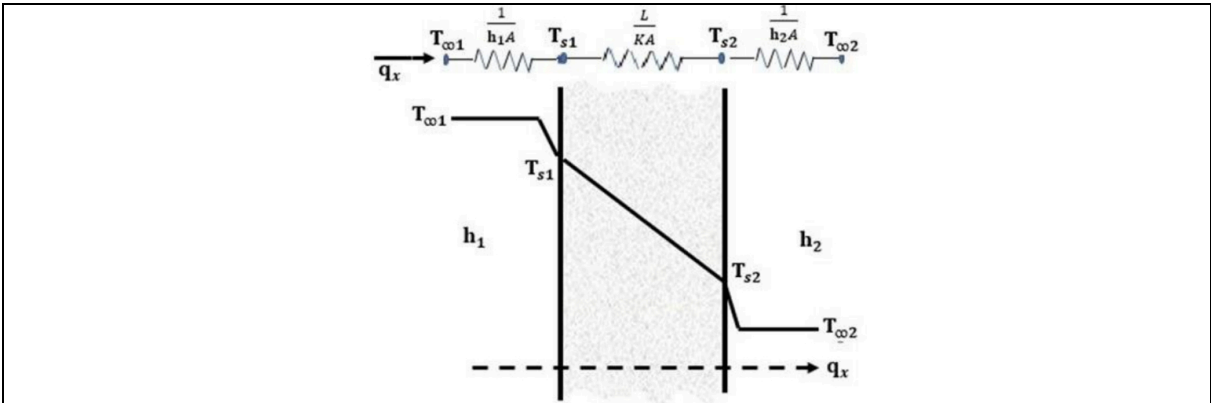


Fig. 4.1 1D Heat transfer model prediction through the pilot furnace refractory wall; showing both the temperature profile and the equivalent thermal circuit [38]

4.1.2 Thermal performance of components

All five components investigated in this work, including opaque components, windows, BIPV, BAPV, and PV Glazing, have been individually analyzed to calculate their heat flows under various boundary conditions. To achieve this, the potential combinations of material assemblies defining the thermal performance of these components have been determined and integrated into the calculations. The final results for the thermal performance of these different components have been obtained by applying specific thermal properties based on the state of the art as observed in the investigated pilot projects.

4.1.3 Electrical power of components

BIPV, BAPV, and PV Glazing were chosen as the three primary configurations for installing PV systems on both opaque and transparent building components. The impact of constantly changing boundary conditions on the output power of these PV systems has been computed. This analysis considered the geometrical configuration of the "components holding PVs," which is primarily influenced by different angular positions with respect to outside irradiation, outside and inside convection, and outside emission.

4.2 Boundary condition

4.2.1 Inside comfort temperature

The theory defining the relationship between outdoor temperature and indoor comfort, which continuously adjusts the indoor temperature setpoint based on outdoor temperature, has been considered. This adaptive comfort model, as illustrated in ASHRAE Standard 55 (ASHRAE 2004), shows how the optimal comfort temperature for a building can vary at different occupant acceptance levels (figure 4.2). [39]

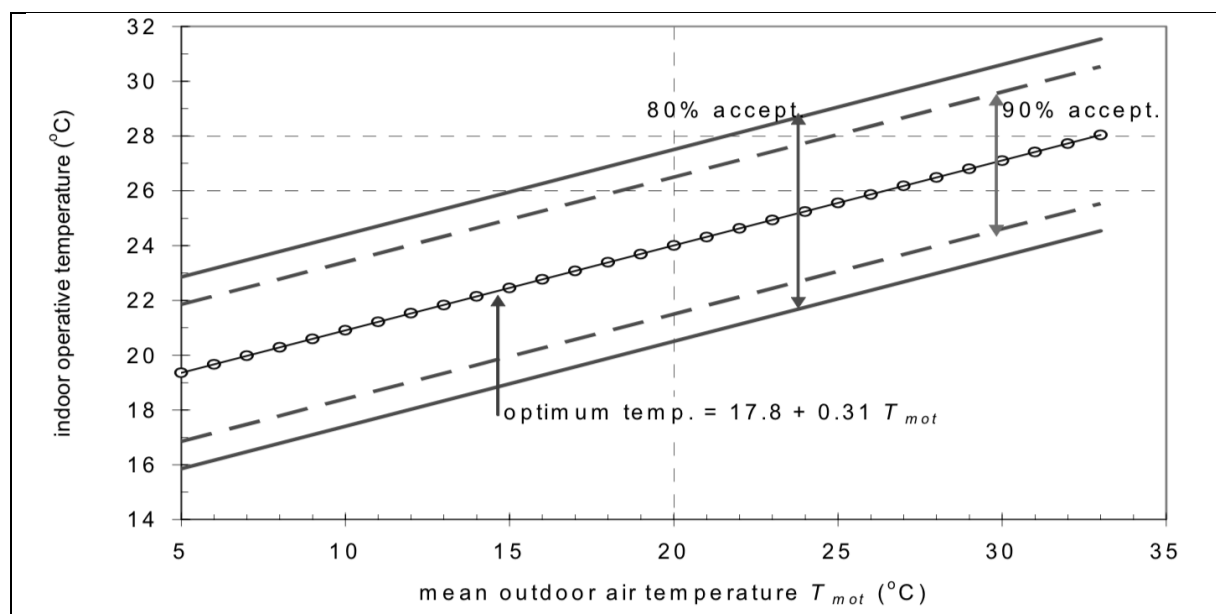


Fig. 4.2 The adaptive comfort model used in ASHRAE Std.55:2004. Optimum indoor comfort in a naturally ventilated building equates to $0.31 \times T_{mot} + 17.8^\circ\text{C}$ [39]

Indoor comfort is a biological parameter that varies from one location to another. Therefore, a German climate comfort definition has been incorporated to establish the dependence of indoor temperature on outdoor temperature. Figure 4.3 illustrates the relationship between indoor and outdoor temperature based on the level of acceptance by occupants. [40]

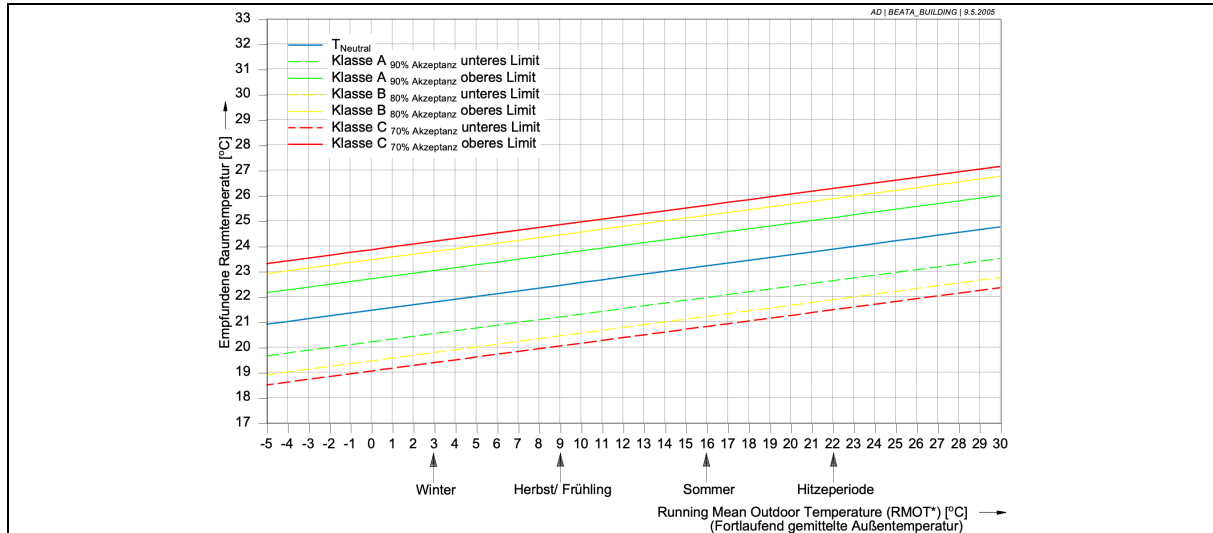


Fig. 4.3 The perceived room temperature in connection with outside temperature and level of acceptance [40]

The graph illustrates three distinct indoor temperature levels corresponding to outdoor temperature. The lowest and highest setpoints differ by approximately 4.8° C, resulting in varying amounts of heat transfer under the same external boundary conditions. Therefore, based on the graph, a linear equation has been derived to represent the integration of the lowest, middle, and highest levels of indoor temperature. In the final part of this work, to assess the impact of indoor temperature on heat flow quantities and resultant heating and cooling demands, the lowest and highest setpoints have been integrated and compared. The correlation of these three different indoor temperature levels with outdoor temperature is presented in table 4.1.

The lowest	$T_{(in)} = 21.50 + (0.107 \times T_{(out)})$	(4.1)
The middle	$T_{(in)} = 19.00 + (0.111 \times T_{(out)})$	(4.2)
The highest	$T_{(in)} = 23.80 + (0.111 \times T_{(out)})$	(4.3)

Tab. 4.1 The perceived room temperature in connection with outside temperature and level of acceptance

4.2.2 Inside convection heat coefficient

Regarding the low velocity of air on the internal surface of walls in buildings with or without ventilation, the assumption of the inside convection coefficient is based on the wall's configuration concerning wind-free stream velocity. Different investigations based on tests and simulations result in approximately the same inside convection, which converges at the same point. Figure 4.4 shows the drop of convection coefficient when wind velocity drops to 0.00 W/m²·K [41].

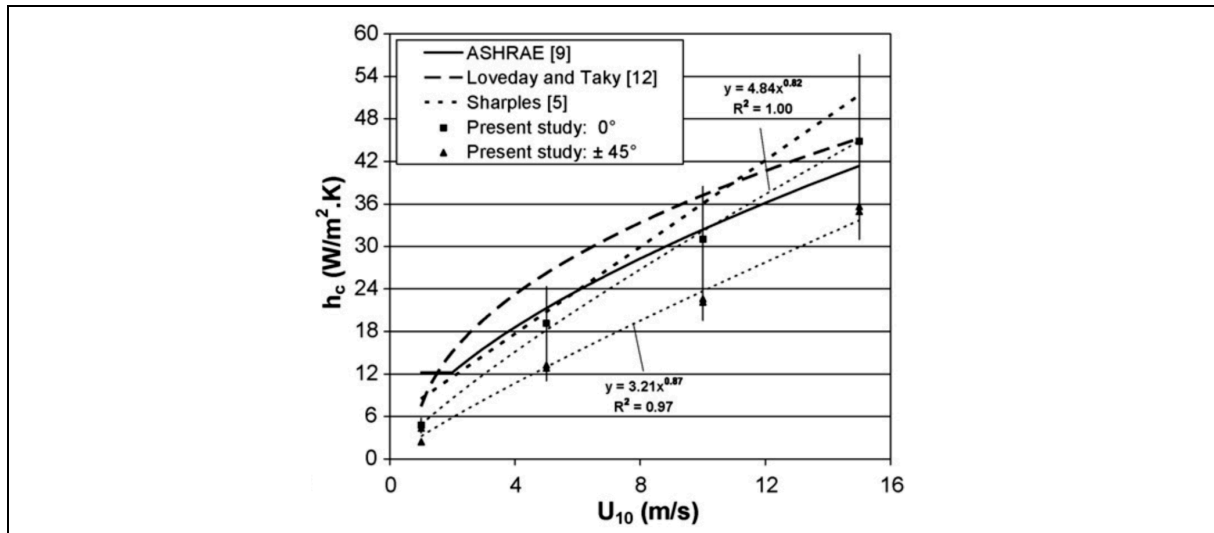


Fig. 4.4 Convective heat transfer coefficient vs. wind free stream velocity for windward conditions - short wall [41]

4.2.3 Irradiation

Percentage of irradiation absorption, rather than light intensity, is directly dependent on the angular configuration of the surface of the component with the axis of light. As a result, both electrical power and thermal performance of components, regarding the amount and direction of heat flow and the rate of electricity production, are directly affected by the domain of irradiation absorption. Direct, diffuse, and reflected radiances are individually calculated and taken into account in each interval of calculations. Figure 4.5 shows the interaction of angular radiance with the surface of the component.

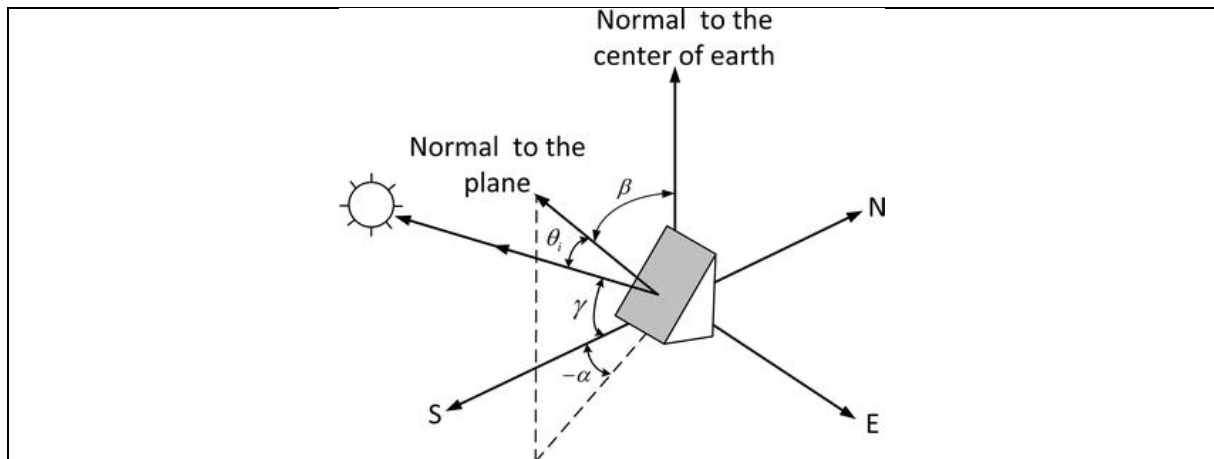


Fig. 4.5 Definition of angles used as coordinates for an element of sky radiation to an inclined plane of tilt β and oriented to α

The total solar radiation density incident on a tilted surface is estimated as [42];

$$G_{Tt} = G_B \cos \theta + G_D R_d + \rho G_E R_r \quad (4.4)$$

Three components of the equation represent portions of direct, diffuse and reflected light that in each geometrical configuration reaches to the surface of a component. Where G_B

is direct beam, θ is angle of incidence of the sun rays on the tilted plane, G_D is diffuse light, R_d is the diffuse transposition factor, ρ is the foreground's albedo and R_r is the transposition factor for ground reflection. G_E is calculated through sum of direct and diffused light and after integrating foreground's albedo and transposition factor, presents amounts of reflected irradiation from surroundings reaching to surface of a component.

To determine direct beam intensity on the surface of component, $\cos\theta$ is calculated through equation 4.5 [43].

$$\cos \theta = \sin \delta \sin \varphi \cos \beta - \sin \delta \cos \varphi \sin \beta \cos \gamma + \cos \delta \cos \varphi \cos \beta \cos \omega + \cos \delta \sin \varphi \sin \beta \cos \gamma \cos \omega + \cos \delta \sin \beta \sin \gamma \sin \omega \quad (4.5)$$

Where;

θ = angle of incidence of beam radiation on a surface (the angle between the beam radiation on a surface and the normal to that surface),

φ = declination of sun,

β = the slope of a tilted surface (angle between the normal of the surface and normal of earth)

ω = hour angle

γ = surface azimuth angle

δ = latitude

Assuming the intensity of diffuse sky radiation to be uniform over the sky, the view factors to the sky $\frac{1+\cos\beta}{2}$ and to the ground $\frac{1-\cos\beta}{2}$, are integrated in related equation [43].

$$G_{Tt} = G_B + (G_D \frac{1+\cos\beta}{2}) + ((G_B + G_D)\rho \frac{1-\cos\beta}{2}) \quad (4.6)$$

Regarding different surroundings and seasonal conditions (summer vs winter), sky clarity (clear-sky vs all-sky conditions) and snow-free ground vs snow on ground, ground albedo (ρ) is estimated at a constant value of 0.2 [42].

The fraction of incident radiation absorption is influenced by the external physical properties of covering components. Different materials exhibit varying levels of absorption, reflection, and transmission of incident radiation. Calculations and assumptions regarding these proportions have been made separately for opaque and transparent components.

4.2.3.1 Reflection in opaque component

The opaque components in this study consist of masonry materials, such as stone, brick, concrete, and adobe, which have porous textures. The percentage of reflected direct, diffuse, and reflected light from the surroundings, which can be absorbed or reflected again, is assumed to be independent of the geometrical configuration of the opaque components.

Figure 4.6 illustrates the principle of reflection from the surface of a non-smooth material, based on the concept that a certain percentage of the combined direct and diffused light will be reflected as diffuse reflection.

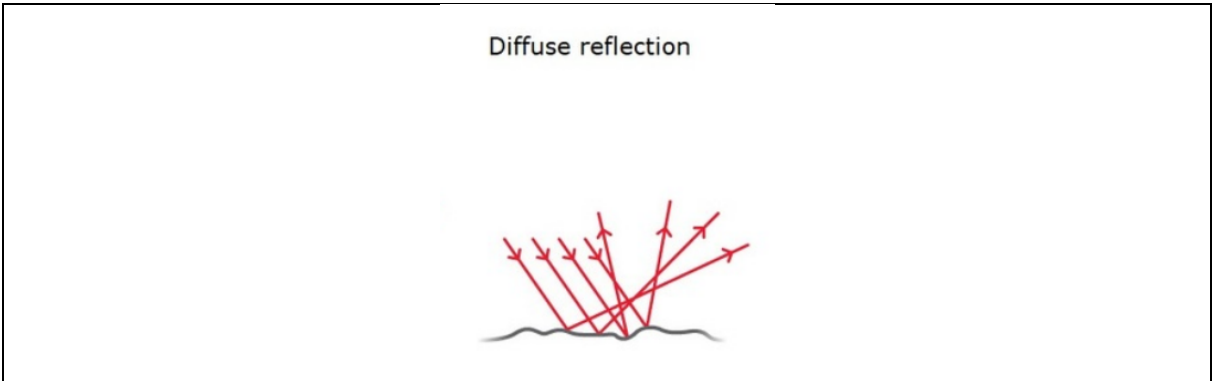


Fig. 4.6 Diffuse reflection in lots of different directions

As a result, the percentage of reflection in opaque components is assumed to be equal to the remaining irradiation after absorption. It should be noted that in steady heat transfer calculations, the quantity of absorbed irradiation is used to determine heat flow by conduction.

4.2.3.2 Reflection in transparent component

A three-layer glazing window is selected as the transparent component in this work. Reflectivity primarily depends on the direction of incident irradiation, wavelength of light, and the type of material. The direction of incident irradiation is calculated based on the geometrical configuration of the component and the direct incident light in each interval. To determine the extent of reflection's dependence on the wavelength of light, we have considered the changing percentages of transmission, absorption, and reflection within a float glass material, as shown in Figure 4.7 [44].

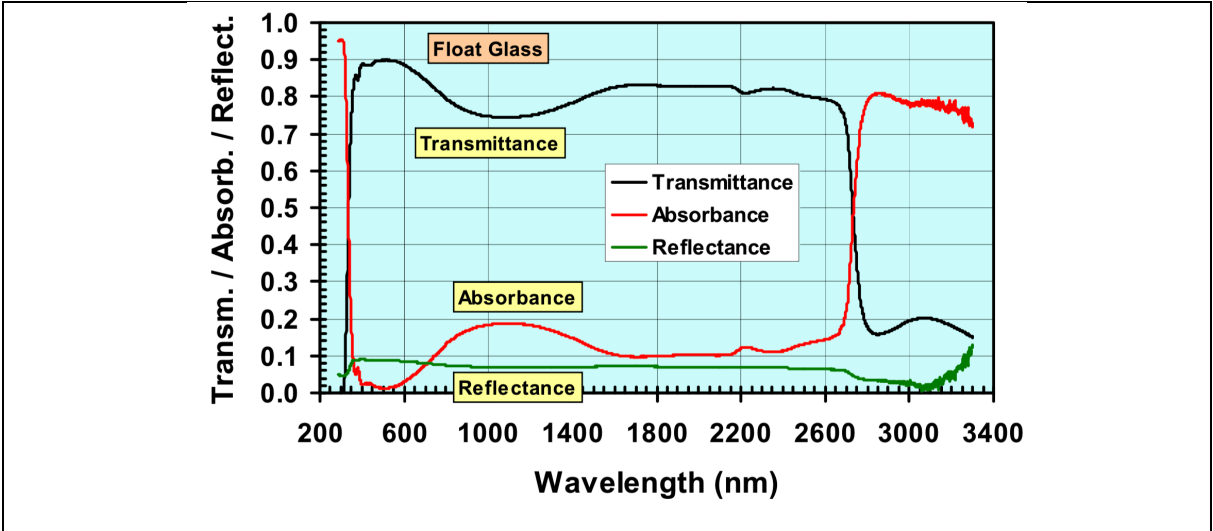


Fig. 4.7 Transmittance, absorbance and reflectance versus wavelength in the whole solar spectrum measured for a float glass [44]

Figure 4.8 [44] displays the spectral irradiance energy and wavelength of sunlight.

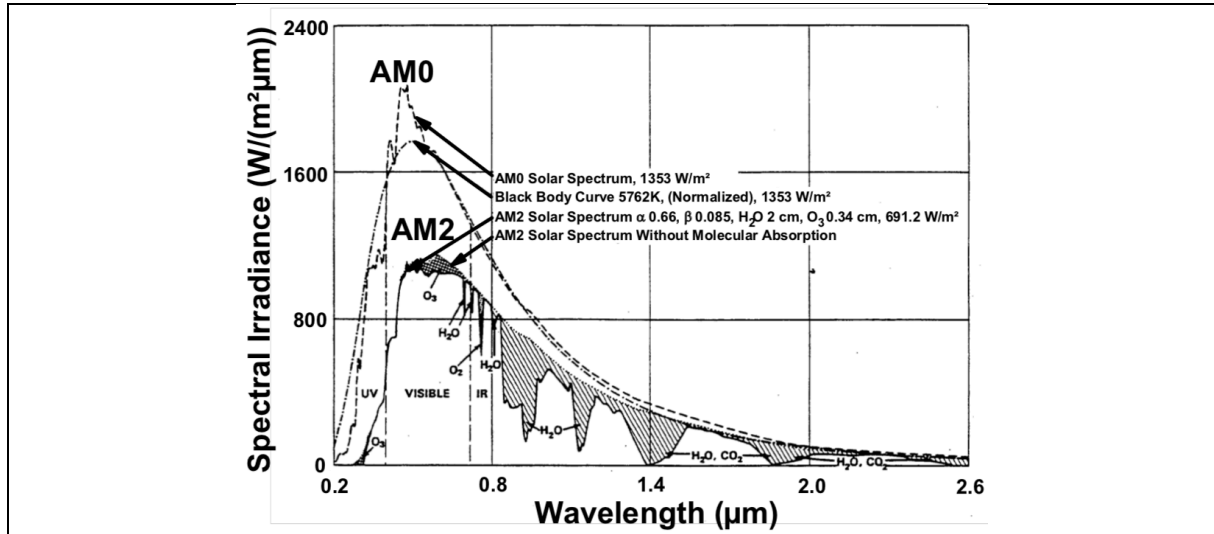


Fig. 4.8 Rate of spectral irradiance energy and wavelength of sunlight [44]

As shown in Figure 4.8, to harness the highest irradiance energy potential, wavelengths between 500 nm and 750 nm have been taken into account. Integrating this wavelength range with the fluctuating curves depicted in Figure 4.7 determines the proportions of transmittance, absorption, and reflection as 75%, 17%, and 8%, respectively. Additionally, the influence of the material type on reflectivity is considered using Equation 4.7, which incorporates two reduction factors that determine the reduction of absorbed light due to reflection [45].

$$q_{Sol(h)} = (B_{(h)}r_{B(\omega)} + D_{(h)}r_{D(\omega)})A_g \cdot g \cdot (F_{SC} \cdot F_S) \quad (4.7)$$

In this equation $r_{B(\omega)}$ and $r_{D(\omega)}$ clarify reduction coefficients changing amounts of direct and diffuse light, respectively. Where;

$B_{(h)}$ = Direct irradiation

$D_{(h)}$ = Diffuse irradiation

A_g = Area

g = Transmittance coefficient

F_{SC} = Shading factor to take the contamination of the glass into accounts

F_S = Shading factor to take buildings and their surroundings into accounts

In this equation the emerged reduction factors are;

Reduction factor for direct light is [45];

$$r_{B(\omega)} = 1 - (1 - \cos \omega)^{\epsilon'} \quad (4.8)$$

And reduction factor for diffuse light is [45];

$$r_{D(\omega)} = \frac{\epsilon' \cdot (\epsilon' + 3)}{(\epsilon' + 1) \cdot (\epsilon' + 2)} \quad (4.9)$$

In these two reduction factors;

ϵ' = Exponent that determines the reduction in radiation transmittance as a function of the type of glass used

$\cos \omega$ = Direct beam intensity coefficient on the surface of component

In this work, the integration of two reduction factors determines the proportion of total irradiation divided into reflection and transmission. This correlation allows for the definition of different g-values for transparent components, as per the German standard [45]. By determining the quantity of reflection, the remaining total irradiation is apportioned based on the assumed proportions of 75% for transmission and 17% for absorption. Consequently, varying reduction factors for direct and diffuse light, influenced by the diverse material properties of the transparent component (ϵ') and the geometrical configuration of the component with respect to the angle of direct incident irradiation, result in different percentages of reflection.

4.2.4 Outside convection heat coefficient

The convective heat transfer coefficient value is a function of wind velocity and its direction, taking into account the three-dimensional relative angle of the component [41]. In this context, the coefficient has been determined by considering both 'wind speeds' and the resulting angles between the geometrical configurations of the component and the wind, which are influenced by different orientations and inclinations of the component. To ensure a more accurate estimation of the heat convection coefficient, both windward and leeward conditions have been studied, taking into account the turbulent intensity of the airflow along separated building edges. This approach has been used to derive the resulting convective heat transfer coefficients for both windward and leeward conditions [41] (Figure 4.9).

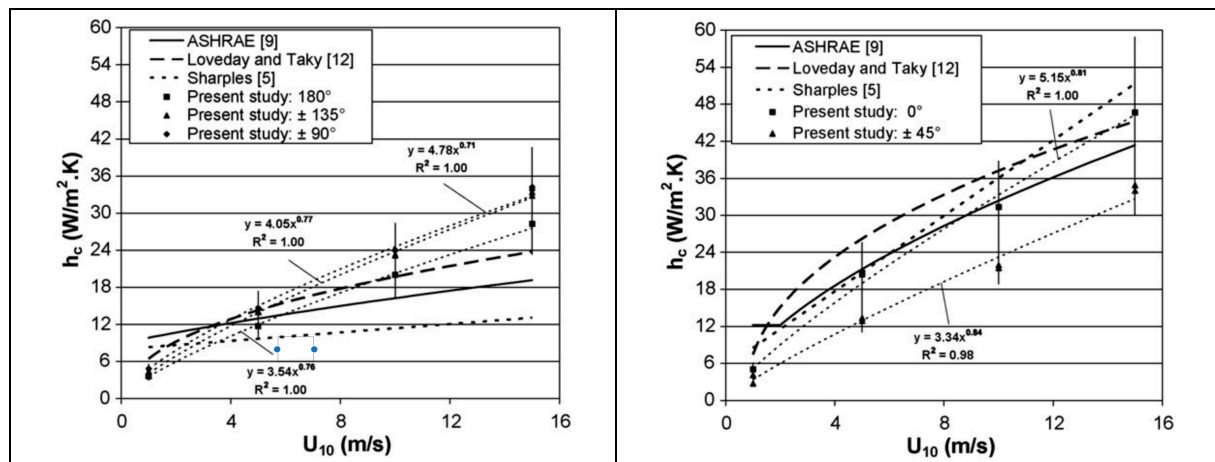


Fig. 4.9 Convective heat transfer coefficient for leeward (left) and windward (right) conditions [41]

In the correlation shown in Figure 4.9, the effect of different orientations of the component in the building with respect to the wind direction and varying turbulence has been calculated. In leeward conditions, three angle variants between the wind and component have been determined: $\pm 90^\circ$, $\pm 135^\circ$, and 180° . In windward conditions, two variants have been determined with angles of 0° and $\pm 45^\circ$.

The convective heat transfer coefficient for the roof at various wind velocities has also been presented (Figure 4.10) [41].

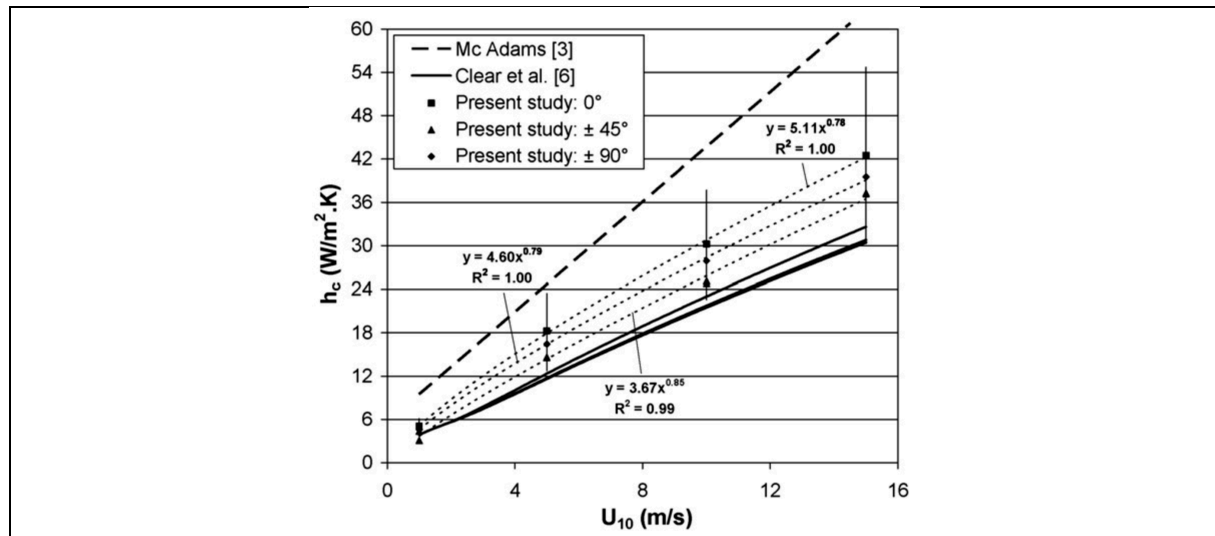


Fig. 4.10 Convective heat transfer coefficient in long-wall-to-wind angle for roof [41]

To determine the angle of the component and the average wind direction, relevant weather data from Stuttgart, Germany, have been utilized (Figure 4.11) [46].

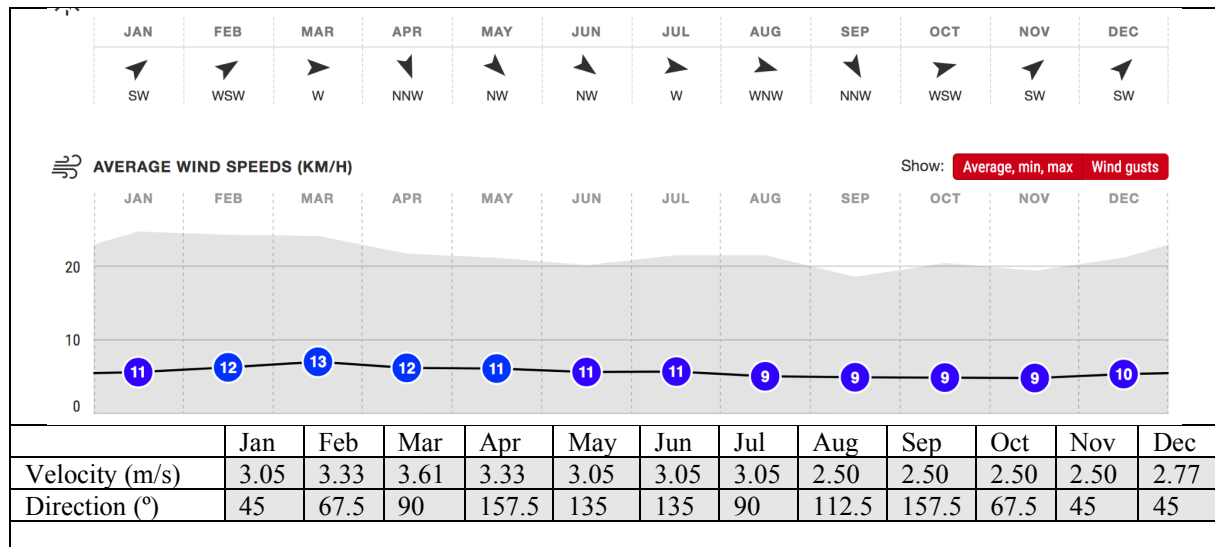


Fig. 4.11 Wind speed averages and directions – Assumption of a pure south as 0° - Stuttgart airport [46]

By integrating the provided convective heat transfer coefficients for walls and roofs in different angular variants defined as leeward and windward with the wind speed averages and directions in Stuttgart, Table 4.2 shows the determination of heat transfer coefficients based on the relative angle of the component to the wind.

Wind velocity (m/s)					
Configuration	2.50	2.78	3.06	3.33	3.61
Windward conditions - 0°	11	12	13	13.8	14.8
Windward conditions - ±45°	7.2	7.9	8.7	9.3	9.9
Leeward conditions - ±90°	9	9.9	10.5	11.3	12
Leeward conditions - ±135°	8.1	9	9.5	10.3	11
Leeward conditions - 180°	7	7.7	8.2	8.8	9.5
Roof	10.3	11.2	12	13.1	13.9

Tab. 4.2 Emerged convective heat transfer coefficients based on angle between component and wind regarding wind velocities – W/m².K

4.2.5 Sky emissivity

Emissivity of each component is the result of the interaction between surface temperature and the surrounding environment. To calculate sky temperature, we determine the sky emissivity using equation 4.10 [47].

$$Sky_{emissivity} = 0.787 + \left(0.767 \times \ln\left(\frac{T_{dewpoint}}{273}\right)\right) + 0.0224N - 0.0035N^2 + 0.00028N^3 \quad (4.10)$$

Where;

$T_{dewpoint}$ = The temperature to which the air would have to cool (at constant pressure and constant water vapor content) in order to reach saturation. In this work, dewpoint temperature is available by integrating weather data of Stuttgart with resolution of one hour.

N = Opaque sky cover (tenths), the expected amount of opaque clouds covering the sky valid for the indicated hour where N equals 0 for clear sky and 10 for overcast sky.

Determination of Opaque sky cover (N)

Figure 4.12, presents annual average cloud coverage in Stuttgart [48].

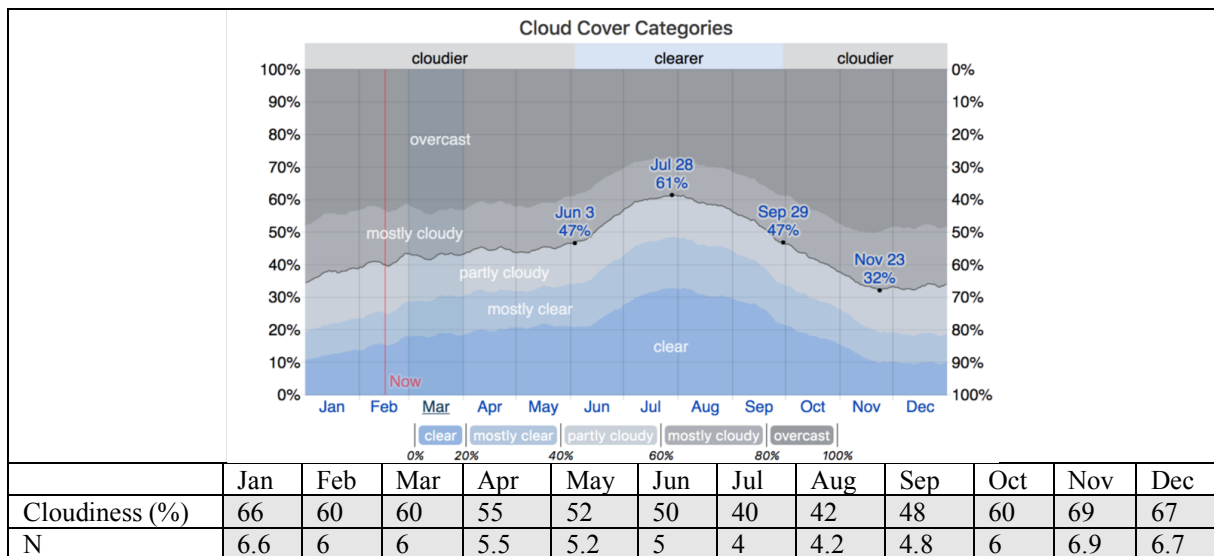


Fig. 4.12 Monthly cloud cover categories– Stuttgart [48], estimation of opaque sky cover coefficient

4.2.6 Sky temperature

The sky temperature at a specific location primarily depends on variables like altitude, dewpoint temperature, cloud cover, and the presence of airborne particles such as dust or pollution. To predict radiative losses from the building envelope components, we calculate this temperature using equation 4.11 [49].

$$T_{sky} = (\varepsilon_{sky})^{0.25} \times T \quad (4.11)$$

Where;

ε = Sky emissivity

T = Dry bulb temperature

4.3 Component emissivity

Regarding the assumption of emissivity for the components, previous research indicates an average value of 0.90 [50]. As the five main components in this study are a combination of opaque materials with semi-glazing coatings, we consider the emissivity of masonry materials with similar construction (see table 4.4) [50].

Material	Density kg/m ³	Conductivity W/(m·K)	Specific Heat Capacity J/(kg·K)	Emissivity -
ceramic tile	2300	1.3	700	0.92
concrete	2200	2.00	880	0.93
cork	400	0.07	1700	0.70
granite	2600	2.80	750	0.85
gypsum	850	0.40	840	0.90
limestone	2000	1.70	900	0.94
mortar	1900	1.30	930	0.90
solid brick	1800	0.45	920	0.88
stainless steel	7900	17.0	480	0.16
untreated wood	610	0.18	2000	0.85

Tab. 4.4 Average emissivity of masonry materials [50]

4.4 Sol-air temperature

Sol-air temperature is used to determine the rate of heat transfer through a surrounding component due to the combined effects of the actual outdoor temperature distribution, along with the incident solar radiation, which is influenced by both outside convection and emission. Sol-air temperature is calculated by integrating component absorptivity with its emissivity, taking into account sky temperature, wind velocity, irradiation, and the direct effect of dry-bulb temperature (see figure 4.13).

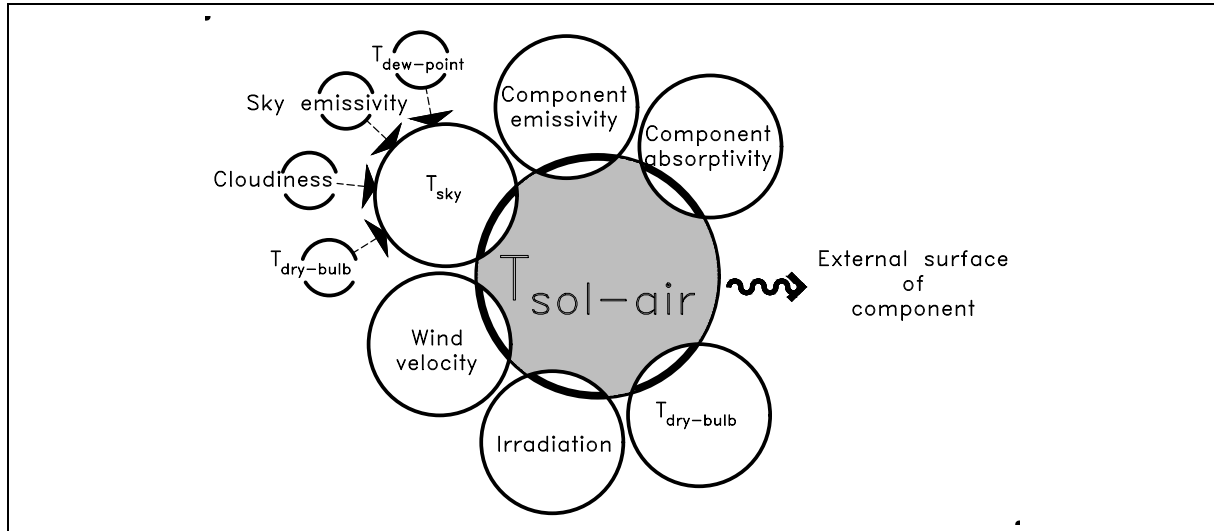


Fig. 4.13 Schematic of integrated parameters regarding outside emission, convection in parallel to component absorptivity and emissivity to perform sol-air temperature

In the upcoming heat transfer calculations, a combination of external weather parameters that define the outside boundary condition yields the 'sol-air temperature.' This temperature is then used in the main equation for heat transfer to determine the quantity and direction of heat flow. The accuracy of integrating sol-air temperature, as opposed to simply integrating dry-bulb temperature, arises from considering the effects of dew-point temperature, sky cloudiness, and sky temperature. Consequently, the simultaneous interaction of 'convection' and 'emission' is calculated and the result is integrated at the outside surface of the component. Sol-air temperature is calculated using equation 4.12 [51].

$$T_{Sol-air} = \left(T + \frac{a_s \cdot Q_{Sol}}{h_c} \right) - \left(\frac{\epsilon \cdot \sigma (T^4 - T_{Sky}^4)}{h_c} \right) \quad (4.12) *$$

Where;

T	Dry-bulb temperature
a _s	Solar absorptivity
Q _{Sol}	Cumulative solar irradiation
h _c	Outside convective heat transfer coefficient
ε	Emissivity of component
σ	Stefan–Boltzmann constant = 5670400 × 10 ⁻⁸ W/m ² K ⁴
T _{sky}	Sky temperature

4.5 Surface temperatures and heat flow

A steady-state heat transfer analysis is employed to determine temperature distribution and heat flow. This analysis can be conducted when the temperature at every point within the model, including the surfaces, remains constant over time. Once the sol-air temperature is determined, the outside surface temperature (T_{S-Out}) can be calculated using equation 4.13 [52].

$$T_{s-out} = \frac{h_o \cdot T_{sol-air} + \left(\frac{T_{in}}{\sum R_I} \right)}{\left(\frac{1}{\sum R_I} \right) + h_o} \quad (4.13)$$

* Accuracy and history of development of this equation is exclusively discussed in appendix 1

Integrating the 'outside surface temperature' and 'solar-air temperature' yields the inside surface temperature (T_{S-In}) as represented in equation 4.14 [52].

$$T_{S-in} = T_{S-out} + (h_o \cdot \Sigma R_{II} \cdot (T_{S-out} - T_{sol-air})) \quad (4.14)$$

Hence, heat transfer through a wall (q) is derived using equation 4.15 [52]





$$q = h_o \cdot (T_{sol-air} - T_{S-out}) = \frac{T_{S-out} - T_{in}}{\Sigma R_I} = \frac{T_{S-out} - T_{S-in}}{\Sigma R_{II}} \quad (4.15)$$

Where;

- T_{S-out} outside surface temperature
- h_o convective heat transfer coefficient
- $T_{sol-air}$ sol-air temperature
- T_{in} inside ambient temperature
- ΣR_I thermal resistance of the wall excluding outside air film resistance
- T_{S-in} inside surface temperature
- ΣR_{II} thermal resistance of the wall excluding inside and outside air film resistances
- q heat transfer

4.6 Value of heat flow

The heat transfer index quantifies both the quantity and direction of heat flow through the component assembly. To determine the component's heating and cooling demands, we consider the heat flow in different boundary conditions based on the temperature differences between the inside and outside ambient temperatures. This information is summarized in table 4.5.

Direction of heat flow Air temperature difference	From "inside" into "outside"	From "outside" into "inside"	Heating demand $\tau \cdot \text{air out} < \tau \cdot \text{air in}$ 	Heating auxiliary $\tau \cdot \text{air out} < \tau \cdot \text{air in}$ 
	$T_{out} < T_{in}$	Heating demand	Heating auxiliary	
			Cooling auxiliary $\tau \cdot \text{air out} > \tau \cdot \text{air in}$ 	Cooling demand $\tau \cdot \text{air out} > \tau \cdot \text{air in}$ 
$T_{out} > T_{in}$	Cooling auxiliary	Cooling demand		

Tab. 4.5 Defining values for heat flow considering different boundary conditions

4.6.1 Heating demand

This value is applicable when a component is losing heat as long as the outside air temperature is lower than the inside air temperature set-point for comfort. Indeed, as long as the outside air temperature remains lower than the inside temperature set-point in the absence of irradiation, the building's envelope components continue to lose heat. Each component that

transfers heat flow toward the outside contributes to an increased heating demand for the building. This condition persists even when irradiation is present during the day, as the percentage of the entire building receiving irradiance is much smaller than the components that do not receive irradiation.

4.6.2 Cooling demand

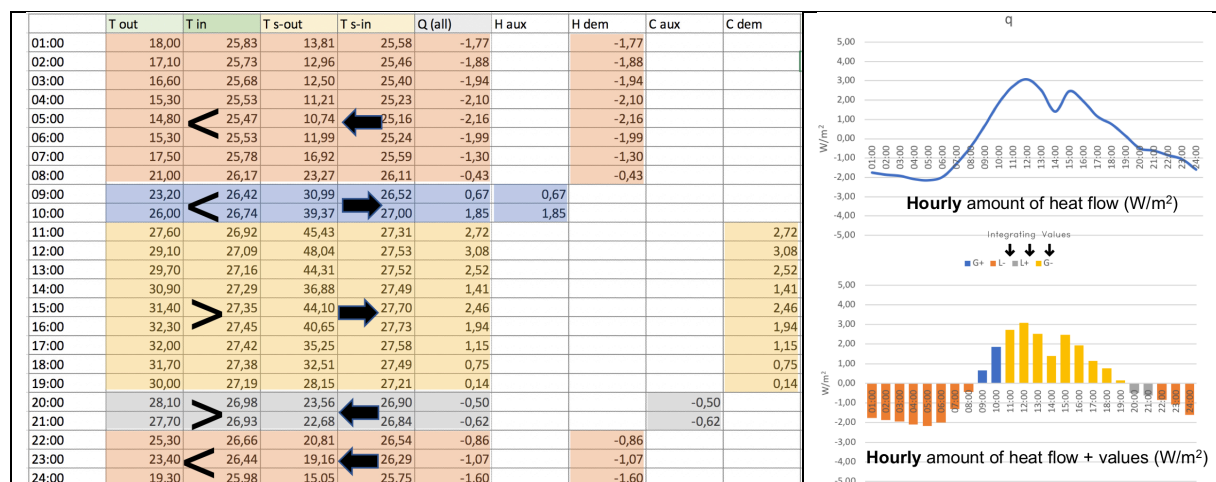
This value is applicable in situations where a component is gaining heat as long as the outside air temperature is higher than the inside air temperature set-point for comfort. Indeed, as long as the outside air temperature remains higher than the inside temperature set-point, the building's envelope components continue to gain heat. Each component that transfers heat flow toward the inside contributes to an increased cooling demand for the building.

4.6.3 Heating auxiliary

This value is applied in situations where a component is gaining heat as long as the outside air temperature is lower than the inside air temperature set-point for comfort. Indeed, as long as the outside air temperature remains lower than the inside temperature set-point, any amount of heat gained by a component can offset the heating demand resulting from other segments of the component integrated on the same facade. This heat gain does not increase cooling demand because, through natural ventilation of windows, any excess heat can be dissipated, as long as the outside air temperature is lower than the inside temperature set-point.

4.6.4 Cooling auxiliary

This value is applied in situations where a component is losing heat as long as the outside air temperature is higher than the inside air temperature set-point for comfort. Indeed, as long as the outside air temperature remains higher than the inside temperature set-point, any amount of heat loss by a component can offset the cooling demand resulting from other segments of the component integrated on the same facade. Table 4.6 represents a matrix of heat flow directions for different boundary condition variants and defines the values of heat flows (as an example).



Tab. 4.6 Values of heat flow considering direction of heat flow and boundary conditions (left), transformation of heat flow curve to indicating heating/cooling demand + heating/cooling auxiliary (right)

4.6.5 Energy demand of combination of components

In each facade combination of opaque, transparent, or components holding PVs that produce electricity, different combinations of heating and cooling demands and/or auxiliaries emerge. Considering the interaction of thermal performance of each component at separate intervals will define a more accurate level of demand. For instance, during winter with low irradiation and colder outside air compared to inside air, a facade of the building composed of windows and walls is simultaneously influenced by the performance of its opaque and transparent components. Due to high irradiation transmittance through windows, there are intervals where cumulative heat transfer in windows occurs in the opposite direction of heat flows transferring through walls by conduction. Therefore, portions of the heating demand of walls, calculated over the same time intervals, can be compensated by auxiliary heating from the windows. As a result, the cumulative heating demand of each facade, integrating different types of components, will consider parts of heat flows that act as auxiliary segments to compensate for the demand of the entire facade. Figure 4.14 illustrates this configuration.

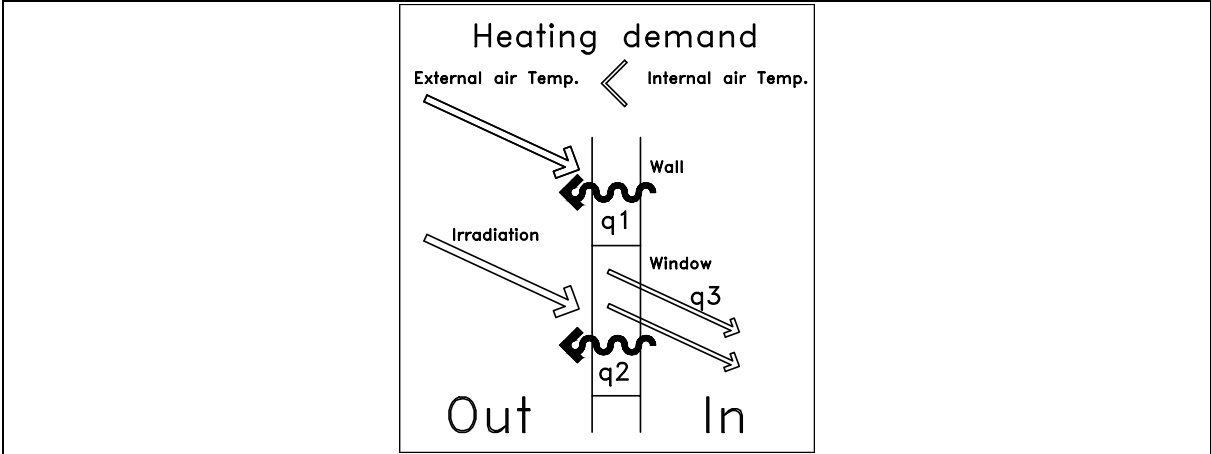


Fig. 4.14 Influencing of heating demand of wall by heating auxiliary of window integrated in the same facade

In the configuration shown in Figure 4.14, when integrating an opaque and transparent component in one facade, the simplification of cumulative heat flow is determined based on correlation 4.16.

$$\text{Cumulative heat flow} = q_1 + q_2 - q_3 \quad (4.16)$$

Where;

- q₁ Heat flow of wall - Conduction
- q₂ Heat flow of window - Conduction
- q₃ Transmitted irradiation through window - Transmission

In the upcoming calculations for transparent components, the cumulative interaction of heat flow through conduction and the amount of transmitted irradiation through transmission indicate the final heat flow of the transparent component.

4.7 Dividing effect of convection and emission

As sol-air temperature has been used as the cumulative integration of irradiation, convection, and emission, the heat flow into an outside surface of a building subjected to solar radiation can be expressed as correlation 4.17 [52].

$$q = \alpha I + h_o(T_{out} - T_{s-out}) - \epsilon \Delta R \quad (4.17)$$

Where;

q	heat flow
h_o	convective heat transfer coefficient
T_{out}	outside dry bulb temperature
T_{s-out}	outside surface temperature
$\epsilon \Delta R$	radiation exchange with the sky and the surrounding surfaces
α	absorptance
I	solar radiation

So, when considering the outside surface of an opaque component, the amount of heat flow (q) is determined by subtracting irradiation (αI) from convection ($h_o(T_{out} - T_{s-out})$) and emission ($\epsilon \Delta R$). Direction of convection is determined based on these two possible configurations.

1. $T_{out} > T_{s-out} \rightarrow$ Convection is positive (heat gain through convection)
2. $T_{out} < T_{s-out} \rightarrow$ Convection is negative (heat loss through convection)

For the determination of the contribution of convection and emission in transparent components, the principle of calculation is the same. However, a certain quantity of irradiation also passes through the component and will be deducted from the total amount of irradiation. The coefficient α , representing the absorptance of the transparent component, will be derived from the transmittance, absorption, and reflection proportions of irradiation, which have already been estimated (Figure 4.15).

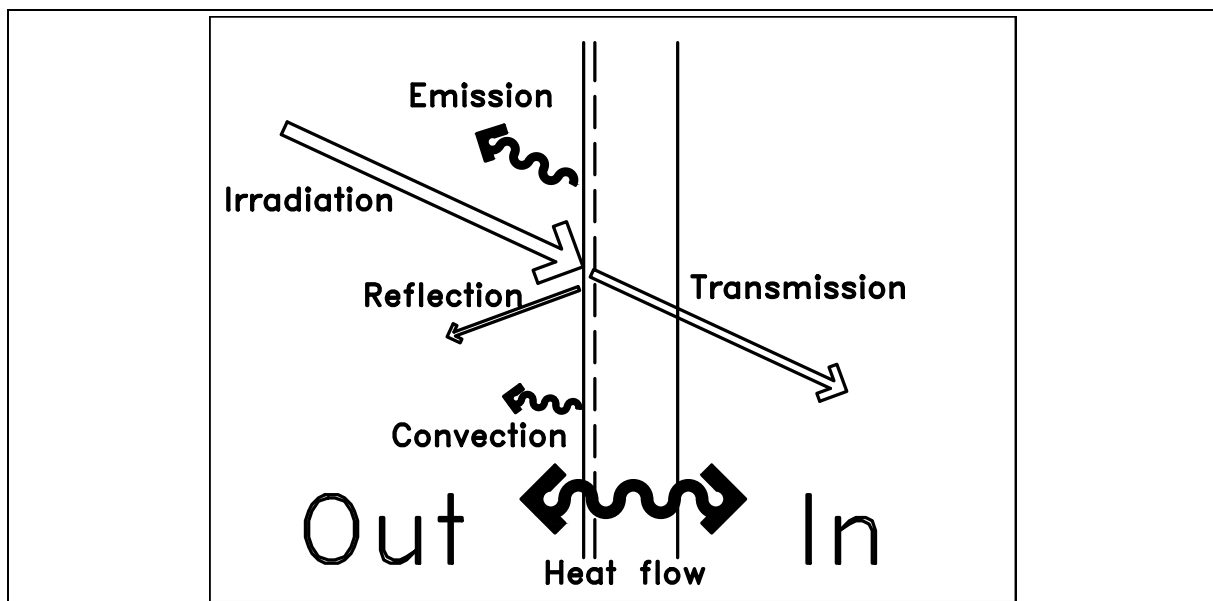


Fig. 4.15 Interaction of main phenomena to perform quantity and direction of heat flow

In a transparent component, the transmission of irradiation can be derived from equation 4.17 [52] and expressed as equation 4.18, taking into account the portion of irradiation that is transmitted.

$$q = \alpha I + h_o(T_{out} - T_{s-out}) - \varepsilon \Delta R - q_{tr} \quad (4.18)$$

Where;

q_{tr} transmitted irradiation through transmission

4.7.1 Net radiation loss

Determining $\varepsilon \Delta R$, which represents the net radiation loss from the outer surfaces of bodies exposed to the sky, can be approximated using the equation [53]:

$$q_{rad} = \varepsilon \sigma (T_{s-out}^4 - \varepsilon_{sky} T_{out}^4) \quad (4.19)$$

Where;

q_{rad} emission from the outer surface of component
 ε emissivity of component
 σ Stefan-Boltzmann constant
 T_{s-out} outside surface temperature
 ε_{sky} emissivity of sky
 T_{out} outside dry bulb temperature

4.8 Geometrical configuration

The geometrical configuration of all five components is primarily based on various possible orientations and inclinations. To account for all faces of a building, we have considered key angular orientations. The main orientations considered are the four primary geographical directions, along with intermediate angles at 30° intervals. For inclinations, we have chosen four main angles: 90°, 60°, 30°, and 0°. A 90° inclination represents a vertical component, commonly used for integrating walls and windows. The 60° inclination can serve as either inclined walls or the top floor of a building. In Germany and European countries, there's a tradition of integrating these roofs as they provide usable space beneath an inclined wall. The 30° inclination represents an inclined roof, which is often used for mounting PV applications with various orientations. Finally, the 0° inclination represents a flat roof. We have examined twelve orientations with angular differences of 30° to account for possible component directions.

In Figure 4.16, the primary and secondary angles of orientations and inclinations are depicted.

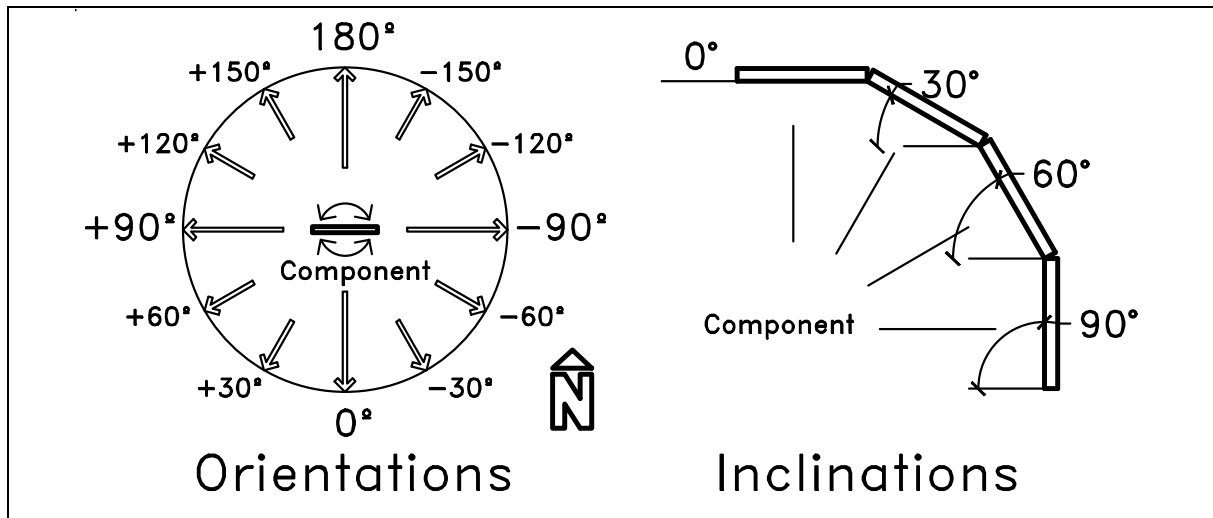


Fig. 4.16 Orientations and inclinations applied to component

The combination of orientations and inclinations results in a three-dimensional geometry representing various configurations for a component. Intermediate geometrical configurations are not considered in the final comparisons, but the developed method allows for the calculation of each favored configuration using the same procedure. Figure 4.17 illustrates the algorithm for three-dimensional geometry and possible configurations.

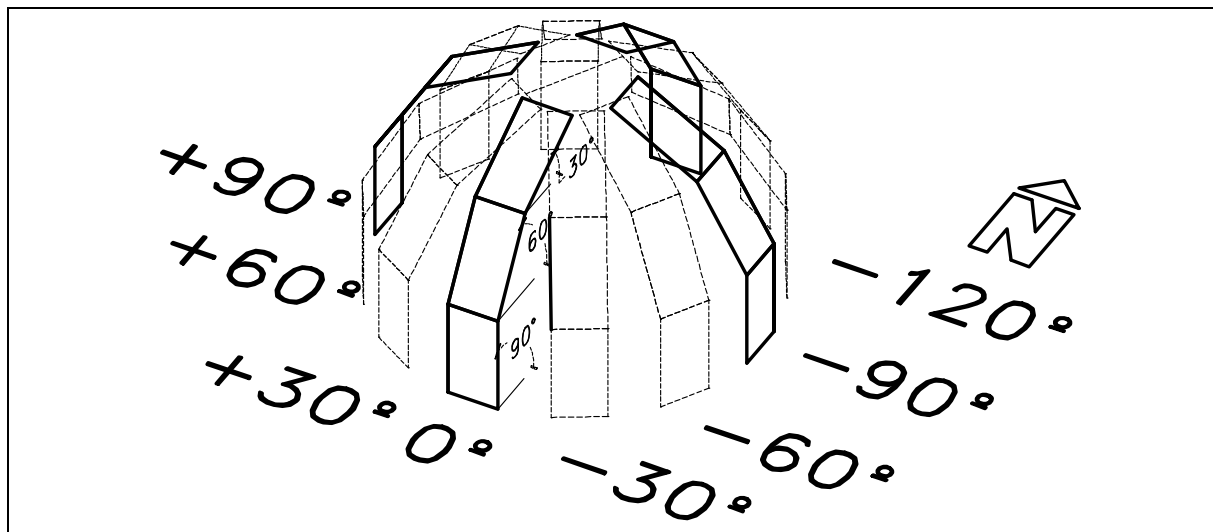


Fig. 4.17 Three-dimensional geometry representing possible configurations of defined orientations and inclinations

4.9 Components

The five applicable components in this work include opaque components, transparent components, BIPV (Building-Integrated Photovoltaics), BAPV (Building-Attached Photovoltaics), and PV glazing. The individual physical characteristics and the procedure for deriving the thermal performance of each component have been explained.

4.9.1 Opaque component

4.9.1.1 Physical characteristics

The thermal conductivity of the assembly of an opaque component, which is an effective characteristic, has been considered in terms of the U-value index. The U-value represents the rate of heat transfer through a structure, divided by the temperature difference across that structure. It primarily determines the insulation properties of materials and their resistance to heat transfer through conduction. To calculate this, the average U-value of integrated materials in the opaque components of 35 pilot zero-energy buildings from the ZUKUNFT-BAU program has been used. Figure 4.18 illustrates the estimated average U-value of walls in these constructed pilot projects [54].

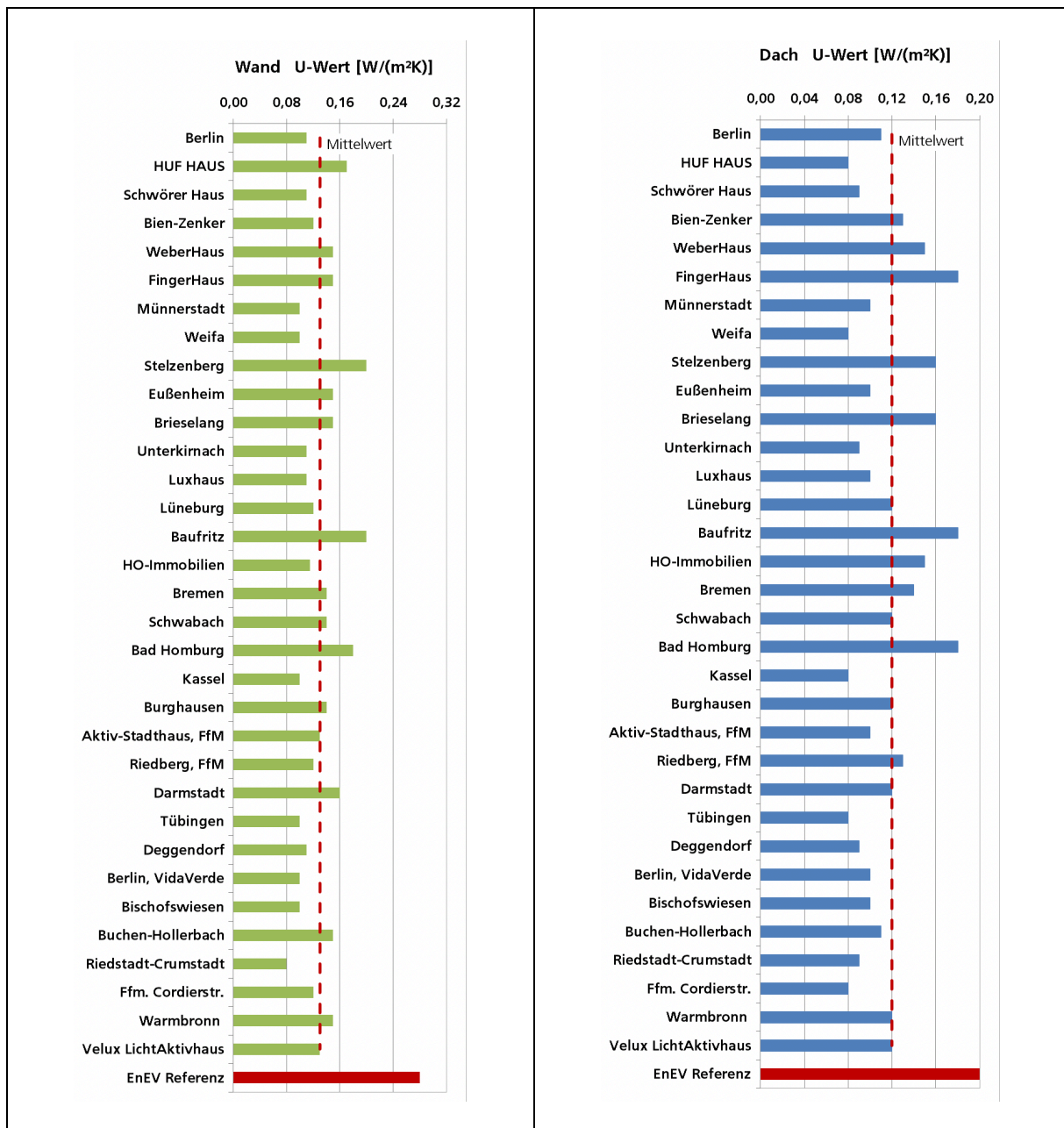


Fig. 4.18 U-value of the wall (left) and roof (right) in construction of the demonstration project in the Efficiency House Plus Standard [54]

The graph shows that for wall construction, the minimum U-value is 0.10 W/m²K, and a maximum of 0.20 W/m²K has been recorded, with an average of 0.13 W/m²K [54]. As for the roof, the right graph indicates a minimum U-value of 0.08 W/m²K, a maximum of 0.18 W/m²K, and an average of 0.12 W/m²K.

In the final demonstrated sample building, the exact U-values of the sample building are used in calculations to indicate deviations in heating and cooling demands.

4.9.1.2 Conduction heat transfer coefficient

Conduction heat transfer is the process of heat flow through a solid material. It depends on several factors, including the thickness (m) of each material and its thermal conductivity (λ). Conduction heat transfer is inversely proportional to the conduction heat transfer coefficient (1/R), which is a key factor used to represent the U-value [55].

$$R = \sum_1^N \left(\frac{d_i}{\lambda_i} \right) \quad (4.20)$$

$$U = \frac{1}{R} \quad (4.21)$$

Where;

- R Thermal resistance of material
- d Thickness of material
- λ Heat conductivity
- U U-value

As a result, in a uniform construction of a component, the conduction heat transfer coefficient is calculated as a correlation between the material thickness (d) and its thermal conductivity (λ). Equation 4.22 is used to calculate the U-value of a uniform wall [55].

$$U = \frac{\lambda_{Uniform\ wall}}{d_{Uniform\ wall}} \quad (4.22)$$

Construction of opaque components involves various U-values derived from either a uniform wall consisting of one material or a complex combination of different materials with varying thermal conductivities. Table 4.7 simplifies these integrated materials. The equal mathematical distance between each material to the next (which is four times greater) provides a fixed proportion for comparing different heat flows of walls with the same thickness but different thermal conductivities.

	Thermal conductivity	Representing assortment of material
Material 01	0.03	Polyurethane foam
Material 02	0.12	Wood
Material 03	0.48	Brick
Material 04	1.92	Sand stone

Tab. 4.7 Thermal conductivity of representative materials with harmonized mathematical ratio

4.9.1.3 Heat transfer algorithm

The flowchart presented in Figure 4.19 illustrates the procedure for integrating inside and outside boundary conditions to determine heat flow through opaque and transparent components. The quasi-static heat transfer principle implies that the heat flow at each interval of calculation between each two nodes of temperature remains the same. Therefore, determining the heat flow between nodes of $T_{\text{sol-air}}$, $T_{\text{s-out}}$, $T_{\text{s-in}}$, and T_{in} results in the same amount.

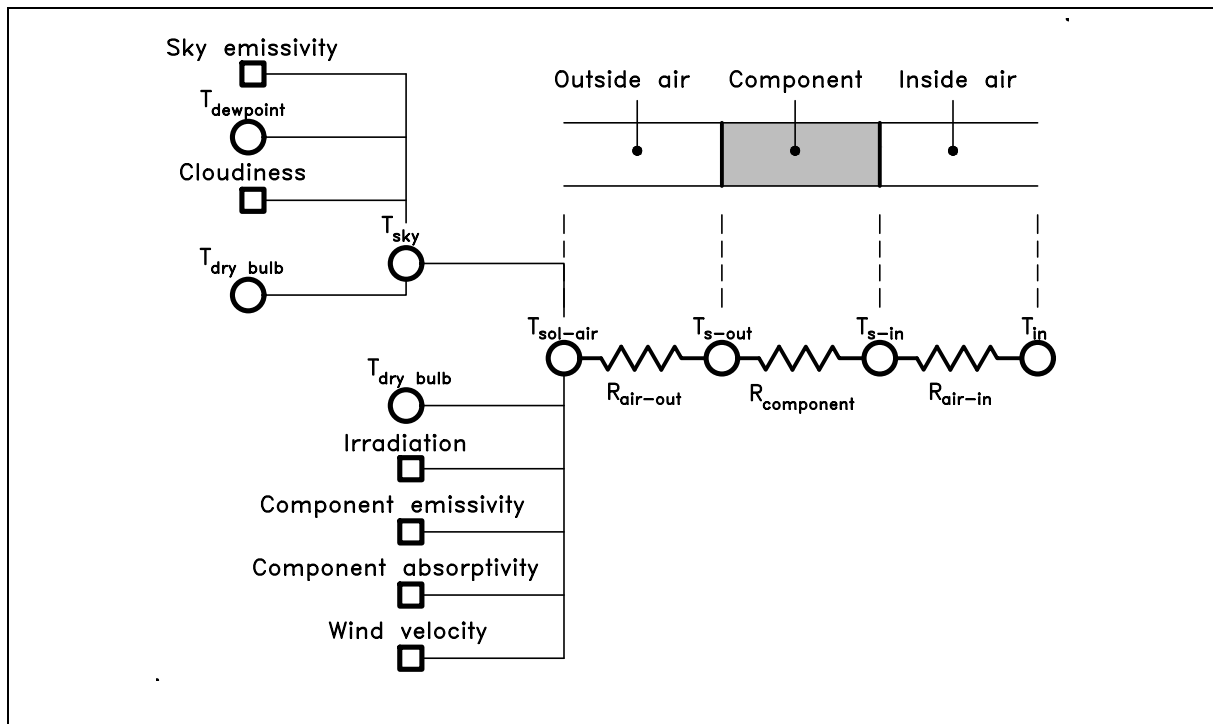


Fig. 4.19 Heat transfer resistances in opaque and transparent component consisting from a uniform material

4.9.2 Transparent component

4.9.2.1 Physical characteristics

Similar to opaque components, the thermal conductivity of windows, which is a parameter of transparent materials determining their U-value, is taken into account. Additionally, the U-value can be assumed to be a constant value under normal temperature conditions of boundary conditions. Therefore, assuming that the thickness of windows in two-glazing or three-glazing layers is fixed and is a combination of different layers, the assumption of U-value can be made based on the standards of German norms (table 4.8) [45].

		U_g	$\tau_{e,Licht}$	$\tau_{e,R}$	g	ε			
Bestand	Verglasung	1-fach	5,8	0,90	0,85	0,87	3,1	unbeschichtet ⁽¹⁾	
		2-fach	2,8	0,81	0,72	0,75	2,3		
		3-fach	2,0	0,72	0,64	0,67	2,0		
		4-fach	1,5	0,63	0,55	0,60	2,0		
Bestand	Profilbauglas	1-fach	5,8	0,80	0,80	0,82	3,0		
		2-fach	2,8	0,71	0,67	0,70	2,0		
Bestand	Verglasung	2-fach	1,9	0,80	0,67	0,71	2,5		beschichtet ⁽²⁾
		2-fach	1,7	0,80	0,64	0,69	2,5		
		2-fach	1,5	0,80	0,61	0,67	2,5		
		2-fach	1,3	0,80	0,58	0,65	2,5		
Neubau und Sanierung	Verglasung	2-fach	1,1	0,80	0,55	0,65	2,5		beschichtet ⁽³⁾
		2-fach	1,1	0,70	0,40	0,50	2,5		
		2-fach	1,1	0,60	0,30	0,35	3,0		
		2-fach	1,1	0,50	0,20	0,25	3,0		
		3-fach	0,7	0,70	0,45	0,50	1,5		
		3-fach	0,5	0,70	0,45	0,50	1,5		
	Profilbauglas	3-fach	0,7	0,50	0,20	0,25	2,0		
		3-fach	0,5	0,50	0,20	0,25	2,0		
		2-fach	1,1	0,70	0,50	0,60	2,0		
		2-fach	1,1	0,50	0,25	0,30	2,0		

Tab. 4.8 Default values for different types of glass in accordance with ÖNORM B 8110-3 [45]

The derivation of U_g as the "U-value" of windows and ε as the "coefficient that determines the reduction in radiation transmittance as a function of the type of glass used" has been done based on table 4.8, which represents standard thermal and optical parameters of integrated windows. Additionally, the average thermal properties of integrated windows in the investigated pilot projects, as measured by "ZUKUNFT-BAU," have been considered. Figure 4.20 shows the estimation of the average U-value in windows in constructed pilot projects [54].

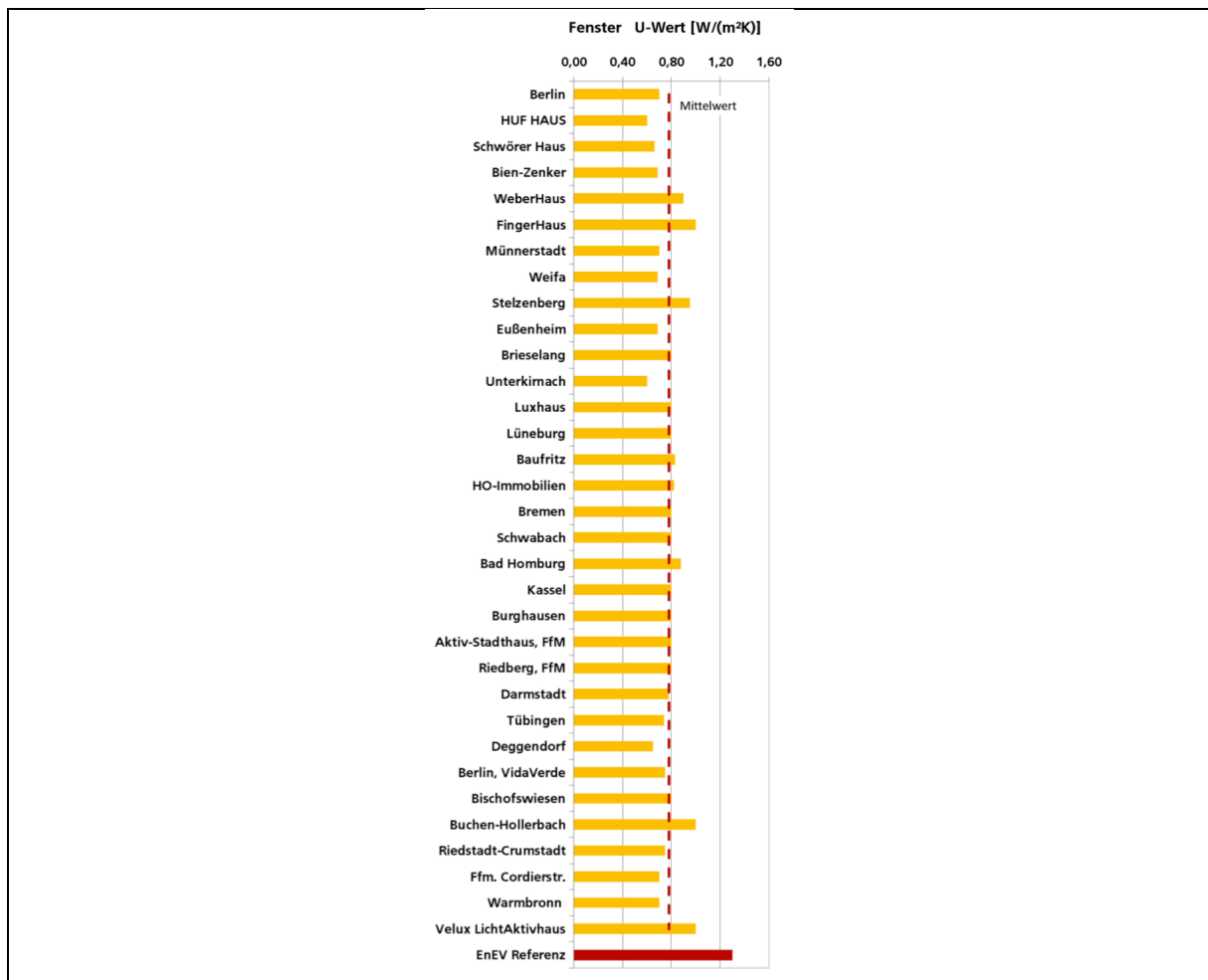


Fig. 4.20 U-value of window of the demonstration projects in the Efficiency House Plus Standard [54]

Figure 4.20 shows that U-values in these pilot projects range between a minimum of 0.60 W/m²K and a maximum of 1.00 W/m²K. The average U-value of windows in these projects is 0.78 W/m²K [54].

4.9.3 BIPV (building integrated photovoltaic system)

As defined, BIPV integration refers to a configuration in which photovoltaic materials are used to replace conventional building materials in a building's envelope. For this reason, the thermal behavior of this configuration, in terms of its heat flow, differs from mounting PVs on the surface of the building with a certain distance from the building's façade.

4.9.3.1 Physical characteristics

Material properties of constructional layers of BIPV has been introduced by Misara (2014) [55]. Table 4.9 describes parameters of material used in a BIPV module that is employed in this work as well.

Material used	Density ρ_m (kg/m ³)	Conductivity λ (W/mK)	heat capacity C_m (J/kgK)	Thickness d_m (mm.)
Frontside				
Front glass	2500	0.76 - 1.00	500	3.000
TiO ₂	2400	7.1	691	0.075
EVA-Foil	960	0.35	2090	0.380
PV Cell	2330	148	677	0.200
Backside				
EVA-Foil	960	0.35	2090	0.380
Backsheet	1200	0.20	1250	0.760
Gypsum	2400	0.21	1.09	10.000
Isofloc	40-60	0.045	2150	75.000
Styrodur	33	0.033	1500	50.000
Air	1.184	0.02587	1.006	16.000
Argon	1.784	0.01172	0.5203	16.000

Tab. 4.9 Material properties of constructional layer in BIPV configuration [55]

4.9.3.2 Heat transfer algorithm

The flowchart in Figure 4.21 illustrates the procedure for integrating boundary conditions to determine heat flow through a BIPV module. Similar to opaque and transparent components, the principles of quasi-static heat transfer imply that the heat flow remains consistent at each interval of calculation between two temperature nodes. Consequently, the heat flow between the outermost node, which integrates with $T_{sol-air}$, and the innermost node, which determines T_{in} , remains constant. In most standard PV-modules, the temperature difference between the cell and surface is considered negligible due to the extremely low thickness of the PV cell. Therefore, T_{1PV} and T_{2PV} , representing the outside and inside surface

temperatures of the PV module, respectively, are assumed to be the same. The very low thermal resistance of the PV is included in the calculation of heat flow for the overall component assembly using Equation 4.15.

Both $\sum R_I$ (referring to the thermal resistance of the wall excluding the outside air film resistance) and $\sum R_{II}$ (referring to the thermal resistance of the wall excluding inside and outside air film resistances) incorporate the PV modules as an integral part of the assembly. Given the multi-layered configuration of a BIPV module, the conduction heat transfer coefficient becomes a crucial parameter in determining surface temperatures, which in turn influence various thermal dissipations (as depicted in Figure 4.21).

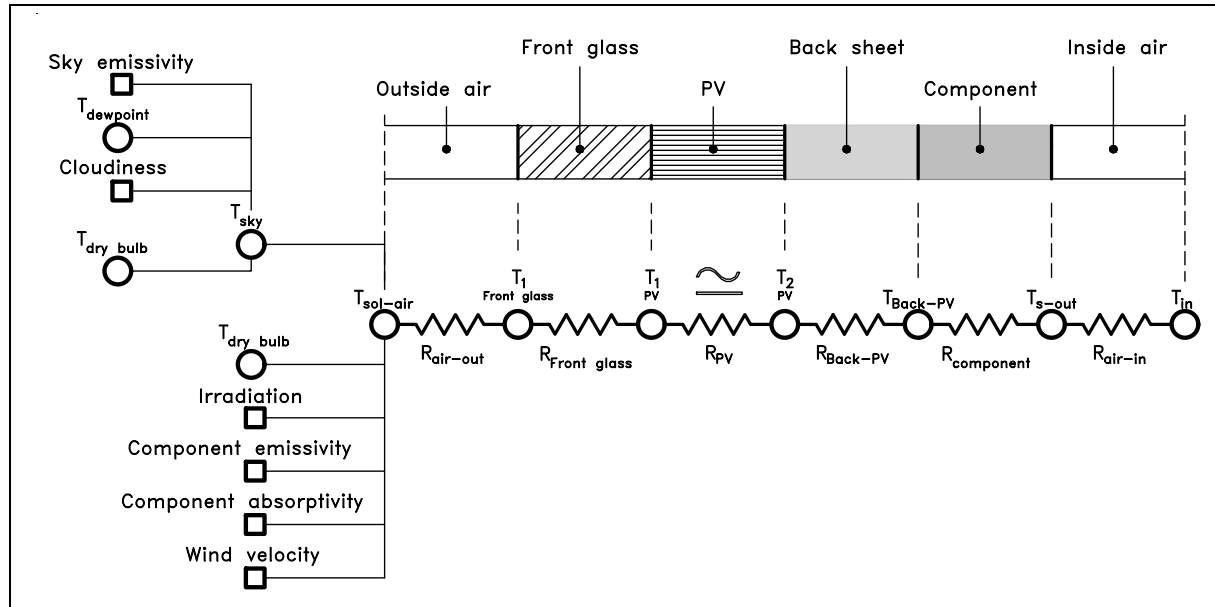


Fig. 4.21 Heat transfer resistances in BIPV module consisting from frontside, PV, backside and uniform material (opaque component)

4.9.4 BAPV (building-applied photovoltaics)

The term "BAPV" refers to photovoltaic systems that are retrofitted or integrated into existing buildings. Many of the building-integrated solar installations in use today are actually of the BAPV configuration. While some manufacturers distinguish between new construction of BIPV (Building-Integrated Photovoltaics) and BAPV, they often use the same types and assembly of materials, typically consisting of a transparent glass front layer and a PV module. In the case of BAPV, the backside construction does not include insulation, and the additional distance between the PV module and the building provides back-cooling effects. This configuration results in lower surface temperatures for the modules, potentially leading to higher electricity generation compared to BIPV configurations with the same efficiency rates.

4.9.4.1 Physical characteristics

In order to facilitate a fair comparison of the performance between BAPV and BIPV, the same "front side" and "PV" integration used in BIPVs have also been incorporated into the BAPV construction. When it comes to the backside of BAPV panels, the first two layers used in BIPV, namely "EVA-Foil" and "Back-sheet," have been employed in the construction of the BAPV backside. Table 4.10 outlines the common layers in the construction of these two configurations, BIPV and BAPV [55].

	Material used	Density ρ_m (kg/m ³)	Conductivity λ (W/mK)	heat capacity C_m (J/kgK)	Thickness d_m (mm.)
↑ BIPV	Frontside				
	Front glass	2500	0.76 - 1.00	500	3.000
	TiO ₂	2400	7.1	691	0.075
↑ BAPV	EVA-Foil	960	0.35	2090	0.380
	PV Cell	2330	148	677	0.200
↓ BIPV	Backside				
	EVA-Foil	960	0.35	2090	0.380
	Backsheet	1200	0.20	1250	0.760
	Gypsum	2400	0.21	1.09	10.000
	Isofloc	40-60	0.045	2150	75.000
	Styrodur	33	0.033	1500	50.000
	Air	1.184	0.02587	1.006	16.000
Argon	1.784	0.01172	0.5203	16.000	

Tab. 4.10 Material properties of constructional layers in BIPV and BAPV – Common construction in “frontside”, “PV Cell” and different construction in “Backside” [55]

4.9.4.2 Thermal resistance

When determining the temperatures of nodes in the BAPV configuration, it's essential to consider that the thermal resistances, denoted as $\sum R_I$ (referring to "Thermal resistance of the wall excluding outside air film resistance") and $\sum R_{II}$ (referring to "thermal resistance of the wall excluding inside and outside air film resistances"), differ from those in the BIPV configuration. In this context, the thermal resistances in the BAPV are lower compared to those in the BIPV due to variations in the constructional layers between the two configurations. Specifically, by eliminating the last five layers present in BIPV and integrating them into BAPV, the thermal resistance of BAPV becomes lower than that of BIPV (Table 4.11).

Thermal resistance	
BIPV	$R_{BIPV} = R_{Frontside} + R_{PV} + R_{Backside} = R = \sum_1^N \left(\frac{d_i}{\lambda_i} \right)$ $\frac{0.003}{0.88} + \frac{0.000075}{7.10} + \frac{0.00038}{0.35} + \frac{0.0002}{148} + \frac{0.00038}{0.35} + \frac{0.00076}{0.20} + \frac{0.01}{0.21} + \frac{0.075}{0.045} + \frac{0.05}{0.033} + \frac{0.016}{0.025} + \frac{0.016}{0.011} = 5.22$
BAPV	$R_{BAPV} = R_{Frontside} + R_{PV} + R_{(part\ of)\ Backside} = R = \sum_1^N \left(\frac{d_i}{\lambda_i} \right)$ $\frac{0.003}{0.88} + \frac{0.000075}{7.10} + \frac{0.00038}{0.35} + \frac{0.0002}{148} + \frac{0.00038}{0.35} + \frac{0.00076}{0.20} = 0.01$

Tab. 4.11 Calculation of thermal resistance in BIPV and BAPV (m².K/W)

4.9.4.3 Heat transfer algorithm

The flowchart depicted in Figure 4.22 illustrates the procedure for integrating boundary conditions to determine heat flow through a BAPV module. Much like BIPV components, the fundamentals of quasi-static heat transfer imply that the heat flow remains constant at each interval of calculation between two temperature nodes.

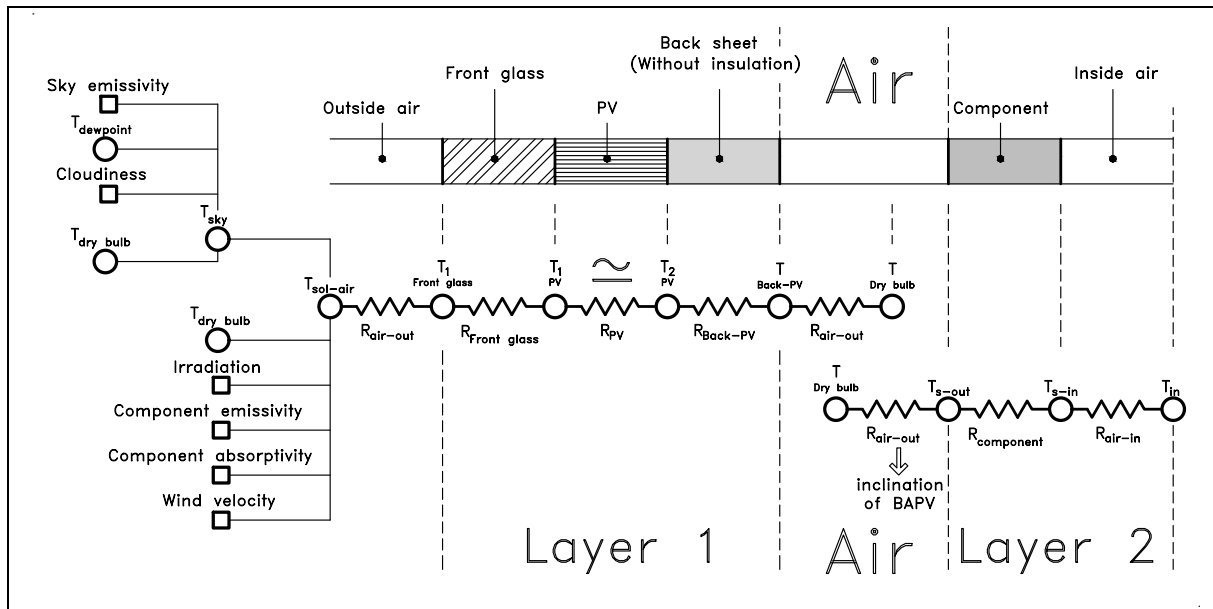


Fig. 4.22 Heat transfer resistances in BAPV module consisting from layer-01; frontside, PV, backside and layer-02; uniform material (opaque component)

4.9.5 PV glazing

The term "PV glazing" refers to a recent technology where a transparent component, such as the glass of a window, incorporates transparent semiconductor-based photovoltaic cells. These cells are typically sandwiched between two sheets of glass. Another definition of transparency in this context considers the percentage of the window area that contains photovoltaic material. In this study, we have considered encapsulating opaque particles of PV modules.

For our analysis, we have applied an additional material assembly to the external side of a "three-glazing window," which is used as the "transparent component" in this work. This assembly consists of 'front glass + PV + back glass,' resulting in an entire component that represents a three-glazing window with encapsulated PV between two glass layers on its external side. While PV glazing may have lower efficiency rates compared to PVs in BIPVs and BAPVs, for the purpose of comparing energy performance with the other two configurations, we have assumed the same efficiency of PV modules. By setting the efficiency rate of the three main components (BIPV, BAPV, and PV glazing), we can conduct a more precise parametric analysis. Comparing the performance of PV glazing with the other four components is important because this configuration serves as an intermediary between "opaque and transparent" components and offers the flexibility to adjust the "efficiency-transparency" level by defining the "area percentage" of encapsulated PV modules.

4.9.5.1 Thermal resistance

In the determination of temperatures at nodes in a PV glazing configuration, thermal resistance of $\sum R_I$ is calculated for the component, excluding the outside air film resistance. Additionally, thermal resistance of $\sum R_{II}$ is calculated for the wall, excluding both inside and outside air film resistances. These calculations are performed separately for parts of the component with and without PV modules. Considering the negligible thickness of the encapsulated PV modules (0.2 mm) and their thermal conductivity (148 W/m.K), a very low thermal resistance value of 0.000001 m²·K/W is applied during assembly. Consequently, the effective thermal resistance of the assembly, whether with or without PV modules, will be nearly the same (as shown in Table 4.12).

In parts with PV;

$$\begin{aligned}\sum R_I &= R_{Front\ glass} + R_{PV} + R_{Back\ glass} + R_{Window} + R_{internal\ air} \\ \sum R_{II} &= R_{Front\ glass} + R_{PV} + R_{Back\ glass} + R_{Window}\end{aligned}$$

And in parts without PV;

$$\begin{aligned}\sum R_I &= R_{Front\ glass} + R_{Back\ glass} + R_{Window} + R_{internal\ air} \\ \sum R_{II} &= R_{Front\ glass} + R_{Back\ glass} + R_{Window}\end{aligned}$$

By integration equation 4.20;

The R_{Window} value has been calculated based on an assumed U-value of the integrated window, which is 0.50 W/m²·K.

$$\begin{aligned}R_{window} &= \frac{1}{U_{window}} = \frac{1}{0.50} = 2.00\text{ m}^2\cdot\text{K/W} \\ R_{internal\ air} &= \frac{1}{h_{internal\ air}} = \frac{1}{7.00} = 0.14\text{ m}^2\cdot\text{K/W}\end{aligned}$$

	Thermal resistance
With PV and without PV	$\sum R_I = R_{Front\ glass} + R_{PV} + R_{Back\ glass} + R_{Window} + R_{internal\ air} =$
	$\frac{0.003}{0.88} + \frac{0.000075}{7.10} + \frac{0.00038}{0.35} + \frac{0.0002}{148} + \frac{0.00038}{0.35} + 2.00 + 0.14 = 2.15$
	$2.15 - 0.000001 \cong 2.15$
	$\sum R_{II} = R_{Front\ glass} + R_{PV} + R_{Back\ glass} + R_{Window} =$
	$\frac{0.003}{0.88} + \frac{0.000075}{7.10} + \frac{0.00038}{0.35} + \frac{0.0002}{148} + \frac{0.00038}{0.35} + 2.00 = 2.01$
	$2.01 - 0.000001 \cong 2.01$

Tab. 4.12 $\sum R_I$ and $\sum R_{II}$ for assembly of PV glazing with and without PVs (m²·K/W)

4.9.5.2 Heat transfer algorithm

The flowchart represented in Figure 4.23 shows the procedure for integrating boundary conditions to determine heat flow through PV glazing. The basics of quasi-static heat transfer are applied to calculate heat transfer. Since PV glazing consists of parts of the assembly, both with and without PV, calculations have been performed for both main configurations.

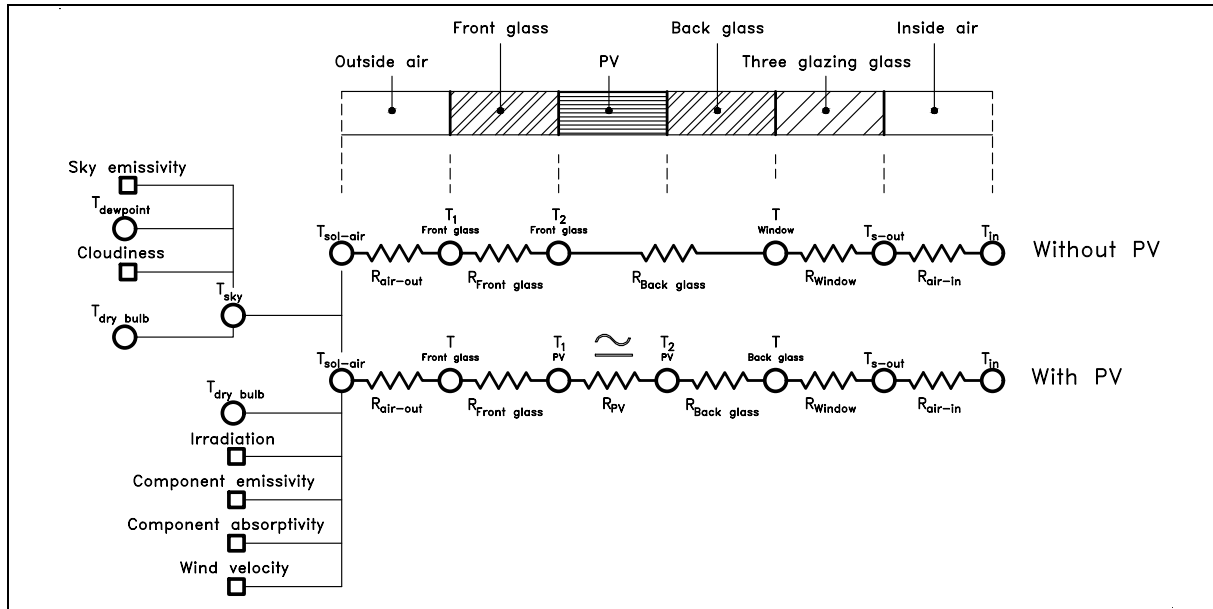


Fig. 4.23 Heat transfer resistances in PV glazing – Two configurations with and without encapsulated PV module

4.9.5.3 Surface temperatures and heat flow

To calculate surface temperatures and heat flow for a combination of a certain proportion of 'parts with PV' and 'parts without PV,' percentage ratios such as 'percentage of PV area' and 'percentage of transparent area' have been defined and applied. Assuming a PV module is an opaque component, transmission in PV glazing is applied only in areas of the 'transparent assembly' that integrate PVs. The final outside and inside surface temperatures of the combination represent different temperatures and are shown as 'Multi-temperatures' in the final results. To calculate the final heat flow for the combination and assess the level of heating demand, cooling demand, heating auxiliary, and cooling auxiliary, 'percentage of PV area' and 'percentage of transparent area' have been applied as follows:

$$N_{with PV} + N_{without PV} = 1 \quad (\text{Constant condition}) \quad (4.23)$$

$$Q_{combination} = (N_{with PV} \times q_{with PV}) + (N_{without PV} \times q_{without PV}) \quad (4.24)$$

Where;

$N_{with PV}$	Percentage of module in parts with encapsulated PV
$q_{with PV}$	Heat flow of module in parts with encapsulated PV
$N_{without PV}$	Percentage of module in parts without encapsulated PV
$q_{without PV}$	Heat flow of module in parts without encapsulated PV

4.9.5.4 Assembly of PV glazing

Instead of heat flow, different proportional combinations of 'percentage of PV area' and 'percentage of transparent area' result in varying amounts of convection, emission, transmission, and electricity generation. The same principle of applying these proportional percentages has been used to calculate the quantity of heat flow diffraction. The parameter of reflection, as an exception, will not be altered since both configurations with and without PVs are covered by the same glass type, resulting in the same quantities of reflection for each irradiation amount and direction. As a result,

$$\begin{aligned}
 q_{con-combination} &= (N_{with\ PV} \times q_{con-with\ PV}) + (N_{without\ PV} \times q_{con-without\ PV}) \\
 q_{em-combination} &= (N_{with\ PV} \times q_{em-with\ PV}) + (N_{without\ PV} \times q_{em-without\ PV}) \\
 q_{tr-combination} &= (N_{with\ PV} \times q_{tr-with\ PV}) + (N_{without\ PV} \times q_{tr-without\ PV}) \\
 q_e-combination &= (N_{with\ PV} \times q_{e-with\ PV}) + (N_{without\ PV} \times q_{e-without\ PV})
 \end{aligned}
 \tag{4.25}$$

Where;

$q_{con-combination}$	Total heat flow of combination
$q_{con-with\ PV}$	heat flow of parts with encapsulated PV
$q_{con-without\ PV}$	Heat flow of parts without encapsulated PV
$q_{em-combination}$	Amount of emission of all combination
$q_{em-with\ PV}$	Amount of emission of parts with encapsulated PV
$q_{em-without\ PV}$	Amount of emission of parts without encapsulated PV
$q_{tr-combination}$	Amount of transmission of all combination
$q_{tr-with\ PV}$	Amount of transmission of parts with encapsulated PV
$q_{tr-without\ PV}$	Amount of transmission of parts without encapsulated PV
$q_e-combination$	Amount of electricity generation of all combination
$q_e-with\ PV$	Amount of electricity generation of parts with encapsulated PV
$q_e-without\ PV$	Amount of electricity generation of parts without encapsulated PV = 0

4.10 Power Balance Model

A power balance model has been employed to justify the thermal behavior of PV in relation to its power generation. Through this model and by identifying the relevant thermal characteristics affecting building functions, the surface temperature of the module is taken into account [44]. This power balance model operates based on the concept of the total power input and power output of the PV panels, which is integrated into the calculation of electrical power and thermal dissipation for three configurations: BIPV, BAPV, and PV glazing. Integrating this model facilitates the goal of this work, which is to assess the electrical power and thermal performance of components integrating PVs, taking into consideration the heat flows of 'components holding PVs,' which affect their efficiencies and result in different surface temperatures. Indeed, the thermal absorption power increases the module temperature until it reaches a steady state. This increase in module temperature decreases the electrical power and increases the thermal dissipation power [56].

Figure 4.24 describes the principle of thermal dissipation and electrical power in this model.

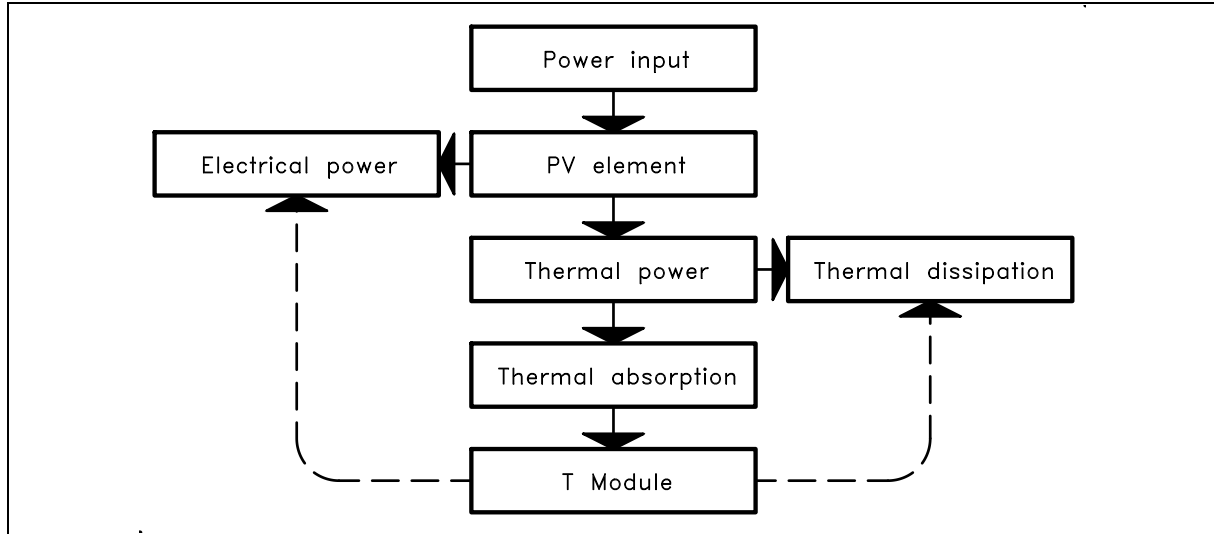


Fig. 4.24 Temperature model based on power balance – Action and interaction of temperature and power regarding boundary condition and PV efficiency [56]

Equivalents of the 'temperature model based on power balance' have been introduced through these correlations [56].

$$Power\ input = (1 - \gamma_f - \alpha_f - \alpha_b \cdot \tau_{PV} \cdot \tau_f - \tau_b \cdot \tau_{PV} \cdot \tau_f) \cdot G$$

$$Electrical\ power = [\eta \cdot (1 - \alpha_{coeff} \cdot (T_M - T_{STC})) \cdot \tau_f \cdot G]$$

$$Thermal\ dissipation = \left[\sum_j^{f,b} h_j \cdot (T_M - T_j) \right]$$

$$Thermal\ absorption = \left[C_M \cdot \left(\frac{\Delta T_M}{\Delta t} \right) \right]$$

Where;

γ_f	reflection factor of front layer
α_f	absorption factor of front layer
α_b	absorption factor of back layer
τ_{PV}	transmission factor of PV
τ_f	transmission factor of front layer
τ_b	transmission factor of back layer
G	irradiation
η	module efficiency
α_{coeff}	temperature co-efficiency of module
T_M	temperature of module
T_{STC}	temperature of module at STC
h_j	outside and inside heat transfer coefficient
T_j	outside and inside surface temperature
C_M	module heat capacity
Δt	time

In this work, the steady-state method will be employed, so the thermal absorption power is no longer considered. The thermal dissipation power can be achieved through conduction heat transfer resistances. In terms of thermal dissipation, it is assumed that the surface temperature is equal to the cell temperature [55]. By eliminating thermal absorption from the presented temperature model based on power balance [56], the temperature model based on power balance will be based on Figure 4.25.

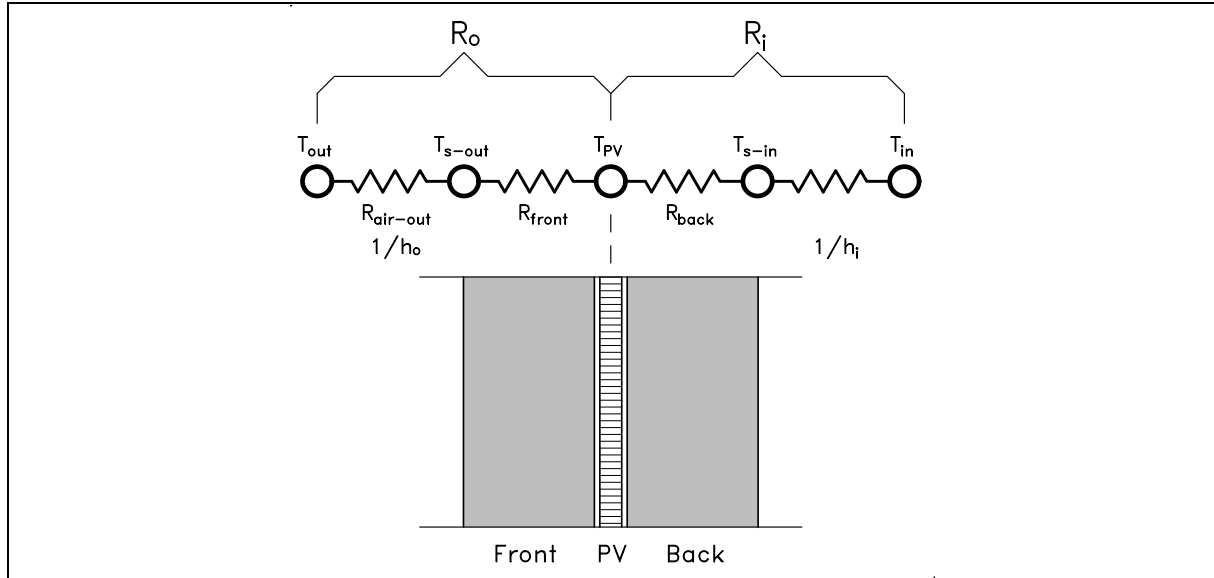


Fig. 4.25 Temperature model of PV module regarding front and back thermal resistances of construction [56]

The temperature model of the PV, represented in Figure 4.25, is applied to all three configurations of BIPV, BAPV, and PV glazing. The correlation of heat transfer elements (conduction, convection, and radiation) along with module configuration is presented in Equation 4.26 [56].

$$(1 - \gamma_f - \alpha_f - \alpha_b \cdot \tau_{PV} \cdot \tau_f - \tau_b \cdot \tau_{PV} \cdot \tau_f) \cdot G = \left[\eta \cdot (1 - \alpha_{coeff} \cdot (T_M - T_{STC})) \cdot \tau_f \cdot G \right] + \left[\sum_j^{f,b} \left(\frac{1}{R_{x,j}} + h_j \right) \cdot (T_M - T_j) \right] \quad (4.26)$$

Where;

- $R_{x,j}$ thermal resistance of representative layer
- h_j convective heat transfer coefficient of representative layer

4.10.1 Power input

Power input, as a direct effect of total irradiation, considering the sequence of construction of the assembly of the component and its geometrical configuration, has been introduced in [56].

$$(1 - \gamma_f - \alpha_f - \alpha_b \cdot \tau_{PV} \cdot \tau_f - \tau_b \cdot \tau_{PV} \cdot \tau_f) \cdot G$$

In this correlation, α_f , γ_f , and τ_f determine the absorption, reflection, and transmission factors of the front layer, respectively. All three coefficients have been calculated in the

calculations of 'transparent component properties' and will be applied to the equation in the upcoming simulations to calculate the power input of components holding PVs. Also, considering the selected type of PV cell in all three configurations, which represents an opaque component, the transmission factor of PV (τ_{PV}) is zero. As a result, the terms ' $\tau_b \cdot \tau_{PV} \cdot \tau_f$ ' consistently remain as zero and will be eliminated from the calculations. The parameter G , representing irradiation, is formally calculated as 'the total solar radiation density incident'

4.10.2 Electrical power

Electrical power is a direct result of total irradiation, taking into account the efficiency of the PV module. In this regard, the operating temperature has been introduced through the upcoming correlation [56].

$$[\eta \cdot (1 - \alpha_{coeff} \cdot (T_M - T_{STC})) \cdot \tau_f \cdot G]$$

In this correlation, η represents the efficiency of the PV module, which, by definition, is the solar cell efficiency determining the portion of energy in the form of sunlight converted via photovoltaics into electricity ($0 < \eta < 1$). The term α_{coeff} represents the 'temperature coefficient of the module' and indicates how strongly the PV power output depends on the cell temperature, specifically the surface temperature of the PV. Due to the extremely low thickness of the PV and its constant material construction, it is assumed that the outside, middle, and inside temperatures of the PV are the same. Since power output decreases with increasing cell temperature, this coefficient defines the sensitivity of the PV to temperature increases, resulting in drops in electrical power. Consequently, higher values of α_{coeff} indicate more electrical power losses for the same temperature differences between T_M and T_{STC} . The term ' $T_M - T_{STC}$ ' indicates the difference in operating temperature from the 'standard test conditions' (STC) provided in the datasheet of each PV panel. Therefore, the ideal temperature set-point to produce electricity equal to the nominal efficiency of the PV occurs when the term ' $T_M - T_{STC}$ ' is equal to zero. This means that the operating temperature of the PV is equal to the temperature of the STC specified by the manufacturer.

4.10.3 Thermal dissipation

Thermal dissipation, as the interaction of both inside and outside surface temperatures of the component's construction, which are influenced by boundary conditions and geometrical configuration, has been expressed in [56].

$$\sum_j^{f,b} \left(\frac{1}{R_{x,j}} + h_j \right) \cdot (T_M - T_j)$$

Regarding the use of the outside temperature, $T_{sol-air}$ has been employed to integrate 'convection,' 'emission,' and 'irradiation' all together, where the 'convection heat transfer coefficient' is already included. The integration of the quantity of thermal dissipation in the balance relation of total irradiation regarding heat flows, electrical power, and the remaining irradiation is justified through correlation 4.27 [56].

$$G_{irradiation} = q_{thermal\ dissipation} + q_{electrical\ power} + q_{transmission+reflection} \quad (4.27)$$

5. Simulation

To calculate the heat flow and its contribution to increasing or decreasing the heating and cooling demand of the building, as well as the interaction of their auxiliary heating and cooling systems with each other, the introduced equations, assumptions, and correlations in the explained method are integrated. Indeed, all the equations employed are within the framework of quasi-static heat transfer methods.

5.1 Geographical location

To better align with the local context of the research and incorporate German standards, regulations, and codes into the developed method and calculations, the city of Stuttgart has been chosen as the geographical location for all calculations. The exact coordinates of the integrated location are shown in table 5.1 [46].

Location	Stuttgart
Latitude	48.68°
Longitude	9,22°

Tab. 5.1 Coordinates of simulation, Stuttgart – Germany [46]

5.2 Weather data

“EnergyPlus Hourly Weather Data” [57] has been integrated to provide meteorological data for performing simulations in this work. According to the claims of “EnergyPlus,” the provided weather data are composite files from multiple years. Therefore, the critical concern when evaluating and drawing conclusions from calculations based on weather data from just one year, considering the changing average cloudiness or wind speed and direction, is mitigated. In this regard, two temperature parameters represent the outside temperature effects in boundary conditions: 'outside dry-bulb temperature' (°C) and 'outside dew-point temperature' (°C).

5.2.1 Dry-bulb temperature

Dry-bulb temperature refers to the ambient air temperature indicated by a thermometer that is not affected by the moisture of the air (T_{out}).

5.2.2 Outside dew-point temperature

Dew point is the temperature at which air must be cooled to become saturated with water vapor. When cooled further, the airborne water vapor will condense to form liquid water (dew). When air cools to its dew point through contact with a surface that is colder than the air, water will condense on the surface [58]. This temperature parameter has been used in the calculation of sky emissivity ($T_{dewpoint}$).

5.2.3 Wind velocity and direction

The accuracy of the obtained wind speed and direction is evident in each interval. To moderate the effect of wind in the calculation procedure, a monthly average of wind speed and direction has been selected and incorporated.

5.2.4 Solar altitude and azimuth

The solar altitude is defined as the angle between the sun's rays and the vertical direction, while the solar azimuth angle represents the azimuth angle of the Sun's position. Both of these parameters are used to determine the percentage of irradiation influence on the proposed component with a specific orientation and inclination. In the integrated equation for calculating the total amount of irradiation, considering direct, diffuse, and reflected irradiation, two parameters, the declination of the sun (ϕ) and the hour angle (ω), are employed [59].

5.2.5 Direct normal and diffuse horizontal irradiation

Both parameters, 'direct normal solar irradiation' (G_B) and 'diffuse horizontal solar irradiation' (G_D), are provided in hourly intervals and are used to calculate the 'total solar radiation density incident' (G_{Tt}).

5.3 Intervals of calculation

In each month two days have been selected as representative days. For this purpose, 11th and 26th of each month deliver demanded data for the representative month. Combination of emerged weather data in interval of one hour is partly shown in table 5.2 as a small segment of the entire annual weather data.

	Date	Time	Date	Time	Date	Time	Next data
	11 th May	09:00	11 th May	10:00	11 th May	11:00	
Outside Dry-Bulb Temperature (°C)	11.3		13.2		14.7		
Outside Dew-Point Temperature (°C)	7.3		7.8		8.3		
Wind Speed (m/s)	0		1.5		2.6		
Wind Direction (°)	0		60		20		
Solar Altitude (°)	42.96		51.19		57.1		
Solar Azimuth (°)	115.16		132.38		154.73		
Direct Normal Solar (W/m ²)	51		449		635		
Diffuse Horizontal Solar (W/m ²)	212		275		242		

Tab. 5.2 Sample segment of annual weather data integrated in calculations [57]

5.4 Simulated variants

Five components of this work, namely opaque, transparent, BIPV, BAPV, and PV glazing, in various geometrical configurations, including different orientations and inclinations, have been simulated. Additionally, each configuration of the component has been separately simulated under two different boundary conditions, considering inside set temperatures within the comfort temperature ranges. Using two representative days per month results in a total of 24 days per year that have been comprehensively simulated and calculated. Furthermore, the effect of integrating different materials, altering thermal conductivity, and defining various 'u-

values' for the opaque component, which is fundamentally integrated into BIPV and BAPV, has been explored. Figure 5.1 illustrates the diversity of calculations performed, considering the possible resulting variants.

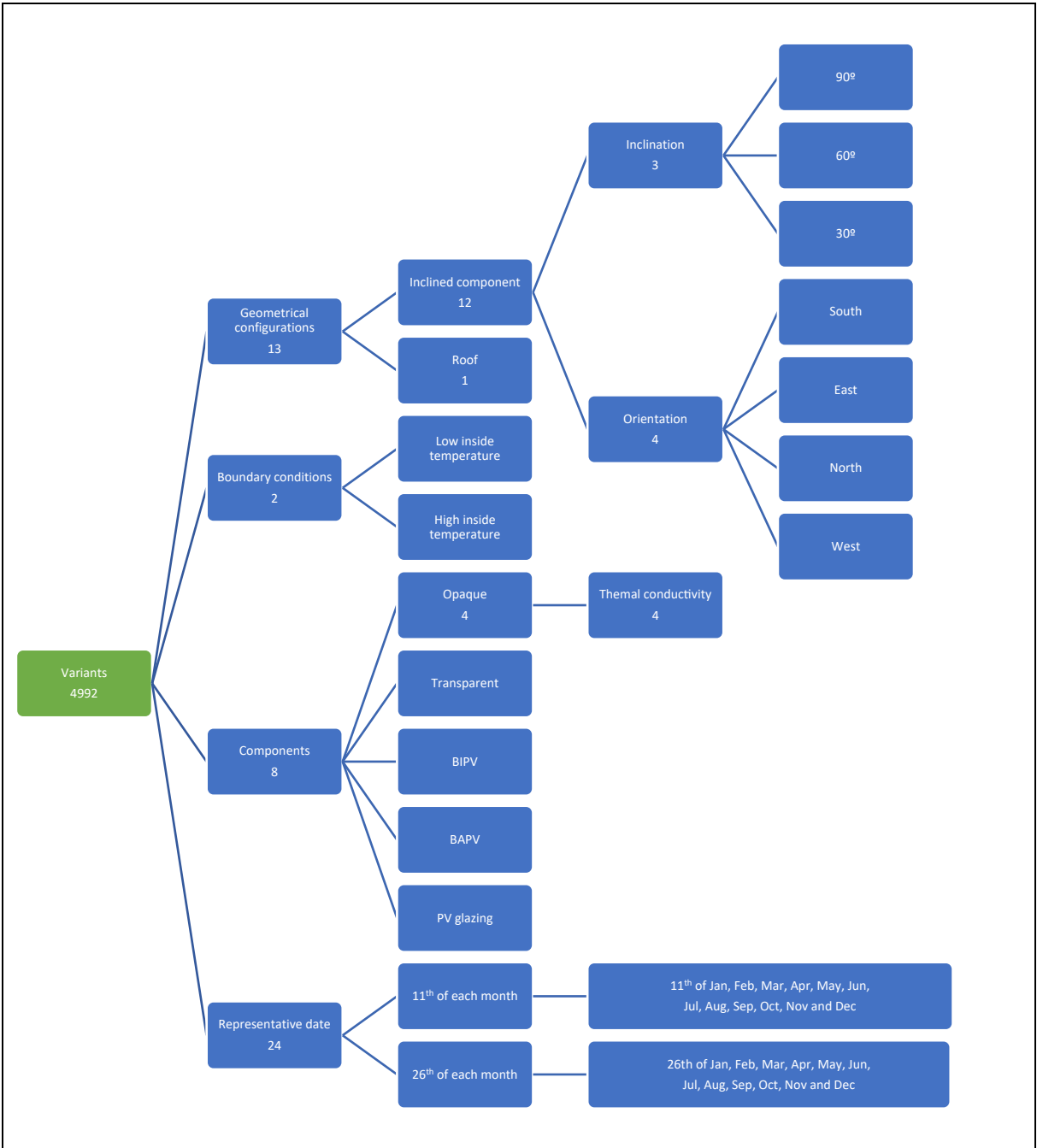


Fig. 5.1 Possible variants considering interaction of geometrical configurations, boundary conditions, components and representative date

While the ultimate graphs that illustrate the annual performance of each component within each geometrical configuration encompass all representative dates (namely, the 11th and 26th of each month, totaling 24 days per year), these are not featured in the current presentation due to the limited scope. For comprehensive data, readers can refer to the appendix 3 of this work where detailed results of the entire calculation process are available.

5.4.1 Geometrical configuration

Three inclinations of 90° , 60° , and 30° represent vertical and inclined components with equal angular differences of 30° . All these three inclinations have been applied to four main orientations of 0° (south), -90° (east), 180° (north), and $+90^\circ$ (west). The interaction of these 3 inclinations through 4 orientations results in 12 different geometrical configurations. The roof, as a component with an inclination of 0° , defines the 13th configuration, as different orientations don't change the angular position of a roof.

Intermediate orientations of -30° , -60° , -120° , -150° , $+150^\circ$, $+120^\circ$, $+60^\circ$, and $+30^\circ$ are also employed in the developed software.

As a result, the primary inclination of 90° representing vertical walls in the four main orientations of 0° (south), -90° (east), 180° (north), and $+90^\circ$ (west), and the inclination of 0° representing the roof in the initial phase of simulations are discussed. In the upcoming phases, the performance of components in these 4 main orientations, along with two additional inclinations of 60° and 30° , will be presented and compared.

5.4.2 Boundary condition

The weather data related to the geometrical configuration of the component and the properties of the coating material (used to calculate the reflection ratio) define the outside parameters of the boundary condition. Regarding the interior of the components throughout the entire simulations, two different boundary conditions, 'low inside temperature' and 'high inside temperature,' have been employed and will be discussed.

5.4.3 Components

Performance of all five components of opaque, transparent, BIPV, BAPV and PV glazing will be calculated and discussed.

5.4.4 Representative date

Two different scenarios for the number of calculated days per year have been investigated and compared. The simplest variant, which involves selecting 1 day per month and results in 12 days per year, has been ignored due to its low-resolution interval. Instead, for a higher resolution, 2 days from each month have been chosen as representative, specifically the 11th and 26th of each month, with equal intervals of 15 days. Consequently, 24 days in each year have been individually calculated. While the entire set of 24 days for each component has been disregarded, two representative days, one for summer and one for winter, are presented. The complete calculations and simulations for all 24 days for each component can be found in the appendix of this work.

To select representative days for summer and winter, we used both the monthly temperature and sun irradiation data for Stuttgart. The two graphs we employed determine the months with the maximum and minimum temperatures and irradiation, respectively. As our choices for representative days, we selected the 26th of July to represent a summer day and the 26th of January to represent a winter day, from among all 365 days of the year. Figure 5.2 displays the monthly temperature and irradiation data for Stuttgart [60] (Figure 5.2).

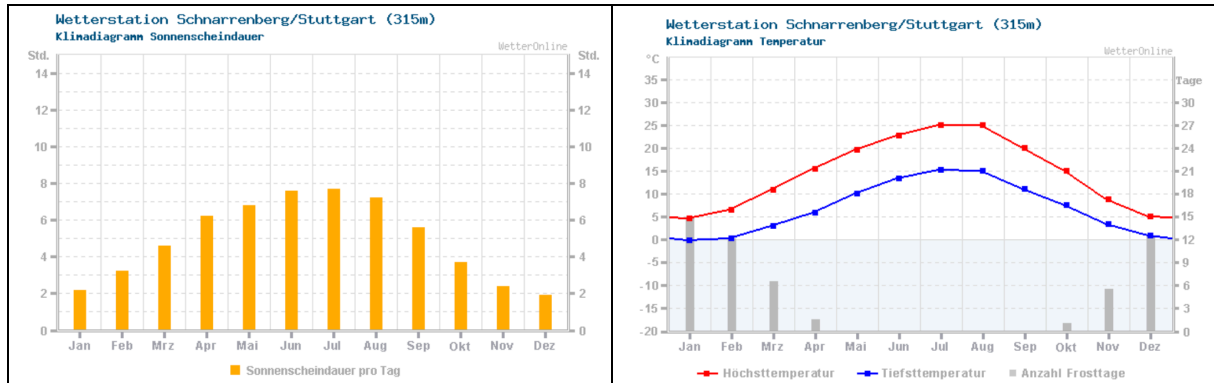


Fig. 5.2 Monthly irradiation period (left) and Monthly maximum and minimum temperature (right)- Stuttgart [60]

It should be noted that the representative summer and winter days are selected for presentation within the limited scope of this work. However, the calculation of the annual energy performance of all five components has been conducted based on the entire set of 24 days per year. Similarly, in the calculation of the final indexes of this work, namely 'self-sufficiency' and 'self-consumption,' all 24 days of the year, broken down into hourly intervals (24 intervals per day), have been simulated and integrated. This means that the final simulation resolution of this work is conducted as follows:

$$Resolution_{calculations} = Number\ of\ days_{year} \times Number\ of\ hours_{day}$$

$$Resolution_{calculations} = 24 \times 24 = 576$$

5.5 Opaque component

Since the inclination of 90° can be considered as representing vertical walls with the highest rate of applicability, and the primary masonry configuration of the construction involves opaque materials, this configuration is taken into account. Table 5.3 provides details of the configuration and boundary conditions for the proposed component.

Component	Inclination (°)	Orientation (°)	Inside temperature (Set)	Date	Heat conductivity (W/m.K)	Thickness (m)	U-value (W/m ² .K)	α _s (%)	h _i (W/m ² .K)
Opaque	90	0	High *	26 th Jan 26 th Jul	0.03	0.20	0.15	50 **	7

Tab. 5.3 Boundary condition – Opaque component

* “High” determines “high inside temperature” and “Low” determines “low inside temperature”

* α_s determines irradiance absorption assumption (%)

h_i determines inside convective heat transfer coefficient (W/m².K)

5.5.1 Daily performance - Summer day

On a summer day, specifically on the 26th of July at 11:00, the calculation procedure is described in Table 5.4, which indicates the parameters used and the equations employed.

Weather parameters & position					Assumption of ratios				
n	Parameter	Symbol	Value	Unit	n	Parameter	Symbol	Value	Unit
	Direct beam	G _B	778	W/m ²		albedo ratio	ρ	0.20	-
	Diffuse beam	G _D	177	W/m ²					
	Solar declination	δ	23.31	°					
	Hour angle	ω	-20.89	°					
	T dry-bulb	T _{out}	298.15	°K					
	T dew-point	T _{dew}	286.85	°K					
	Wind Speed	W _s	3.06	m/s					
	Wind Direction	W _d	90	°					
	Latitude (Stuttgart)	ϕ	48.68	°					
Convective heat transfer coefficient					Component properties & geometry				
n	Parameter	Symbol	Value	Unit	n	Parameter	Symbol	Value	Unit
	Outside Convective heat transfer coefficient	h _o	9.50	W/m ² .K		Heat conductivity	λ	0.03	W/mK
	Inside Convective heat transfer coefficient	h _i	7.00	W/m ² .K		Thickness	d	0.2	m
						Reflection coefficient	γ_r	0.50	-
						Absorption coefficient	α_r	0.50	-
						Component emissivity	ϵ	0.90	
						Surface tilt	β	90	°
						Surface azimuth	α	0	°

Tab. 5.4 Weather data, component property and assumptions – Opaque component – 26th July

In relation to Table 5.4, which represents the 26th of July as a representative summer day, the procedure for the interaction of weather data through component properties for calculating surface temperatures, heat flows, and the diffraction of irradiation is detailed in Table 5.5.

N	Parameter	Symbol	Equation	Result	Unit
01	Angle of incidence of beam radiation	cos θ	4.5	0.40	-
02	Total solar radiation density incident on tilted surface	Q _{sol}	4.6	479.02	W/m ²
03	Opaque sky cover	N	Weather data	5	-
04	Sky emissivity	ϵ_{sky}	4.10	0.88	
05	Sky temperature	T _{sky}	4.11	291.40	°C

Tab. 5.5 Constant amounts of parameters in all 5 components with the same geometrical configuration

Absorption, emissivity, and the outside convective heat coefficient are combined to calculate T_{sol-air}. The inside convective heat coefficient, thermal resistance of the component, and its thermal conductivity are integrated to calculate the inside and outside surface temperatures, ultimately resulting in heat flow (see Table 5.6).

N	Parameter	Symbol	Equation	Result	Unit
06	Solar-air temperature	T _{sol-air}	4.12	318.84	°C
07	Thermal resistance excluding outside air film resistance	$\sum RI$	4.20	6.81	m ² k/W
08	Thermal resistance excluding inside and outside air film resistances	$\sum RII$	4.20	6.67	m ² k/W
09	Outside surface temperature	T _{s-out}	4.13	318.84	°K
10	Inside surface temperature	T _{s-in}	4.14	300.46	°K
11	Heat flow	q	4.15	2.72	W/m ²

Tab. 5.6 Calculation of surface temperatures – heat flow – Opaque component

The division of the diffraction of irradiation is calculated based on the proportions of reflection, emission, and convection, respectively (see Table 5.7).

N	Parameter	Symbol	Equation	Result	Unit
12	outside reflection from surface of component	q_{ref}	$100 (\%) - Reflection (\%)$	-239.51	W/m^2
13	outside emission from surface of component	q_{rad}	4.19	-157.73	W/m^2
14	outside convection from surface of component	q_{con}	4.18	-79.06	W/m^2

Tab. 5.7 Dividing diffraction of irradiation – Opaque component

Table 5.8 displays the calculated inside and outside surface temperatures of the component and the resulting heat flows over a 24-hour period on the 26th of July.

	T out	T in	T s-out	T s-in	Q (all)	Direction	G+	L-	L+	G-	Irradiation	Reflection	Convection	Emission
01:00	18,00	25,83	13,81	25,58	-1,77	L-		-1,77			0,00	0,00	23,35	-25,12
02:00	17,10	25,73	12,96	25,46	-1,88	L-		-1,88			0,00	0,00	23,23	-25,10
03:00	16,60	25,68	12,50	25,40	-1,94	L-		-1,94			0,00	0,00	23,13	-25,07
04:00	15,30	25,53	11,21	25,23	-2,10	L-		-2,10			0,00	0,00	23,34	-25,44
05:00	14,80	25,47	10,74	25,16	-2,16	L-		-2,16			0,00	0,00	23,28	-25,45
06:00	15,30	25,53	11,99	25,24	-1,99	L-		-1,99			15,60	-7,80	18,84	-28,63
07:00	17,50	25,78	16,92	25,59	-1,30	L-		-1,30			74,50	-37,25	3,17	-41,72
08:00	21,00	26,17	23,27	26,11	-0,43	L-		-0,43			138,46	-69,23	-11,89	-57,77
09:00	23,20	26,42	30,99	26,52	0,67	G+	0,67				257,93	-128,97	-38,75	-89,55
10:00	26,00	26,74	39,37	27,00	1,85	G+	1,85				382,78	-191,39	-62,27	-127,26
11:00	27,60	26,92	45,43	27,31	2,72	G-				2,72	479,02	-239,51	-79,06	-157,73
12:00	29,10	27,09	48,04	27,53	3,08	G-				3,08	507,77	-253,89	-81,67	-169,13
13:00	29,70	27,16	44,31	27,52	2,52	G-				2,52	418,27	-209,13	-64,37	-142,25
14:00	30,90	27,29	36,88	27,49	1,41	G-				1,41	239,50	-119,75	-27,48	-90,87
15:00	31,40	27,35	44,10	27,70	2,46	G-				2,46	383,39	-191,69	-55,42	-133,81
16:00	32,30	27,45	40,65	27,73	1,94	G-				1,94	291,68	-145,84	-37,10	-106,80
17:00	32,00	27,42	35,25	27,58	1,15	G-				1,15	178,39	-89,20	-14,96	-73,08
18:00	31,70	27,38	32,51	27,49	0,75	G-				0,75	122,50	-61,25	-3,81	-56,69
19:00	30,00	27,19	28,15	27,21	0,14	G-				0,14	69,80	-34,90	8,99	-43,75
20:00	28,10	26,98	23,56	26,90	-0,50	L+			-0,50		9,60	-4,80	22,88	-28,18
21:00	27,70	26,93	22,68	26,84	-0,62	L+			-0,62		0,00	0,00	25,49	-26,12
22:00	25,30	26,66	20,81	26,54	-0,86	L-			-0,86		0,00	0,00	23,30	-24,16
23:00	23,40	26,44	19,16	26,29	-1,07	L-			-1,07		0,00	0,00	22,43	-23,50
24:00	19,30	25,98	15,05	25,75	-1,60	L-			-1,60		0,00	0,00	23,38	-24,99

Tab. 5.8 Inside and outside surface temperatures (°C) – Effect of reflection, convection and emission (W/m^2) – Opaque component – Boundary condition in table 5.3

The total amount of heat flow is presented in Figure 5.3.

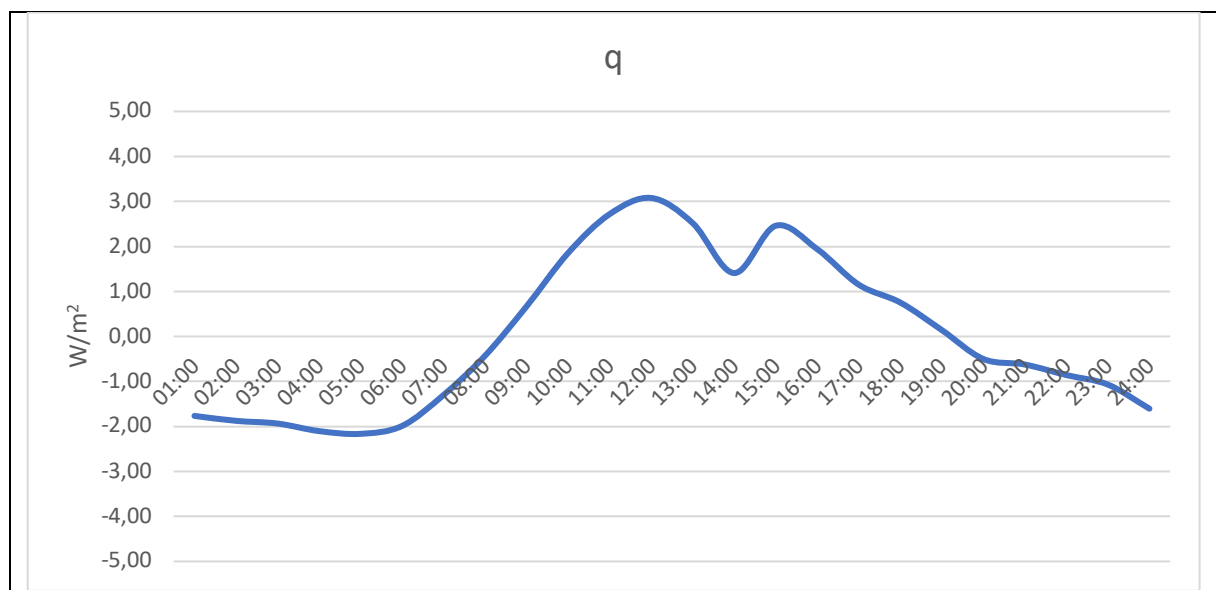


Fig. 5.3 Hourly amount of heat flow (W/m^2) – Opaque component – Boundary condition in table 5.3

The calculated quantities of heat flow are shown in Figure 5.4.

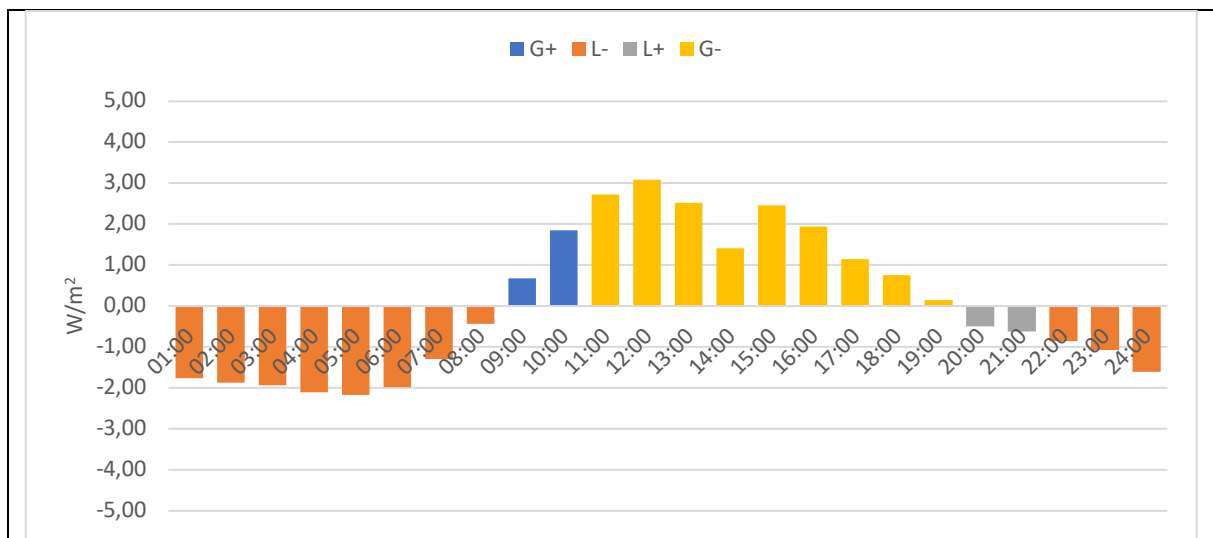


Fig. 5.4 Hourly amount of heat flow + values (W/m^2) - Opaque component – Boundary condition in table 5.3

All four heat flow values are observed after applying the values to the quantity of heat flow, considering the boundary condition. On the representative date, from the beginning of the day until 09:00, the direction of heat flow is 'from inside into outside,' and ' $T_{out} < T_{in}$,' indicating heat loss. From 09:00 until 11:00, the direction of heat flow is 'from outside into inside,' and ' $T_{out} < T_{in}$,' signifying heating demand. From 11:00 until 20:00, the direction of heat flow remains 'from outside into inside,' but the dry-bulb temperature is higher than the inside air temperature, resulting in ' $T_{out} > T_{in}$,' identifying cooling demand, which typically occurs during a summer afternoon. From 20:00 until 22:00, the direction of heat flow changes to 'from inside into outside,' during which these two hours still have the boundary condition showing ' $T_{out} > T_{in}$,' identifying cooling auxiliary. During the last three hours of the day, the direction of heat flow is 'from inside into outside,' and ' $T_{out} < T_{in}$,' indicating heat loss or the same heat flow value as in the initial 8 hours of the day (Figure 5.5).

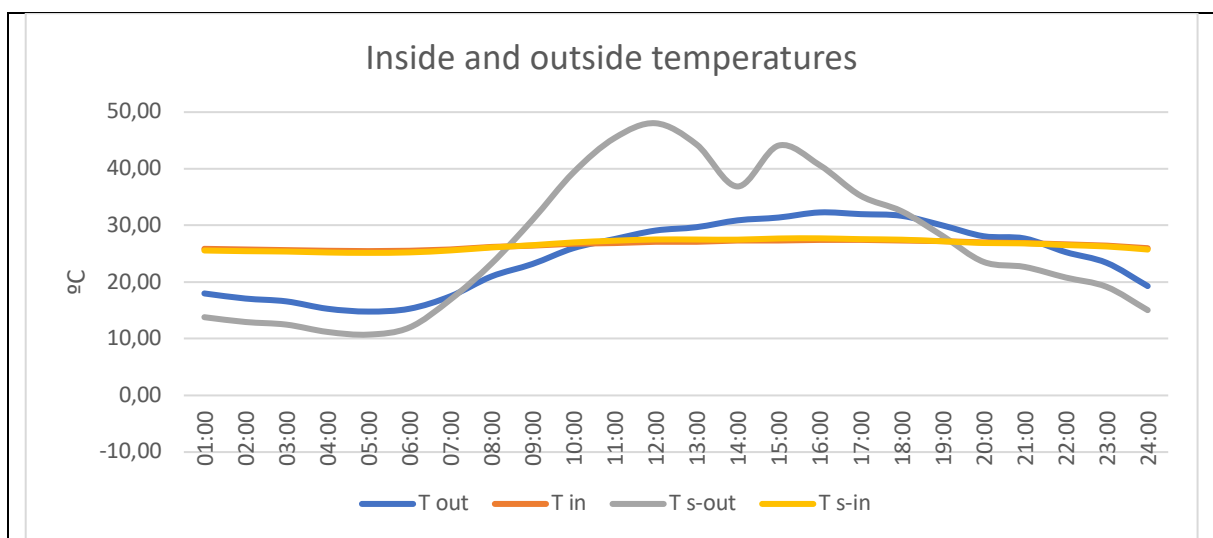


Fig. 5.5 outside temperature ($^{\circ}C$), inside temperature ($^{\circ}C$), outside surface temperature ($^{\circ}C$) and inside surface temperature ($^{\circ}C$) - Opaque component – Boundary condition in table 5.3. As there are only small differences between the calculated inside temperature (T_{in}) and inside surface temperature (T_{s-in}), both curves seem almost the same. The differences are detectable in Table 5.8.

The calculated temperatures reveal that from the beginning of the day until 09:00 and from 20:00 until 24:00, the inside surface temperature is lower than the outside air temperature. Between 09:00 and 20:00, the inside surface temperature is higher than the outside air temperature.

Similarly, from the beginning of the day until 07:00 and from 19:00 until the end of the day, the outside surface temperature is lower than the outside air temperature. From 07:00 until 19:00, the outside surface temperature is higher than the outside air temperature.

5.5.2 Daily performance - Winter day

Inside and outside temperatures are calculated at one-hour intervals using equations 4.13 and 4.14. The determination of the value of 'q' is based on the direction of heat flow and the difference between the dry-bulb temperature and the inside air temperature. In this instance, as throughout the entire 24-hour interval, both conditions of ' $T_{out} < T_{in}$ ' and heat flow direction 'from inside to outside' are applied, all quantities of heat flows are considered as heating demand. Table 5.9 provides an abbreviation of the values of heat flows.

Heat flow	G+	L-	L+	G-
Value	Heating auxiliary	Heating demand	Cooling auxiliary	Cooling demand

Tab. 5.9 Abbreviation of values of heat flow

Table 5.10 displays the calculated inside and outside surface temperatures of the component and the resulting heat flows. The right side of the table illustrates the effect of each phenomenon on the quantities of heat flow.

	T out	T in	T s-out	T s-in	q	Direction	G+	L-	L+	G-	Irradiation	Reflection	Convection	Emission
01:00	-0,80	23,71	-5,03	23,11	-4,22	L-		-4,22			0,00	0,00	19,75	-23,97
02:00	-1,10	23,68	-5,21	23,07	-4,24	L-		-4,24			0,00	0,00	19,26	-23,50
03:00	-1,00	23,69	-5,18	23,08	-4,24	L-		-4,24			0,00	0,00	19,58	-23,82
04:00	-1,30	23,65	-5,44	23,04	-4,27	L-		-4,27			0,00	0,00	19,43	-23,70
05:00	-1,90	23,59	-6,08	22,96	-4,36	L-		-4,36			0,00	0,00	19,73	-24,09
06:00	-2,00	23,57	-6,18	22,95	-4,37	L-		-4,37			0,00	0,00	19,75	-24,12
07:00	-2,40	23,53	-6,59	22,90	-4,42	L-		-4,42			0,00	0,00	19,88	-24,31
08:00	-2,10	23,56	-6,29	22,94	-4,38	L-		-4,38			0,00	0,00	19,82	-24,20
09:00	-2,20	23,55	-5,59	22,94	-4,28	L-		-4,28			13,20	-6,60	16,00	-26,88
10:00	-2,40	23,53	0,97	23,06	-3,31	L-		-3,31			133,26	-66,63	-15,39	-54,55
11:00	-1,40	23,64	-1,24	23,12	-3,65	L-		-3,65			77,62	-38,81	-0,76	-41,71
12:00	-1,30	23,65	0,17	23,16	-3,45	L-		-3,45			100,74	-50,37	-6,72	-47,10
13:00	-0,90	23,70	1,08	23,22	-3,32	L-		-3,32			109,60	-54,80	-9,00	-49,12
14:00	-1,80	23,60	6,65	23,24	-2,49	L-		-2,49			224,49	-112,25	-37,43	-77,31
15:00	-1,20	23,66	5,18	23,28	-2,71	L-		-2,71			189,37	-94,68	-28,39	-69,01
16:00	-1,70	23,61	-0,35	23,11	-3,52	L-		-3,52			97,30	-48,65	-6,18	-45,99
17:00	-1,70	23,61	-5,27	23,00	-4,24	L-		-4,24			10,80	-5,40	16,77	-26,41
18:00	-2,10	23,56	-6,26	22,94	-4,38	L-		-4,38			0,00	0,00	19,69	-24,07
19:00	-2,40	23,53	-6,54	22,90	-4,42	L-		-4,42			0,00	0,00	19,63	-24,04
20:00	-3,30	23,43	-7,41	22,78	-4,53	L-		-4,53			0,00	0,00	19,64	-24,17
21:00	-3,40	23,42	-7,51	22,77	-4,54	L-		-4,54			0,00	0,00	19,66	-24,20
22:00	-3,40	23,42	-7,48	22,77	-4,54	L-		-4,54			0,00	0,00	19,54	-24,07
23:00	-3,70	23,38	-7,79	22,73	-4,58	L-		-4,58			0,00	0,00	19,64	-24,22
24:00	-0,60	23,73	-4,83	23,13	-4,19	L-		-4,19			0,00	0,00	19,70	-23,90

Tab. 5.10 Inside and outside surface temperatures (°C) – Effect of reflection, convection and emission (W/m²) - Opaque component – Boundary condition in table 5.3

The reflection amount of total irradiation is calculated based on the average reflection of masonry materials with a mild color, representing neither an extremely light nor a dark coating. Emission has been calculated by integrating equation 4.19. Similarly, the quantity of convection has been calculated by integrating the explained equation of 4.17. Hourly amounts of heat flow are presented in Figure 5.6.

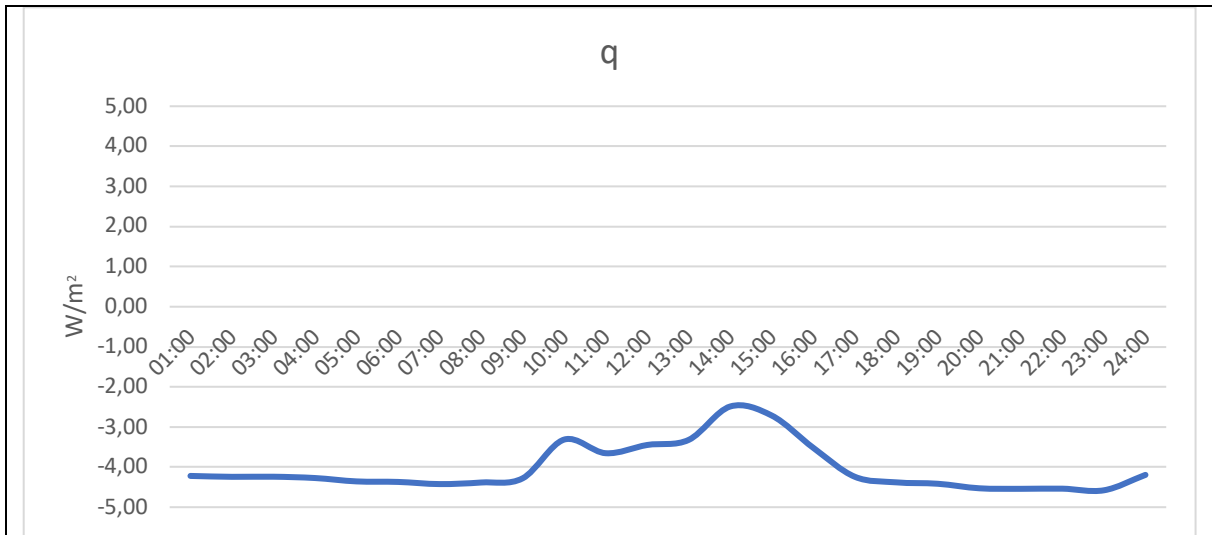


Fig. 5.6 Hourly amount of heat flow (W/m²) - Opaque component – Boundary condition in table 5.3

The graph illustrates that during the representative date, the component experiences heat loss of approximately 4.30 W/m², and with the onset of irradiation, it decreases to its minimum of about -2.50 W/m² around 14:00. The application of values of heat flows to their quantities is presented in Figure 5.7.

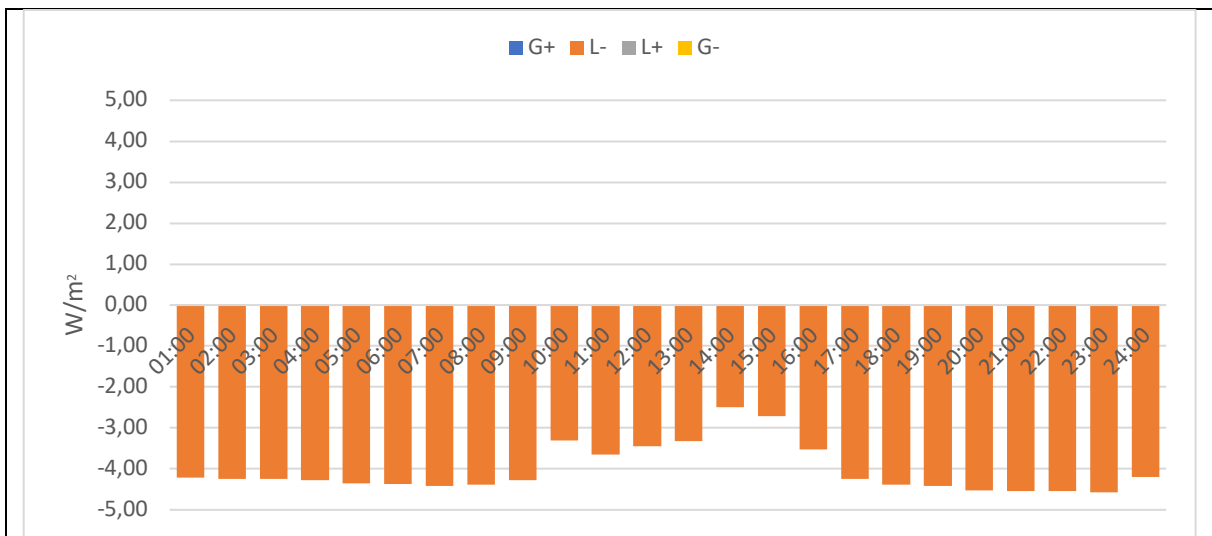


Fig. 5.7 Hourly amount of heat flow + values (W/m²) - Opaque component – Boundary condition in table 5.3

The graph shows that due to the constant inside and outside temperature difference ($T_{out} < T_{in}$) and the direction of heat flow towards the outside, throughout the entire 24 hours of the representative date, all quantities of heat flows are categorized as 'heating demand'.

Outside and inside surface and air temperatures are presented in Figure 5.8.

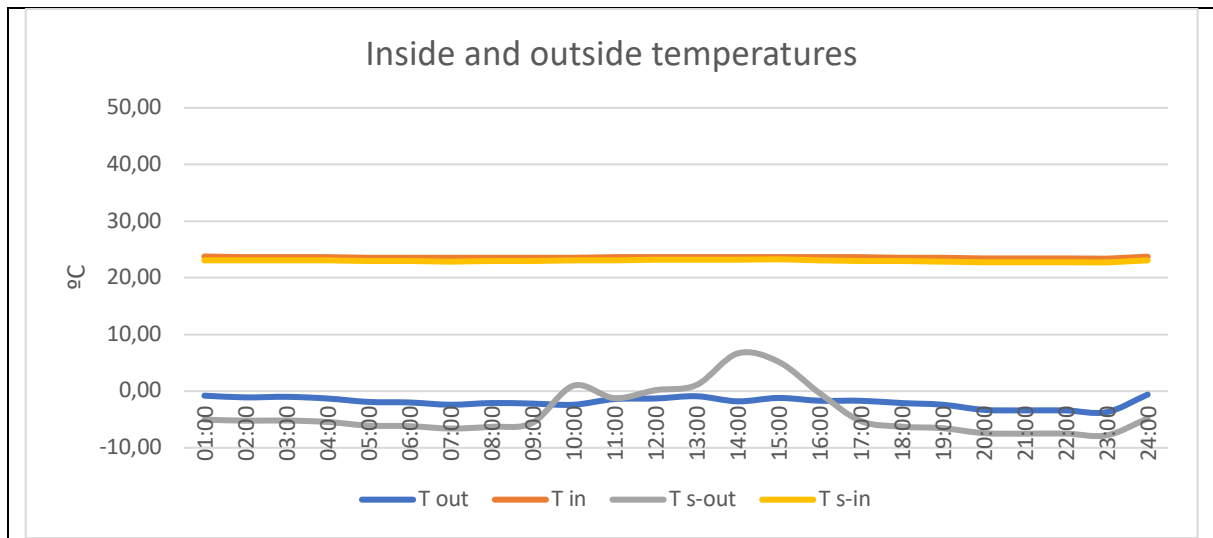


Fig. 5.8 outside temperature (°C), inside temperature (°C), outside surface temperature (°C) and inside surface temperature (°C) - Opaque component – Boundary condition in table 5.3. As there are only small differences between the calculated inside temperature (T_{in}) and inside surface temperature (T_{s-in}), both curves seem almost the same. The differences are detectable in Table 5.10.

The quantities of inside air temperature and inside surface temperature indicate that the surface temperature remains consistently lower than the inside air temperature, resulting in simultaneous heat loss through convection.

5.5.3 Monthly performance

On an hourly basis, the cumulative amounts of the calculated parameters over all 24 selected days are presented in the following table, which indicates the quantity and value of heat flows. It should be noted that the recorded amounts of heating and cooling auxiliary do not alter the quantities of heating and/or cooling demand of the component itself. Instead, they will be used in combination with different components through a facade (for example, integrated windows as a transparent component with an opaque component) for the final calculation of the amounts of heating and/or cooling demand that can be compensated by other components. The second part of this annual table describes the hourly intervals for recording parameters that indicate the cumulative quantities of reflection, convection, and emission. Tables 5.11 and 5.12 display the annual cumulative quantities of these parameters (Figure 5.9).

	Jan	-	Feb	-	Mar	-	Apr	-	May	-	Jun	-
G+	0,00	0,00	0,00	0,00	0,69	10,51	0,40	0,00	12,21	20,23	2,05	11,48
L-	-83,75	-96,66	-89,54	-91,47	-70,87	-53,40	-60,64	-69,78	-39,70	-26,18	-37,86	-23,29
H Demand	83,75	96,66	89,54	91,47	70,87	53,40	60,64	69,78	39,70	26,18	37,86	23,29
H Auxiliary	0,00	0,00	0,00	0,00	-0,69	-10,51	-0,40	0,00	-12,21	-20,23	-2,05	-11,48
L+	0,00	0,00	0,00	0,00	0,00	0,00	0,00	0,00	0,00	0,00	0,00	-0,01
G-	0,00	0,00	0,00	0,00	0,00	0,00	0,00	0,00	0,00	0,00	0,00	7,82
C Demand	0,00	0,00	0,00	0,00	0,00	0,00	0,00	0,00	0,00	0,00	0,00	7,82
C Auxiliary	0,00	0,00	0,00	0,00	0,00	0,00	0,00	0,00	0,00	0,00	0,00	-0,01
Irradiation	222,60	956,39	363,60	479,40	2491,90	5391,14	1912,68	2277,78	4111,69	4427,43	2862,51	4004,08
Reflection	-111,30	-478,19	-181,80	-239,70	-1245,95	-2695,57	-956,34	-1138,89	-2055,85	-2213,71	-1431,26	-2002,04
Convection	380,28	223,59	456,21	418,59	-134,92	-843,00	61,10	-4,24	-376,20	-370,88	-158,18	-298,10
Emission	-575,34	-798,45	-727,55	-749,76	-1181,21	-1895,45	-1077,67	-1204,43	-1707,13	-1848,78	-1308,89	-1707,95

Tab. 5.11 First six months - cumulative quantities of parameters (W/m^2) - Opaque component – Boundary condition in table 5.3

	Jul	-	Aug	-	Sep	-	Oct	-	Nov	-	Dec	-
G+	5,09	2,53	16,46	0,00	17,07	25,45	0,18	0,00	4,94	13,31	0,00	0,00
L-	-31,57	-17,09	-26,90	-38,37	-34,22	-44,82	-56,00	-71,86	-58,35	-76,57	-104,54	-85,44
H Demand	31,57	17,09	26,90	38,37	34,22	44,82	56,00	71,86	58,35	76,57	104,54	85,44
H Auxiliary	-5,09	-2,53	-16,46	0,00	-17,07	-25,45	-0,18	0,00	-4,94	-13,31	0,00	0,00
L+	0,00	-1,12	0,00	0,00	0,00	0,00	0,00	0,00	0,00	0,00	0,00	0,00
G-	0,00	16,17	0,00	0,00	0,00	0,00	0,00	0,00	0,00	0,00	0,00	0,00
C Demand	0,00	16,17	0,00	0,00	0,00	0,00	0,00	0,00	0,00	0,00	0,00	0,00
C Auxiliary	0,00	-1,12	0,00	0,00	0,00	0,00	0,00	0,00	0,00	0,00	0,00	0,00
Irradiation	3109,22	3569,19	3616,21	1479,90	3254,99	4323,56	1371,13	778,31	2242,96	3891,93	250,04	371,25
Reflection	-1554,61	-1784,60	-1808,11	-739,95	-1627,49	-2161,78	-685,56	-389,15	-1121,48	-1945,96	-125,02	-185,63
Convection	-166,79	-211,97	-175,22	140,03	-17,26	-45,37	141,48	305,27	-4,22	-202,71	389,76	307,95
Emission	-1414,30	-1572,15	-1643,32	-918,35	-1627,39	-2135,78	-882,86	-766,28	-1170,66	-1806,51	-619,32	-579,01

Tab. 5.12 Second six months - cumulative quantities of parameters (W/m^2) - Opaque component – Boundary condition in table 5.3

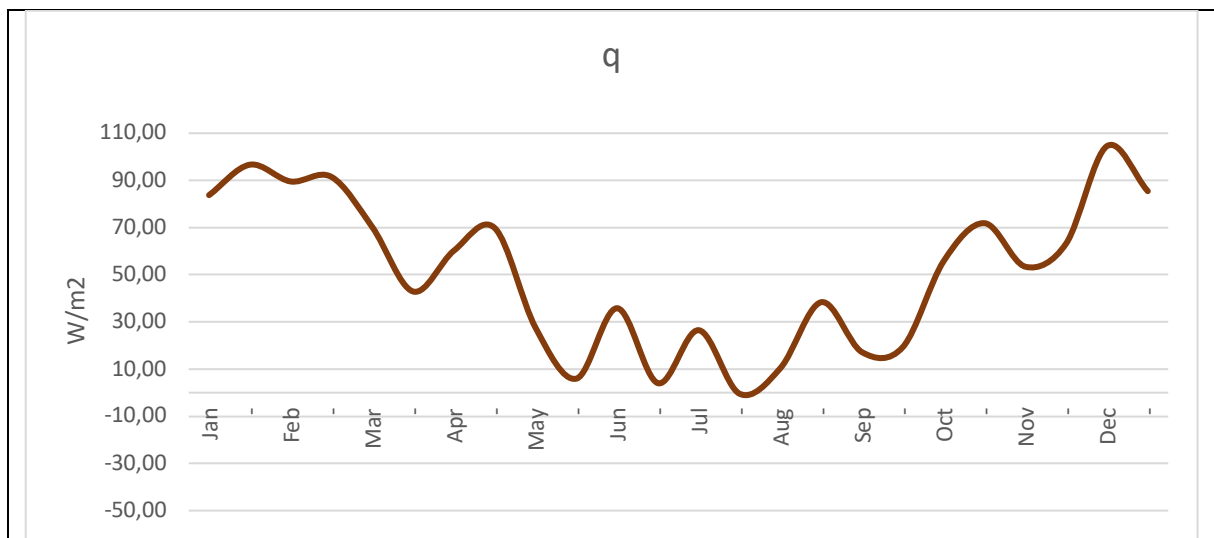


Fig. 5.9 Monthly amount of heat flow – cumulative calculation (W/m^2) - Opaque component – Boundary condition in table 5.3

The cumulative quantities of heat flow show an amount of $83.75 W/m^2$ on the 11th of January, while in the middle of summer on the 26th of July, it reaches a minimum of $17.09 W/m^2$, and in winter on the 11th of December, it reaches a maximum of $104.54 W/m^2$. The application of values of heat flows to the monthly quantities is depicted in Figure 5.10.

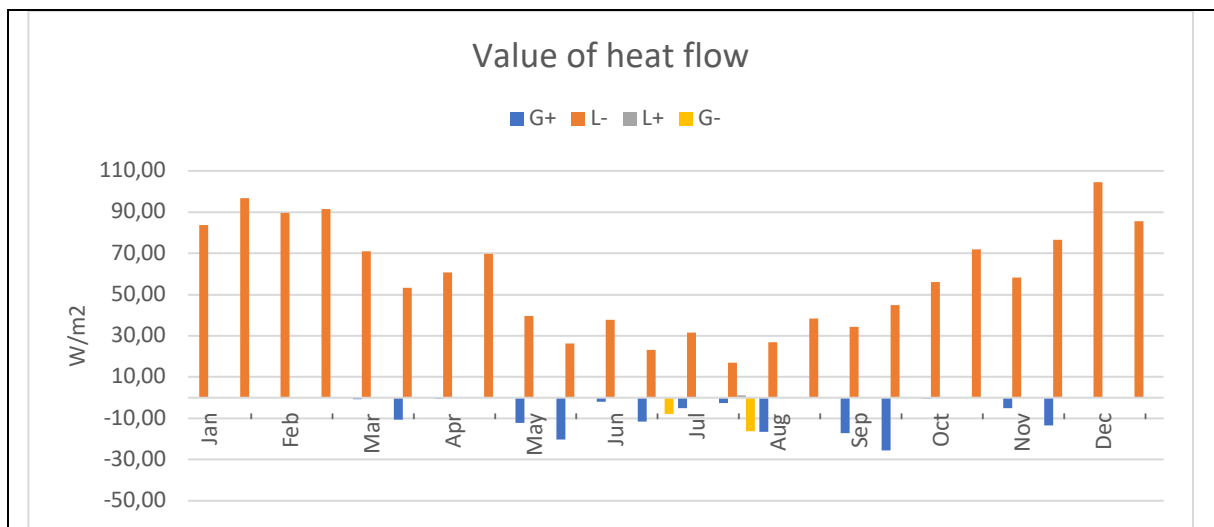


Fig. 5.10 Monthly amount of heat flow + values (W/m^2) – Interval 15 days - Opaque component – Boundary condition in table 5.3

By applying values of heat flows based on the difference between inside and outside air temperatures, portions of heat flow that can be used as heating auxiliary are observed in the middle months of the year (highlighted in blue). Similarly, on the 26th of June, 7.82 W/m² has been recorded as cooling demand, and an extremely low amount of 0.01 W/m² as cooling auxiliary (not notable in Figure 5.13). On the 26th of July, 16.17 W/m² is recorded as cooling demand, and a low amount of 1.12 W/m² as cooling auxiliary. Integrating the quantities of heat flows with their relative values for heating demand, cooling demand, heating auxiliary, and cooling auxiliary results in the annual performance of the component, illustrating its energy demands and auxiliaries (Figure 5.11).

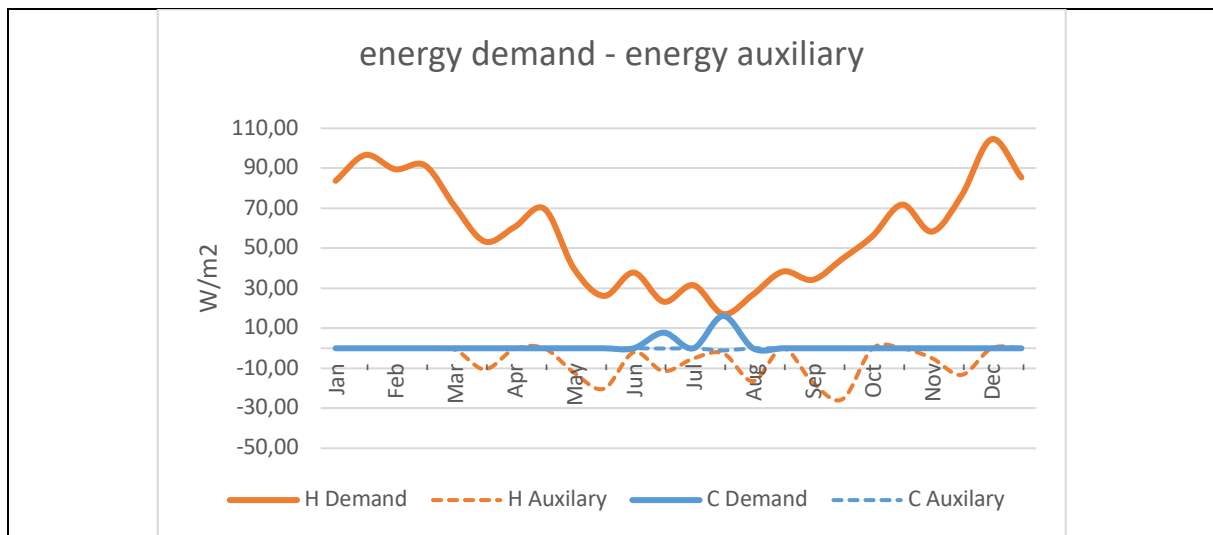


Fig. 5.11 Monthly heating demand, heating auxiliary, cooling demand, cooling auxiliary (W/m²) - Opaque component – Boundary condition in table 5.3

The monthly energy performance of the component demonstrates heating demand with a maximum and minimum of about 105 W/m² and 20 W/m², respectively. There are quantities of cooling demands occurring in the middle of summer with an average amount of 10 W/m². Additionally, a considerable proportion of heat flow from the beginning of March until the end of the year is allocated to auxiliary heating, with a maximum of 25.45 W/m² on the 26th of March.

This demonstrates that integrating values of heat flows results in the calculation of the amount of heating demand, as some parts of the heat flows are not considered as heating demand, and the final demand is moderated. Additionally, in upcoming parts of the work, the quantities of these heating (or cooling) auxiliaries will be used to compensate for the heating (or cooling) demand of united facades of the building, which simultaneously use different components. Integrating the quantities of auxiliaries will moderate the final demand of the entire considered facade. In the next three orientations of -90° (east), 180° (north), and +90° (west), representing daily performances of the component has been purposefully ignored. For the monthly energy performance of the component, the 'energy demand - energy auxiliary' graph is mainly discussed as it indicates the fundamental indexes for the upcoming work, namely 'self-sufficiency' and 'self-consumption'.

5.5.4 Orientation

To compare the energy performance of the component in different orientations with a constant inclination of 90°, Table 5.13 provides details of the configuration and boundary conditions of the proposed component.

Component	Inclination (°)	Orientation (°)	Inside temperature (Set)	Date	Heat conductivity (W/m.K)	Thickness (m)	U-value (W/m ² .K)	α_s (%)	h_i (W/m ² .K)
Opaque	90	0, -90, 180, +90	High	A year	0.03	0.20	0.15	50	7

Tab. 5.13 Boundary condition – Opaque component – different orientations

Integrating the quantities of heat flows based on relative values results in the monthly 'energy demand - energy auxiliary' of the component (Figure 5.12).

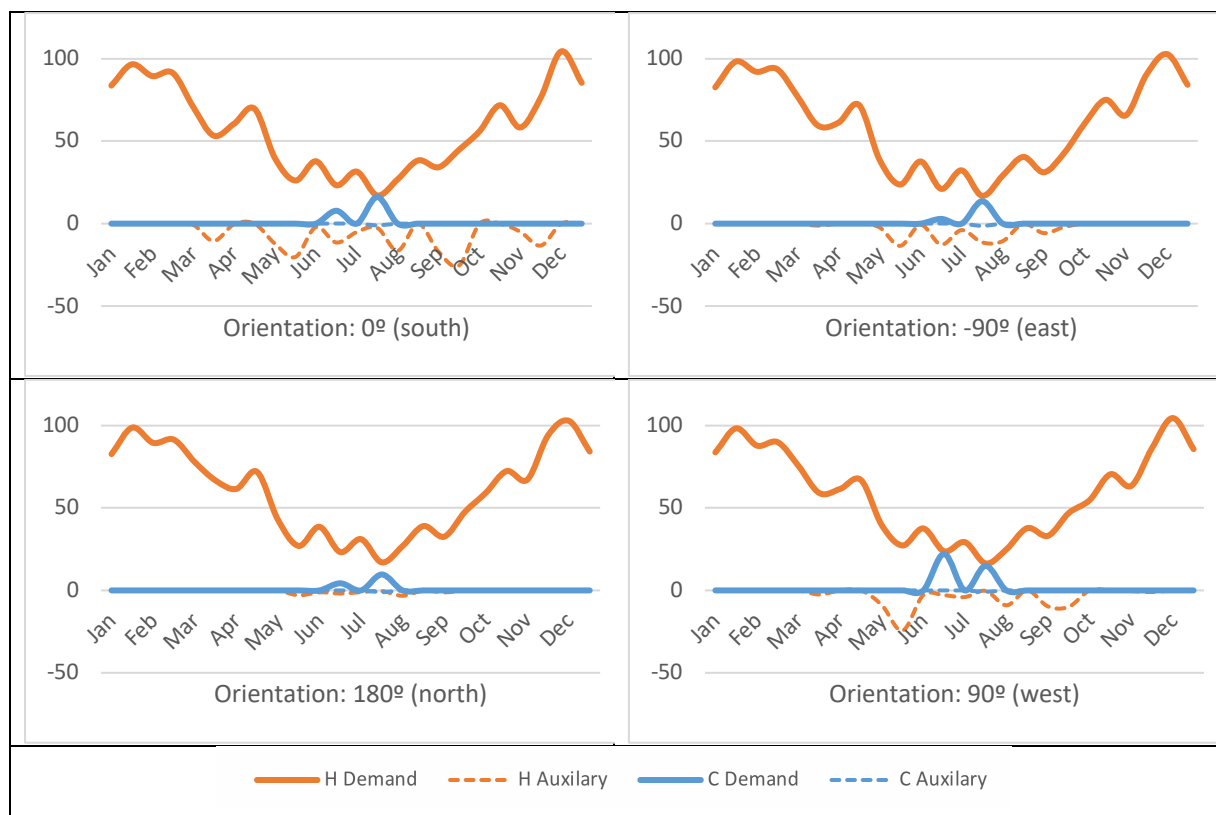


Fig. 5.12 Monthly heating demand, heating auxiliary, cooling demand, cooling auxiliary(W/m²) – Opaque component, Inclination 0°, all four orientations - Boundary condition in table 5.13

Comparing the curves reveals a notable difference in the quantities of cooling demand between different orientations. The most significant distinction is observed in heating auxiliary, where the north-facing component has nearly zero heating auxiliary, while the south-facing component provides a considerable amount of heating auxiliary. When comparing the quantities and time steps of heating auxiliary in the east and west orientations, it becomes evident that these orientations also differ in the quantities of their heating auxiliaries.

5.5.5 Inclination

Four inclinations of 90°, 60°, 30°, and 0° (roof) with a constant orientation of 0° (south) under different boundary conditions regarding 'inside air temperature' have been calculated and will be presented in upcoming graphs. A selective geometrical configuration, representing the south-facing component, has been chosen as an example to illustrate the effectiveness of inclination in altering the fluctuation and quantity of the final calculated indexes (heating and cooling demand and auxiliary). Table 5.14 provides details of the configuration and boundary conditions of the proposed component, and the results for each inclination are presented in Figure 5.13.

Component	Inclination (°)	Orientation (°)	Inside temperature (Set)	Date	Heat conductivity (W/m.K)	Thickness (m)	U-value (W/m ² .K)	α_s (%)	h_i (W/m ² .K)
Opaque	0, 30, 60, 90	0	High	A year	0.03	0.20	0.15	50	7

Tab. 5.14 Boundary condition – Opaque component – different inclinations

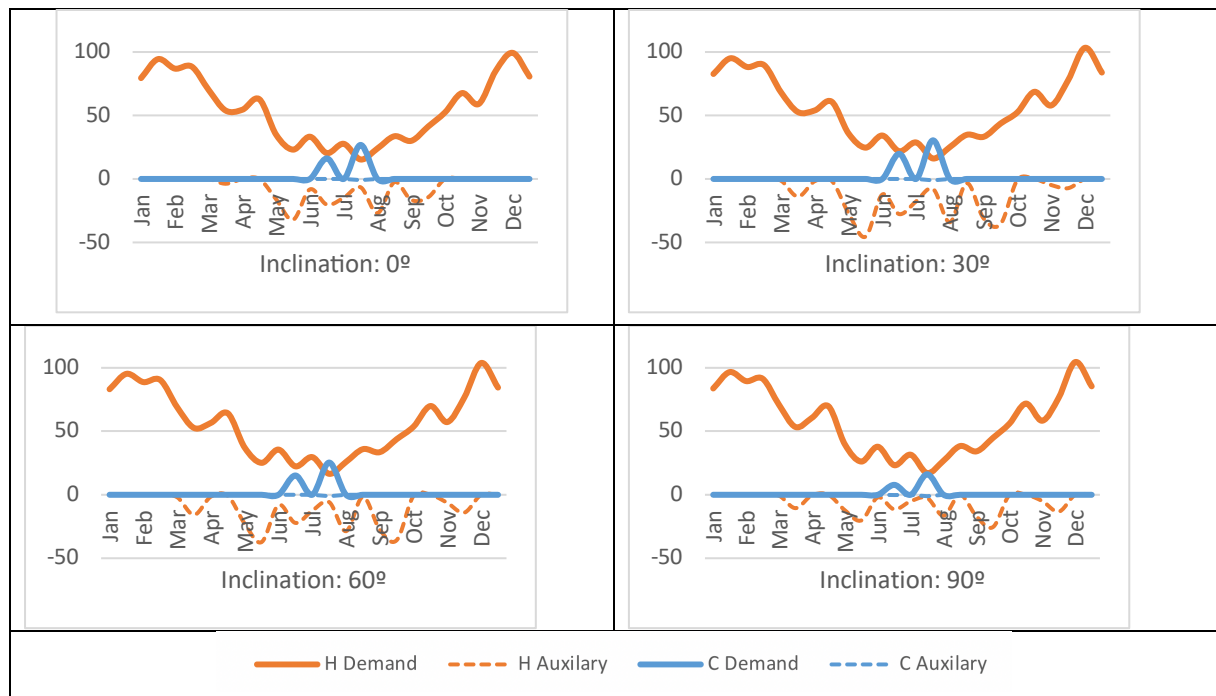


Fig. 5.13 Monthly heating demand, heating auxiliary, cooling demand, cooling auxiliary(W/m²) – Opaque component, All four inclinations, Orientation 0° - Boundary condition in table 5.14

More vertical components exhibit a higher maximum of heating demand during cold months, while cooling demand in more vertical components is lower. An inclination of 30° results in the highest amount of heating auxiliary compared to the other three inclinations.

5.5.6 Inside air temperature

A cumulative comparison of the quantity of indexes has been conducted in parallel. It should be noted that identifying the final indexes of this work as self-sufficiency and self-consumption will not be based on cumulative quantities but on the difference of quantities in intervals of calculation (1 hour). Regarding the representative component under the defined

boundary condition, a comparison of cumulative quantities of indexes through the four main orientations is shown in Figure 5.14.

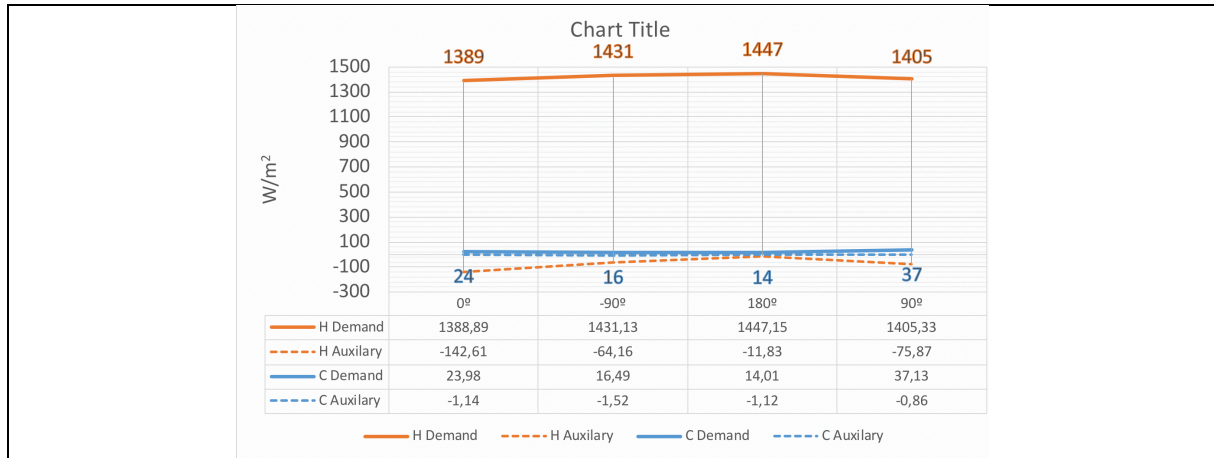


Fig. 5.14 Cumulative amount of heating demand, heating auxiliary, cooling demand, cooling auxiliary (W/m²) – Opaque component, Inclination 0°, all four orientations – Inside temperature: high

In terms of cumulative quantities of indexes, the orientation of 0° (south-facing) exhibits the lowest energy demand of 1389 W/m² and the highest heating auxiliary of 142 W/m². For the lowest cooling demand, the orientation of 180° (north-facing) demonstrates the lowest energy demand of 14 W/m². Changing the inside temperature setpoint under the same boundary conditions results in the same sequence of parameters but with different quantities. The upcoming boundary condition in Table 5.15 and the related comparison in Figure 5.15 are presented to illustrate the effectiveness of the inside temperature setpoint in cumulative quantities of energy indexes.

Component	Inclination (°)	Orientation (°)	Inside temperature (Set)	Date	Heat conductivity (W/m.K)	Thickness (m)	U-value (W/m ² .K)	α _s (%)	h _i (W/m ² .K)
Opaque	90	0, -90, 180, +90	Low	A year	0.03	0.20	0.15	50	7

Tab. 5.15 Boundary condition – Opaque component – different orientations – Inside set temperature: low

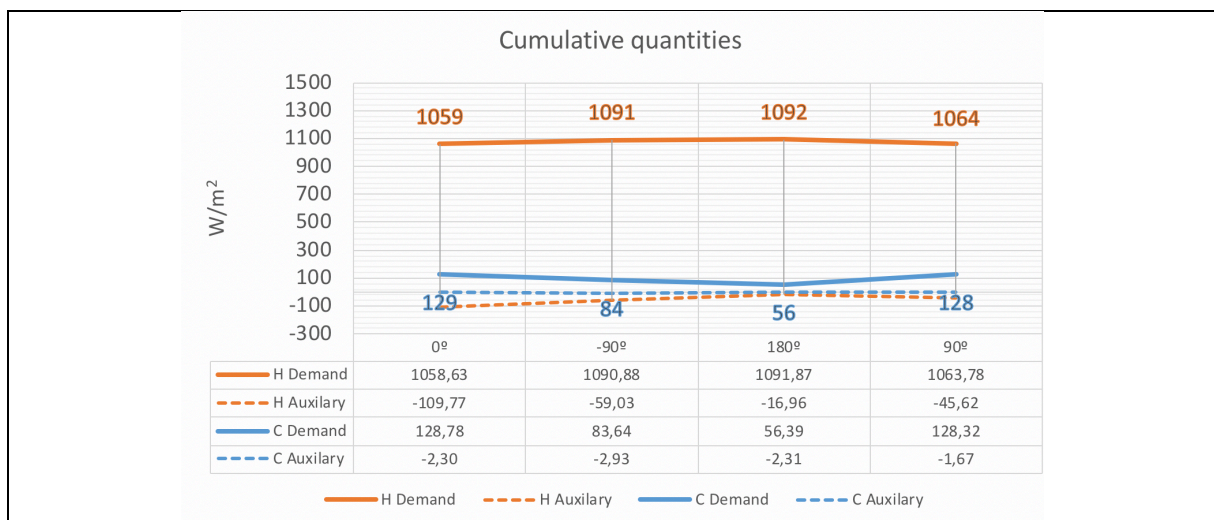


Fig. 5.15 Cumulative amount of heating demand, heating auxiliary, cooling demand, cooling auxiliary (W/m²) – Opaque component, Inclination 0°, all four orientations – Inside temperature: Low

To emphasize the differences in quantities of changing energy indexes solely based on the inside temperature setpoint, Figure 5.16 provides a comparative analysis of the results.

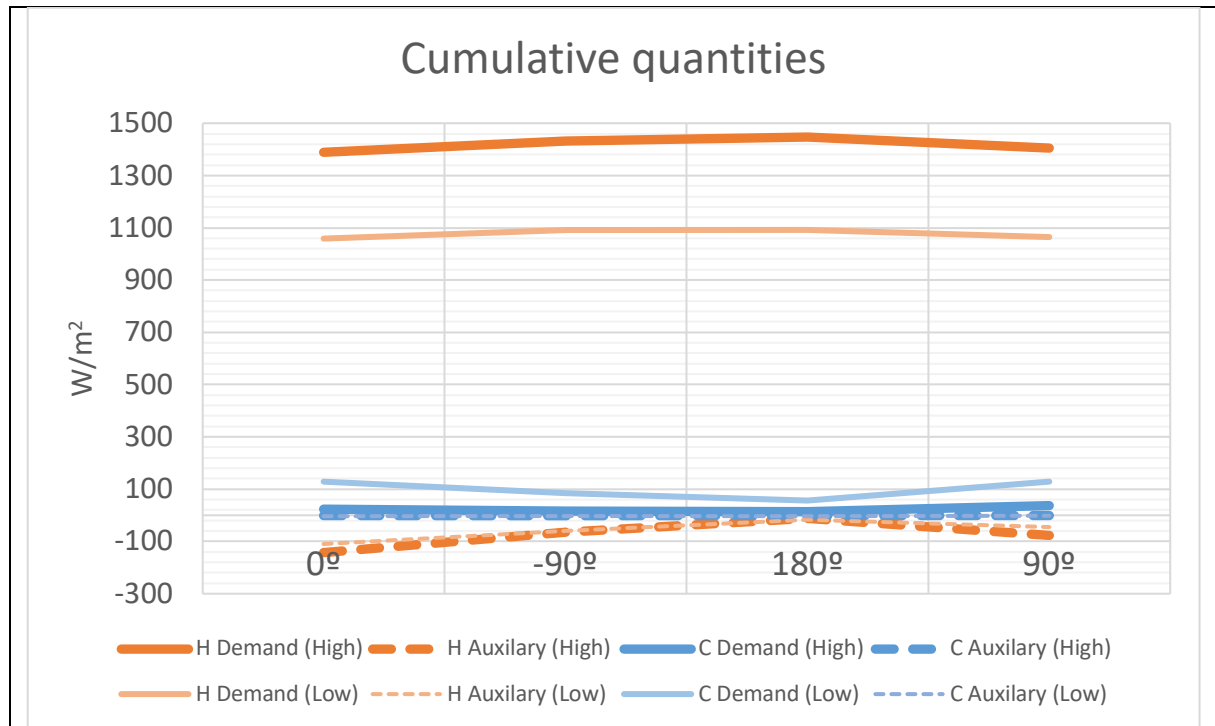


Fig. 5.16 Cumulative amount of heating demand, heating auxiliary, cooling demand, cooling auxiliary (W/m^2) – Opaque component, Inclination 0° , all four orientations – Inside temperature: high, low

Instead of cumulative differences resulting from applying different inside temperature setpoints, the quantity of changes in energy indexes based on an hourly calculation interval shows significant variations in terms of when demands are applied and their quantities. It can be concluded that different inside air temperature setpoints clearly impact the performance of a component with the same geometrical configuration. Figure 5.17 illustrates the performance under the same boundary conditions (Table 5.16), differing in inside air temperatures.

Component	Inclination ($^\circ$)	Orientation ($^\circ$)	Inside temperature	Date	Heat conductivity ($W/m.K$)	Thickness (m)	U-value ($W/m^2.K$)	α_s (%)	h_i ($W/m^2.K$)
Opaque	90	0	High, Low	A year	0.03	0.20	0.15	50	7

Tab. 5.16 Boundary condition – Opaque component – Inside set temperature: high / low

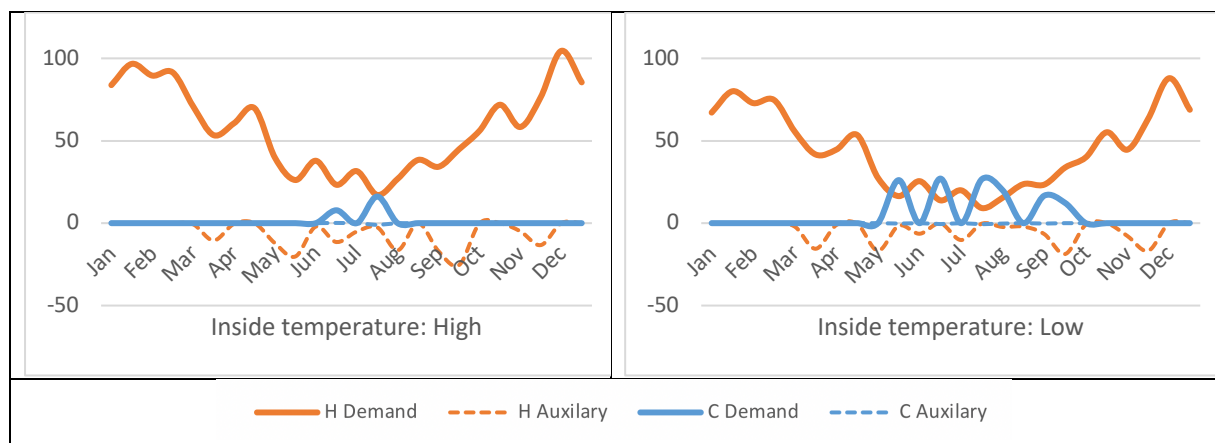


Fig. 5.17 Monthly heating demand, heating auxiliary, cooling demand, cooling auxiliary (W/m^2) – Opaque component, Inclination 0° , orientation 0° , Inside temperature; high (left), low (right)

Different inside air temperature setpoints, assumed from equations 4.1 and 4.3 for high and low setpoints, respectively, result in different quantities of all indexes. In the 'inside air temperature setpoint; high' scenario (left graph), the quantity of heating demand is higher during cold months, and this also leads to lower cooling demand compared to the same configuration when the inside air temperature is set to 'low'. The fluctuation of heating auxiliary is also partly different in each month for each 'inside air temperature set-point'. Cooling auxiliary for both 'inside air temperature' settings remains at approximately zero. To highlight the effectiveness of inclination in cumulative amounts of energy indexes for the proposed component, considering the boundary condition in Table 5.17, Figure 5.18 illustrates the differences in quantities and sequences of indexes.

Component	Inclination	Orientation	Inside temperature (Set)	Date	Heat conductivity (W/m.K)	Thickness (m)	U-value (W/m ² .K)	α_s (%)	h_i (W/m ² .K)
Opaque	0, 30, 60, 90	0	high, low	A year	0.03	0.20	0.15	50	7

Tab. 5.17 Boundary condition – Opaque component – different inclinations - Inside set temperature: high / low

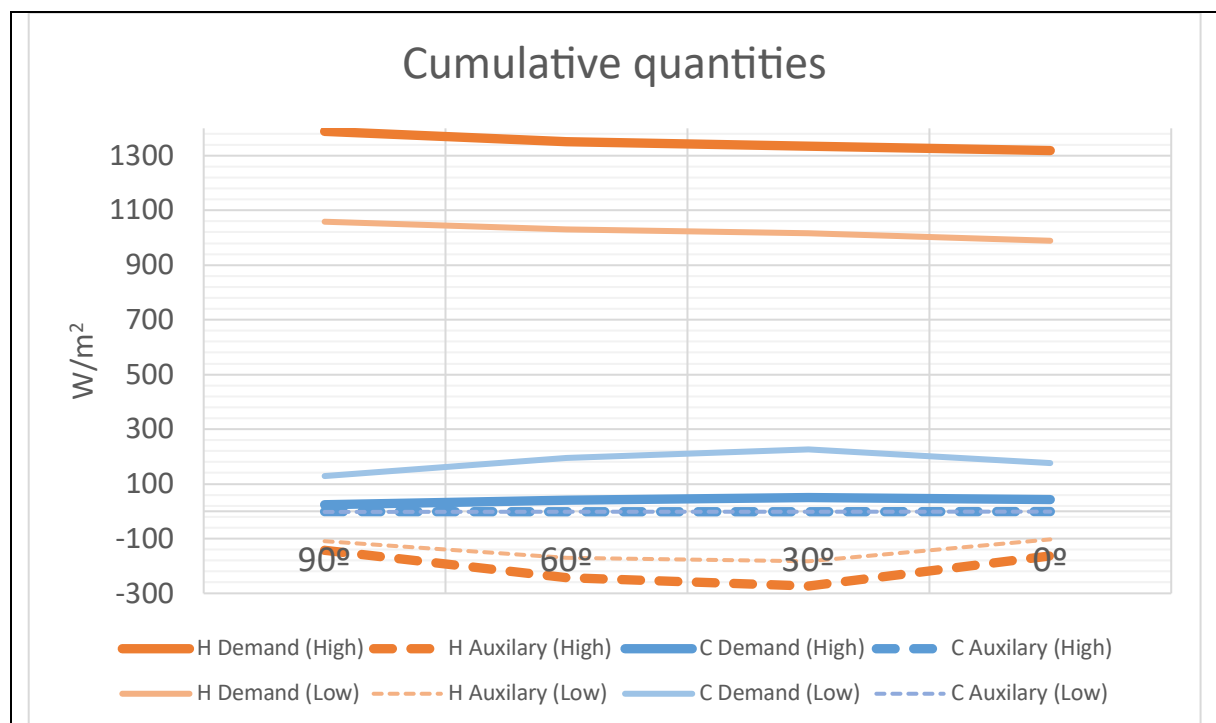


Fig. 5.18 Cumulative amount of heating demand, heating auxiliary, cooling demand, cooling auxiliary (W/m²) – Opaque component, orientation: 0°, inclinations: 0°, 30°, 60° and 90° – Inside temperature: high, low

5.6 Calibration of calculated surface temperature

Sol-air temperature is directly employed to calculate the 'outside surface temperature.' As a result, the accuracy of the calculated 'inside surface temperature' as well as the 'heat flow' depends on the accuracy of the 'calculated outside surface temperature.' To assess this accuracy, simulation software such as DesignBuilder, which serves as an advanced user interface for EnergyPlus, is employed. EnergyPlus offers advanced dynamic thermal simulation at sub-hourly timesteps. Therefore, while this work employs the 'steady heat transfer' method in calculating temperatures, comparing the recorded results with software that provides dynamic simulations using the 'unsteady heat transfer' method can help identify deviations in the recorded temperatures.

5.6.1 Winter day

As a winter day, the 26th of January has been chosen. To compare the results of the recorded 'T_{s-out}' with those obtained from simulation software, an east-oriented vertical opaque component was selected. The boundary conditions for the calculated wall is: (Table 5.18)

Component	Inclination (°)	Orientation (°)	Inside temperature (Set)	Heat conductivity (W/m.K)	Thickness (m)	U-value (W/m ² .K)	α _s (%)	h _i (W/m ² .K)
Opaque	90	-90 east	high	0.03	0.2	0.15	50	7

Tab. 5.18 Boundary condition – Opaque component

Figure 5.19 shows the calculated outside surface temperature on the 26th of January.



Fig. 5.19 Outside air and surface temperature of component – boundary condition table 5.18

The fluctuation of temperature in DesignBuilder is shown in Figure 5.20.

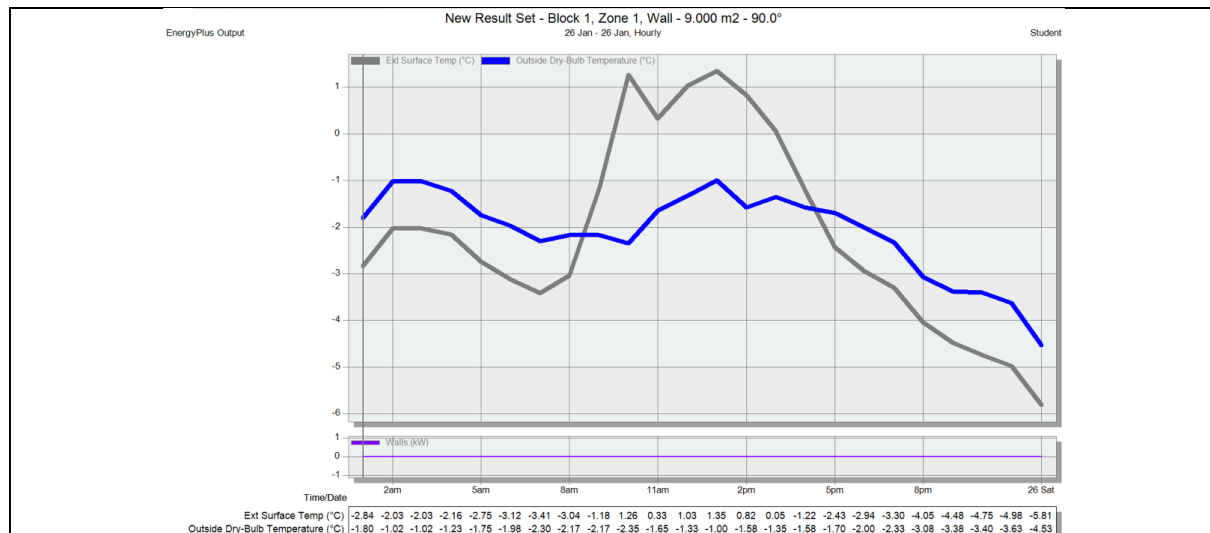


Fig. 5.20 Outside air and surface temperature of component –calculated by DesignBuilder - boundary condition table 5.18

Comparing the fluctuations of recorded outside surface temperature in the work and the simulations in DesignBuilder demonstrates that the same sequence of increasing and decreasing temperatures is calculated. Extensive recorded temperatures for each hour are included in both the calculated temperatures in this work and the simulated temperatures produced by DesignBuilder.

5.6.2 Summer day

The same comparison was conducted on a summer day. Therefore, July 26th was selected, and the same component with the same geometrical setup was calculated and simulated. Figure 5.21 shows the calculated outside surface temperature on July 26th.



Fig. 5.21 Outside air and surface temperature of component – boundary condition table 5.18

With the same boundary conditions, the fluctuation of temperature calculated by DesignBuilder is shown in Figure 5.22.

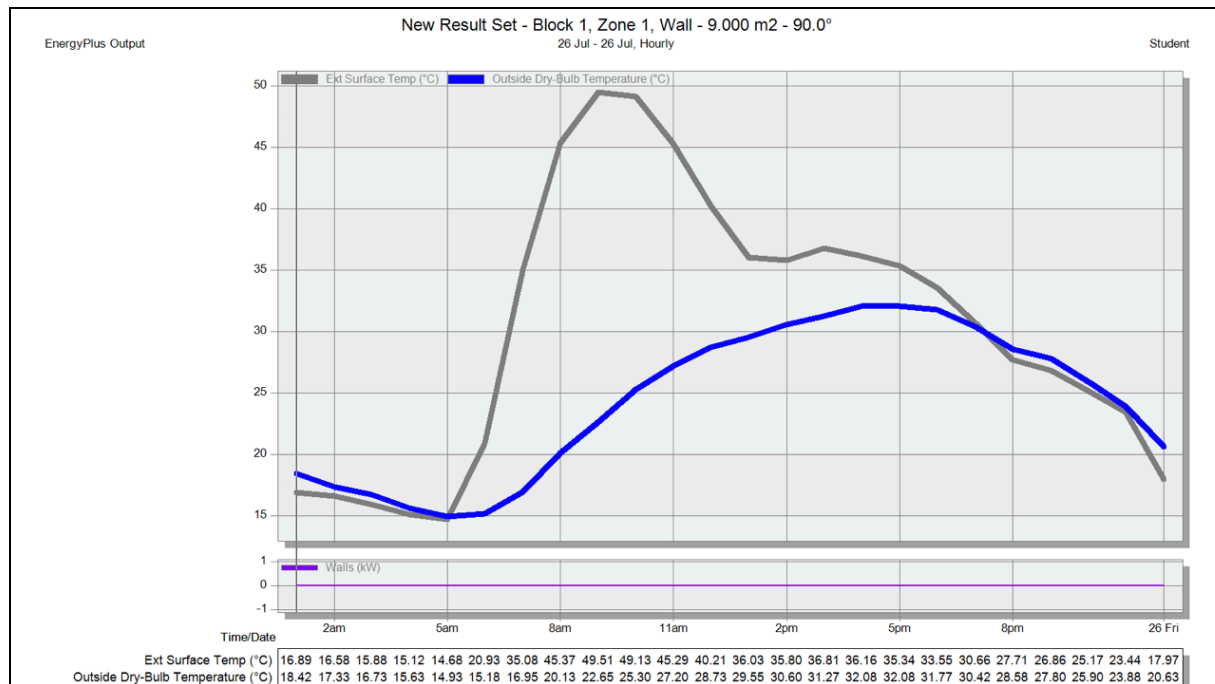


Fig. 5.22 Outside air and surface temperature of component – calculated by DesignBuilder - boundary condition table 5.18

Comparing the calculated temperatures in the work with the simulated temperatures in DesignBuilder shows the same intervals of increases and decreases in the graphs. Extensive recorded temperatures for each hour are included in both the calculated temperatures of this work and the simulated temperatures generated by DesignBuilder.

5.6.3 Deviation

Comparison of the calculated surface temperatures (T_{s-out}) of the east-oriented vertical opaque component in winter with the surface temperatures obtained from the simulation tools of DesignBuilder is presented in Figure 5.23.

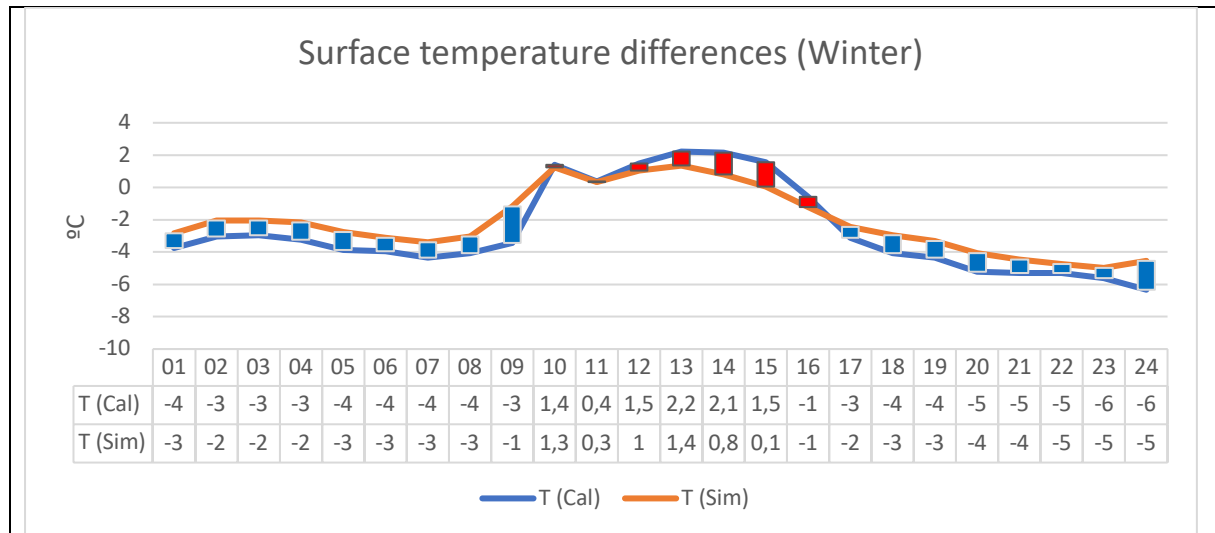


Fig. 5.23 Deviation of outside surface temperature of component – winter day - Calculations and simulation-boundary condition table 5.18

Considering the entire 24 hours of a winter day as calculation intervals and taking into account the temperature differences between the calculations in this work and the simulation tool of DesignBuilder, an average difference of $-0.537\text{ }^{\circ}\text{C}$ is calculated across all 24 calculation points. This calculated deviation should be studied in relation to the range of outside surface temperatures recorded by 'DesignBuilder,' which indicates a minimum of $-4.98\text{ }^{\circ}\text{C}$ (at 23:00) and a maximum of $+1.35\text{ }^{\circ}\text{C}$ (at 13:00), resulting in a fluctuation of $6.33\text{ }^{\circ}\text{C}$. Table 5.19 displays the outside surface temperature of the component on a winter day as calculated and simulated using the software.

Hr	01	02	03	04	05	06	07	08	09	10	11	12	13	14	15	16	17	18	19	20	21	22	23	24
Cal	-	-	-	-	-	-	-	-	-	+	+	+	+	+	+	-	-	-	-	-	-	-	-	-
	3.7	3.0	2.9	3.2	3.8	3.9	4.3	4.0	3.4	1.4	0.3	1.4	2.2	2.1	1.5	0.5	3.1	4.0	4.3	5.2	5.3	5.3	5.6	6.3
Sim	-	-	-	-	-	-	-	-	-	+	+	+	+	+	+	-	-	-	-	-	-	-	-	-
	2.8	2.0	2.0	2.1	2.7	3.1	3.4	3.0	1.1	1.2	0.3	1.0	1.3	0.8	0.0	1.2	2.4	2.9	3.3	4.0	4.4	4.7	4.9	4.5
Dif.	-	-	-	-	-	-	-	-	-	+	+	+	+	+	+	+	-	-	-	-	-	-	-	-
	0.9	1.0	0.9	1.0	1.1	0.8	0.9	1.0	2.2	0.1	0.0	0.4	0.8	1.3	1.4	0.6	0.6	1.1	1.0	1.1	0.8	0.5	0.6	1.8

Tab. 5.19 Outside surface temperature of component – winter day - Calculations and simulation

So, a deviation of $-0.537\text{ }^{\circ}\text{C}$ is recorded within a temperature fluctuation of $6.33\text{ }^{\circ}\text{C}$ in the calculated outside surface temperature of the component on a winter day. The colors red and blue represent higher and lower calculated temperatures compared to the results from DesignBuilder, respectively.

Furthermore, a comparison of the calculated surface temperatures (T_{s-out}) of the same component in the summer with the surface temperature obtained from the simulation tool of DesignBuilder is presented in Figure 5.24.

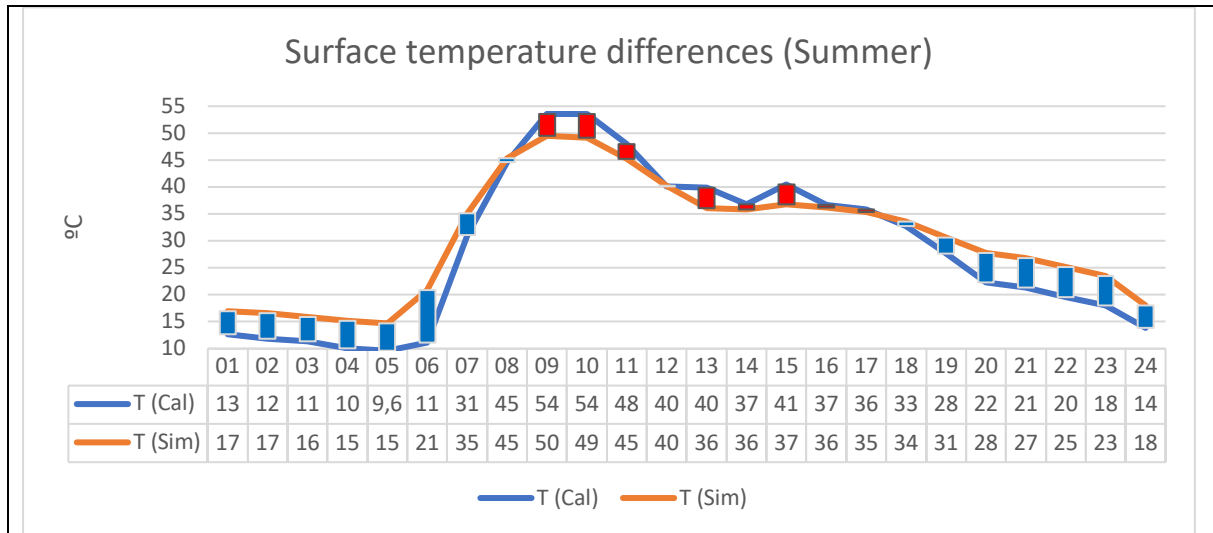


Fig. 5.24 Deviation of outside surface temperature of component – summer day - Calculations and simulation-boundary condition table 5.18

Considering the entire 24 hours of a summer day as calculation intervals and taking into account the temperature differences between the calculations in this work and the simulation tool of DesignBuilder, an average difference of $-1.987\text{ }^{\circ}\text{C}$ is calculated across all 24 calculation points. This calculated deviation should be studied in relation to the range of outside surface temperatures recorded by 'DesignBuilder,' which indicates a minimum of $+14.68\text{ }^{\circ}\text{C}$ (at 05:00) and a maximum of $+49.51\text{ }^{\circ}\text{C}$ (at 09:00), resulting in a fluctuation of $34.83\text{ }^{\circ}\text{C}$. Table 5.20 displays the outside surface temperature of the component on a summer day as calculated and simulated using the software.

Hr	01	02	03	04	05	06	07	08	09	10	11	12	13	14	15	16	17	18	19	20	21	22	23	24
Cal	+12.6	+11.8	+11.3	+10.0	+9.6	+11.0	+31.0	+44.6	+53.5	+53.5	+47.9	+40.0	+39.8	+36.7	+40.5	+36.6	+35.8	+32.7	+27.6	+22.3	+21.3	+19.5	+17.9	+13.8
Sim	+16.8	+16.5	+15.8	+15.1	+14.6	+20.9	+35.0	+45.3	+49.5	+49.1	+45.2	+40.2	+36.0	+35.8	+36.8	+36.1	+35.3	+33.5	+30.6	+27.7	+26.8	+25.1	+23.4	+17.9
Dif.	-4.2	-4.7	-4.5	-5.0	-5.0	-9.8	-4.1	-0.7	-4.6	-4.4	-2.6	-0.1	+3.8	+0.9	+3.6	+0.4	+0.4	+0.8	-3.2	-5.4	-5.5	-5.5	-5.4	-4.0

Tab. 5.20 Outside surface temperature of component – summer day - Calculations and simulation

A deviation of $-1.987\text{ }^{\circ}\text{C}$ is observed within a temperature fluctuation of $34.83\text{ }^{\circ}\text{C}$ in the calculated outside surface temperature of the component on a summer day. Regarding the equations employed in the calculation method of this work under steady-state conditions, fluctuations in the calculated temperatures for both winter and summer representative days indicate 'higher maximums' and 'lower minimums' compared to the results of 'DesignBuilder,' a simulation tool that employs dynamic equations in its calculations. As a result, in the absence of a 'time lag' of heat flow under steady-state conditions, despite differences in recorded temperatures, the temperature curves over 24 hours in both winter and summer days demonstrate acceptable ranges of calculated temperatures compared to DesignBuilder. When considering the red and blue colors indicating higher and lower recorded temperatures compared to DesignBuilder, it becomes apparent that the difference in the numerical sum of recorded temperatures under steady-state conditions is moderated in comparison with DesignBuilder's results under unsteady-state conditions.

5.7 Transparent component

5.7.1 Daily performance - Summer day

On a summer day, specifically on the 26th of July at 11:00, the calculation procedure and the employed parameters are described in detail in Table 5.21, presenting the configuration and boundary conditions of the proposed component.

Component	Inclination (°)	Orientation (°)	Inside temperature (Set)	Date	Transmittance factor	U-value (W/m ² .K)	h _i (W/m ² .K)
Transparent	90	0	High	26 th Jan 26 th Jul	1.5	0.50	7

Tab. 5.21 Boundary condition – Transparent component

Table 5.22 presents constant values of parameters.

Component properties & geometry				
n	Parameter	Symbol	Value	Unit
	Thermal transmittance	U-value	0.50	W/ m ² k
	coefficient of reduction in radiation transmittance (Type of glass)		1.50	-
	Reduction factor for direct light	r(B(ω)) *	0.54	
	reduction factor for diffuse light	r(D(ω)) **	0.77	
	Reflection ratio	γ _f	0,38	
	Absorption coefficient	α _f	0,11	
	Transmission coefficient	τ _f	0,51	
	Component emissivity	ε	0.90	
	Surface tilt	β	90	°
	Surface azimuth	α	0	°
(* equation 4.8, ** equation 4.9)				

Tab. 5.22 Transparent component – properties and specific geometrical configuration - Boundary condition table 5.21

Specific reduction factors for direct and diffuse light, taking into account the reduction coefficient (type of glass) and 'cos ω' as the direct beam intensity coefficient on the surface of the component, have been applied. This consideration results in different proportions of reflection, absorption, and transmission for various types of glass, which also vary with different angles of irradiation (as shown in Table 5.22). Calculations of surface temperatures and heat flow are presented in Table 5.23.

N	Parameter	Symbol	Equation	Result	Unit
06	Solar-air temperature	T _{sol-air}	4.12	301,27	°C
07	Thermal resistance excluding outside air film resistance	ΣRI	4.20	2,14	m ² k/W
08	Thermal resistance excluding inside and outside air film resistances	ΣRII	4.20	2,00	m ² k/W
09	Outside surface temperature	T _{s-out}	4.13	301,22	°K
10	Inside surface temperature	T _{s-in}	4.14	300,15	°K
11	Heat flow	q	4.15	0,54	W/m ²

Tab. 5.23 Calculation of surface temperatures – heat flow – Transparent component - Boundary condition table 5.21

The division of irradiation diffraction is calculated based on the proportions of reflection, emission, and convection, respectively, as shown in Table 5.24.

N	Parameter	Symbol	Equation	Result	Unit
12	outside reflection from surface of component	q_{ref}	$q_{ref} = Q_{sol} - (B_{(h)}r_{B(\omega)} + D_{(h)}r_{D(\omega)})$	-181,51	W/m ²
13	outside emission from surface of component	q_{rad}	4.19	-52,18	W/m ²
14	outside convection from surface of component	q_{con}	4.18	-2,32	W/m ²
15	Transmission	q_{tr}	$0.815 \cdot (q_{sol} - q_{ref})$	-242,47	W/m ²

Tab. 5.24 Dividing diffraction of irradiation – Transparent component - Boundary condition table 5.21

On the 26th of July, as a summer day, using the same calculations and procedures, the results are presented in the upcoming table and graph. Table 5.25 displays the calculated inside and outside surface temperatures of the transparent component and the resulting heat flows.

	T _{out}	T _{in}	T _{s-out}	T _{s-in}	q	Direction	G+	L-	L+	G-	Irradiation	Reflection	Convection	Emission	Transmission	Conduction
01:00	18,00	25,83	14,16	25,06	-5,45	L-		-5,45			0,00	0,00	21,36	-26,81	0,00	-5,45
02:00	17,10	25,73	13,34	24,91	-5,79	L-		-5,79			0,00	0,00	21,10	-26,89	0,00	-5,79
03:00	16,60	25,68	12,88	24,82	-5,97	L-		-5,97			0,00	0,00	20,93	-26,90	0,00	-5,97
04:00	15,30	25,53	11,63	24,60	-6,49	L-		-6,49			0,00	0,00	20,92	-27,40	0,00	-6,49
05:00	14,80	25,47	11,17	24,52	-6,68	L-		-6,68			0,00	0,00	20,78	-27,46	0,00	-6,68
06:00	15,30	25,53	11,87	24,62	3,44	G+	3,44				15,60	-3,57	19,49	-28,09	-9,81	-6,37
07:00	17,50	25,78	14,76	25,04	41,70	G+	41,70				74,50	-17,03	15,26	-31,03	-46,84	-5,14
08:00	21,00	26,17	18,70	25,67	76,68	G+	76,68				138,46	-40,09	12,35	-34,04	-80,17	-3,49
09:00	23,20	26,42	21,47	26,09	112,40	G+	112,40				257,93	-117,19	9,06	-37,41	-114,71	-2,31
10:00	26,00	26,74	25,26	26,64	178,87	G+	178,87				382,78	-162,46	3,72	-45,17	-179,56	-0,69
11:00	27,60	26,92	28,07	27,00	243,01	G-				243,01	479,02	-181,51	-2,32	-52,18	-242,47	0,54
12:00	29,10	27,09	29,99	27,28	277,40	G-				277,40	507,77	-169,07	-4,32	-56,98	-276,04	1,36
13:00	29,70	27,16	29,75	27,33	243,58	G-				243,58	418,27	-120,89	-0,25	-53,55	-242,37	1,21
14:00	30,90	27,29	28,69	27,38	145,64	G-				145,64	239,50	-61,59	10,68	-42,94	-144,99	0,65
15:00	31,40	27,35	30,44	27,55	209,33	G-				209,33	383,39	-128,31	4,59	-50,34	-207,88	1,44
16:00	32,30	27,45	29,85	27,61	140,42	G-				140,42	291,68	-120,76	11,62	-42,12	-139,30	1,12
17:00	32,00	27,42	29,14	27,53	109,60	G-				109,60	178,39	-44,90	13,68	-37,58	-108,80	0,80
18:00	31,70	27,38	28,37	27,45	77,48	G-				77,48	122,50	-28,00	16,02	-33,04	-77,02	0,46
19:00	30,00	27,19	25,85	27,10	43,26	G-				43,26	69,80	-15,95	20,45	-31,04	-43,88	-0,63
20:00	28,10	26,98	23,35	26,73	4,34	G-				4,34	9,60	-2,19	23,98	-27,04	-6,04	-1,69
21:00	27,70	26,93	22,81	26,66	-1,92	L+					0,00	0,00	24,85	-26,77	0,00	-1,92
22:00	25,30	26,66	20,98	26,28	-2,65	L+					0,00	0,00	22,40	-25,05	0,00	-2,65
23:00	23,40	26,44	19,37	25,97	-3,30	L-					0,00	0,00	21,29	-24,59	0,00	-3,30
24:00	19,30	25,98	15,37	25,27	-4,95	L-					0,00	0,00	21,60	-26,55	0,00	-4,95

Tab. 5.25 Inside and outside surface temperatures (°C) – Effect of reflection, convection and emission (W/m²) – Transparent component - Boundary condition table 5.21

The quantities of heat flow through 'conduction' are shown in Figure 5.25, while the cumulative quantities of heat flow resulting from 'conduction and transmission' are shown in Figure 5.26.

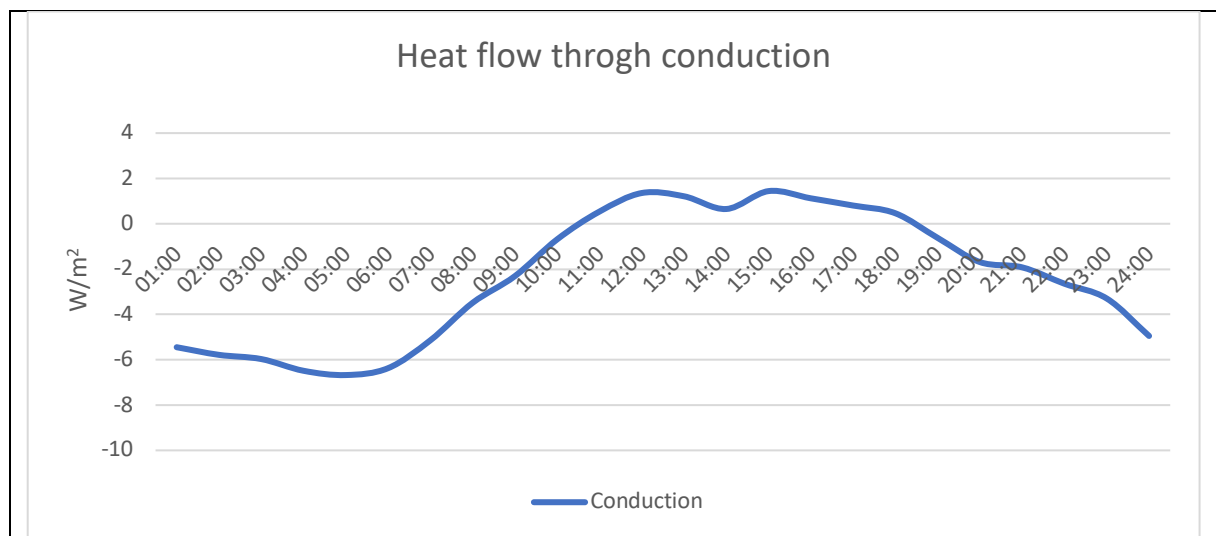


Fig. 5.25 Quantities of heat flow through “conduction” (W/m²) – transparent component- Boundary condition table 5.21

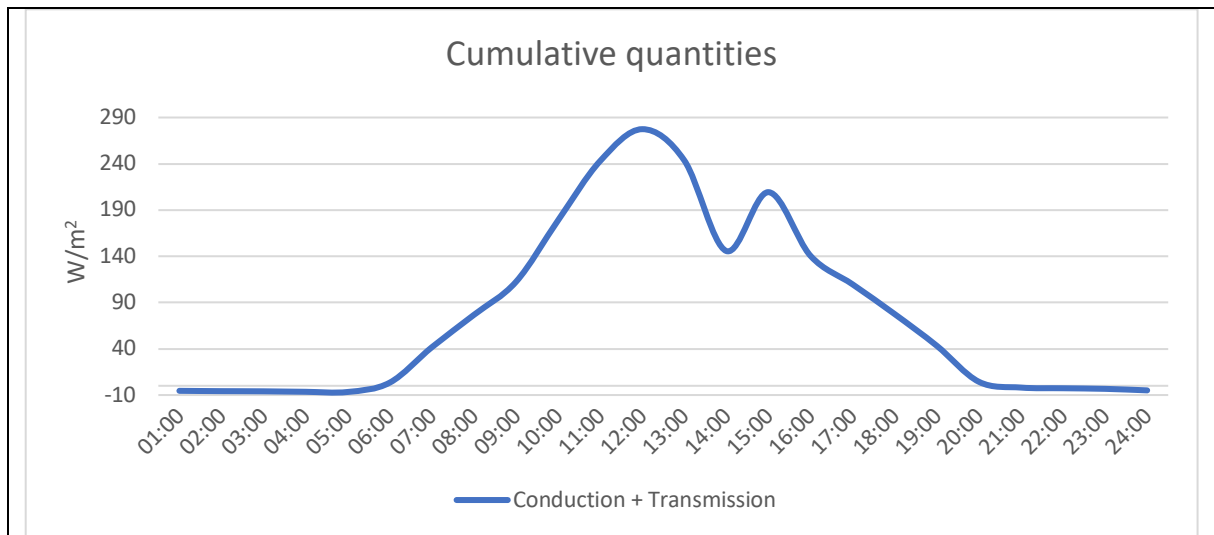


Fig. 5.26 Cumulative quantities of heat flow resulted by “conduction and transmission” (W/m^2) - Transparent component - Boundary condition table 5.21

Applying the values of heat flows to their quantities results in the graph shown in Figure 5.27.

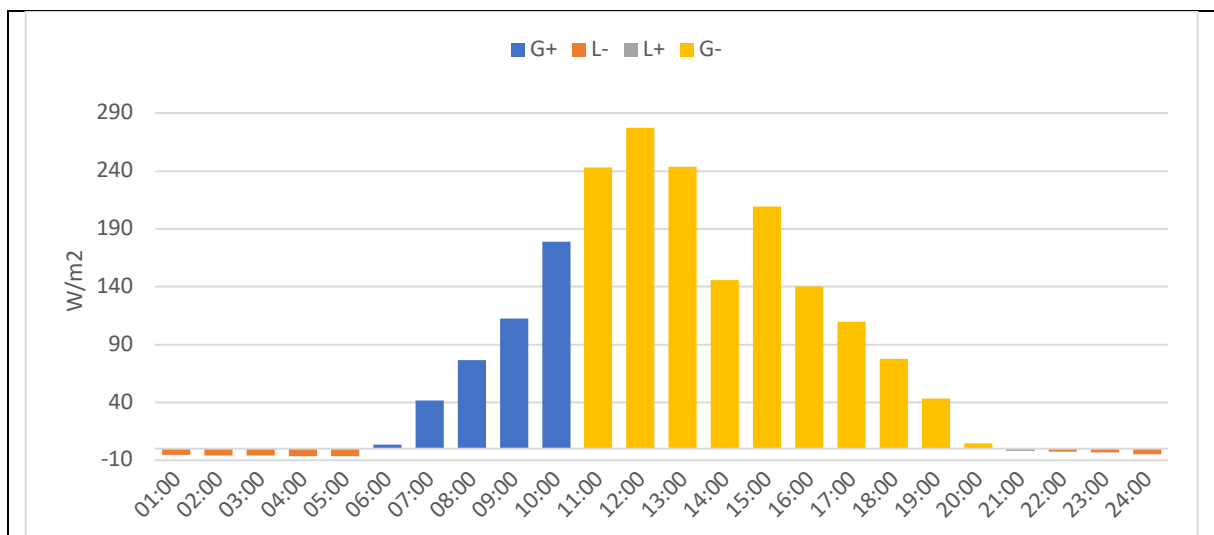


Fig. 5.27 Hourly amount of heat flow + values (W/m^2) - Transparent component - Boundary condition table 5.21

All four heat flow values are observed after applying values to the quantity of heat flow, considering the defined boundary conditions. On a representative day, from the beginning of the day until 06:00, the component indicates equal quantities of heating demand. From 06:00 until 11:00, it indicates heating auxiliary. From 11:00 until 21:00, during a summer afternoon, the component delivers considerable amounts of cooling demand. From 21:00 until 22:00, it shows cooling auxiliary. During the last three hours of the day, it again shows quantities of heating demand.

The outside and inside surface temperatures as well as air temperatures are shown in Figure 5.28.

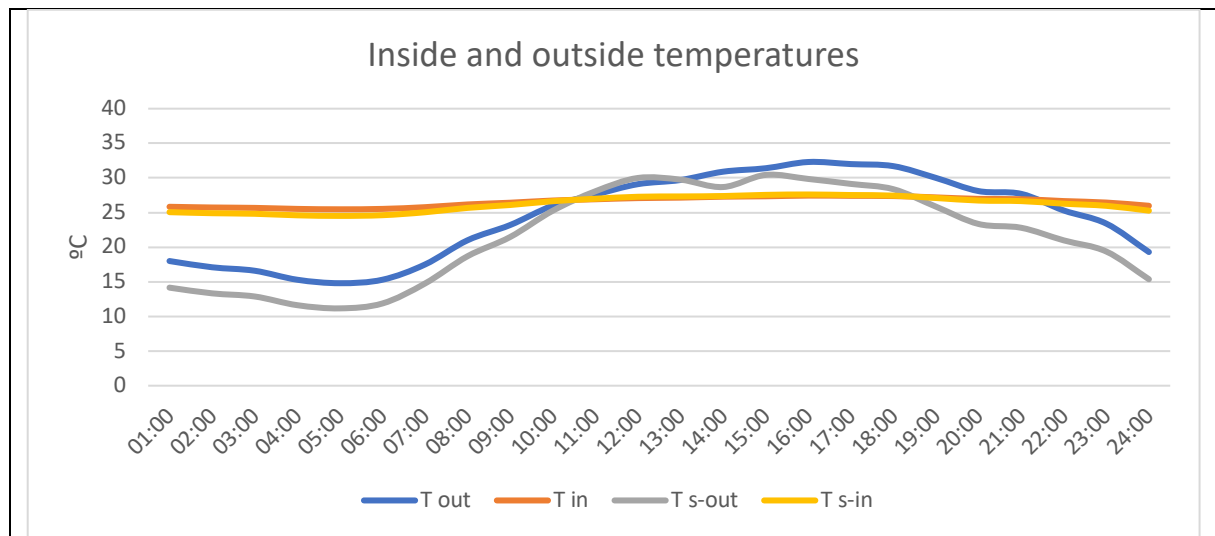


Fig. 5.28 outside temperature (°C), inside temperature (°C), outside surface temperature (°C) and inside surface temperature (°C) - Transparent component - Boundary condition table 5.21

5.7.2 Daily performance - Winter day

Table 5.26 displays the calculated inside and outside surface temperatures of the supposed transparent component with respect to the employed boundary conditions.

	T out	T in	T s-out	T s-in	q	Direction	G+	L-	L+	G-	Irradiation	Reflection	Convection	Emission	Transmission	Conduction
01:00	-0,80	23,71	-4,02	21,86	-12,94	L-		-12,94			0,00	0,00	14,99	-27,93	0,00	-12,94
02:00	-1,10	23,68	-4,20	21,82	-13,01	L-		-13,01			0,00	0,00	14,47	-27,48	0,00	-13,01
03:00	-1,00	23,69	-4,18	21,83	-13,00	L-		-13,00			0,00	0,00	14,79	-27,80	0,00	-13,00
04:00	-1,30	23,65	-4,43	21,78	-13,10	L-		-13,10			0,00	0,00	14,60	-27,70	0,00	-13,10
05:00	-1,90	23,59	-5,05	21,68	-13,36	L-		-13,36			0,00	0,00	14,78	-28,14	0,00	-13,36
06:00	-2,00	23,57	-5,14	21,66	-13,40	L-		-13,40			0,00	0,00	14,78	-28,18	0,00	-13,40
07:00	-2,40	23,53	-5,54	21,59	-13,57	L-		-13,57			0,00	0,00	14,83	-28,39	0,00	-13,57
08:00	-2,10	23,56	-5,25	21,64	-13,45	L-		-13,45			0,00	0,00	14,82	-28,27	0,00	-13,45
09:00	-2,20	23,55	-5,09	21,64	-5,07	L-		-5,07			13,20	-3,02	13,60	-28,85	-8,30	-13,37
10:00	-2,40	23,53	-3,22	21,75	80,10	G+	80,10				133,26	-19,65	3,84	-37,34	-92,59	-12,48
11:00	-1,40	23,64	-3,36	21,84	37,55	G+	37,55				77,62	-16,08	9,11	-33,09	-50,15	-12,60
12:00	-1,30	23,65	-2,89	21,88	52,71	G+	52,71				100,74	-20,87	7,38	-34,54	-65,10	-12,39
13:00	-0,90	23,70	-2,35	21,96	58,68	G+	58,68				109,60	-22,68	6,69	-34,93	-70,84	-12,16
14:00	-1,80	23,60	-1,08	21,95	146,76	G+	146,76				224,49	-30,28	-3,31	-44,13	-158,28	-11,52
15:00	-1,20	23,66	-1,28	22,00	118,36	G+	118,36				189,37	-29,86	0,38	-41,53	-130,00	-11,64
16:00	-1,70	23,61	-3,28	21,82	49,84	G+	49,84				97,30	-20,74	7,35	-34,06	-62,39	-12,55
17:00	-1,70	23,61	-4,68	21,72	-6,41	L-		-6,41			10,80	-2,47	13,97	-28,71	-6,79	-13,20
18:00	-2,10	23,56	-5,22	21,64	-13,43	L-		-13,43			0,00	0,00	14,70	-28,13	0,00	-13,43
19:00	-2,40	23,53	-5,49	21,59	-13,54	L-		-13,54			0,00	0,00	14,58	-28,12	0,00	-13,54
20:00	-3,30	23,43	-6,33	21,44	-13,89	L-		-13,89			0,00	0,00	14,43	-28,32	0,00	-13,89
21:00	-3,40	23,42	-6,43	21,43	-13,93	L-		-13,93			0,00	0,00	14,43	-28,36	0,00	-13,93
22:00	-3,40	23,42	-6,41	21,43	-13,92	L-		-13,92			0,00	0,00	14,31	-28,22	0,00	-13,92
23:00	-3,70	23,38	-6,71	21,38	-14,04	L-		-14,04			0,00	0,00	14,35	-28,39	0,00	-14,04
24:00	-0,60	23,73	-3,83	21,89	-12,86	L-		-12,86			0,00	0,00	14,98	-27,85	0,00	-12,86

Tab. 5.26 Inside and outside surface temperatures (°C) – Effect of reflection, convection, emission and transmission (W/m²), transparent component, winter day, 26th January

The quantity of heat flow through conduction has been calculated using the same equation as that used for conductive heat flows in opaque components (equation 4.15). To calculate heating and cooling demands and the resulting auxiliaries of a transparent component, the quantities of irradiation that pass through the component via transmission are cumulatively added to the quantities of heat flow resulting from conduction. For example, in Figure 5.31, on a winter day, such as the 26th of January, from 09:00 until 17:00, the total calculated 'heat' represents the cumulative sum of 'conductive heat flow' and 'transmitted irradiation'. It is assumed that the contribution of a transparent component like a window is not only through its conductive heat transfer but also through the quantities of transmitted irradiation.

Figure 5.29 shows cumulative amount of conduction and transmission in transparent component regarding the defined boundary condition.

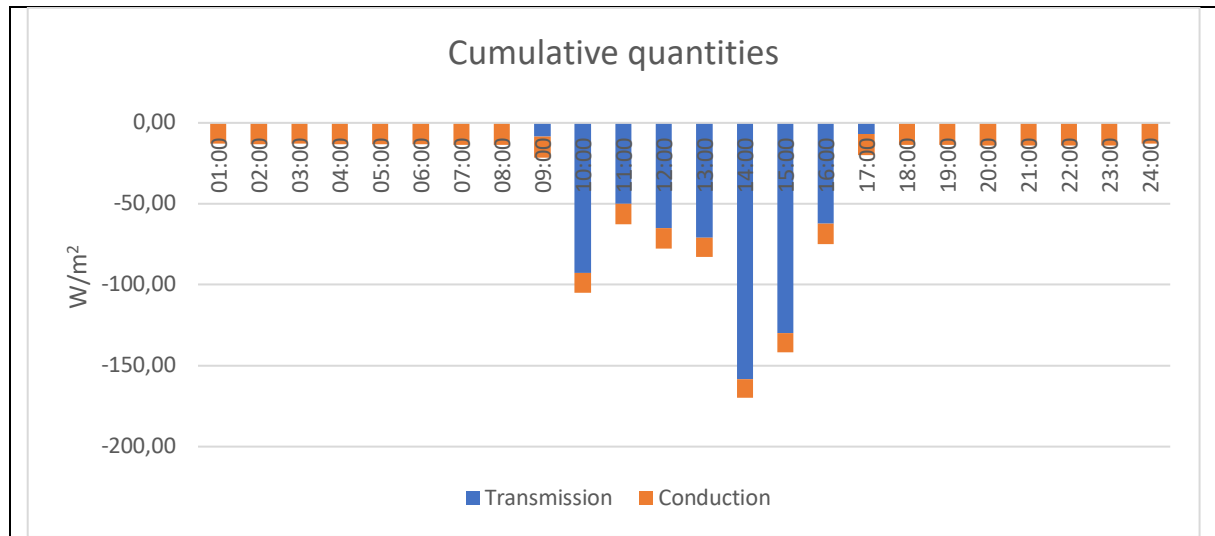


Fig. 5.29 Cumulative amount of conduction and transmission in transparent component (W/m²) - Boundary condition table 5.21

Applying values of heat flows to cumulative quantities of conduction and transmission results the graph shown in figure 5.30.

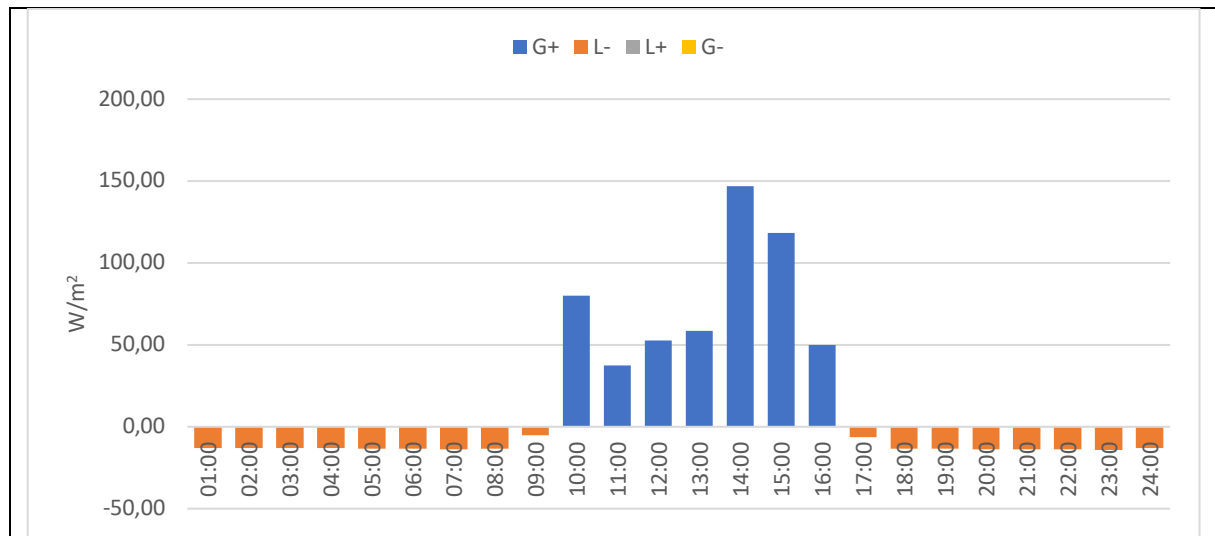


Fig. 5.30 Hourly amount of heat flow + values (W/m²), transparent component - Boundary condition table 5.21

The graph shows that during the day, when applying transmitted segments of irradiation to conducted heat flow, the proposed transparent component provides significant quantities of 'heating auxiliary.' The exceptions are at the beginning and end of the day (09:00 and 17:00) when the amount of transmitted irradiation is lower than the amount of heat flows toward the outside, resulting in a low quantity of heat flow that can be considered as heating demand. Figure 5.30 explains these two exceptional hours.

$$q_{09:00} = q_{conduction(09:00)} + q_{transmission(09:00)} = (-13.37) + (+8.30) = -5.07 \text{ W/m}^2$$

$$q_{17:00} = q_{conduction(17:00)} + q_{transmission(17:00)} = (-13.20) + (+6.79) = -6.41 \text{ W/m}^2$$

Outside and inside surface and air temperatures are shown in figure 5.31.

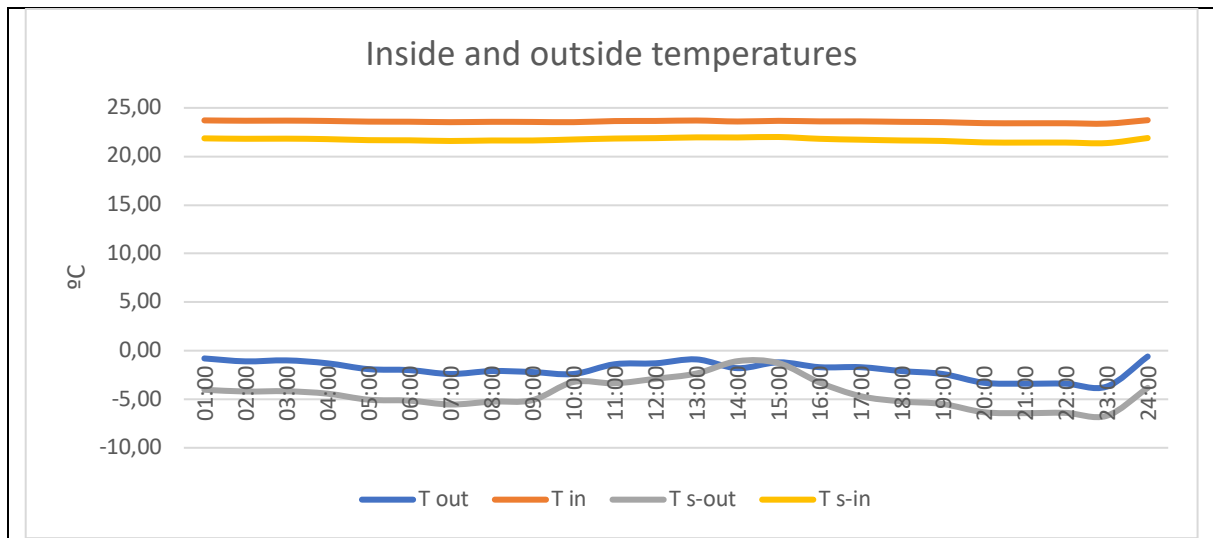


Fig. 5.31 outside temperature (°C), inside temperature (°C), outside surface temperature (°C) and inside surface temperature (°C) - Transparent component - Boundary condition table 5.21

Considering the inside air temperature and inside surface temperature reveals that the inside surface temperature consistently remains lower than the inside air temperature, resulting in simultaneous heat loss through convection. On the outside, the surface temperature remains below the air temperature until 09:30, then remains above the outside temperature until 16:00, and finally, after 16:00, it falls below the outside temperature.

5.7.3 Monthly performance

On an hourly basis, the cumulative amounts of calculated parameters for all 24 selected days result in the upcoming graphs for the transparent component, taking into account the defined boundary conditions. The monthly cumulative heat flow of conduction is shown in Figure 5.32.

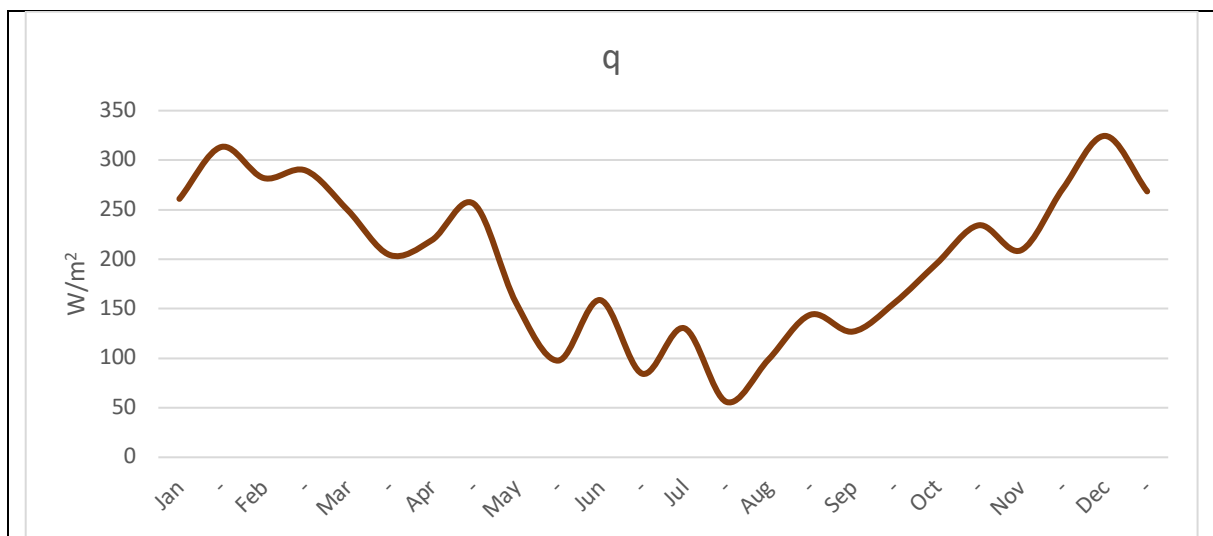


Fig. 5.32 Monthly amount of heat flow – (W/m²) - Transparent component - Boundary condition table 5.21

Applying values of heat flows to the quantity of monthly heat flows considering conduction and transmission is shown in figure 5.33.

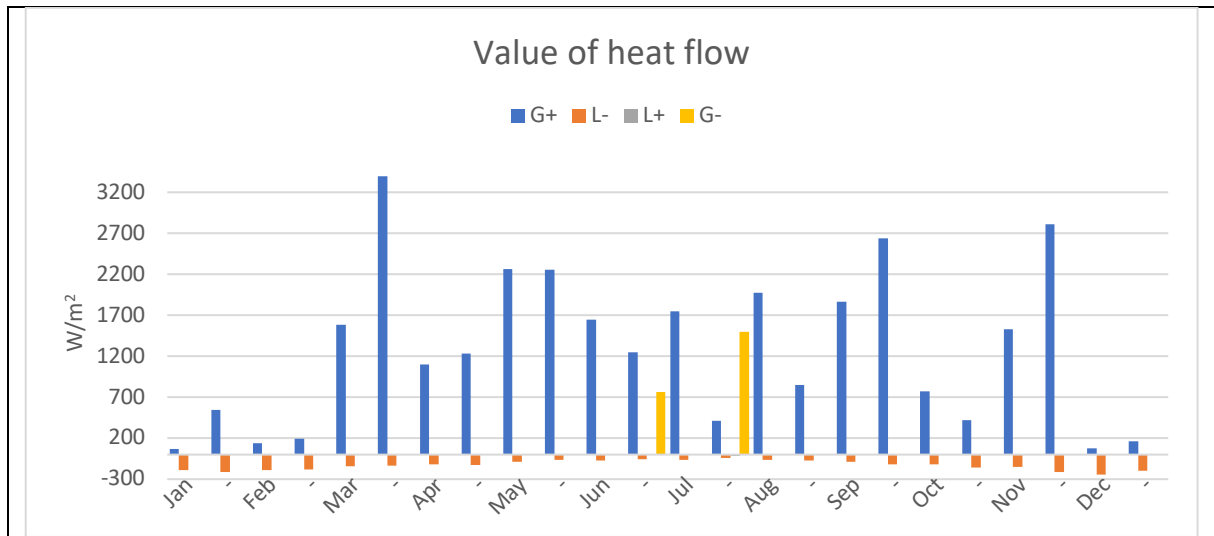


Fig. 5.33 Monthly amount of heat flow + values (W/m^2) – Interval 15 days - Transparent component - Boundary condition table 5.21

Integrating quantities of heat flows through the definition of demands and auxiliaries (table 4.5) determines annual energy performance of component (figure 5.34).

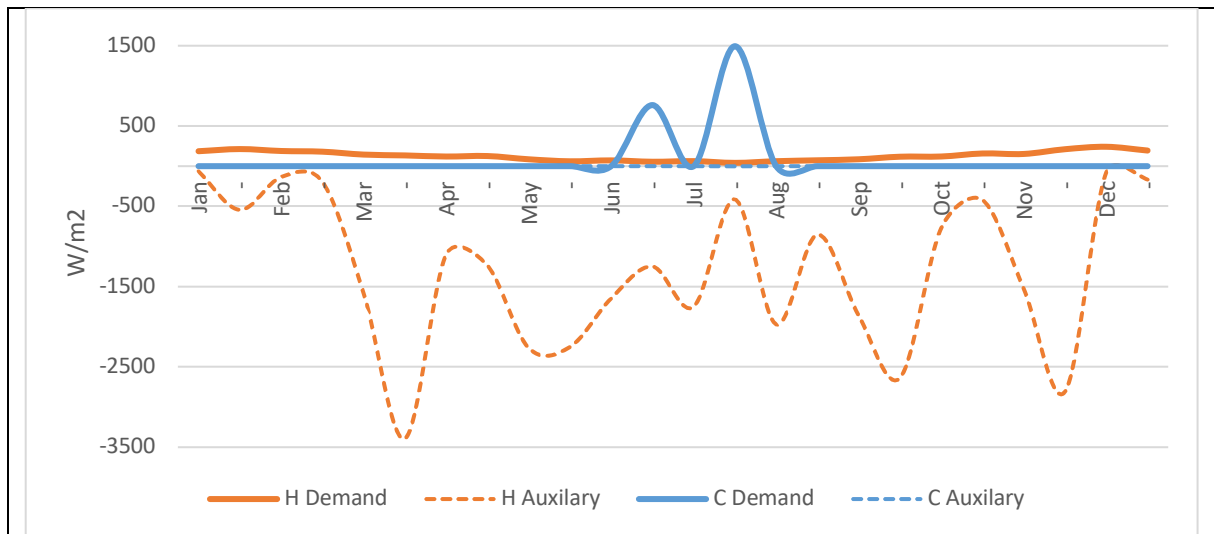


Fig. 5.34 Monthly heating demand, heating auxiliary, cooling demand, cooling auxiliary (W/m^2) – Transparent component - Boundary condition table 5.19

The monthly energy performance of the transparent component highlights the importance of considering 'cooling demand.' It shows that at the beginning and end of the year, there is a heating demand of $180 W/m^2$, while in summer, it reaches a minimum of $50 W/m^2$. The cooling demand peaks at $1500 W/m^2$ on the 26th of July. This emphasizes that for a precise calculation of a building's energy performance, cooling demand should also be continuously taken into account.

5.7.4 Orientation

Comparison of energy performance of a vertical (inclination: 90°) transparent component in all 4 main orientations has been done (Table 5.27).

Component	Inclination (°)	Orientation (°)	Inside temperature (Set)	Date	Transmittance factor	U-value (W/m ² .K)	h _i (W/m ² .K)
Transparent	90	0, -90, 180, +90	High	A year	1.5	0.50	7

Tab. 5.27 Boundary condition – Transparent component – different orientations

Integrating the quantities of heat flows to determine relative values results in the monthly 'energy demand - energy auxiliary' for the component. Figure 5.35 presents the monthly heating demand, heating auxiliary, cooling demand, and cooling auxiliary of the transparent component under the defined boundary conditions in all four main orientations.

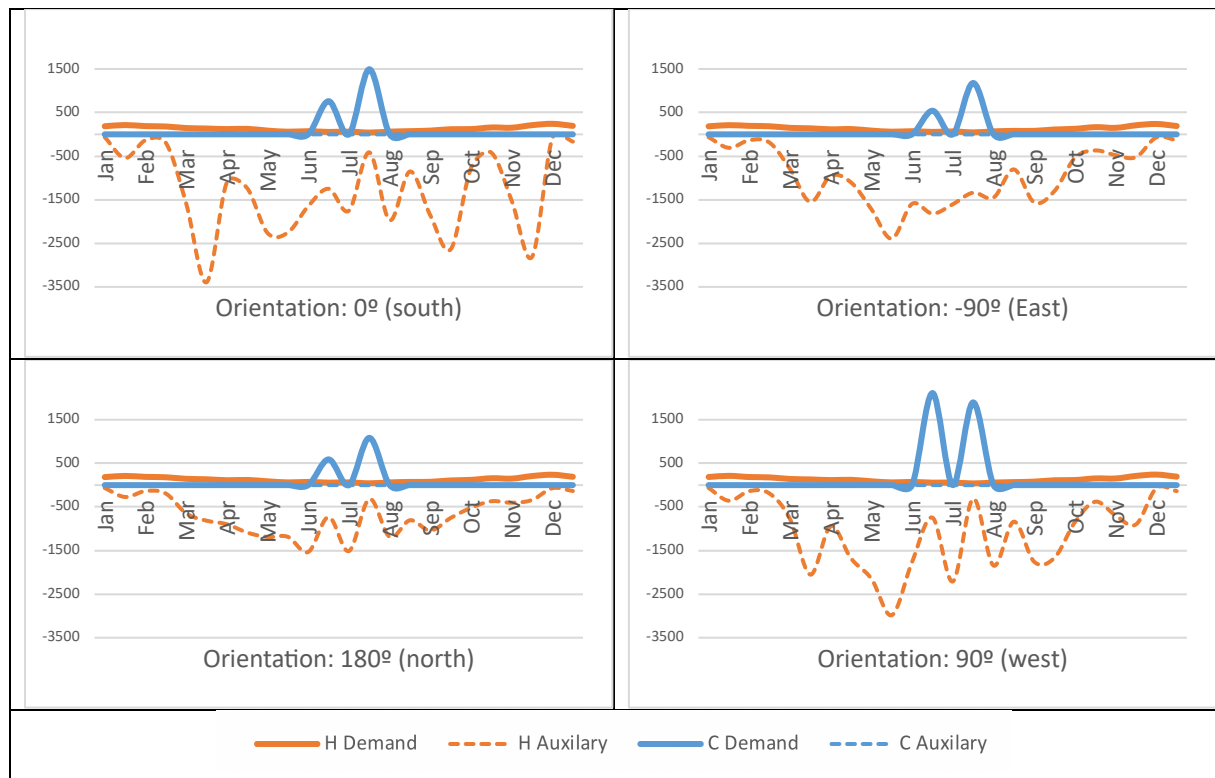


Fig. 5.35 Monthly heating demand, heating auxiliary, cooling demand, cooling auxiliary(W/m²) – Transparent component, Inclination 0°, all four orientations - Boundary condition table 5.27

Comparing the curves reveals a significant difference in the quantities of cooling demand among different orientations. The west-facing component indicates 2,100 W/m², while this amount is reduced to less than 1,100 W/m² for the north-facing component. Heating demand remains relatively consistent in terms of quantity and sequence, but the maximum heating auxiliary belongs to the south-facing component, reaching approximately 3,400 W/m² on March 26th. Moderated amounts are observed in the east-facing and west-facing components, around 2,500 W/m², while the minimum is found in the north-facing component at approximately 1500 W/m². The notable variation in heating auxiliary quantities underscores the importance of defining heat flow values accurately to make informed decisions regarding whether the heat flow results in heating and/or cooling demand or can be easily compensated for by natural ventilation, which can be achieved by partially opening windows.

5.7.5 Inclination

Three inclinations of 90°, 60°, and 30° in all four orientations, under various boundary conditions with respect to the 'inside air temperature,' have been considered. A specific geometric configuration, representative of the south-facing component, was selected for comparison. Additionally, an inclination of 0° is compared as the last orientation, representing a flat roof. Table 5.28 provides details of the configurations and boundary conditions of the transparent component, and the energy performance of each inclination is illustrated in Figure 5.36.

Component	Inclination (°)	Orientation (°)	Inside temperature	Date	Transmittance factor	U-value (W/m ² .K)	h _i (W/m ² .K)
Transparent	0, 30, 60, 90	0	High	A year	1.5	0.50	7

Tab. 5.28 Boundary condition – Transparent component – different inclinations

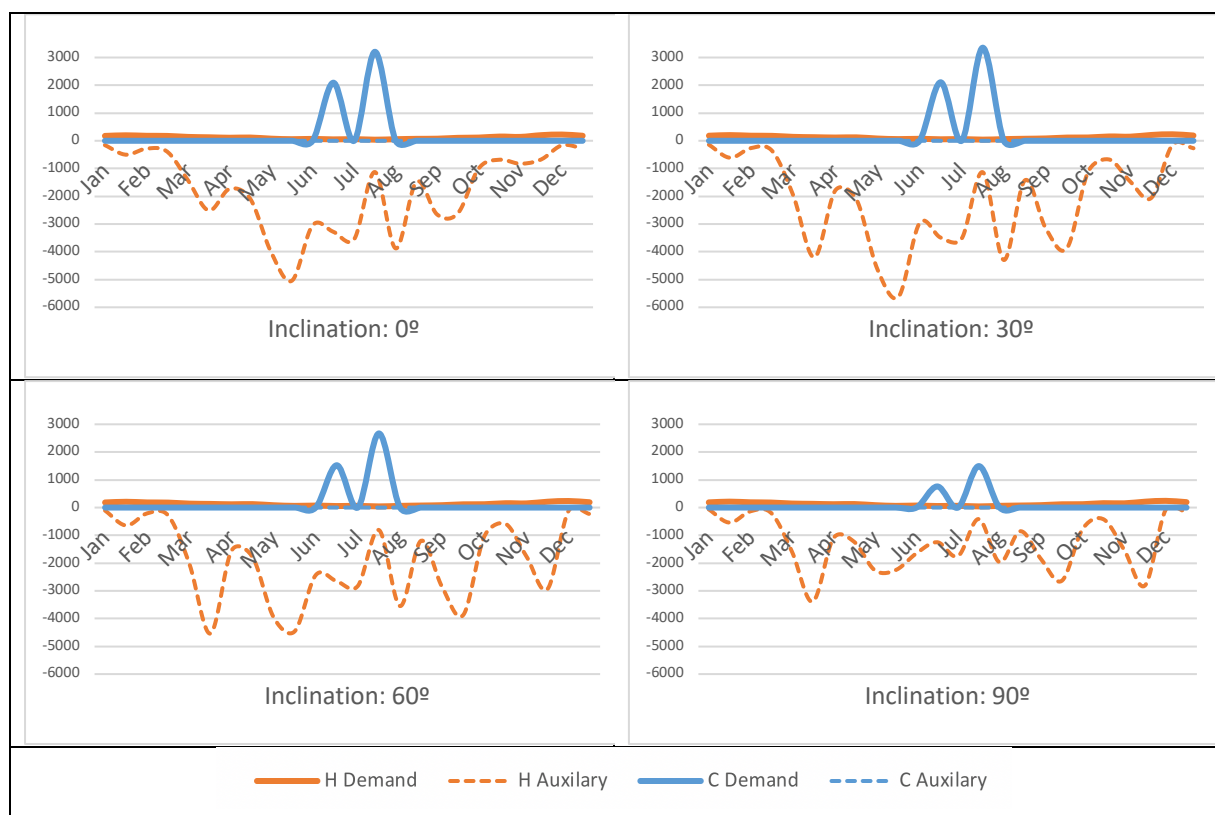


Fig. 5.36 Monthly heating demand, heating auxiliary, cooling demand, cooling auxiliary(W/m²) – Transparent component, Inclination 0°, all four orientations - Boundary condition table 5.28

Comparing the results of a south-facing transparent component in four orientations (90° vertical, 60°, 30°, and 0° flat roof) shows almost the same quantities of heating demand but significant differences in cooling demand. For instance, on July 26th, the cooling demand for the 90° vertical orientation is about 1,500 W/m², while the 60°, 30°, and 0° orientations show 2,700, 3,350, and 3,200 W/m², respectively. Therefore, in the defined component, the 30° inclination results in higher cooling demand compared to other inclinations. Additionally, auxiliary heating also indicates higher quantities in the 30° inclination, reaching a maximum of about 5,500 W/m², while in the 90° vertical orientation, it is moderated to approximately 3,200 W/m².

5.7.6 Inside air temperature

With respect to the representative transparent component and the defined boundary conditions (as listed in Table 5.29), a comparison of the cumulative quantities of indexes across the four main orientations is presented in Figure 5.37.

Component	Inclination (°)	Orientation (°)	Inside temperature (Set)	Date	Transmittance factor	U-value (W/m ² .K)	h _i (W/m ² .K)
Transparent	0, 30, 60, 90	0	High	A year	1.5	0.50	7

Tab. 5.29 Boundary condition – Transparent component – different inclinations – Inside set temperature: high

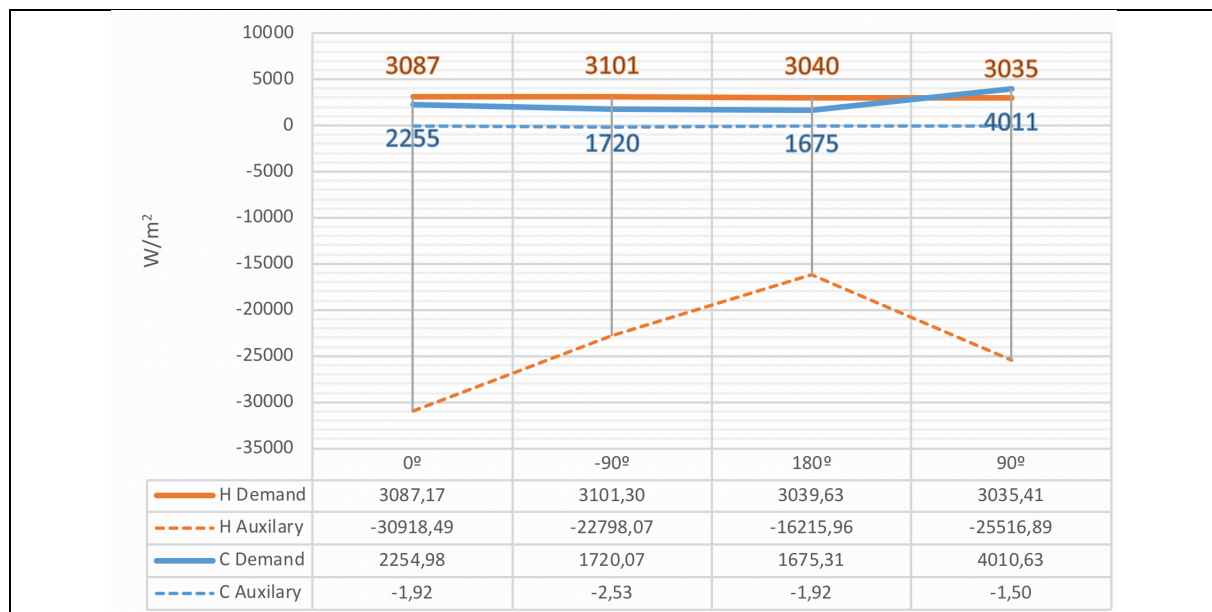


Fig. 5.37 Cumulative amount of heating demand, heating auxiliary, cooling demand, cooling auxiliary (W/m²) – Transparent component, Inclination 0°, all four orientations – Inside temperature: high - Boundary condition table 5.29

A quantitative comparison of the indexes reveals a minor difference in annual heating demand, with the 90° inclination (west-faced) indicating 3,035 W/m², while the 0° inclination (south-faced) shows 3,087 W/m². The lowest cumulative cooling demand is observed in the 180° inclination (north-faced) with a quantity of 1,720 W/m², while the 90° inclination (west-faced) records 4,011 W/m². The maximum heating auxiliary is delivered by the 0° inclination (south-faced) with approximately 30,000 W/m², while the 180° inclination (north-faced) shows the minimum at about 16,000 W/m². Cooling auxiliary remains at low rates.

The upcoming boundary conditions in Table 5.30 and the related comparisons in Figure 5.38 are presented to illustrate the differences in quantities of indexes when the inside temperature set-point changes.

Component	Inclination (°)	Orientation (°)	Inside temperature (Set)	Date	Transmittance factor	U-value (W/m ² .K)	h _i (W/m ² .K)
Transparent	0, 30, 60, 90	0	Low	A year	1.5	0.50	7

Tab. 5.30 Boundary condition – Transparent component – different inclinations – Inside set temperature: low

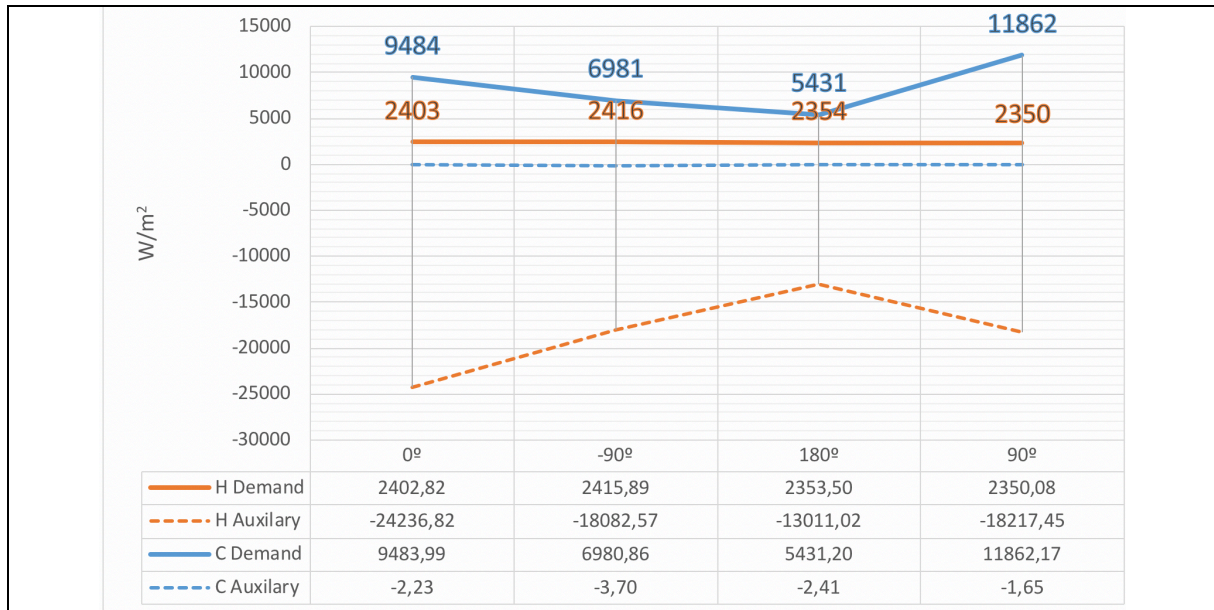


Fig. 5.38 Cumulative amount of heating demand, heating auxiliary, cooling demand, cooling auxiliary (W/m^2) – Transparent component, Inclination 0° , all four orientations – Inside temperature: Low

Comparing quantities of cumulative amounts of indexes in two boundary conditions (different inside temperatures) in the defined transparent component is shown in figure 5.39.

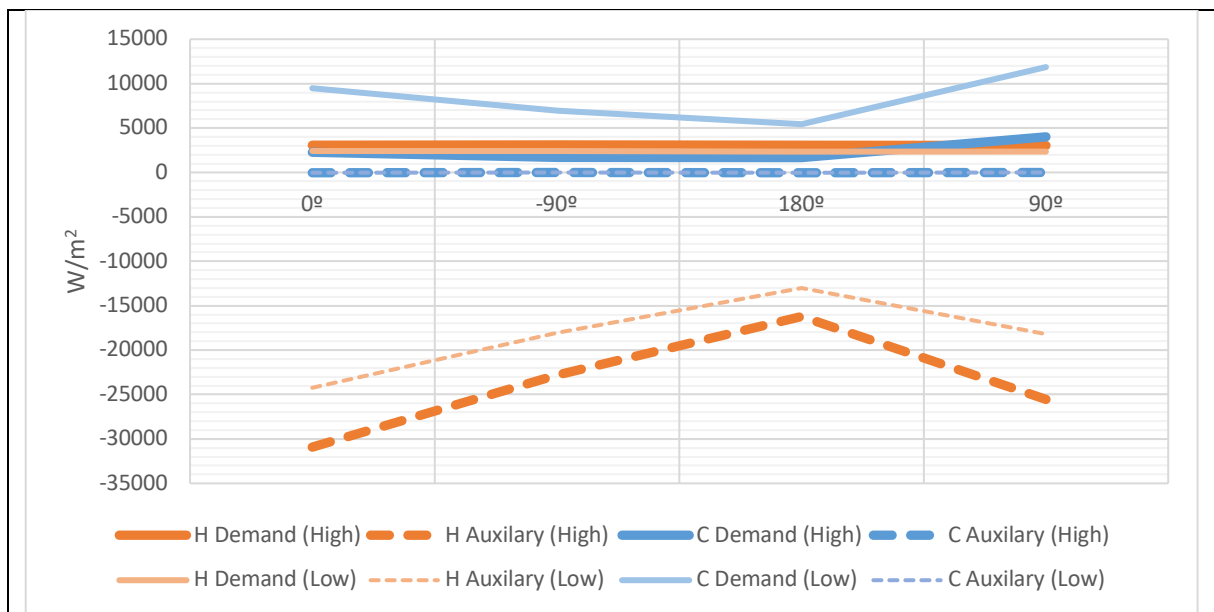


Fig. 5.39 Cumulative amount of heating demand, heating auxiliary, cooling demand, cooling auxiliary (W/m^2) – Transparent component, Inclination 0° , all four orientations – Inside temperature: high, low

The quantity of changing energy indexes, based on an hourly interval of calculation, in the considered transparent component with the defined boundary conditions, is shown in Figure 5.38. A selective inclination of 90° (vertical) with an orientation of 0° (south-faced) is employed using the defined boundary conditions in Table 5.31 (results are presented in Figure 5.40).

Component	Inclination ($^\circ$)	Orientation ($^\circ$)	Inside temperature (Set)	Date	Transmittance factor	U-value ($W/m^2.K$)	h_i ($W/m^2.K$)
Transparent	90	0	high, low	A year	1.5	0.50	7

Tab. 5.31 Boundary condition – Transparent component - Inside set temperature: high / low

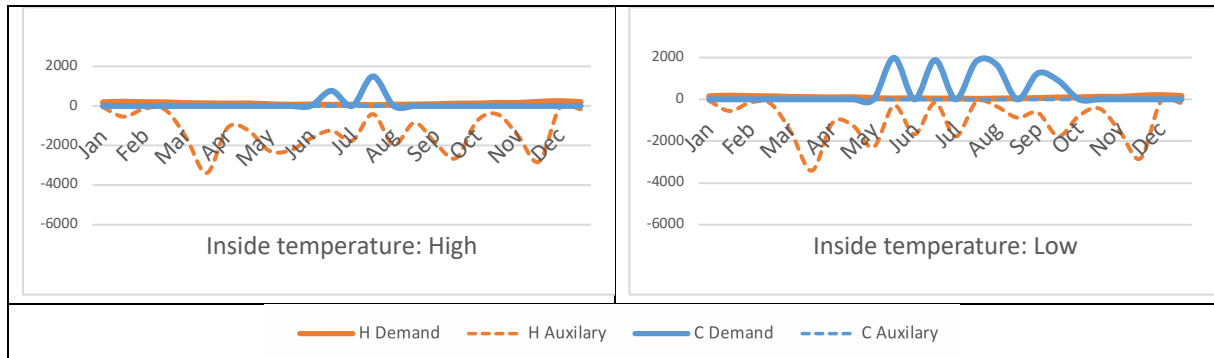


Fig. 5.40 Monthly heating demand, heating auxiliary, cooling demand, cooling auxiliary (W/m^2) – Transparent component, Inclination 90° , orientation 0° , Inside temperature; high (left), low (right)

Comparing performance of transparent component in two different inside temperature set-points indicate a remarkable difference in cooling demand quantities and periods. Boundary condition in table 5.32 and related comparison in figure 5.41 show changes of cumulative amounts of indexes.

Component	Inclination ($^\circ$)	Orientation ($^\circ$)	CT	Date	Transmittance factor	U-value ($W/m^2.K$)	h_i ($W/m^2.K$)
Transparent	0, 30, 60, 90	0	high, low	A year	1.5	0.50	7

Tab. 5.32 Boundary condition - Transparent component - Different inclinations - CT: high / low

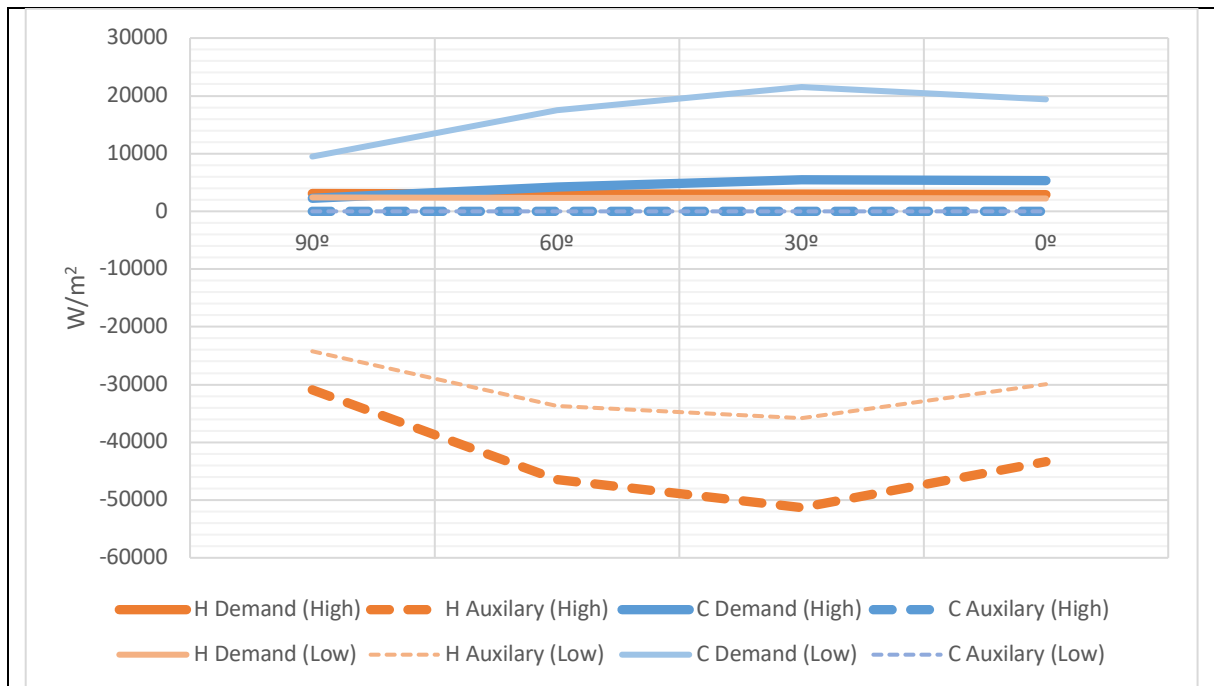


Fig. 5.41 Cumulative amount of heating demand, heating auxiliary, cooling demand, cooling auxiliary (W/m^2) – Transparent component, orientation: 0° , inclinations: 0° , 30° , 60° and 90° – Inside temperature: high, low

Comparing the cumulative annual indexes in the transparent component with a selective orientation of 0° (south-faced through all four main orientations) reveals that cooling demand and heating auxiliary are primarily affected by altering the inclination of the proposed component. An inclination of 30° results in the highest cooling demand and heating auxiliary, making it more sensitive to changes in the inside temperature setpoint. When changing the inside temperature setpoint from high to low, the cooling demand for the 30° inclination increases by more than $1,600 W/m^2$, while its heating auxiliary increases by about $1,500 W/m^2$.

5.8 BIPV

In calculating the amounts, direction, and values of heat flows in BIPV using the steady heat transfer method, the 'power balance model' correlation has been integrated. The employment of Equation 4.26 indicates the interaction of the temperature of the PV system in drops of efficiency, as well as the contributions of irradiation and the thermal effects of boundary conditions to be calculated in the dissipation of heat in both directions. Regarding the assembly of materials for BIPV, as listed in Table 4.9, additional thermal resistance of BIPV is included in the calculation of the final U-value for the combination of BIPV with the opaque component. As a result,

$$\Sigma R_{II_{BIPV+wall}} = R_{wall} + R_{BIPV} = 6.66 + 5.22 = 11.88 \text{ m}^2 \cdot \text{k/W}$$

$$U - \text{value}_{wall+BIPV} = \frac{1}{11.88} = 0.084 \text{ W/m}^2 \cdot \text{k}$$

Considering Equation 4.20, $R_{wall+BIPV}$ is considered as ΣR_{II} , which refers to the 'thermal resistance of the wall excluding inside and outside air film resistances.' To calculate ΣR_{I} , referring to the 'thermal resistance of the wall excluding outside air film resistance,' the following correlation has been applied:

$$\Sigma R_{I_{BIPV+wall}} = \Sigma R_{II_{BIPV+wall}} + R_{inside \text{ air}} = 11.88 + \frac{1}{h_{in}} = 11.88 + 0.14 = 12.03 \text{ m}^2 \cdot \text{k/W}$$

For the assumption of the transmittance factor of the front glass, the same type of integrated glass used in the transparent component has been assumed for the front glass layer of BIPV. In the assumptions of parameters in Equation 4.26, which determines the power input by integrating portions of irradiation reaching the surface of the PV, the same coefficients as those of the transparent component have been applied. In the calculation of electrical power, electrical and thermal parameters have been assumed based on the sample data sheet for the production of BIPV (as shown in Table 5.33) [61].

Coefficient de température I_{sc}	α	[%/K]	+0,04	Coefficient de température U_{oc}	β	[%/K]	-0,27
Coefficient de température P_{MPP}	γ	[%/K]	-0,35	Nominal Module Operating Temperature	NMOT	[°C]	43±3
CARACTÉRISTIQUES POUR LE DIMENSIONNEMENT DU SYSTÈME							
Tension maximale du système	U_{sys}	[V]	1000	Classification des modules PV	Classe II		
Courant de retour admissible	I_r	[A]	20	Classe de résistance au feu basée sur l'ANSI / UL 61730	C / TYPE 2		
Charge max. admissible de compression / de traction		[Pa]	3600/2667	Température admissible des modules avec un ensoleillement maximal	-40°C - +85°C		
Charge max. d'essai de compression / de traction		[Pa]	5400/4000				

Tab. 5.33 Electrical and thermal characteristics of photovoltaic (Q-Cells) [61]

As a result, to assume a normal range of efficiency for PVs that will be integrated into all three configurations of BIPV, BAPV, and PV glazing, an efficiency value of 0.2 is applied. A nominal module operating temperature of 43 °C is also applied to all three configurations of BIPV, BAPV, and PV. Considering the temperature coefficient of PVs, different ranges of sensitivities are observed for different types of panels, which indicate lower values of the α coefficient. On average, an α coefficient of 0.02% per degree Kelvin (°C) has been applied in the calculations.

5.8.1 Daily performance – summer day

Table 5.34 shows calculated inside and outside surface temperatures of defined BIPV integrated on existing opaque component through employed boundary condition.

Component	Inclination (°)	Orientation (°)	CT	Date	Transmittance factor (front glass)	U-value (W/m ² .K)	h _i (W/m ² .K)	α _{coeff} (%/K)	T _{STC} (°C)	η
BIPV	90	0	High	26 th Jan 26 th Jul	1.5	0.084	7	0.02	43	0.20

Tab. 5.34 Thermal and electrical characteristic of applied BIPV to opaque component and boundary condition

On a summer day, specifically the 26th of July at 11:00, the procedure for calculations and the employed equations are described in the following tables. Equation 4.20 is used to calculate T_M, which represents the operating temperature of the PV cell, by considering the thermal resistance of the combination of the PV backside and the wall introduced in the opaque component. For the PV cell, which is assumed to have an extremely low thickness of 0.2 mm and a homogeneous construction, a constant temperature is calculated. As a result, three main segments of Equation 4.26 are employed to calculate the balance of 'power input,' 'electrical power,' 'thermal dissipation,' as well as the quantity of surface temperatures and T_M. Power input, considering the reflection, absorption, and transmission properties of the front layer of BIPV, is calculated through Equation 4.26. To integrate T_{sol-air} directly at the surface of the PV cell, a low thermal resistance value for the front side of BIPV is calculated and applied in the calculations for R_{II combination} and R_{I combination} (The rest of the calculations in Table 5.35).

N	Parameter	Symbol	Equation	Result	Unit
06	Effective irradiation	I	$Power\ input = (1 - \gamma_f - \alpha_f - \alpha_b \cdot \tau_{PV} \cdot \tau_f - \tau_b \cdot \tau_{PV} \cdot \tau_f) \cdot Q_{sol}$	191,61	W/m ²
07	Solar-air temperature	T _{sol-air}	(4.12)	314,50	°C
08	Thermal resistance of the wall excluding outside air film resistance	ΣRI	$R_{I\ combination} = R_{front\ glass} + R_{PV} + R_{back} + R_{wall} + R_{air\ in}$ (4.20)	12,03	m ² k/W
09	Thermal resistance of the wall excluding inside and outside air film resistances	ΣRII	$R_{II\ combination} = R_{front\ glass} + R_{PV} + R_{back} + R_{wall}$ (4.20)	11,89	m ² k/W
10	PV operating temperature	T _M	$T_M = \frac{h_o \cdot T_{sol-air} + \left(\frac{T_{in}}{\Sigma R_I}\right)}{\left(\frac{1}{\Sigma R_I}\right) + h_o}$ (4.13)	314,38	°K
11	Inside surface temperature	T _{s-in}	$T_{s-in} = T_M + (h_o \cdot \Sigma R_{II} \cdot (T_M - T_{sol-air}))$ (4.14)	300,24	°K
12	Heat flow	q	$q = h_o \cdot (T_{sol-air} - T_M)$ (4.15)	1,19	W/m ²

Tab. 5.35 Calculation of surface temperatures – heat flow – BIPV – boundary condition in table 5.34

The division of irradiation diffraction is calculated based on the proportion of generated electricity, utilizing the 'electrical power' segment of the energy balance equation in BIPV. Diffractions of reflection, emission, and convection are calculated separately (Table 5.36).

N	Parameter	symbol	Equation	result	Unit
13	Electricity generation	q _e	$Electrical\ power = [\eta \cdot (1 - \alpha_{coeff} \cdot (T_M - T_{STC})) \cdot \tau_f \cdot G]$	-48,92	W/m ²
14	outside reflection	q _{ref}	$q_{ref} = Q_{sol} - (B_{(h)} r_{B(\omega)} + D_{(h)} r_{D(\omega)})$	-181,51	W/m ²
15	outside emission	q _{rad}	4.19	-130,57	W/m ²
16	outside convection	q _{con}	4.18	-116,83	W/m ²

Tab. 5.36 Dividing diffraction of irradiation – electricity generation – BIPV - boundary condition in table 5.34

By integrating thermal and electrical characteristic of applied BIPV to opaque component in representative day of summer (26th Jul), table 5.37 is resulted;

	T out	T in	T s-out	T s-in	q	Direction	G+	L-	L+	G-	Irradiation	Reflection	Convection	Emission	Electricity
01:00	18,00	25,83	13,74	25,69	-1,01	L-		-1,01			0,00	0,00	23,77	-24,78	0,00
02:00	17,10	25,73	12,89	25,58	-1,07	L-		-1,07			0,00	0,00	23,68	-24,75	0,00
03:00	16,60	25,68	12,42	25,52	-1,10	L-		-1,10			0,00	0,00	23,60	-24,70	0,00
04:00	15,30	25,53	11,12	25,36	-1,20	L-		-1,20			0,00	0,00	23,85	-25,04	0,00
05:00	14,80	25,47	10,65	25,30	-1,23	L-		-1,23			0,00	0,00	23,81	-25,04	0,00
06:00	15,30	25,53	11,91	25,37	-1,13	L-		-1,13			15,60	-3,57	17,37	-28,27	-2,27
07:00	17,50	25,78	16,89	25,67	-0,74	L-		-0,74			74,50	-17,03	-6,06	-41,56	-10,59
08:00	21,00	26,17	22,77	26,13	-0,28	L-		-0,28			138,46	-40,09	-25,87	-55,12	-17,66
09:00	23,20	26,42	27,50	26,43	0,09	G+	0,09				257,93	-117,19	-46,08	-69,86	-24,72
10:00	26,00	26,74	34,93	26,84	0,68	G+	0,68				382,78	-162,46	-82,09	-100,19	-37,36
11:00	27,60	26,92	41,23	27,09	1,19	G+				1,19	479,02	-181,51	-116,83	-130,57	-48,92
12:00	29,10	27,09	45,04	27,30	1,49	G-				1,49	507,77	-169,07	-133,46	-149,10	-54,65
13:00	29,70	27,16	42,96	27,34	1,31	G-				1,31	418,27	-120,89	-114,05	-133,54	-48,48
14:00	30,90	27,29	36,58	27,40	0,77	G-				0,77	239,50	-61,59	-58,16	-89,05	-29,93
15:00	31,40	27,35	41,80	27,52	1,20	G-				1,20	383,39	-128,31	-93,08	-118,97	-41,83
16:00	32,30	27,45	37,48	27,57	0,83	G-				0,83	291,68	-120,76	-54,37	-87,09	-28,63
17:00	32,00	27,42	35,09	27,51	0,64	G-				0,64	178,39	-44,90	-38,10	-72,14	-22,62
18:00	31,70	27,38	32,58	27,44	0,43	G-				0,43	122,50	-28,00	-20,80	-57,06	-16,21
19:00	30,00	27,19	28,18	27,20	0,08	G-				0,08	69,80	-15,95	-0,44	-43,89	-9,43
20:00	28,10	26,98	23,55	26,93	-0,28	L+				-0,28	9,60	-2,19	21,73	-28,10	-1,32
21:00	27,70	26,93	22,66	26,88	-0,36	L+				-0,36	0,00	0,00	25,64	-25,99	0,00
22:00	25,30	26,66	20,78	26,59	-0,49	L-		-0,49			0,00	0,00	23,50	-23,99	0,00
23:00	23,40	26,44	19,12	26,36	-0,61	L-		-0,61			0,00	0,00	22,68	-23,29	0,00
24:00	19,30	25,98	14,99	25,85	-0,91	L-		-0,91			0,00	0,00	23,76	-24,68	0,00

Tab. 5.37 Inside and outside surface temperatures (°C), heat flow (W/m²)– Effect of reflection, convection, emission and transmission + generated electricity (W/m²), BIPV, summer day, 26th July - boundary condition in table 5.34

Air and surface temperatures, values of heat flows are shown in figure 5.42.

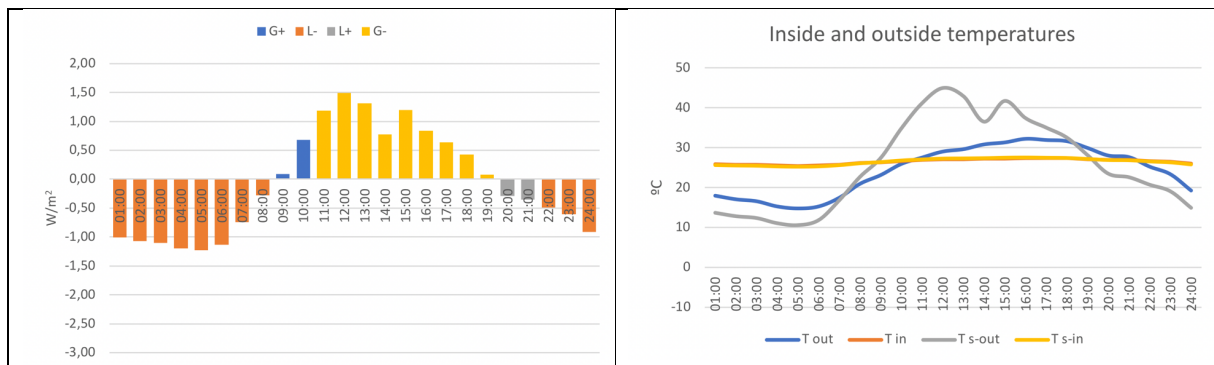


Fig. 5.42 Air and surface temperatures, values of heat flows, BIPV, summer day - boundary condition in table 5.34

Resulted heating and cooling demands and electricity generation and diffraction of irradiation are shown in figure 5.43.

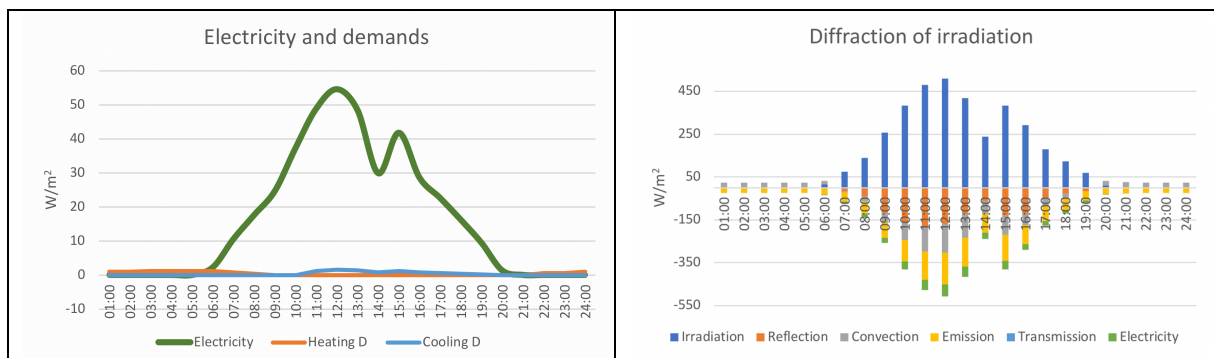


Fig. 5.43 Air and surface temperatures, values of heat flows, BIPV, summer day - boundary condition in table 5.34

5.8.2 Daily performance – Winter day

By integrating thermal and electrical characteristic of applied BIPV to opaque component in representative day of winter (26th Jan), table 5.38 is resulted;

	T _{out}	T _{in}	T _{s-out}	T _{s-in}	q	Direction	G+	L-	L+	G-	Irradiation	Reflection	Convection	Emission	Electricity
01:00	-0,80	23,71	-5,23	23,37	-2,41	L-		-2,41			0,00	0,00	20,75	-23,16	0,00
02:00	-1,10	23,68	-5,42	23,33	-2,42	L-		-2,42			0,00	0,00	20,27	-22,69	0,00
03:00	-1,00	23,69	-5,39	23,34	-2,42	L-		-2,42			0,00	0,00	20,59	-23,00	0,00
04:00	-1,30	23,65	-5,65	23,31	-2,44	L-		-2,44			0,00	0,00	20,45	-22,89	0,00
05:00	-1,90	23,59	-6,29	23,23	-2,48	L-		-2,48			0,00	0,00	20,78	-23,26	0,00
06:00	-2,00	23,57	-6,39	23,22	-2,49	L-		-2,49			0,00	0,00	20,80	-23,30	0,00
07:00	-2,40	23,53	-6,81	23,17	-2,52	L-		-2,52			0,00	0,00	20,95	-23,47	0,00
08:00	-2,10	23,56	-6,51	23,21	-2,50	L-		-2,50			0,00	0,00	20,87	-23,37	0,00
09:00	-2,20	23,55	-5,80	23,20	-2,44	L-		-2,44			13,20	-3,02	15,52	-26,08	-2,06
10:00	-2,40	23,53	1,65	23,27	-1,82	L-		-1,82			133,26	-19,65	-35,65	-57,43	-22,35
11:00	-1,40	23,64	-1,27	23,35	-2,07	L-		-2,07			77,62	-16,08	-9,78	-41,58	-12,25
12:00	-1,30	23,65	0,20	23,37	-1,95	L-		-1,95			100,74	-20,87	-18,82	-47,20	-15,81
13:00	-0,90	23,70	1,13	23,43	-1,88	L-		-1,88			109,60	-22,68	-22,34	-49,32	-17,13
14:00	-1,80	23,60	8,16	23,41	-1,28	L-		-1,28			224,49	-30,28	-74,22	-84,11	-37,17
15:00	-1,20	23,66	6,11	23,46	-1,46	L-		-1,46			189,37	-29,86	-57,08	-73,09	-30,80
16:00	-1,70	23,61	-0,38	23,32	-1,99	L-		-1,99			97,30	-20,74	-17,50	-45,87	-15,19
17:00	-1,70	23,61	-5,47	23,26	-2,42	L-		-2,42			10,80	-2,47	16,55	-25,61	-1,69
18:00	-2,10	23,56	-6,48	23,21	-2,50	L-		-2,50			0,00	0,00	20,74	-23,24	0,00
19:00	-2,40	23,53	-6,76	23,17	-2,52	L-		-2,52			0,00	0,00	20,69	-23,21	0,00
20:00	-3,30	23,43	-7,63	23,06	-2,58	L-		-2,58			0,00	0,00	20,74	-23,32	0,00
21:00	-3,40	23,42	-7,73	23,05	-2,59	L-		-2,59			0,00	0,00	20,77	-23,36	0,00
22:00	-3,40	23,42	-7,71	23,05	-2,59	L-		-2,59			0,00	0,00	20,64	-23,23	0,00
23:00	-3,70	23,38	-8,02	23,01	-2,61	L-		-2,61			0,00	0,00	20,75	-23,37	0,00
24:00	-0,60	23,73	-5,03	23,39	-2,39	L-		-2,39			0,00	0,00	20,70	-23,09	0,00

Tab. 5.38 Inside and outside surface temperatures (°C), heat flow (W/m²) – Effect of reflection, convection, emission and transmission + generated electricity (W/m²), BIPV, winter day, 26th January - boundary condition in table 5.34

Air and surface temperatures, values of heat flows are shown in figure 5.44.

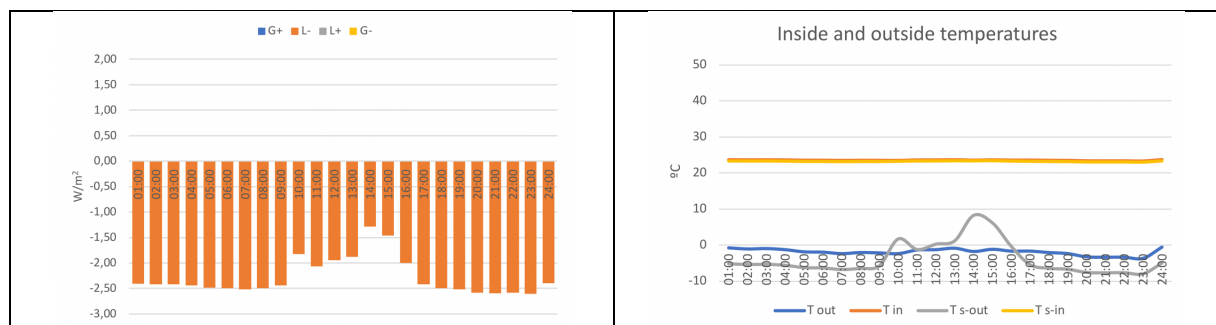


Fig. 5.44 Air and surface temperatures (left), values of heat flows (right), BIPV, winter day - boundary condition in table 5.34

The resulting heating and cooling demands, electricity generation, and diffraction of irradiation are shown in Table 5.45.

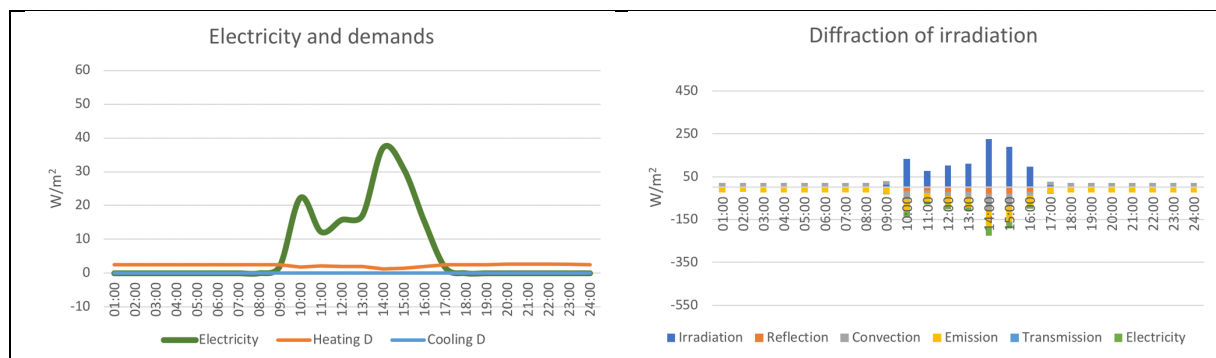


Fig. 5.45 Air and surface temperatures (left), diffraction of irradiation (right), BIPV, winter day - boundary condition in table 5.34

5.8.3 Monthly performance

Monthly cumulative heat flow in BIPV regarding the defined boundary condition, applying values and resulted energy demands is shown in figure 5.46.

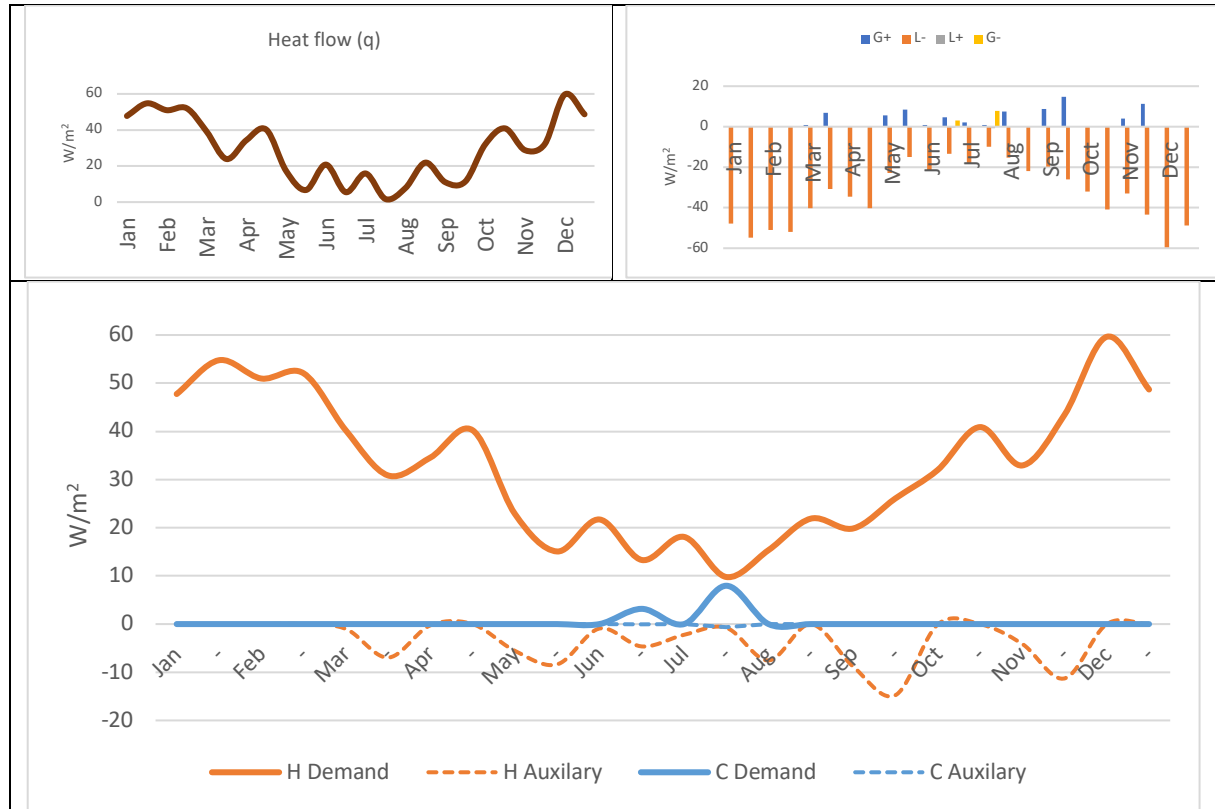


Fig. 5.46 Monthly cumulative heat flow (top left) – Values of heat flow (top right) – Heating demand, heating auxiliary, cooling demand and cooling auxiliary (bottom) – BIPV (W/m^2) - Geometrical setup and boundary condition in table 5.34

Applying power balance model considering interaction of thermal dissipation and power input regarding selective geometrical setup and boundary condition, results annual energy performance of BIPV representing fluctuation of electricity generation (figure 5.47).

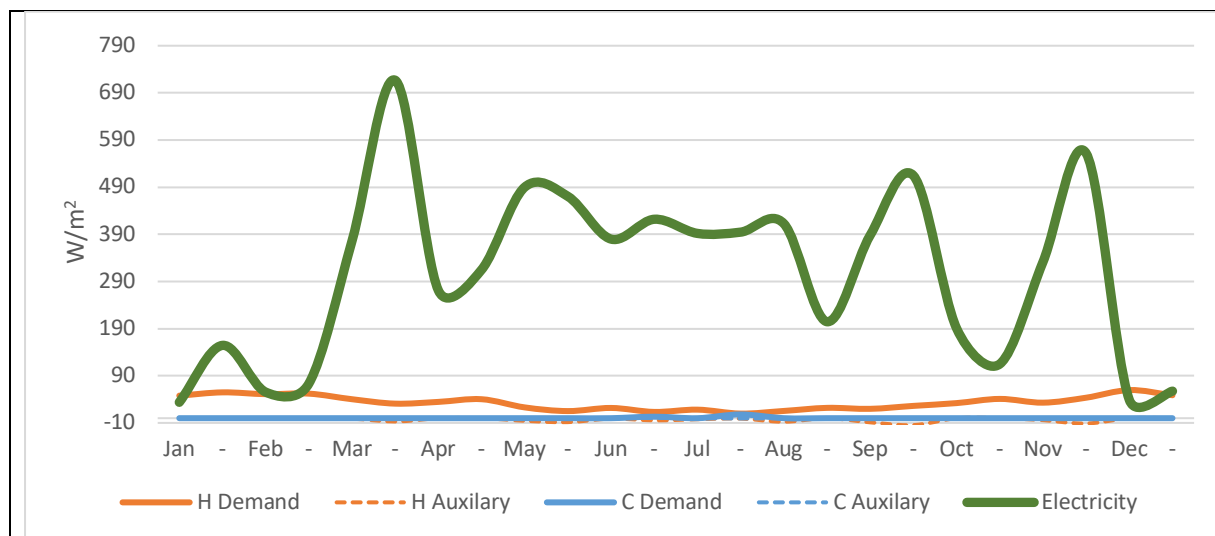


Fig. 5.47 Monthly energy demands – electricity generation (W/m^2) - BIPV - Geometrical setup and boundary condition in table 5.34

5.8.4 Orientation

Comparison of energy performance of a vertical (inclination 90°) BIPV in all 4 main orientations has been done. Table 5.39 shows detail of configuration and boundary condition of the purposed component.

Component	Inclination (°)	Orientation (°)	Inside temperature (Set)	Date	Transmittance factor (front glass)	U-value (W/m ² .K)	h _i (W/m ² .K)	α _{coeff} (%/K)	T _{stc} (°C)	η
BIPV	90	0, -90, 180, +90	High	A year	1.5	0.084	7	0.02	43	0.20

Tab. 5.39 Thermal and electrical characteristic of applied BIPV to opaque component and boundary condition

The results of comparing the effects of the four main orientations in the vertical position (inclination 90°) of BIPV are presented in Figure 5.48 and Figure 5.49.

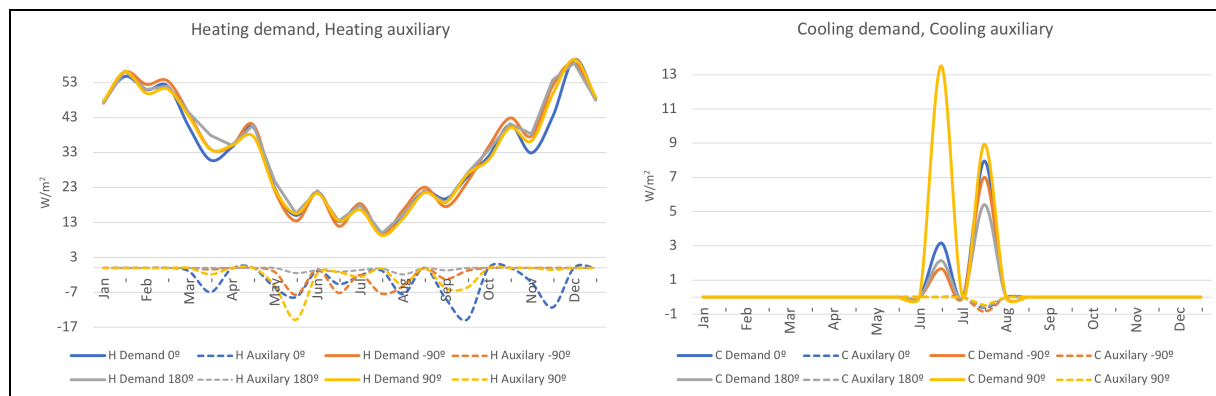


Fig. 5.48 heating demand + heating auxiliary (left), cooling demand + cooling auxiliary (right) (W/m²) BIPV - Geometrical setup and boundary condition in table 5.39 – Different orientations

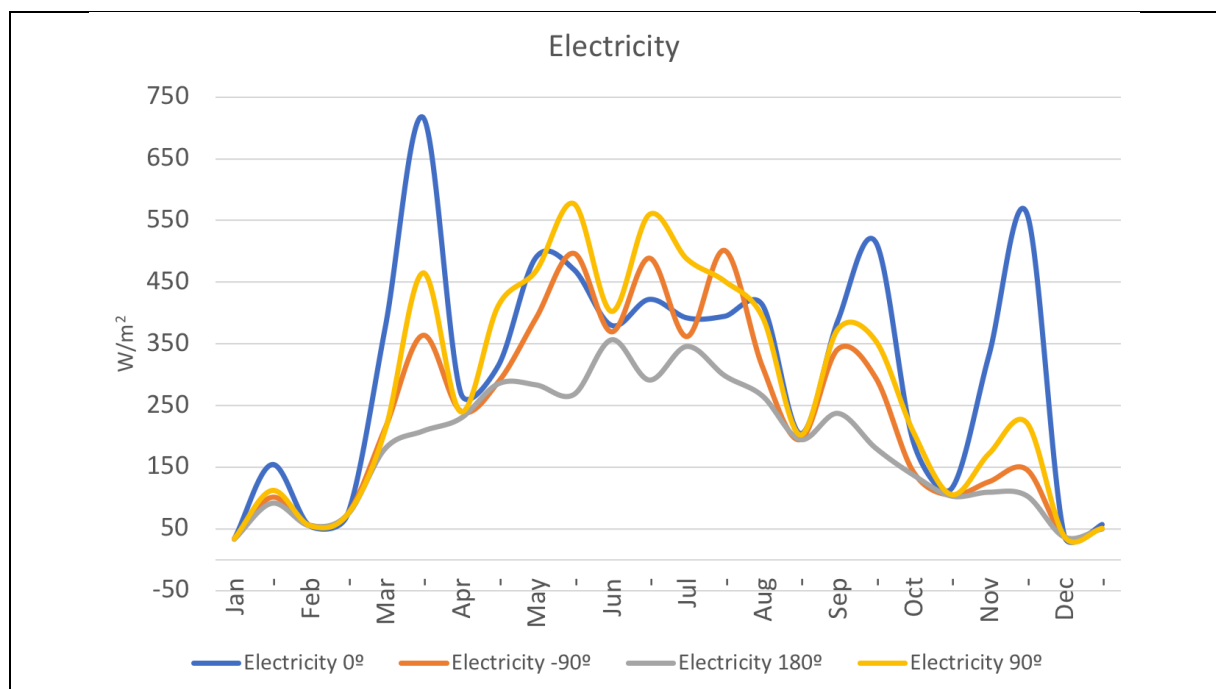


Fig. 5.49 Monthly electricity generation (W/m²) - BIPV - Geometrical setup and boundary condition in table 5.39 – Different orientations

5.8.5 Inclination

Comparison of energy performance of a south-faced (orientation: 0°) BIPV in all 4 main inclinations has been done. Table 5.40 shows detail of configuration and boundary condition of the purposed component.

Component	Inclination (°)	Orientation (°)	Inside temperature (Set)	Date	Transmittance factor (front glass)	U-value (W/m ² .K)	h _i (W/m ² .K)	α _{coeff} (%/K)	T _{stc} (°C)	η
BIPV	0, 30, 60, 90	0	High	A year	1.5	0.084	7	0.02	43	0.20

Tab. 5.40 Thermal and electrical characteristic of applied BIPV to opaque component – Different inclinations

The results of comparing the effects of the four main inclinations in a south-faced (orientation 0°) BIPV are presented in Figure 5.50 and Figure 5.51.

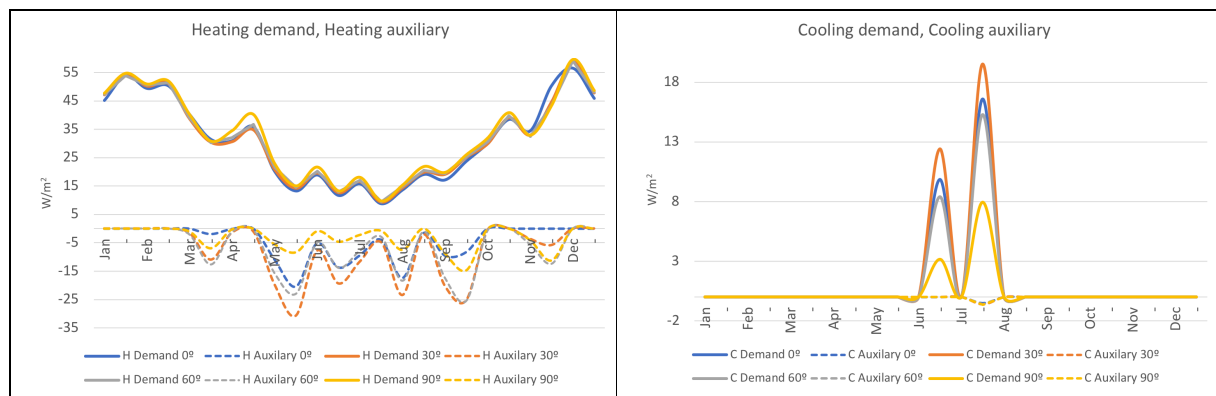


Fig. 5.50 heating demand + heating auxiliary (left), cooling demand + cooling auxiliary (right) (W/m²) BIPV - Geometrical setup and boundary condition in table 5.40 – Different inclinations

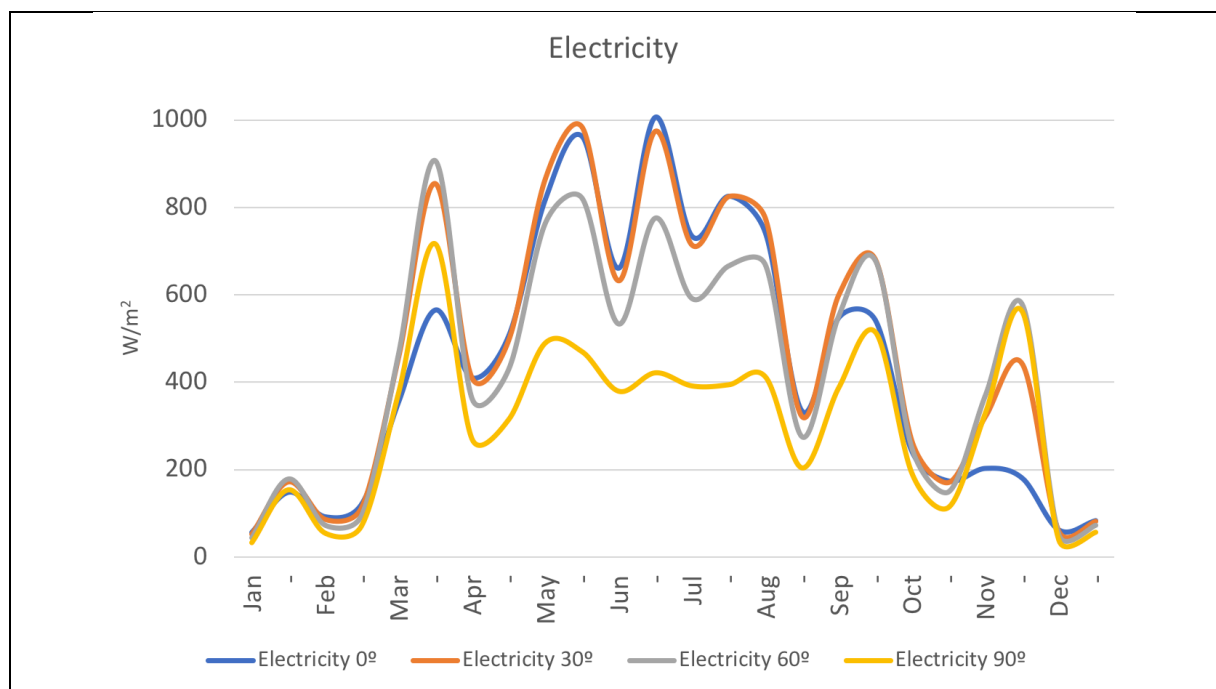


Fig. 5.51 Monthly electricity generation (W/m²) - BIPV - Geometrical setup and boundary condition in table 5.40 – Different inclinations

5.9 BAPV

The configuration of BAPV involves the integration of PV panels at a certain distance from the outer surface of the opaque component. This distance affects the operating temperature of PV panels. Additionally, thermal dissipations need to be calculated considering different quantities of convective thermal transfer, which is influenced by the backside distance. In this work, an average backside distance of 10 cm is applied for BAPV. The construction consists of two separate layers. The first layer includes frontside glass, PV panels, and backside glass. The second layer is composed of a uniform material (opaque component). Different inclinations of BAPV result in varying backside air velocities, which in turn alter the convective heat transfer coefficient. Consequently, different coefficients are applied to both layers of BAPV under steady-state conditions. These coefficients, resulting from different inclinations, are employed for the 'backside of layer 1' and the 'frontside of layer 2,' as illustrated in Figure 5.52 [55].

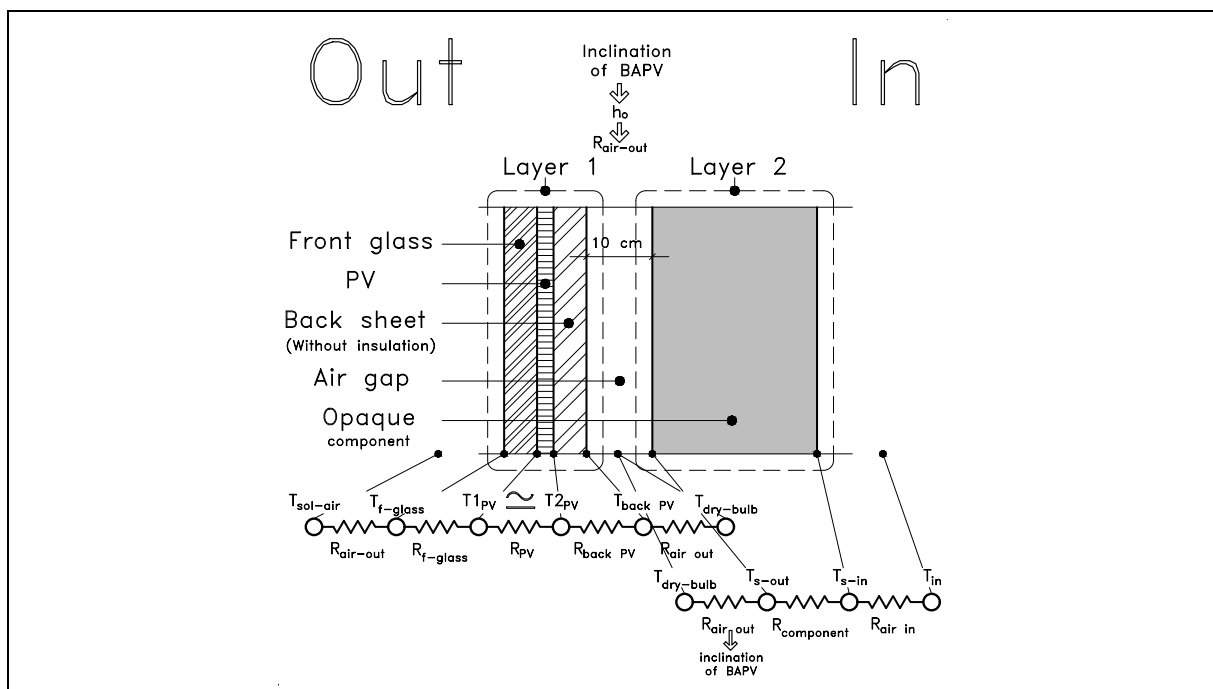


Fig. 5.52 Physical construction of defined BAPV + thermal resistance algorithm

Assumption of changing convective heat transfer coefficient in different inclinations for BAPV (the same constructive setup) with 10 cm backside air gap is shown in table 5.41 [55].

Gap	Tilt angle	Measurement		
		Temperature (°C)		$h_{i,gap}$ (W/m ² K)
		$T_{m,back}$	T_{wall}	
10cm	Vertical	59,0	41,6	12,7
	Tilted	60,0	43,5	12,6
	Horizontal	64,0	46	12,0

Tab. 5.41 Measurement of operating temperature of PV module at backside and wall temperature and total gap heat transfer coefficient ($h_{i,gap}$) (W/m²K) [55]

So, an assumption of a convective heat transfer coefficient ranging from 12.00 W/m²K for 0° inclination to 12.70 W/m²K for 90° inclination is applied.

5.9.1 Daily performance – summer day

BAPV consists primarily of two basic layers: Layer-01 and Layer-02, representing the outside integrated PV and the inside opaque component, respectively. Therefore, we consider two separate heat transfers—one on the outside and one on the inside of the component. These layers are separated by a 10 cm air gap, and it is assumed that the same outside air can naturally ventilate through this gap. Consequently, in both boundary conditions, the temperature of the intermediate air is assumed to be equal to T_{out} . The effect of different air velocities in this air gap, which leads to varying convective heat transfer coefficients due to different inclinations, has been continuously calculated and is employed as h_o . It's important to note that two different quantities of heat flow are calculated in Layer-01 and Layer-02. This discrepancy arises because the heat flow in Layer-02 is disconnected from the building's envelope, and the interaction of heat flow occurs within the 10 cm air layer, which is in constant contact with the outside air. However, the significance of Layer-02 (the outside layer) lies in the operating temperature of PV, directly impacting the 'electrical power' segment of the power balance. Consequently, while the heat flow of both the inside and outside layers of BAPV can be calculated, only the heat flow of Layer-02 will be taken into account. Tables 5.43 and 5.44 illustrate the calculation of parameters in Layer-01 for the 26th of July.

The boundary condition applied to the considered BAPV in Table 5.42 is supplemented with new values of individual 'u-value,' which are separately calculated based on thermal resistances of $\sum R_I$ and $\sum R_{II}$ for each layer.

Component	Inclination (°)	Orientation (°)	Inside temperature	Date	Transmittance factor (front glass)	U-value (W/m ² .K)	h_i (W/m ² .K)	α_{coeff} (%/K)	T_{STC} (°C)	η
Layer-01	90	0	-	26 th Jan 26 th Jul	1.5	100	12.70	0.02	43	0.20
Layer-02	90	0	High	26 th Jan 26 th Jul	-	0.15	7.00	-	-	-

Tab. 5.42 Thermal and electrical characteristic of applied BAPV to opaque component and boundary condition

N	Parameter	Symbol	Equation	Result	Unit
06	Effective irradiation	I	$Power\ input = (1 - \gamma_f - \alpha_f - \alpha_b \cdot \tau_{PV} \cdot \tau_f - \tau_b \cdot \tau_{PV} \cdot \tau_f) \cdot Q_{sol}$	191,61	W/m ²
07	Solar-air temperature	$T_{sol-air}$	(4.12)	314,50	°C
08	Thermal resistance of the wall excluding outside air film resistance	$\sum R_I$	$R_{I\ combination} = R_{front\ glass} + R_{PV} + R_{back} + R_{air}$ (4.20)	0,09	m ² k/W
09	Thermal resistance of the wall excluding inside and outside air film resistances	$\sum R_{II}$	$R_{II\ combination} = R_{front\ glass} + R_{PV} + R_{back}$ (4.20)	0,01	m ² k/W
10	PV operating temperature	T_{PV}	$T_M = \frac{h_o \cdot T_{sol-air} + \left(\frac{T_{in}}{\sum R_I}\right)}{\left(\frac{1}{\sum R_I}\right) + h_o}$ (4.13)	307,36	°K

Tab. 5.43 Calculation of surface temperatures – heat flow – BAPV – Layer-01 –boundary condition; table 5.40

N	Parameter	Symbol	Equation	Result	Unit
11	electricity generation	q_e	$Electrical\ power = [\eta \cdot (1 - \alpha_{coeff} \cdot (T_M - T_{STC})) \cdot \tau_f \cdot G]$	-50,63	W/m ²
12	Outside reflection	q_{ref}	$q_{ref} = Q_{sol} - (B_{(h)} r_{B(\omega)} + D_{(h)} r_{D(\omega)})$	-181,51	W/m ²
13	Outside emission	q_{rad}	4.19	-87,48	W/m ²
14	Outside convection	q_{con}	4.18	-84,43	W/m ²

Tab. 5.44 Dividing diffraction of irradiation – electricity generation – BAPV - Layer-02 - boundary condition in table 5.40

In Layer-02 (the inner layer), a different boundary condition is applied, supposing the absence of irradiation and a disconnection from the effect of sky emission as it is covered by Layer-01. In this regard, instead of $T_{sol-air}$, T_{out} has been employed to calculate surface temperatures. The value of h_o is based on considering the special configuration of BAPV, including its 10 cm air gap and 90° inclination, and has been assumed to be 12.70 W/m²·K.

Table 5.45 shows the calculated surface temperatures and heat flow in Layer-02.

N	Parameter	Symbol	Equation	Result	Unit
01	Effective irradiation	I	(shaded)	0.00	W/m ²
02	Thermal resistance of the wall excluding outside air film resistance	ΣRI	$RI_{combination} = R_{opaque\ component} + R_{air-in}$ 4.20	6.81	m ² k/W
03	Thermal resistance of the wall excluding inside and outside air film resistances	ΣRII	$RII_{combination} = R_{opaque\ component}$ 4.20	6.67	m ² k/W
04	Outside-surface temperature	T_{pv}	4.13	300,74	°K
05	Inside-surface temperature	T_{pv}	4.14	300,08	°K
06	Heat flow	q	4.15	0,10	W/m ²

Tab. 5.45 Surface temperatures and heat flow – BAPV - Layer-02 - boundary condition in table 5.42

In the absence of irradiation, Layer-02 also experiences no diffraction of irradiation. Considering both layers of BAPV, Table 5.46 presents the resulting surface temperatures, heat flows, and the diffraction of irradiation (resulting from Layer-01).

	Outside air temperature	Inside air temperature	Outside surface temperature	Inside surface temperature	Total heat flow	Value of heat flow	Total irradiation	Reflection	Convection	Emission	Transmission	Electricity	Conduction
	T_{out}	T_{in}	T_{s-out}	T_{s-in}	q_{all}	Value	Q_{sol}	q_{ref}	q_{con}	q_{emi}	q_{tra}	q_{ele}	q_{cond}
	°C	°C	°C	°C	W/m ²	W/m ²	W/m ²	W/m ²	W/m ²	W/m ²	W/m ²	W/m ²	W/m ²
Layer-01	27,60	27,60	34,21	33,50	74,97	-	479,02	-181,51	-84,43	-87,48	0,00	-50,63	74,97
Layer-02	27,60	26,92	27,59	26,93	0,10	G-	0,00	0,00	0,10	0,00	0,00	0,00	0,10
Result	27,60	26,92	34,21	26,93	0,10	G-	479,02	-181,51	-84,43	-87,48	0,00	-50,63	0,10

Tab. 5.46 Surface temperatures and diffraction of irradiation, BAPV, 10 cm air gap - boundary condition in table 5.42

Regarding the different amounts of heat flow in Layer-01 and Layer-02, the heat flow of Layer-02 is taken into account, as it indicates the quantity of effective heat flow in connection with the building's components. Due to the similarities between the construction of BAPV and BIPV, as well as the calculation procedures, the daily performance of BAPV on a winter day is not explained, and the results of BAPV are discussed directly at the monthly level.

5.9.2 Monthly performance

The monthly cumulative heat flow in BAPV, considering the defined boundary conditions, applied values, and resulting energy demands, is shown in Figure 5.53.



Fig. 5.53 Monthly cumulative heating demand, heating auxiliary, cooling demand and cooling auxiliary – BAPV (W/m²), Geometrical setup and boundary condition in table 5.42

Integrating the electricity generation amounts into the monthly energy performance of BAPV results in its energy performance, as shown in Figure 5.54.

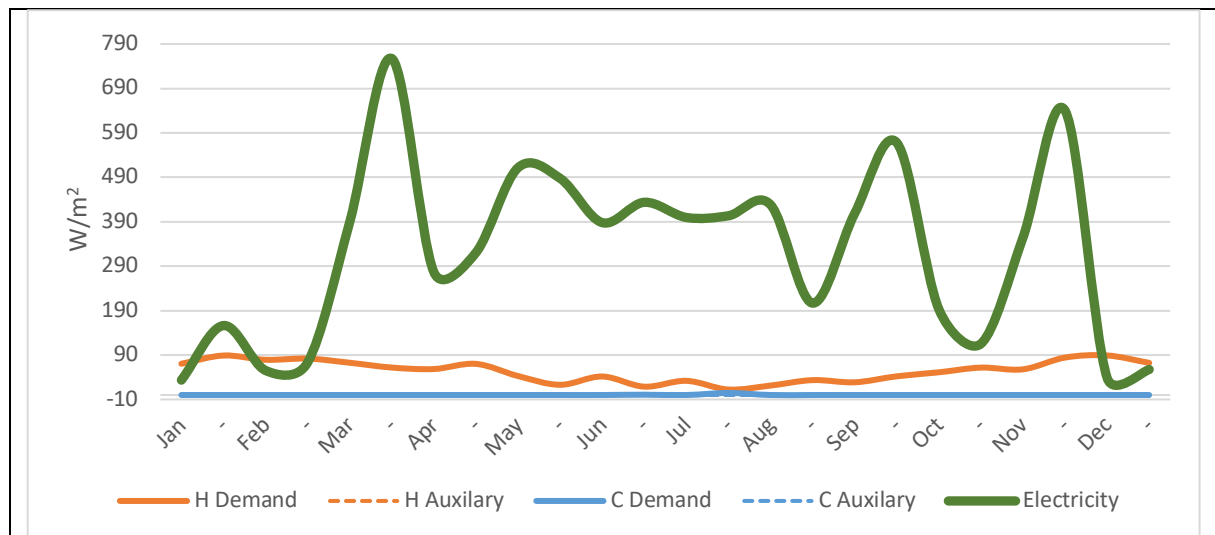


Fig. 5.54 Monthly energy demands – electricity generation (W/m²) - BAPV - Geometrical setup and boundary condition in table 5.42

5.9.3 Inclination and orientation

Regarding the same procedure for assessing the effects of orientation on the energy performance of BAPV and BIPV, performance comparisons of BAPV in different orientations are not presented. Instead, the effect of different inclinations is discussed purposefully, as the assumption of convective heat transfer coefficients in different inclinations in the backside air layer is exclusively employed in BAPV energy performances. A comparison of the energy

performance of a south-facing (orientation: 0°) BAPV in all four main inclinations has been conducted (Table 5.47).

Component	Inclination (°)	Orientation (°)	Inside temperature (Set)	Date	Transmittance factor (front glass)	U-value (W/m ² .K)	h _i (W/m ² .K)	α _{coeff} (%/K)	T _{STC} (°C)	η
Layer-01	0, 30, 60, 90	0	-	annual	1.5	100	12.70	0.02	43	0.20
Layer-02			High	annual	-	0.15	7.00	-	-	-

Tab. 5.47 Thermal and electrical characteristic of applied BAPV to opaque component and boundary condition

The results of comparing the effects of the four main orientations in vertical inclination are shown in Figure 5.55.

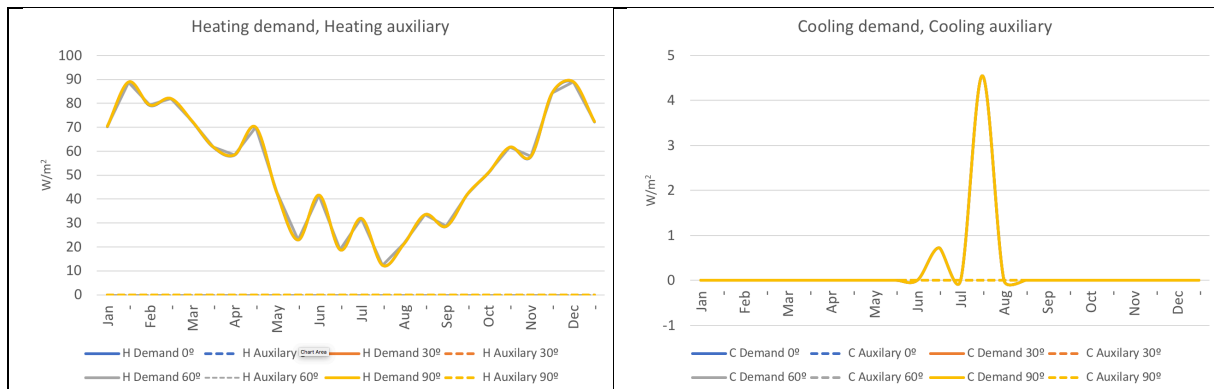


Fig. 5.55 heating demand + heating auxiliary (left), cooling demand + cooling auxiliary (right) (W/m²) BAPV - Geometrical setup and boundary condition in table 5.47 – Different inclinations

Regarding the absence of irradiation and outside emission in Layer-02 of BAPV (the inside layer), the fluctuation of heating and cooling demands shows approximately the same levels. Similarly, the effects of different convective heat transfer coefficients due to varying wind velocities will not significantly affect the final performance. On the outside, electricity generation is continuously influenced by all weather parameters dependent on geometrical configurations as well. The fluctuation of electricity generation under the defined boundary conditions in different inclinations is shown in Figure 5.56.

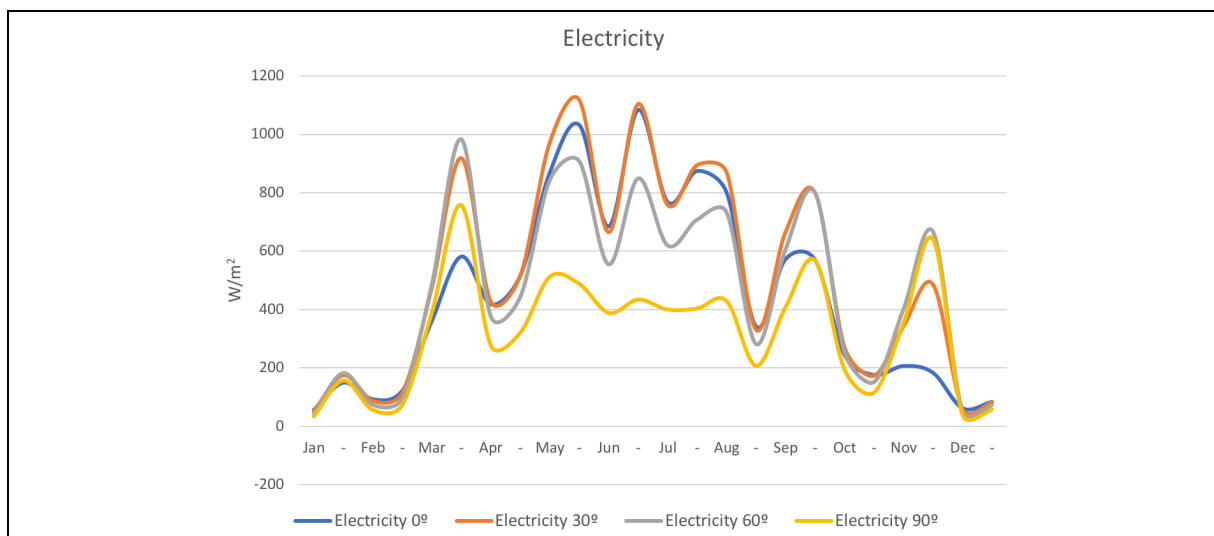


Fig. 5.56 Monthly electricity generation (W/m²) - BAPV - Geometrical setup and boundary condition in table 5.44 – Different inclinations – boundary condition in table 5.47

5.10 PV glazing

Supposing partial integration of PVs on existing transparent components in this work, two different parts have been separately calculated. The first part indicates areas of the component that are covered by PVs (encapsulated between two transparent layers), and the second part indicates areas of the component that remain transparent without any PV coverage. Regarding different possible proportions of 'areas with PVs' and 'areas without PVs,' the possibility of applying different proportional ratios is considered in calculations, but a certain ratio of 75% allocated to 'areas with PVs' and 25% to 'areas without PVs' is selected for different types of PV glazing. Figure 5.57 shows the applied proportional area of PV glazing.

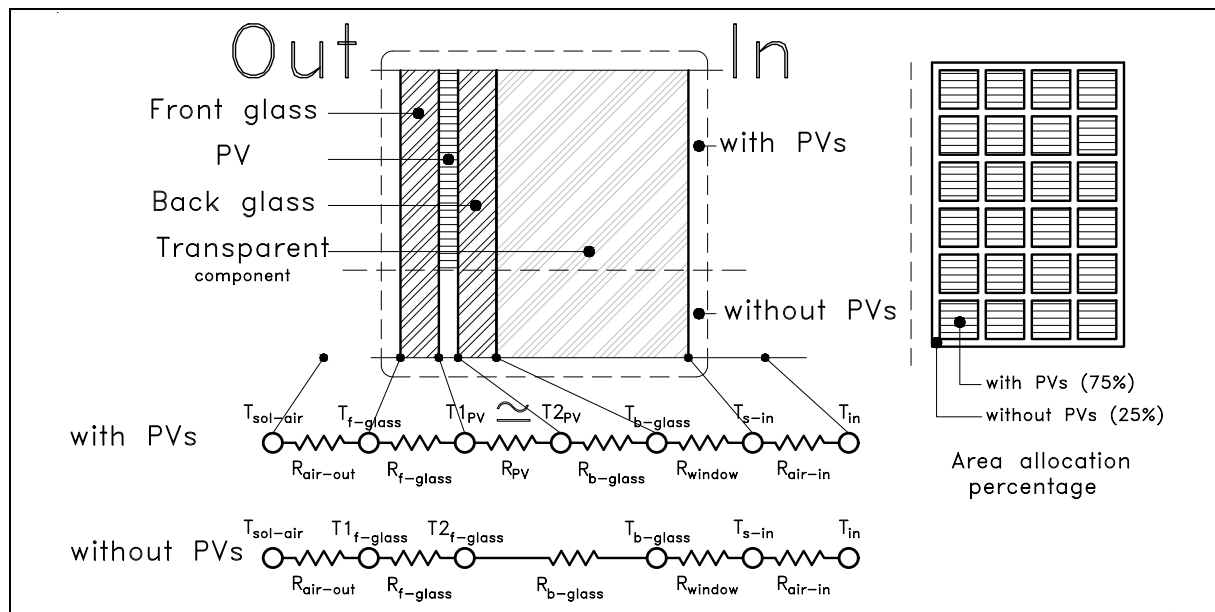


Fig. 5.57 Physical construction of considered PV glazing + thermal resistance algorithm + considered area allocation percentage

5.10.1 Daily performance - Summer day

Electrical power and thermal performance calculations for 'areas with PVs' and 'areas without PVs' on the representative day of July 26th at 11:00 are separately displayed in Table 5.48.

Component	Inclination	Orientation	Inside temperature	Date	Transmittance factor (front glass)	U-value (W/m ² .K)	h _i (W/m ² .K)	α _{coeff} (%/K)	T _{STC} (°C)	η
With PVs	90 (°)	0 (°)	High	26 th Jul 1	1.5		7.00	0.02	43	0.20
Without PVs	90	0	High	26 th Jul	1.5	0.497	7.00	-	-	-

Tab. 5.48 Thermal and electrical characteristic of PV glazing and boundary condition

The calculation of surface temperatures and heat flow is displayed in Table 5.49, and the division of diffraction of irradiation is shown in Table 5.50.

N	Parameter	Symbol	Equation	Result	Unit
06	Effective irradiation	I	$Power\ input = (1 - \gamma_f - \alpha_f - \alpha_b \cdot \tau_{PV} \cdot \tau_f - \tau_b \cdot \tau_{PV} \cdot \tau_f) \cdot Q_{sol}$	191,61	W/m ²
07	Solar-air temperature	T _{sol-air}	4.12	314,50	°C
08	Thermal resistance of wall excluding outside air resistance	∑RI	$RI_{combination} = R_{front\ glass} + R_{PV} + R_{back} + R_{Window} + R_{air\ in}$	2,15	m ² k/W
09	Thermal resistance of wall excluding inside and outside air resistances	∑RII	$RII_{combination} = R_{front\ glass} + R_{PV} + R_{back} + R_{Window}$	2,01	m ² k/W
10	PV operating temperature	T _{PV}	$T_M = \frac{h_o \cdot T_{sol-air} + \left(\frac{T_{in}}{\sum RI}\right)}{\left(\frac{1}{\sum RI}\right) + h_o}$ (4.13)	313,89	°K
11	Inside surface temperature	T _{s-in}	$T_{s-in} = T_M + (h_o \cdot \sum RII \cdot (T_M - T_{sol-air}))$ (4.14)	301,60	°K
12	Heat flow	q	$q = h_o \cdot (T_{sol-air} - T_M)$ (4.15)	6,12	W/m ²

Tab. 5.49 Surface and operating temperatures, PV glazing, Areas with PVs – boundary condition in table 5.48

N	Parameter	Symbol	Equation	Result	Unit
13	Electricity generation	q _e	$Electrical\ power = [\eta \cdot (1 - \alpha_{coeff} \cdot (T_M - T_{STC})) \cdot \tau_f \cdot G]$	-49,04	W/m ²
12	Outside reflection	q _{ref}	$q_{ref} = Q_{sol} - (B_{(h)}r_{B(\omega)} + D_{(h)}r_{D(\omega)})$	-181,51	W/m ²
13	Outside emission	q _{rad}	4.19	-127,42	W/m ²
14	Outside convection	q _{con}	4.18	-114,93	W/m ²

Tab. 5.50 Diffraction of irradiation, PV glazing, Areas with PVs - boundary condition in table 5.48

And in ‘areas without PVs’ surface temperatures, heat flow and diffractions of irradiation are calculated and shown in table 5.51.

N	Parameter	Symbol	Equation	Result	Unit
06	Effective irradiation	Q _{sol}	4.6	191,61	W/m ²
07	Solar-air temperature	T _{sol-air}	4.12	301,27	°C
08	Thermal resistance of the wall excluding outside air film resistance	∑RI	$RI_{combination} = R_{front\ glass} + R_{back} + R_{Window} + R_{air\ in}$ 4.20	2,15	m ² k/W
09	Thermal resistance of the wall excluding inside and outside air film resistances	∑RII	$RII_{combination} = R_{front\ glass} + R_{back} + R_{Window}$ 4.20	2,01	m ² k/W
10	Outside surface temperature	T _{s-out}	4.13	301,22	°K
11	Inside surface temperature	T _{s-in}	4.14	300,15	°K
12	Heat flow	q	4.15	0,54	W/m ²
13	transmission	q _{tr}	$0.815 \cdot (q_{sol} - q_{ref})$	-242,47	W/m ²
12	outside reflection	q _{ref}	$q_{ref} = Q_{sol} - (B_{(h)}r_{B(\omega)} + D_{(h)}r_{D(\omega)})$	-181,51	W/m ²
13	outside emission	q _{rad}	4.19	-52,18	W/m ²
14	outside convection	q _{con}	4.18	-2,32	W/m ²

Tab. 5.51 Surface temperatures + Diffraction of irradiation, PV glazing, Areas without PVs - boundary condition: table 5.48 * Results of calculated ∑RII and ∑RI indicate no different comparing to the same thermal resistance of ‘areas with PVs’ regarding low quantity of R_{PV} that is 0.000001 m²k/W

To determine the performance of a component that is a combination of areas with and without PVs, the amount of outside convection, emission, transmission, and electricity is calculated using correlation 4.24. Since each configuration indicates different surface temperatures, the result is recorded as 'multi,' indicating two different surface temperatures. The final performance of the component is presented in Table 5.52.

	Outside air temperature	Inside air temperature	Outside surface temperature	Inside surface temperature	Total heat flow	Value of heat flow	Total irradiation	Reflection	Convection	Emission	Transmission	Electricity	Conduction
	T _{out}	T _{in}	T _{s-out}	T _{s-in}	q _{all}	Value	Q _{sol}	q _{ref}	q _{con}	q _{emi}	q _{tra}	q _{ele}	q _{cond}
	°C	°C	°C	°C	W/m ²	W/m ²	W/m ²	W/m ²	W/m ²	W/m ²	W/m ²	W/m ²	W/m ²
With PVs	27,60	26,92	40,74	28,45	6,12	G-	479,02	-181,51	-114,93	-127,42	0,00	-49,04	6,12
Without PVs	27,60	26,92	28,07	27,00	243,01	G-	479,02	-181,51	-2,32	-52,18	-242,47	0,00	0,54
Combination	27,60	26,92	Multi	Multi	65,34	G-	479,02	-181,51	-86,78	-108,61	-60,62	-36,78	4,72

Tab. 5.52 Surface temperatures and diffraction of irradiation, PV glazing (75% with PVs + 25% without PVs) - boundary condition in table 5.48

Since the construction of the assumed PV glazing integrates the same PV technology applied in both BIPV and BAPV, and the inner side consists of a transparent component, the performance in areas of PV glazing without PVs is exactly the same as the performance of the transparent component. The only change is the inclusion of low quantities of additional thermal resistance from the front glass and back glass of the PV glazing, which results in a shift in the U-value of the window from 0.5 W/m²·K to 0.497 W/m²·K.

In areas with PVs, considering the extremely low calculated thermal resistance of the PV material (0.000001 m²·K/W), the final U-value again remains at 0.497 W/m²·K. Therefore, due to the nearly identical energy performance of PV glazing in areas without PVs compared to standard windows, the calculation procedure for daily performance in areas without PVs is not presented.

In areas with PVs, where the PV is attached to an inside thermal resistance (an existing window with a thermal resistance of 2.00 m²·K/W), the calculation procedure is exactly the same as the procedure used for BIPV (the application of PV to an existing thermal resistance of an opaque component). Hence, an explanation of the calculation procedure for areas with PVs is also omitted.

5.10.2 Monthly performance

Monthly cumulative heat flow in PV glazing, considering the defined boundary conditions, applied values, and resulting energy demands, is shown in Figure 5.58.

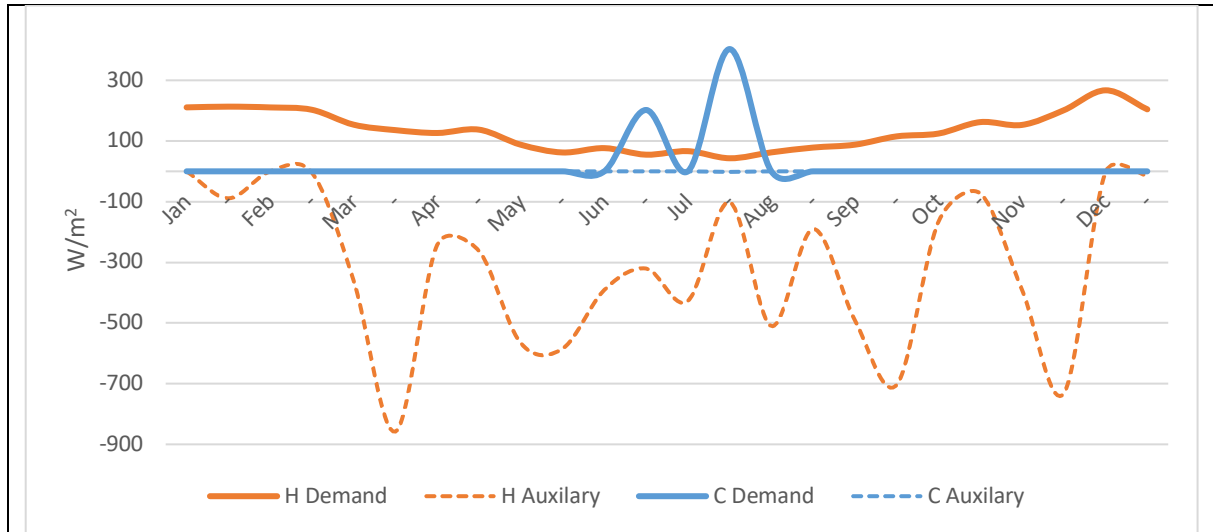


Fig. 5.58 Monthly cumulative heating demand, heating auxiliary, cooling demand and cooling auxiliary – PV glazing (W/m²), Geometrical setup and boundary condition in table 5.48

Integrating electricity generation amounts into the monthly energy performance of PV glazing results in its energy performance, as shown in Figure 5.59.

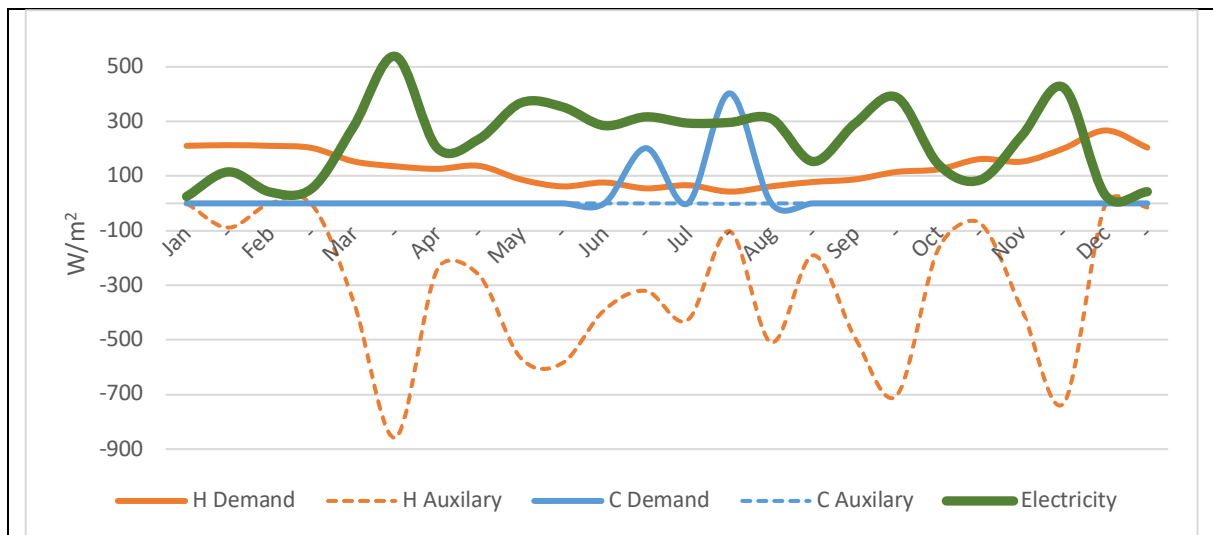


Fig. 5.59 Monthly energy demands – electricity generation (W/m²) – PV glazing - Geometrical setup and boundary condition in table 5.48

5.10.3 Inclination and orientation

Regarding the construction of PV glazing, which combines a transparent component with opaque PV panels, and considering the possibilities of different area allocations (the ratio of areas with PVs to areas without PVs), various energy performance scenarios with different quantities and proportions of energy demands and auxiliaries will be explored. Rates of electricity generation will also be directly related to the percentage of areas with PVs.

5.11 Comparing 5 components

To compare the electrical power and thermal performance of all five defined components in this study, specific geometrical setups representing the most common inclination and orientation have been selected. A comprehensive calculation has been conducted considering possible variants that take into account the interaction of geometrical configurations, boundary conditions, components, and the representative date (Table 5.53). The results obtained are simultaneously used in the calculations of the final indexes of self-sufficiency and self-consumption. For the purpose of discussing and revealing the effects of different geometrical setups across different components, we have chosen some selective geometrical setups. Upcoming graphs will compare the electrical power and thermal performance of these five components at an inclination of 90° (vertical) with an orientation of 0° (south-faced) (Figures 5.60 and 5.61).

Component	Inclination ($^\circ$)	Orientation ($^\circ$)	Inside temperature (Set)	Date	Transmittance factor (front glass)	U-value ($W/m^2.K$) *	h_i ($W/m^2.K$)	α_{coeff} (%/K) **	T_{STC} ($^\circ C$) **	η **
5 components	90	0	High	annual	1.5	a. 0.15 b. 0.5 c. 0.084 d. 0.15 e. 0.497	7.00	0.02	43	0.20

Tab. 5.53 Thermal and electrical characteristic of applied BAPV to opaque component and boundary condition
*. Amount of u-value is assumed regarding construction of each component; a. opaque, b. transparent, c. BIPV, d. BAPV, e. PV glazing
**. Applied to BIPV, BAPV and PV glazing

The comparison of the thermal performance of all five components are in Figure 5.60.

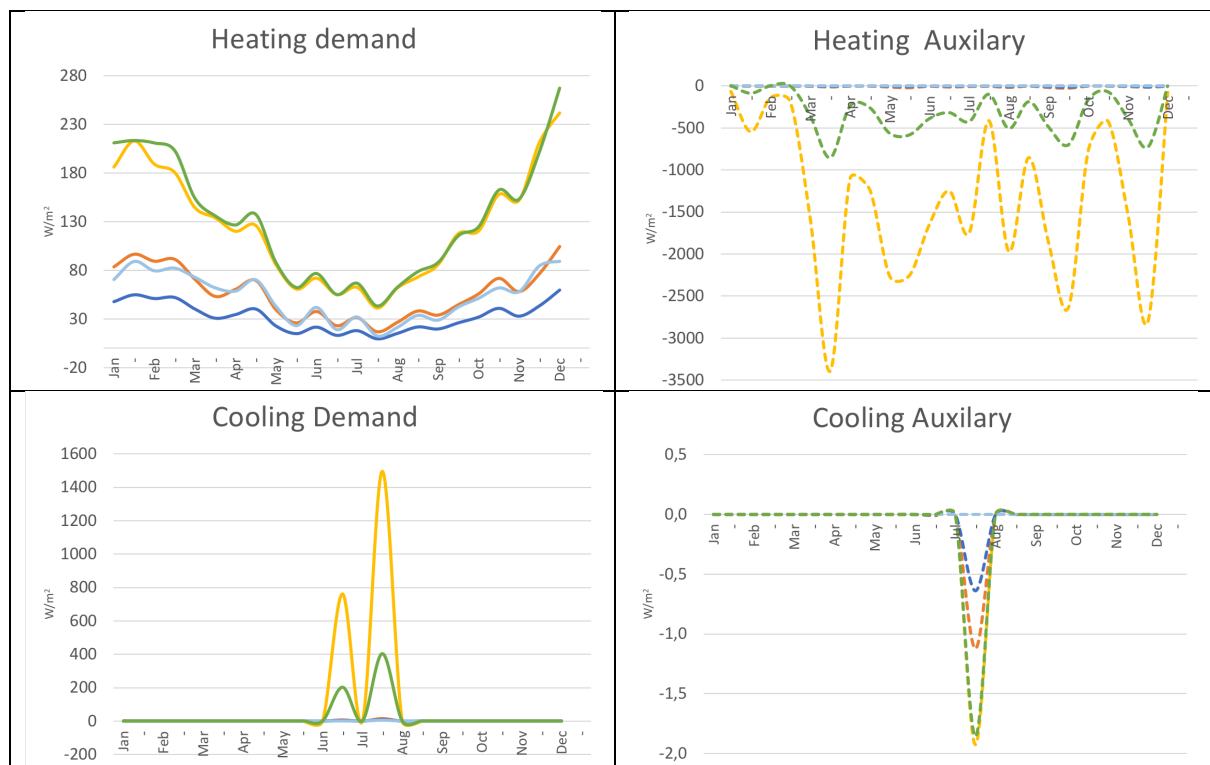


Fig. 5.60 Monthly heating demand, heating auxiliary, cooling demand, cooling auxiliary(W/m^2) – 5 components, Geometrical setup and boundary condition in table 5.53

● Opaque, ● Transparent, ● BIPV, ● BAPV, ● PV glazing

Comparing the heating demand of all five components demonstrates a remarkable effect of the U-value of each component on the calculated heating demand, with the lowest demand belonging to BIPV. It should be noted that the higher cooling demand of PV glazing compared to windows is justified, considering that the total amount of 'transmitted heat' in transparent components is calculated through the cumulative calculation of 'transmission + conduction.' Due to the larger transparent area, windows have more transmitted quantities of irradiation compared to PV glazing, which leads to a higher cooling demand as well. The comparison of electricity generation for the three components equipped with PVs is shown in Figure 5.61.

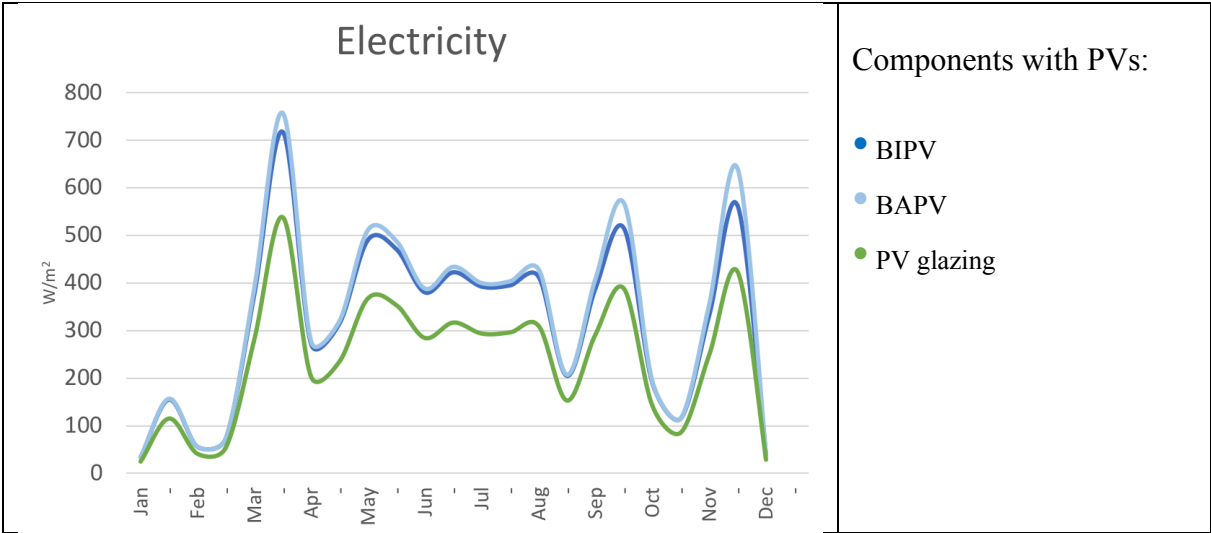


Fig. 5.61 Monthly electricity generation (W/m²) – 3 components, Geometrical setup and boundary condition in table 5.53

The graph demonstrates a higher quantity of generated electricity by BAPV compared to BIPV, primarily due to the comparatively lower operating temperature of BAPV. The lower performance of PV glazing is also a result of the lower integrated PV area percentage compared to BIPV and BAPV, which has been assumed to be 75% of the total area of the module.

5.12 Proportion of outside convection and emission (BIPV)

Other comparisons have also been conducted regarding the proportion of outside convection and emission in different inclinations and orientations. The employed data have been collected based on the available proportion of emission and convection calculated in the diffraction of irradiation within each component. Figures 5.62 and 5.63 illustrate the proportion of convection and emission in BIPV across different inclinations and orientations, respectively, encompassing the four main orientations and four main inclinations.

These comparisons, rather than different quantities of calculated heat flows, determine the quantities of the different proportion of outside convection and emission resulting from various geometrical setups. Further development of these comparisons can be utilized for determining the type of insulation that may be integrated into different orientations and inclinations, as opposed to specifying the amount of integrated insulation. Essentially, the insulation of heat flows resulting from convection suggests different types of insulation materials compared to situations where heat flow is primarily a result of emission. These results are not currently employed in the defined hypothesis of this work but can be utilized for further research into insulation types.

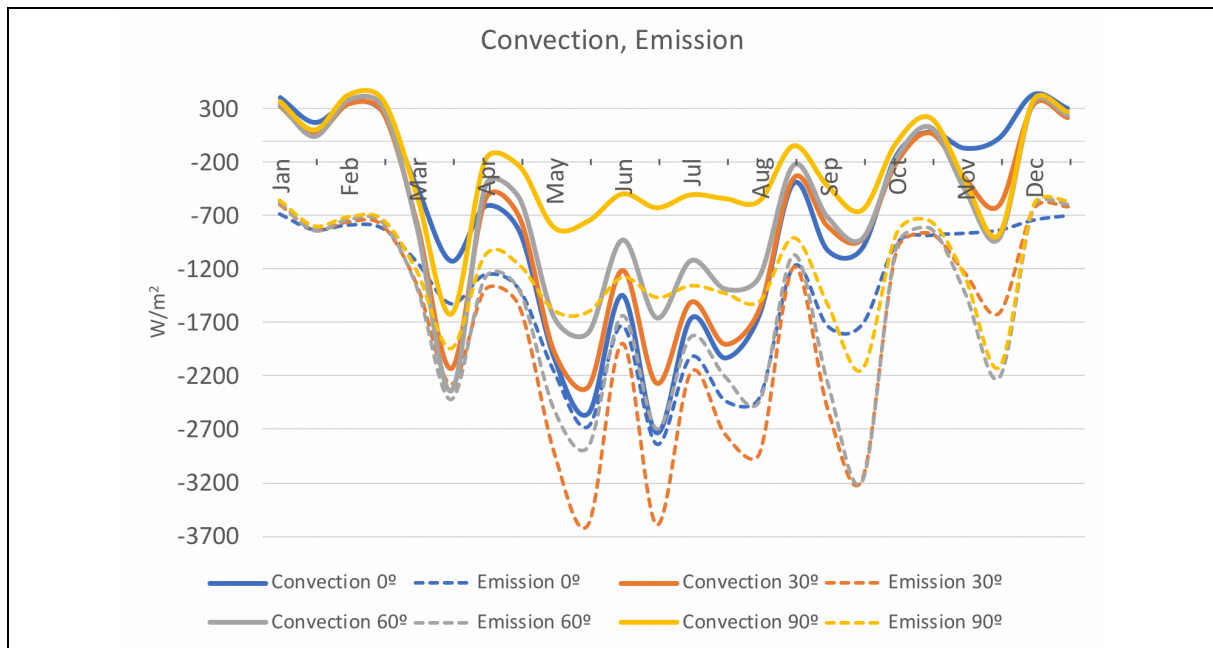


Fig. 5.62 Proportions of outside convection and emission (W/m^2) – BIPV – south-faced - different inclinations - Boundary condition in table 5.40

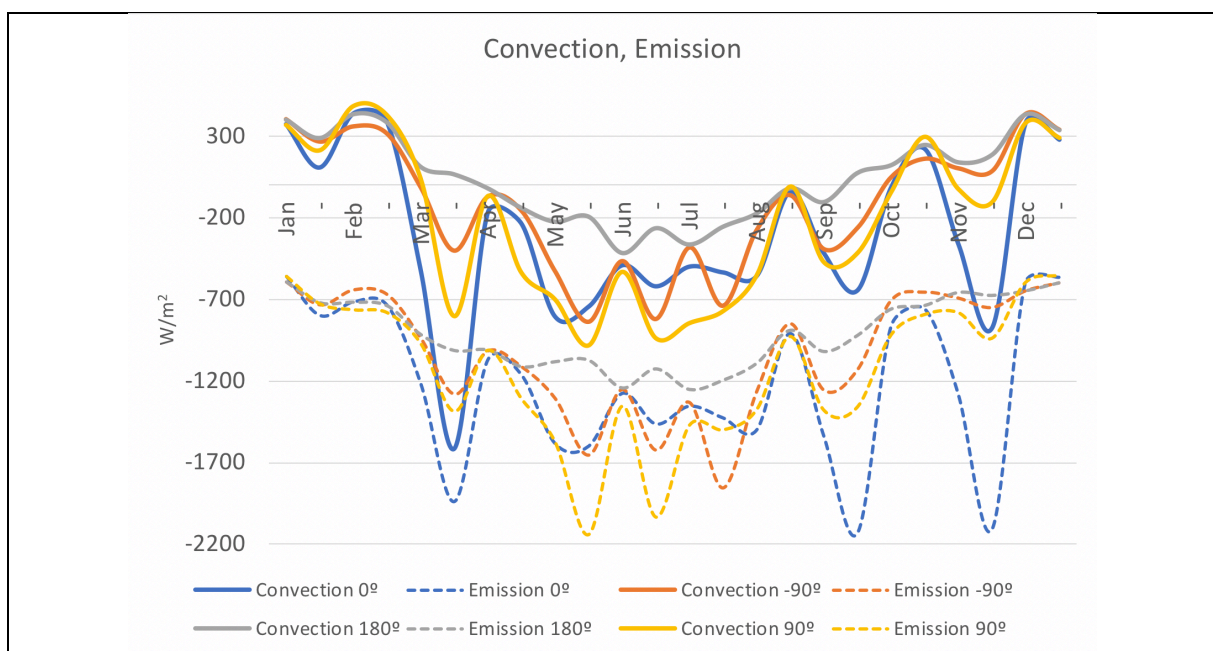


Fig. 5.63 Proportions of outside convection and emission (W/m^2) – BIPV – vertical - different orientations - Boundary condition in table 5.39

The fluctuation of convection and emission is a complex outcome resulting from changes in all integrated parameters and geometrical setups. It should be noted that this fluctuation significantly impacts the inside comfort temperature as well. The variation in both calculated convection and emission across different orientations and inclinations of BIPV demonstrates that each specific component setup resulting from a particular inclination and orientation leads to a unique pattern of changes in convection and emission. These changes vary quantitatively throughout different intervals of the year.

6. Self-sufficiency – self consumption

The two indexes, self-sufficiency and self-consumption, indicate the 'sufficiency of a building to cover its own demand' and the 'potential of a building to consume its own generated electricity,' respectively. The constant consideration of both indexes is the objective of high-efficient buildings. Achieving high degrees of self-sufficiency is relatively easy, but achieving high degrees of self-consumption can be challenging. This means that by integrating more quantities of PVs, self-sufficiency can approach 1.00, indicating a zero-energy building. However, a significant portion of the generated electricity may not be consumed by the building itself, leading to lower degrees of self-consumption.

The index of self-sufficiency has been defined as 'the degree to which on-site generation is sufficient to meet the energy needs of the building' [01], representing the ratio of 'covered energy demand' to 'total energy demand.' In parallel, the index of self-consumption has been defined as 'the self-consumed part of on-site generation relative to the total production' [01]. Figure 6.1 provides a schematic representation of the generation and consumption of electricity particles related to the fluctuation of energy demand during a day.

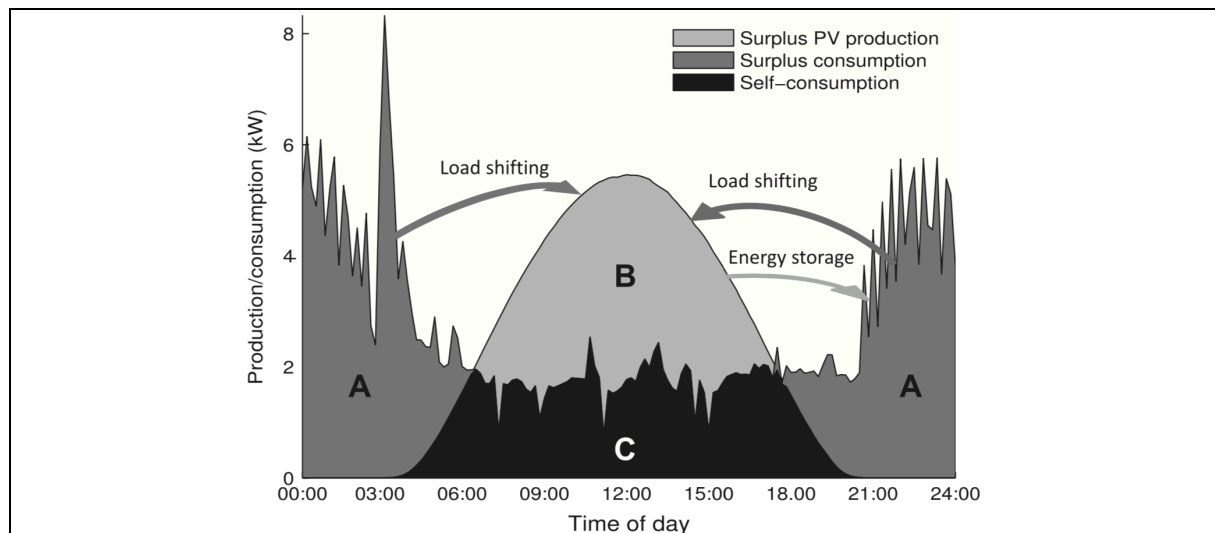


Fig.6.1 Schematic outline of daily net load (A + C) and net generation (B + C) in a building with on-site PV [01]

The daily fluctuation of on-site electricity generation and energy demand (Figure 6.1) can be assumed to represent the annual fluctuation of 'energy generation' and 'energy demand,' especially in a climate like Germany, where energy demand is higher at the beginning and end of the year compared to mid-summer, primarily due to heating demand. Similarly, the maximum electricity generation occurs in mid-summer due to the higher quantities of irradiation. Considering the particles of energy generation and energy demands in Figure 6.1, correlations for self-sufficiency and self-consumption are defined through Equations 6.1 and 6.2 [01].

$$\text{Self} - \text{sufficiency} = \frac{C}{A+C} \quad (6.1)$$

$$\text{Self} - \text{consumption} = \frac{C}{B+C} \quad (6.2)$$

Where;

- A Uncovered demand
- B Unused electricity generation of on-site PV
- C Used electricity generation of on-site PV
- B+C Total electricity generation by on-site PV
- A+C Total energy demand

Assuming that the total amount of energy demand of the building is derived from the 'cumulation of heating and cooling demand' and a 'flat rate of energy demand,' the proportions of 'A+C' referring to 'total energy demand' can be defined as follows:

- A+C (part a) Energy demand through building's envelope
- A+C (part b) Flat rate of energy demand

Considering that 'part a' has been calculated based on the heating and cooling demand of the integrated components in the building's envelope, a flat rate of energy demand mainly coming from the cumulation of lighting, household appliances, cooking, etc., must be assumed. Based on calculations and measurements from 36 pilot projects of efficient houses, it is reasonable to assume a flat rate of energy demand for medium-sized buildings at 20 kWh/m² per year (Table 6.1) [54].

Effizienzhaus Plus Standard	Pauschal [kWh/m ² a]		Maximum je Wohneinheit [kWh/a]
Beleuchtung	3		375
Haushaltsgeräte	10	17	1.250
Kochen	3		375
Sonstiges	4		500
Summe	20		2.500

Tab. 6.1 Flat-rate size of energy to be applied for lighting, household appliances, cooking and other items according to the Efficiency House Plus standard [54]

6.1 Energy demand through building's envelope

To calculate the 'energy demand through the building's envelope,' which is estimated as the 'A+C (part a)' contribution of components integrated in the same façade to compensate parts of their 'energy demand' by 'energy auxiliary,' various proportional combinations of the five defined components in this study are possible. In each calculation interval (each hour), specific 'heating demand' of each component can be offset by the 'heating auxiliary' of other components in the same façade. Similarly, in each calculation interval (each hour), certain 'cooling demand' of each component can be offset by the 'cooling auxiliary' of other components in the same façade.

Consequently, in combined facades (combinations of 2, 3, 4, or 5 types of components), new heating demand, heating auxiliary, cooling demand, and cooling auxiliary values will be calculated in each interval based on the absolute mathematical values recorded.

$$\begin{aligned}
G_{+total} &= (a.G_{+opaque}) + (b.G_{+transparent}) + (c.G_{+BIPV}) + (d.G_{+BAPV}) + (e.G_{+PV\ glazing}) \\
L_{-total} &= (a.L_{-opaque}) + (b.L_{-transparent}) + (c.L_{-BIPV}) + (d.L_{-BAPV}) + (e.L_{-PV\ glazing}) \\
L_{+total} &= (a.L_{+opaque}) + (b.L_{+transparent}) + (c.L_{+BIPV}) + (d.L_{+BAPV}) + (e.L_{+PV\ glazing}) \\
G_{-total} &= (a.G_{-opaque}) + (b.G_{-transparent}) + (c.G_{-BIPV}) + (d.G_{-BAPV}) + (e.G_{-PV\ glazing})
\end{aligned} \tag{6.3}$$

Where;

G+	heating auxiliary
L-	heating demand
L+	cooling auxiliary
G-	cooling demand
G ^{+total}	total heating auxiliary of combination of components
L ^{-total}	total heating demand of combination of components
L ^{+total}	total cooling auxiliary of combination of components
G ^{-total}	total cooling demand of combination of components
a	percentage of opaque component
b	percentage of transparent component
c	percentage of BIPV
d	percentage of BAPV
e	percentage of PV glazing

The result of the interaction between compensating quantities of heating and cooling demands by heating and cooling auxiliaries determines the heating and cooling demands of the composed façade, which result from the combination of components.

$$\begin{aligned}
H_{demand\ (composed\ facade)} &= H_{demand\ (total)} + H_{auxiliary\ (total)} = (L_{-total}) + (G_{+total}) \\
C_{demand\ (composed\ facade)} &= C_{demand\ (total)} + C_{auxiliary\ (total)} = (G_{-total}) + (L_{+total})
\end{aligned} \tag{6.4}$$

After calculating the amounts of heating and cooling demands per square meter, to determine the absolute quantity of heating and cooling demand for each facade, the area of each facade will be used (Equation 6.5).

$$\begin{aligned}
H_{absolute\ demand\ (composed\ facade)} &= H_{demand\ (composed\ facade)} \times Area_{facade} \\
C_{absolute\ demand\ (composed\ facade)} &= C_{demand\ (composed\ facade)} \times Area_{facade}
\end{aligned} \tag{6.5}$$

Assuming that the final heating demand and cooling demand of the building are determined through correlation 6.6, we can proceed with the calculation.

$$\begin{aligned}
H_{demand-building} &= \Sigma H_{absolute\ demand\ (all\ facades+roof+ground)} \\
C_{demand-building} &= \Sigma C_{absolute\ demand\ (all\ facades+roof+ground)}
\end{aligned} \tag{6.6}$$

6.2 Calibration of self-sufficiency and self-consumption

To calibrate the calculation of total energy demand and electricity generation for a building, a real constructed house certified by 'Forschungsinitiative - Zukunft Bau' has been chosen. This house features a simple and compact structure with no protruding or attached components. The living space is distributed over two full floors and an attic. The building is oriented with a 23° rotation toward the east. The geometrical setup of the building and its geographical location is illustrated in Figure 6.2 [62].

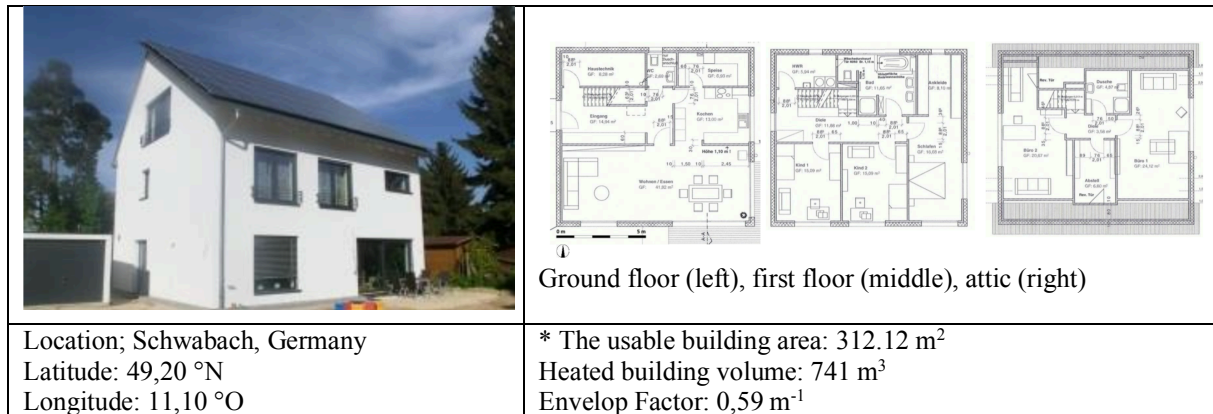


Fig. 6.2 Geographical location and geometrical setup of investigated building [62]

The area of each component and its U-value has been presented in Table 6.2 and Table 6.3 [62].

	Base plate	Window N-E	Window S-E	Window N-W	Window S-W	Door-opaque N-W	Wall N-E	Wall S-E	Wall S-W	Wall N-W	Inclined roof S-W*	Inclined roof N-E
Area (m ²)	113,25	3,74	21,18	6,95	22,71	3,90	69,27	66,06	50,30	76,39	80,50	65,96
U-value (W/m ² .K)	0,14	0,80	0,80	0,80	0,80	1,00	0,14	0,14	0,14	0,14	0,12	0,12

Tab. 6.2 Components in selected building – area – U-value [62]

* 18,2 m² is added to 'inclined roof S-W' to be adequate for holding 99 m² of PV in BAPV setup

Component	Material	Thickness (mm)	u-value (W/m ² .K)
Wall (inside to outside)	Gypsum plaster	15	0,14
	perforated bricks	490	
	Light plaster	20	
Window	Triple-glazed windows (g-value = 0.45)	-	0,80
Inclined roof (top to down)	PV	-	0,12
	Wood fiber insulation board	35	
	Mineral fiber insulation boards	300	
	Vapor barrier	-	
	Plasterboard 2-ply	12,5	
Base plate	Screed	60	0,14
	Impact sound insulation	30	
	Thermal insulation	50	
	Concrete slab	300	
	Perimeter insulation	150	

Tab. 6.3 Assembly of materials in each Components in selected building – thickness – U-value [62]

6.2.1 Energy concept

The entire house is heated by a central ventilation device. The primary integrated parallel devices include an exhaust air fan, a cross-counterflow heat exchanger with a regulated summer bypass, and a frequency-modulated air-to-air heat pump. The heat pump covers the majority of the annual heating workload. For additional conditioning of the supply air during peak heating demand, electrical heaters are installed in the air outlets. Depending on weather conditions, either outside air or preconditioned air is brought in as supply air via a geothermal heat exchanger. The system is controlled through a system-specific bus system, with the central touch control unit located in the living room.

Exhaust air rooms such as bathrooms and toilets are heated by electric convectors. The exhaust air is utilized as a heat source for a downstream air-water heat pump via a branch in the air duct network following the central ventilation unit. This heat pump heats the domestic hot water stored in its integrated 290-liter storage tank, which also includes an additional heating element.

A photovoltaic system is installed on the south side of the roof with a roof pitch of 35°. This system covers a total area of 99 m² and has a nominal output of 14.4 kW. The schematic of the energy concept of the building is depicted in Figure 6.3 [62].

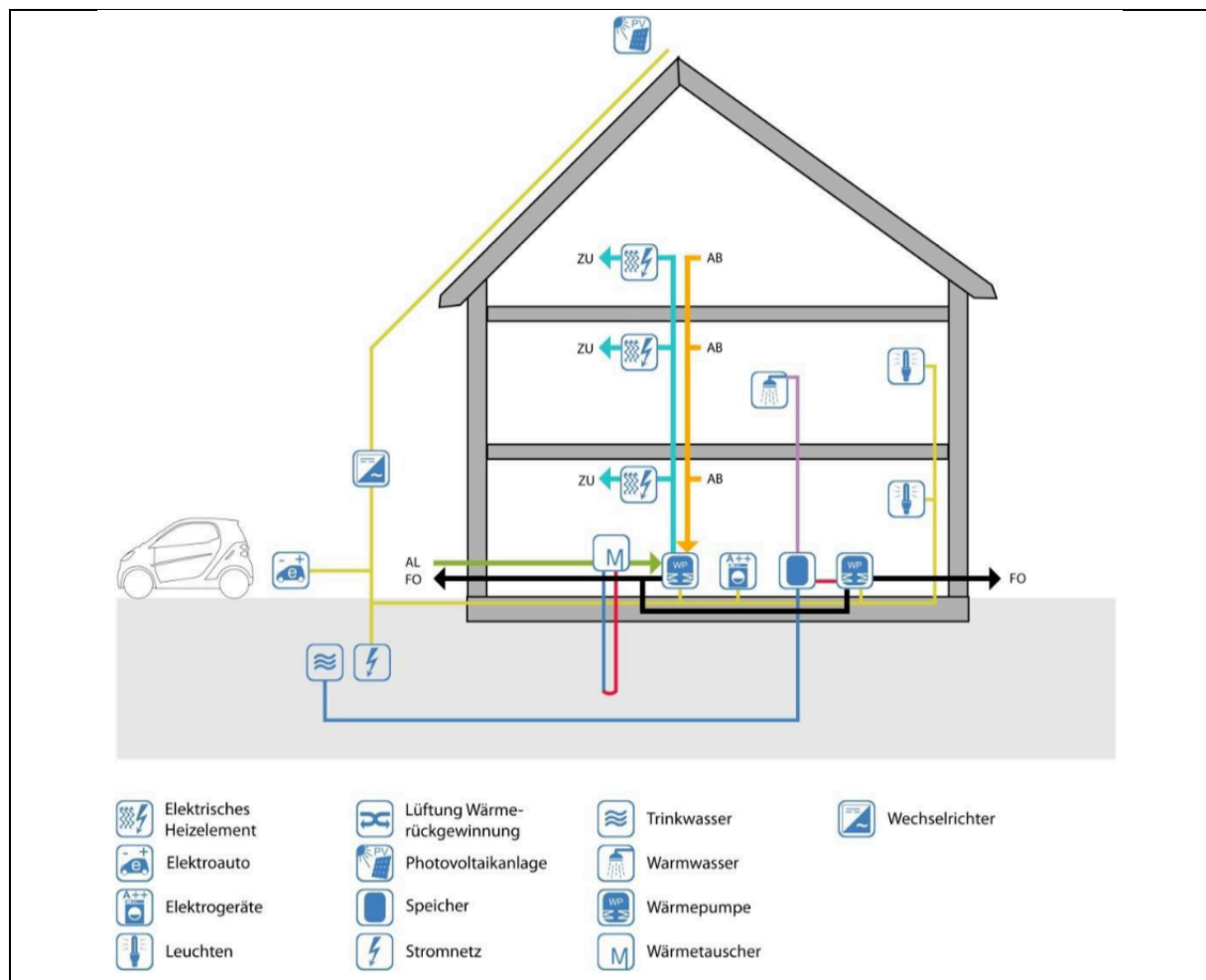


Fig. 6.3 Schematic of energy concept of selected building [62]

6.2.2 Boundary condition

Considering the building's location in Schwabach, the nearest available weather data from Nürnberg have been incorporated, taking into account irradiation, wind, and other relevant factors. In addition to irradiation, local wind velocities and direction have also been included (see Figure 6.4).

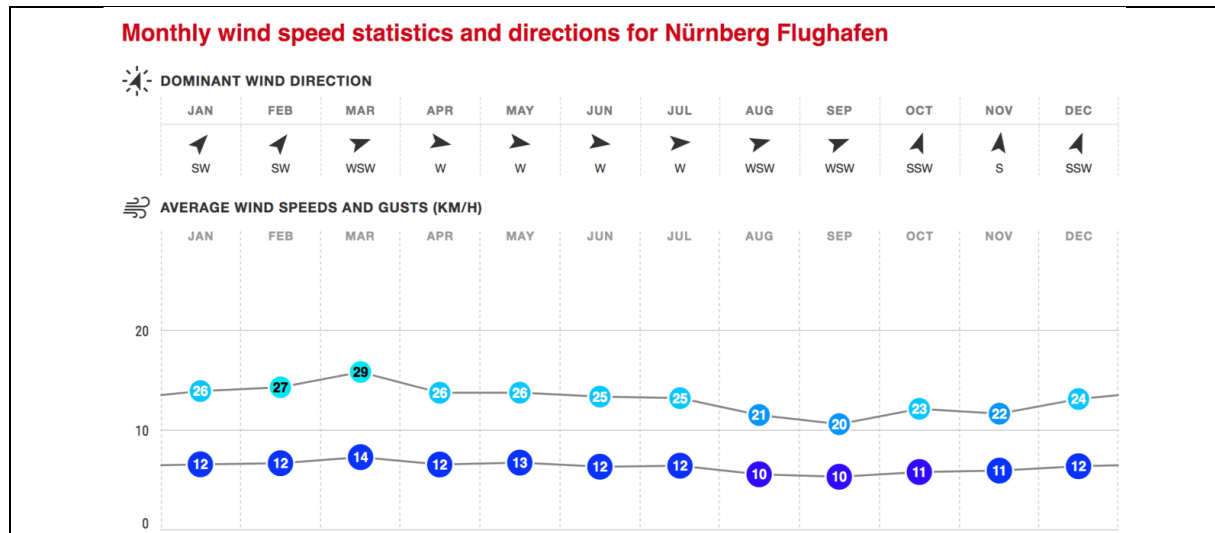


Fig. 6.4 Average and direction of wind – Nürnberg, Germany [46]

Concerning indoor comfort temperature, and based on two years of recorded indoor temperatures, the closest correlation between outside air temperature and the set indoor temperature has been incorporated (see Figure 6.5).

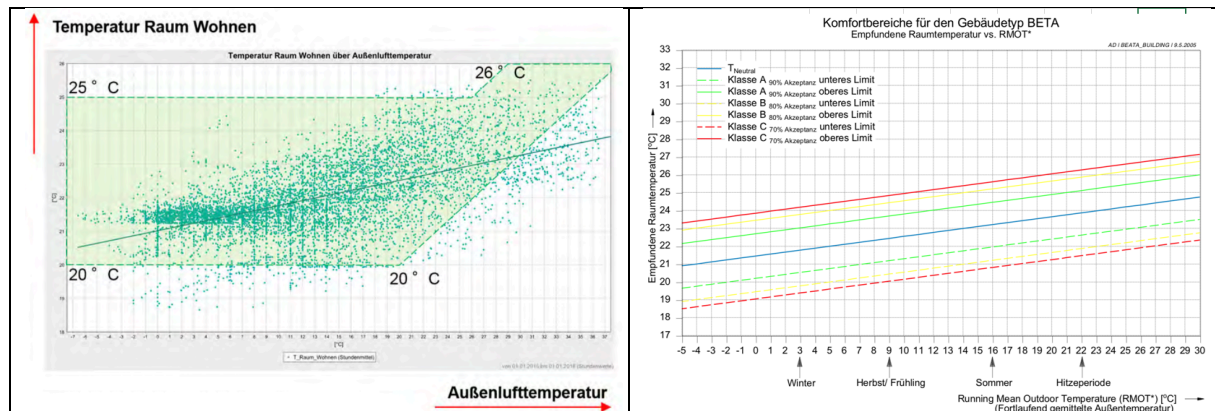


Fig. 6.5 Average of inside temperature in two years (left) [62], integration of 'blue line' as the most equivalent of recorded inside temperature (right) [40]

6.2.3 Energy performance of components

6.2.3.1 Walls

Considering the definition of materials and components, Table 6.4 displays the integrated parameters of the walls.

Component	Inclination (°)	Orientation (°)		Inside temperature (Set)	Heat conductivity (W/m.K)	Thickness (m)	U-value (W/m ² .K)	α_s (%)	h_i (W/m ² .K)
Opaque	90	23	S-W	Middle	0.03	0.21428	0.14	50	7
		113	N-W						
		-67	S-E						
		-157	N-E						

Tab. 6.4 Geometrical setup and material property in Walls

Figure 6.6 presents the results of calculations for heating demand, cooling demand, heating auxiliary, and cooling auxiliary in all four oriented walls.

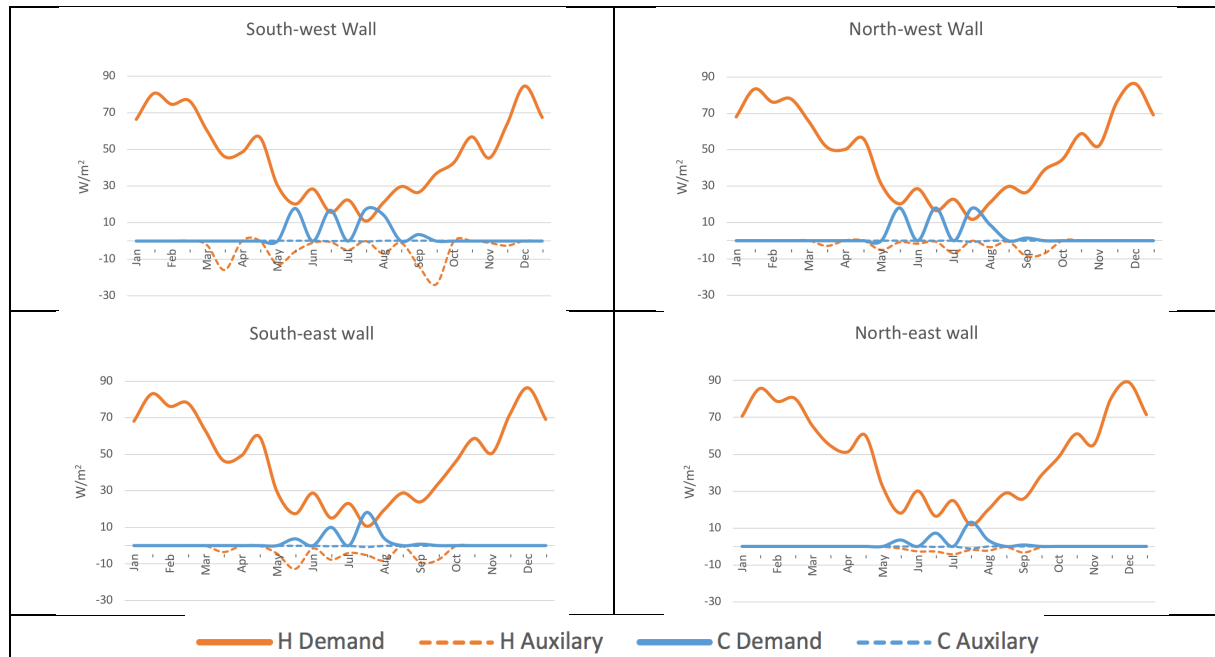


Fig. 6.6 Monthly energy performance of wall in four orientations of 23° (S-W), 113° (N-W), -67° (S-E) and -157° (N-E)

6.2.3.2 Windows

Considering the definition of windows, Table 6.5 displays the integrated parameters of windows.

Component	Inclination (°)	Orientation (°)		Inside temperature (Set)	Transmittance factor	U-value (W/m ² .K)	h_i (W/m ² .K)
Window	90	23	S-W	Middle	0.4	0.80	7
		113	N-W		*		
		-67	S-E				
		-157	N-E				

Tab. 6.5 Geometrical setup and material property in windows

* corresponding to g-value of approx. 0.45

Figure 6.7 presents the results of calculations for heating demand, cooling demand, heating auxiliary, and cooling auxiliary in all four oriented windows.

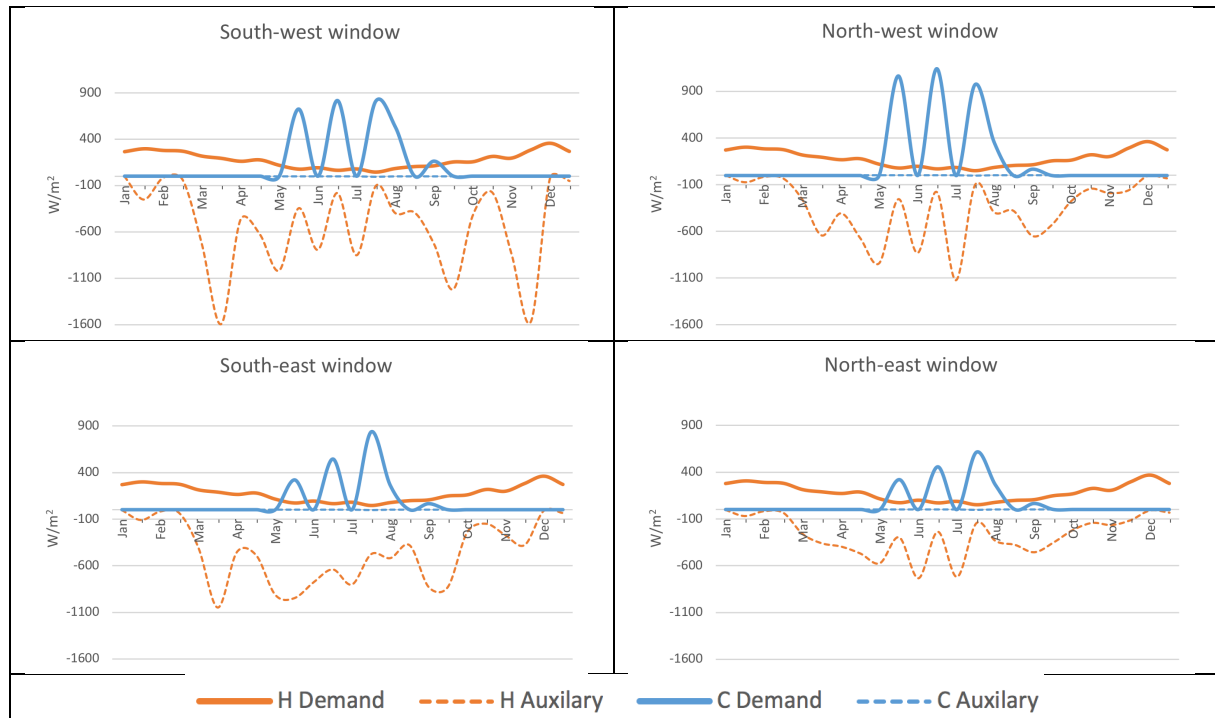


Fig. 6.7 Monthly energy performance of window in four orientations of 23° (S-W), 113° (N-W), -67° (S-E) and -157° (N-E)

6.2.3.3 Floor and door

The integrated parameters of the door (located in the north-west façade) and the floor are shown in Table 6.6.

Component	Inclination	Orientation		Inside temperature (Set)	Heat conductivity (W/m.K)	Thickness (m)	U-value (W/m².K)	h _i (W/m².K)
	(°)	(°)						
Floor	0	0		Middle	0.03	0.21428	0.14	7
Door	90	113	N-W	Middle	0.03	0.03	1.00	7

Tab. 6.6 Geometrical setup and material property in floor (up) and door (down)

The monthly energy performance of the floor and door is displayed in Figure 6.8.

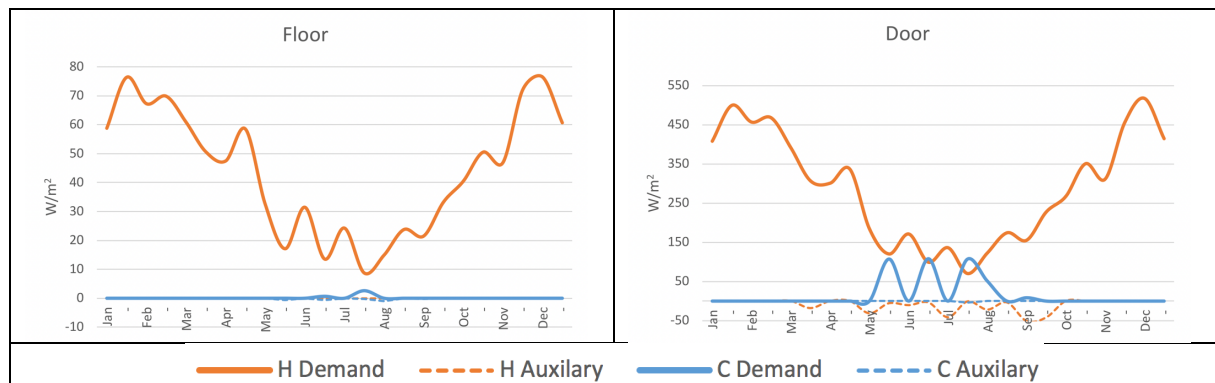


Fig. 6.8 Monthly energy performance of floor (left) and north-west orientated door, orientation 113° (right)

6.2.3.4 Roof

The integrated parameters of inclined roofs in three different setups have been considered. For the south-west roof, two different configurations were calculated: one with PVs as the main roof and the other with PVs as an extension of the roof (see Table 6.7).

Component	Inclination (°)	Orientation (°)	Inside temperature (Set)	Heat conductivity (W/m.K)	Thickness (m)	U-value (W/m ² .K)	α_s (%)	h_i (W/m ² .K)	α_{coeff} (%/K)	T_{STC} (°C)	η
Main roof (With PV)	35	23	Middle	0.03	0.25	0.12	-	7	0.031	48	17
Extended roof (with PV)	35	23	Middle	0.03	0.25	0.12	-	7	0.031	48	17
Main roof (without PV)	35	-157	Middle	0.03	0.25	0.12	50	7	-	48	17

Tab. 6.7 Geometrical setup and material property in inclined south-west and north-east roofs

The monthly energy performance of the three roof setups is displayed in Figure 6.9.

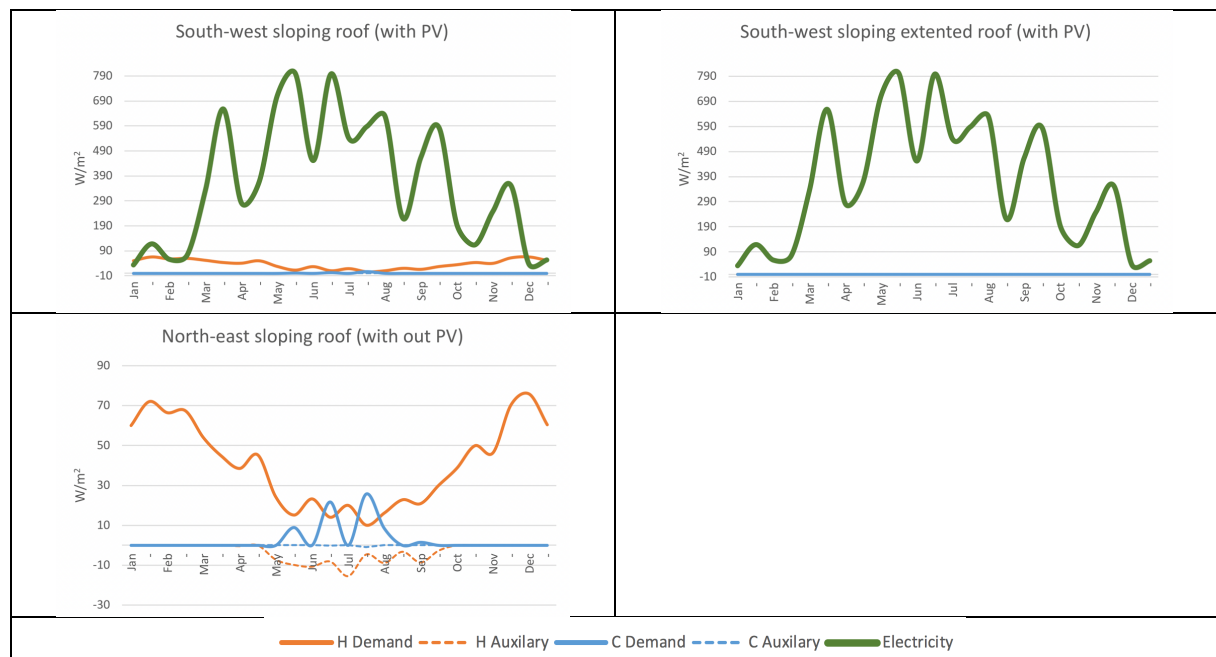


Fig. 6.9 Monthly energy performance of roof with and without PVs. Inclination 35° (all three setups) S-W with PV – main roof (top-left), S-W with PV – extended roof (top-right), N-E without PV (Bottom-left)

6.2.4 Energy demands – Electricity generation

To calculate the final energy demand of each façade, the area of each component (see Table 7.1) is multiplied by its energy performance. Then, considering the defined correlations in 6.3, the percentage of each component in the façade is incorporated. Finally, by using correlation 6.4, the proportions of heating and cooling demands that can be compensated by components integrated in the same façade are determined, thus moderating the quantity of heating demand. It is worth noting that moderating cooling demand is rarely recorded since cooling auxiliary in all components is registered as low amounts. Table 6.8 displays the calculated energy demands (equation 6.6), electricity generation, and their proportional coverage during one year in intervals of 15 days (on the 11th and 26th of each month).

	Jan 11th	Jan 26th	Feb 11th	Feb 26th	Mar 11th	Mar 26th	Apr 11th	Apr 26th	May 11th	May 26th	Jun 11th	Jun 26th
H Demand	48896,37	55907,73	53055,40	52856,15	40685,75	34665,39	31100,41	35748,08	21103,03	13085,76	19009,56	11147,05
H Demand (HP)	16298,79	18635,91	17685,13	17618,72	13561,92	11555,13	10366,80	11916,03	7034,34	4361,92	6336,52	3715,68
Extra Demand	9835,00	9835,00	9835,00	9835,00	9835,00	9835,00	9835,00	9835,00	9835,00	9835,00	9835,00	9835,00
DHW	2085,00	2085,00	2085,00	2085,00	2085,00	2085,00	2085,00	2085,00	2085,00	2085,00	2085,00	2085,00
C Demand	0,00	0,00	0,00	0,00	0,00	0,00	0,00	0,00	0,00	35724,18	0,00	45306,57
C Demand (HP)	0,00	0,00	0,00	0,00	0,00	0,00	0,00	0,00	0,00	11908,06	0,00	15102,19
Sum Demand	28218,79	30555,91	29605,13	29538,72	25481,92	23475,13	22286,80	23836,03	18954,34	28189,98	18256,52	30737,87
Cov Demand C	3406,13	11726,25	5609,34	7436,23	25481,92	23475,13	22286,80	23836,03	18954,34	28189,98	18256,52	30737,87
Un-Cov Demand A	24812,66	18829,66	23995,79	22102,49	0,00	0,00	0,00	0,00	0,00	0,00	0,00	0,00
Un-used E B	0,00	0,00	0,00	0,00	7362,43	41698,01	5795,37	12562,14	51432,54	51196,21	26508,06	48363,03
S-C	1,00	1,00	1,00	1,00	0,78	0,36	0,79	0,65	0,27	0,36	0,41	0,39
S-S	0,12	0,38	0,19	0,25	1,00	1,00	1,00	1,00	1,00	1,00	1,00	1,00
Electricity	3406,13	11726,25	5609,34	7436,23	32844,35	65173,14	28082,17	36398,16	70386,88	79386,19	44764,58	79100,90

	Jul 11th	Jul 26th	Aug 11th	Aug 26th	Sep 11th	Sep 26th	Oct 11th	Oct 26th	Nov 11th	Nov 26th	Dec 11th	Dec 26th
H Demand	15753,04	7855,59	13287,53	18289,04	17998,10	25906,16	29288,03	38672,64	35037,39	52123,66	63046,17	48446,80
H Demand (HP)	5251,01	2618,53	4429,18	6096,35	5999,37	8635,39	9762,68	12890,88	11679,13	17374,55	21015,39	16148,93
Extra Demand	9835,00	9835,00	9835,00	9835,00	9835,00	9835,00	9835,00	9835,00	9835,00	9835,00	9835,00	9835,00
DHW	2085,00	2085,00	2085,00	2085,00	2085,00	2085,00	2085,00	2085,00	2085,00	2085,00	2085,00	2085,00
C Demand	0,00	52626,07	23683,03	0,00	6290,63	0,00	0,00	0,00	0,00	0,00	0,00	0,00
C Demand (HP)	0,00	17542,02	7894,34	0,00	2096,88	0,00	0,00	0,00	0,00	0,00	0,00	0,00
Sum Demand	17171,01	32080,55	24243,52	18016,35	20016,24	20555,39	21682,68	24810,88	23599,13	29294,55	32935,39	28068,93
Cov Demand C	17171,01	32080,55	24243,52	18016,35	20016,24	20555,39	19315,54	11341,67	23599,13	29294,55	3831,88	5365,90
Un-Cov Demand A	0,00	0,00	0,00	0,00	0,00	0,00	2367,14	13469,21	0,00	0,00	29103,51	22703,03
Un-used E B	36241,87	26221,36	38094,44	3799,92	26079,29	37317,22	0,00	0,00	984,14	5674,03	0,00	0,00
S-C	0,32	0,55	0,39	0,83	0,43	0,36	1,00	1,00	0,96	0,84	1,00	1,00
S-S	1,00	1,00	1,00	1,00	1,00	1,00	0,89	0,46	1,00	1,00	0,12	0,19
Electricity	53412,88	58301,91	62337,96	21816,26	46095,53	57872,60	19315,54	11341,67	24583,27	34968,58	3831,88	5365,90

Tab. 6.8 Energy demands and electricity generation – First six months (top), second six months (bottom) (W) *

6.2.5 Flat rate of energy

Estimating the remaining energy demands, including electrical appliances, lighting, and auxiliary electricity for devices, is achieved using data from two years of monitoring this building (Table 6.9).

	Bedarf		Deckung			
	Komponente	Strombedarf		Komponente	Stromertrag	
		[kWh/a]	[kWh/m ² a] *		[kWh/a]	[kWh/m ² a] **
Hilfsenergie für Heizung und Warmwasser Lüftung	1.105	3,5	PV-Dach	12.092	122,0	
Elektrische Geräte Beleuchtung	2.500	8,0	**) bezogen auf die PV-Modulfäche Dach – 99 m ²			
Heizung Warmwasser Lüftung	5.839	18,7				
*) bezogen auf die Gebäudenutzfläche 312,12 m ²						
Gesamt	9.444 kWh/a		Gesamt	12.092 kWh/a		

Tab. 6.9 Energy demands and electricity generation – Average of two years monitoring [62]

Table 7.8 shows that the annual energy demand for 'lighting + electrical appliances' is 8.00 kWh/m². Similarly, the annual 'auxiliary electricity for heating, cooling, and ventilation' has been measured at 3.50 kWh/m². Therefore, the additional energy demand of the building, in addition to 'heating/cooling demands + DHW (domestic hot water),' is 11.50 kWh/m² per year. This flat-rate energy is factored into the upcoming monthly calculations (see Table 6.10).

$$\begin{aligned}
 & \text{Demand}_{\text{Auxiliary electricity + lighting and electrical appliances}} = 8.0 + 3.5 = 11.5 \text{ kWh/m}^2 \text{a} \\
 & 11500 \frac{\text{Wh}}{\text{m}^2 \text{a}} \div 365 \text{ (days)} = 31.51 \frac{\text{Wh}}{\text{m}^2} \text{ (per day)} \\
 & 31.51 \frac{\text{Wh}}{\text{m}^2} \text{ per day} \times 312.12 \text{ m}^2 = 9835 \text{ Wh (per day)} *
 \end{aligned}$$

Tab. 6.10 Calculation of flat-rate of energy base on average of two years monitoring
* The amount has been applied as 'extra demand' in 'Energy demands and electricity generation'

* Accuracy of calculations and employed equations exclusively discussed in appendix 2

The assumption of electricity demand for DHW (Domestic Hot Water) and its auxiliary is based on the same report obtained from two years of monitoring (see Table 6.11).

Verbrauch/Produktion Strom und Wärme	Monat	Nov 14	Dez 14	Jan 15	Feb 15	Mrz 15	Apr 15	Mai 15	Jun 15	Jul 15	Aug 15	Sep 15	Okt 15	Mon. 2014/15
Brauchwassernutzwärme	[kWh]	75	48	64	80	94	94	58	58	38	20	51	81,00	761

Tab. 6.11 Electricity demand for DHW + Auxiliary electricity – Average of two years monitoring [62]

The assumption of a flat-rate electricity consumption for DHW (Domestic Hot Water) in the heat pump and its auxiliary for circulation is presented in Table 6.12.

$$\text{Demand}_{\text{electricity for DHW}} = 761 \text{ kWh/a (For entire building)}$$

$$761000 \frac{\text{Wh}}{\text{a}} \div 365 \text{ (days)} = 2085 \text{ Wh (per day) } *$$

Tab. 6.12 Assumption of ‘electricity demand’ for hot water

* The amount has been applied as ‘DHW’ in ‘Energy demands and electricity generation’

6.2.6 Electricity demand for heating and cooling

The estimation of the final electricity demand for heating and cooling has been calculated based on the energy concept of the selected building, which is equipped with a heat pump. Figure 6.10 illustrates the efficiency of the integrated heat pump (COP) as a function of the outdoor ambient temperature.

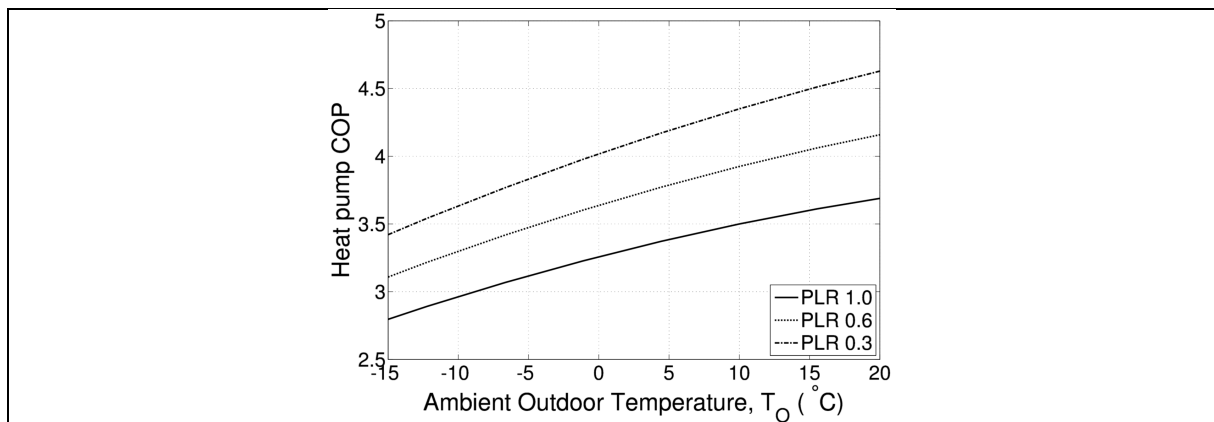


Fig. 6.10 Heat pump coefficient of performance (COP) as a function of ambient outdoor temperature, T_o , and part-load ratio (PLR). [63]

To estimate the average efficiency of the integrated heat pump (PROXON FWT 3 2.0), we have considered the average COP (Coefficient of Performance) of heat pumps as a function of the outdoor ambient temperature. Given the range of employed weather data, which indicates temperature fluctuations between approximately -5°C and 20°C , an average COP of 3.00 has been applied. This means that a certain amount of electricity is used to compensate for three times more heating and cooling demand (see Table 6.13).

$$\text{Electricity demand for heating (11th Jan) for heat pump} = \frac{\text{Heating demand}}{\text{COP of heat pump}} = \frac{48896}{3} = 16298 \text{ Wh}$$

$$\text{Electricity demand for cooling (26th May) for heat pump} = \frac{\text{Cooling demand}}{\text{COP of heat pump}} = \frac{35724}{3} = 11908 \text{ Wh}$$

Tab. 6.13 Examples of electricity demand for heating and cooling after integration of heat pump with average COP of 3 – 11th January for heating demand (top), 26th May for cooling demand (bottom)

Calculating the annual final heating demand and cooling demand of the selected building can be estimated based on the cumulative amounts from all 24 days during the year, which are on the 11th and 26th of each month (see Table 6.14). Table 6.15 provides an estimation of the annual values of parameters based on the 24 calculated days.

E demand of heating $_{24\text{ days}} = \sum E$ demand (heating) $_{11\text{ th and }26\text{ th each month}} = 260988\text{ Wh}/24\text{ days}$
E demand of cooling $_{24\text{ days}} = \sum E$ demand (cooling) $_{11\text{ th and }26\text{ th each month}} = 54543\text{ Wh}/24\text{ days}$

Tab. 6.14 Cumulative electricity demand for heating and cooling for 24 calculated days

	Wh/24 d	kWh/a	
H Demand	782965	11744	A. E demand (24 days) $_{heating} = 260988\text{ Wh}/24\text{ days}$ $260988 \frac{\text{Wh}}{24\text{ days}} \times 15 \div 1000 = 3915\text{ kWh/a}$
H Demand (HP)	260988	3915	
Extra Demand	236040	3541	B. E demand (24 days) $_{cooling} = 54543\text{ Wh}/24\text{ days}$ $54543 \frac{\text{Wh}}{24\text{ days}} \times 15 \div 1000 = 818\text{ kWh/a}$
DHW		761	
C Demand	163630	2454	C. Annual electricity demand for DHW 761 kWh/a *
C Demand (HP)	54543	818	
Sum Demand	601612	9024	Annual electricity demand for heating, cooling and DHW; $E_{heating+cooling+DHW} = 3915 + 818 + 761 = 5494\text{ kWh/a}$
Cov Demand C	444228	6663	
Un-Cov Demand A	157383	2361	
Un-used E B	419330	6290	
S-C	0,51		
S-S	0,74		
Electricity	863558	12953	

Tab. 6.15 Annual energy demands and electricity generation, coverage of demands, SS + SC (left chart)

* The value is emerged from Table 6.11, electricity demand for DHW + Auxiliary electricity – Average of two years

The total measured electricity demand for 'heating, DHW, and ventilation' in Table 6.9 amounts to 5839 kWh/year. Assuming the use of the same integrated heat pump for ventilation during hot months, the electricity used for cooling is included in the same value. Consequently, the following comparison helps to explain the deviation between 'calculated annual electricity demand' and 'measured annual electricity demand'.

6.2.7 Deviation

By utilizing the same datasheet of integrated PV in the building, a comparison between the calculated 'annual electricity demand' and 'annual electricity generation' with its measurement is presented in Table 6.16.

$Annual\ electricity\ demand_{calculated} = 5494\text{ kWh/a}$	$Deviation_{calculated\ E\ demand} = -5.9\%$
$Annual\ electricity\ demand_{measured} = 5839\text{ kWh/a}$	
$Annual\ electricity\ generation_{calculated} = 12953\text{ kWh/a}$	$Deviation_{E\ generation} = +7.91\%$
$Annual\ electricity\ generation_{measured} = 12092\text{ kWh/a}$	

Tab. 6.16 Deviation of calculated and measured (two years monitoring) [62] annual 'E-demand' and 'E-generation'

As the integrated weather data used for calculations are sourced from 'EnergyPlus,' and the measured electricity demand and generation data are collected from two years of monitoring in 2013-2014 and 2014-2015, both deviations can be attributed to differences in the quantity of weather data integrated into the calculations and the geographical location of the tested building.

6.2.8 Daily and annual self-consumption – self-efficiency

Taking into account the acceptable deviation between 'calculated electricity demand for heating and cooling' and 'generated electricity,' two final indexes, 'self-consumption' and 'self-sufficiency,' have been calculated separately for each day (24 days) over the entire year. Table 6.17 provides an example of the calculation for January 11th. Using the data from Table 6.8, the calculated SC and SS values for the 11th and 26th of each month are presented in Table 6.18.

Parameter	Heating demand	E demand for heating	Cooling demand	E demand for cooling	Generated electricity	DHW + Flat rate	Total E demand
Value	48896	16298	0	0	3406	11920	28218
Parameter	Covered demand	Uncovered demand	Unused electricity	SS %	SC %		
Value	3406	24812	0	0.12	1.00		

Tab. 6.17 Electricity demands and generation (Wh/d), 11th January, Self-sufficiency and self-consumption

Date	Jan 11 th	Jan 26 th	Feb 11 th	Feb 26 th	Mar 11 th	Mar 26 th	Apr 11 th	Apr 26 th	May 11 th	May 26 th	Jun 11 th	Jun 26 th	Jul 11 th	Jul 26 th	Aug 11 th	Aug 26 th	Sep 11 th	Sep 26 th	Oct 11 th	Oct 26 th	Nov 11 th	Nov 26 th	Dec 11 th	Dec 26 th
SC	1.00	1.00	1.00	1.00	0.78	0.36	0.79	0.65	0.27	0.36	0.41	0.39	0.32	0.55	0.39	0.83	0.43	0.36	1.00	1.00	0.96	0.84	1.00	1.00
SS	0.12	0.38	0.19	0.25	1.00	1.00	1.00	1.00	1.00	1.00	1.00	1.00	1.00	1.00	1.00	1.00	1.00	1.00	0.89	0.46	1.00	1.00	0.12	0.19

Tab. 6.18 Calculated self-consumption and self-sufficiency on 11th and 26th of each month

An annual energy performance, considering electricity generation and demand coverage for all 24 days of the year, is illustrated in Figure 6.11.

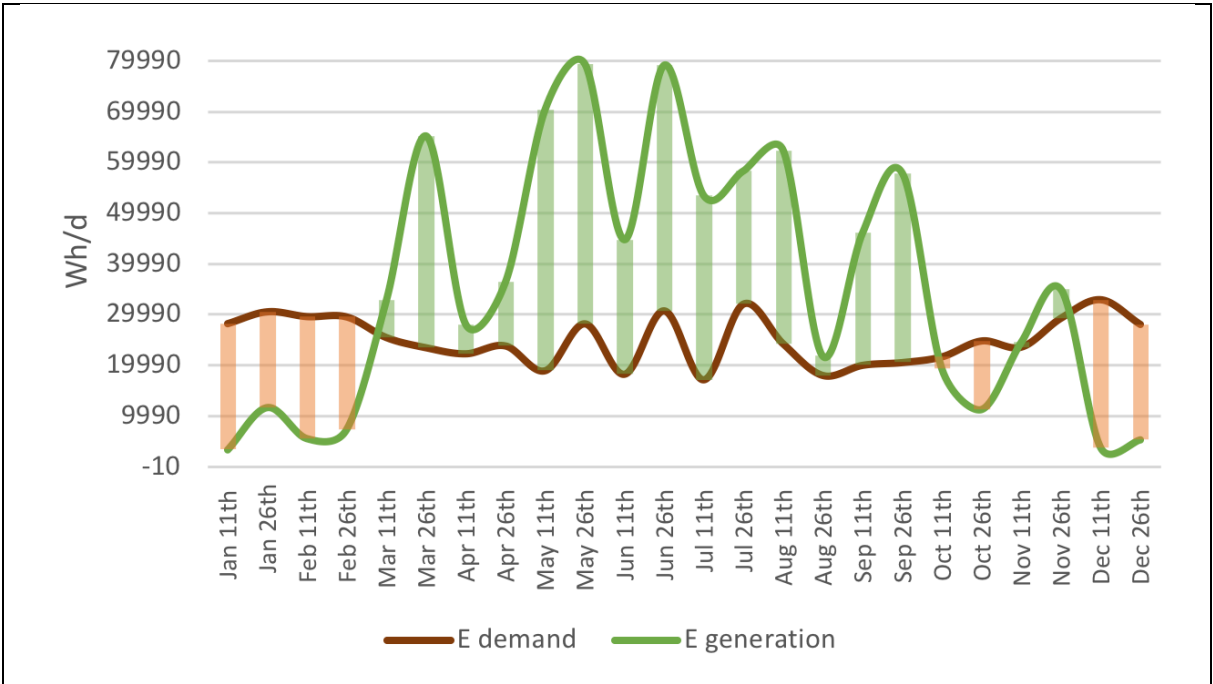


Fig. 6.11 Fluctuation of electricity generation and electricity demand during a year

The final annual values for 'electricity generation' and 'electricity demand' indicate 0.51 and 0.74 for self-consumption and self-sufficiency, respectively.

7. Demonstration of effects of geometry

To assess the effects of different geometrical setups of the building, as well as its various proportional combinations of components, a simple building geometry with a constant area of 200 m² and a limited PV area of 40 m² has been considered. These geometrical modifications were compared across 13 different variants, resulting from these changes in geometry.

The final values of 'self-consumption' and 'self-sufficiency' can be quantitatively compared, and this procedure can be applied in the early stages of 'building design' to predict the approximate energy performance of a proposed building. Alternatively, the window-to-wall ratio (WWR), a critical ratio, can be investigated in parallel. This allows for the exploration of favorable combinations of different components integrated into a facade.

By comparing the final energy performance of these variants, we can estimate the range of change in two key 'energy efficiency indicators': self-sufficiency and self-consumption, influenced by the effects of geometry. The constraints applied to all 13 variants include 'the same building area' of 200 m², 'the same integrated PV area' of 40 m², 'the same PV installation setup' as BAPV, and 'the same WWR' of 0.2. Consequently, in all variants, the same amount of PV is allocated per square meter of living space, which is 0.2 m² (PV/1 m² living space). Changes in WWR, proportions, PV integration positions, roof types, allocation of PVs to one side or both sides of a symmetric sloping roof, and changes in the inclination of a vertical wall holding PVs are the initial geometrical modifications resulting in different levels of 'energy efficiency indicators.' These variations demonstrate the effectiveness of each geometrical parameter in altering the final energy performance of the defined prototype.

7.1 Sample building

The first chart illustrates the estimation of energy performance for a two-story building with vertical walls, a window-to-wall ratio (WWR) of 0.2 in all four facades, and the integration of 40 m² of PV as BAPV on its flat roof (see Table 7.1).

Geometry	Length (x)	Width (y)	Height	N Floors	Area	South Inc	South area	East Inc	East area	North Inc	North area	West Inc	West area	Roof area	Floor area						
	10,00	10,00	6,00	2,00	200,00	90,00	60,00	90,00	60,00	90,00	60,00	90,00	60,00	100,00	100,00						
Components	01(90 0) O + W		Area	02(90 -90) O + W		Area	03(90 180) O + W + BI		Area	04(90 90) O + W		Area	13(0 0) O + BA		Area	Wall area %	0,05	TFA	190	Total TFA	190
Opaque	0,80	48,00	0,80	48,00	0,80	48,00	0,80	48,00	0,80	48,00	0,80	48,00	0,60	60,00							
Window	0,20	12,00	0,20	12,00	0,20	12,00	0,20	12,00	0,20	12,00	0,20	12,00	0,00	0,00							
BIPV	0,00	0,00	0,00	0,00	0,00	0,00	0,00	0,00	0,00	0,00	0,00	0,00	0,00	0,00							
BAPV	0,00	0,00	0,00	0,00	0,00	0,00	0,00	0,00	0,00	0,00	0,00	0,00	0,40	40,00							
PVG	0,00	0,00	0,00	0,00	0,00	0,00	0,00	0,00	0,00	0,00	0,00	0,00	0,00	0,00							
Final performance (W/24 d) + Dimensions																					
Generation + Demands	H demand	C demand	Flat rate	E for heating	E for cooling	Generated E	Covered demand	Self-sufficiency	Self-consumption												
	602645	123115	246240	200882	41038	433316	310574	0,64	0,72												

Tab. 7.1 Variant-01, 2 stories, flat roof

Energy demands and electricity generation (W/24 days), Self-sufficiency and self-consumption

7.2 WWR

By increasing the window-to-wall ratio (WWR) in all four facades of the building from 0.2 to 0.4 while keeping electricity generation constant, the changes in self-sufficiency and self-consumption are presented in Table 7.2.

Geometry	Length (x)	Width (y)	Height	N Floors	Area	South Inc	South area	East Inc	East area	North Inc	North area	West Inc	West area	Roof area	Floor area
	10,00	10,00	6,00	2,00	200,00	90,00	60,00	90,00	60,00	90,00	60,00	90,00	60,00	100,00	100,00
Components	01(90 0)	Area	02(90 -90)	Area	03(90 180)	Area	04(90 90)	Area	13(0 0)	Area	Wall area %	0,05			
	O + W		O + W		O + W + BI		O + W		O + BA		TFA	190			
	Opaque	0,60	36,00	0,60	36,00	0,60	36,00	0,60	36,00	0,00	0,00	Total TFA	190		
	Window	0,40	24,00	0,40	24,00	0,40	24,00	0,40	24,00	0,60	60,00				
	BIPV	0,00	0,00	0,00	0,00	0,00	0,00	0,00	0,00	0,00	0,00				
	BAPV	0,00	0,00	0,00	0,00	0,00	0,00	0,00	0,00	0,40	40,00				
	PVG	0,00	0,00	0,00	0,00	0,00	0,00	0,00	0,00	0,00	0,00				
Final performance (W/24 d) + Dimensions															
	Generation + Demands	H demand	C demand	Flat rate	E for heating	E for cooling	Generated E	Covered demand	Self-sufficiency	Self-consumption					
	695899	237947	246240	231966	79316	433316	331361	0,59	0,76						

Tab. 7.2 Variant-02, 2 stories, flat roof, WWR = 0.40 in all four facades
Energy demands and electricity generation (W/24 days), Self-sufficiency and self-consumption

To compare the effects of different window-to-wall ratios (WWRs) in all four facades of the selected example geometry, Table 7.3 presents the changes in SS and SC.

Variant	WWR S	WWR E	WWR N	WWR W	H demand (W/24 d)	C demand (W/24 d)	SS	SC
W-1	0.2	0.2	0.2	0.2	602645	123115	0.64	0.72
W-2	0.8	0.2	0.2	0.2	673692	203431	0.61	0.75
W-3	0.2	0.8	0.2	0.2	674007	184443	0.61	0.75
W-4	0.2	0.2	0.8	0.2	672588	182921	0.61	0.75
W-5	0.2	0.2	0.2	0.8	678494	266161	0.59	0.76
W-6	0.4	0.4	0.4	0.4	695899	237947	0.59	0.76
W-7	0.6	0.6	0.6	0.6	792994	352780	0.54	0.78
W-8	0.8	0.8	0.8	0.8	890846	467612	0.49	0.80

Tab. 7.3 Comparing self-sufficiency and self-consumption of example building with different setups of WWR – sample geometry of building - Integration of 40 m² of BAPV on flat roof for all variants.

7.3 One storey building

Allocating the entire 200 m² to one storey, with the same area of 40 m² BAPV on the roof, and varying the levels of demands and generation are presented in Table 7.4.

Geometry	Length (x)	Width (y)	Height	N Floors	Area	South Inc	South area	East Inc	East area	North Inc	North area	West Inc	West area	Roof area	Floor area		
	14,14	14,14	3,00	1,00	200,00	90,00	42,43	90,00	42,43	90,00	42,43	90,00	42,43	200,00	200,00		
Components	01(90 0)		Area	02(90 -90)		Area	03(90 180)		Area	04(90 90)		Area	13(0 0)		Area	Wall area %	0,05
	O + W			O + W			O + W + BI			O + W			O + BA			TFA	190
	Opaque	0,80	33,94	0,80	33,94	0,80	33,94	0,80	33,94	0,80	33,94	0,80	33,94	0,80	160,00	Total TFA	190
	Window	0,20	8,48	0,20	8,48	0,20	8,48	0,20	8,48	0,20	8,48	0,20	8,48	0,20	0,00		
	BIPV	0,00	0,00	0,00	0,00	0,00	0,00	0,00	0,00	0,00	0,00	0,00	0,00	0,00	0,00		
	BAPV	0,00	0,00	0,00	0,00	0,00	0,00	0,00	0,00	0,00	0,00	0,00	0,00	0,20	40,00		
PVG	0,00	0,00	0,00	0,00	0,00	0,00	0,00	0,00	0,00	0,00	0,00	0,00	0,00	0,00			
Final performance (W/24 d) + Dimensions																	
	Generation + Demands	H demand	C demand	Flat rate	E for heating	E for cooling	Generated E	Covered demand	Self-sufficiency	Self-consumption							
	756078	92176	246235	252026	30725	433316	315589	0,60	0,73								

Tab. 7.4 Variant-03, 1 storey, flat roof
Energy demands and electricity generation (W/24 days), Self-sufficiency and self-consumption

7.4 Proportion

Changing the primary shape of the building from a square to rectangular (25 m x 8 m) and the resulting energy performance are presented in Table 7.5.

Geometry	Length (x)	Width (y)	Height	N Floors	Area	South Inc	South area	East Inc	East area	North Inc	North area	West Inc	West area	Roof area	Floor area		
	8,00	25,00	3,00	1,00	200,00	90,00	24,00	90,00	75,00	90,00	24,00	90,00	75,00	200,00	200,00		
Components	01(90 0)		Area	02(90 -90)		Area	03(90 180)		Area	04(90 90)		Area	13(0 0)		Area	Wall area %	0,05
	O + W			O + W			O + W + BI			O + W			O + BA			TFA	190
	Opaque	0,80	19,20	0,80	60,00	0,80	19,20	0,80	19,20	0,80	60,00	0,80	19,20	0,80	160,00	Total TFA	190
	Window	0,20	4,80	0,20	15,00	0,20	4,80	0,20	4,80	0,20	15,00	0,20	4,80	0,20	0,00		
	BIPV	0,00	0,00	0,00	0,00	0,00	0,00	0,00	0,00	0,00	0,00	0,00	0,00	0,00	0,00		
	BAPV	0,00	0,00	0,00	0,00	0,00	0,00	0,00	0,00	0,00	0,00	0,00	0,00	0,20	40,00		
PVG	0,00	0,00	0,00	0,00	0,00	0,00	0,00	0,00	0,00	0,00	0,00	0,00	0,00	0,00			
Final performance (W/24 d) + Dimensions																	
	Generation + Demands	H demand	C demand	Flat rate	E for heating	E for cooling	Generated E	Covered demand	Self-sufficiency	Self-consumption							
	794116	115864	246240	264705	38621	433316	326743	0,59	0,75								

Tab. 7.5 Variant-04, 1 storey, proportion: 8 × 25 m, flat roof
Energy demands and electricity generation (W/24 days), Self-sufficiency and self-consumption

7.5 Orientation

Rotating the same building by 90° to create a new proportional geometry results in the same self-sufficiency and 1% lower self-consumption (see Table 7.6).

Geometry	Length (x)	Width (y)	Height	N Floors	Area	South Inc	South area	East Inc	East area	North Inc	North area	West Inc	West area	Roof area	Floor area
	25,00	8,00	3,00	1,00	200,00	90,00	75,00	90,00	24,00	90,00	75,00	90,00	24,00	200,00	200,00
Components	01(90 0)	Area	02(90 -90)	Area	03(90 180)	Area	04(90 90)	Area	13(0 0)	Area	Wall area %	0,05			
	O + W		O + W		O + W + BI		O + W		O + BA		TFA	190			
	Opaque	0,80	60,00	0,80	19,20	0,80	60,00	0,80	19,20	0,80	160,00	Total TFA	190		
	Window	0,20	15,00	0,20	4,80	0,20	15,00	0,20	4,80	0,00	0,00				
	BIPV	0,00	0,00	0,00	0,00	0,00	0,00	0,00	0,00	0,00	0,00				
	BAPV	0,00	0,00	0,00	0,00	0,00	0,00	0,00	0,00	0,00	40,00				
PVG	0,00	0,00	0,00	0,00	0,00	0,00	0,00	0,00	0,00	0,00					
Final performance (W/24 d) + Dimensions															
	Generation + Demands	H demand	C demand	Flat rate	E for heating	E for cooling	Generated E	Covered demand	Self-sufficiency	Self-consumption					
	800517	96862	246240	266839	32287	433316	320618	0,59	0,74						

Tab. 7.6 Variant-05, 1 storey, proportion: 25 × 8 m, flat roof
Energy demands and electricity generation (W/24 days), Self-sufficiency and self-consumption

7.6 Distribution of PV

Allocating 40 m² of BAPVs evenly across all four main facades of the building, with 10 m² applied to each facade, is presented in Table 7.7.

Geometry	Length (x)	Width (y)	Height	N Floors	Area	South Inc	South area	East Inc	East area	North Inc	North area	West Inc	West area	Roof area	Floor area
	10,00	10,00	6,00	2,00	200,00	90,00	60,00	90,00	60,00	90,00	60,00	90,00	60,00	100,00	100,00
Components	01(90 0)	Area	02(90 -90)	Area	03(90 180)	Area	04(90 90)	Area	13(0 0)	Area	Wall area %	0,05			
	O + W		O + W		O + W + BI		O + W		O		TFA	190			
	Opaque	0,63	38,00	0,63	38,00	0,63	38,00	0,63	38,00	1,00	100,00	Total TFA	190		
	Window	0,20	12,00	0,20	12,00	0,20	12,00	0,20	12,00	0,00	0,00				
	BIPV	0,00	0,00	0,00	0,00	0,00	0,00	0,00	0,00	0,00	0,00				
	BAPV	0,17	10,00	0,17	10,00	0,17	10,00	0,17	10,00	0,00	0,00				
PVG	0,00	0,00	0,00	0,00	0,00	0,00	0,00	0,00	0,00	0,00					
Final performance (W/24 d) + Dimensions															
	Generation + Demands	H demand	C demand	Flat rate	E for heating	E for cooling	Generated E	Covered demand	Self-sufficiency	Self-consumption					
	598766	123925	246240	199589	41308	249036	241578	0,50	0,97						

Tab. 7.7 Variant-06, 2 stories, flat roof, 10 m² BAPV on each facade
Energy demands and electricity generation (W/24 days), Self-sufficiency and self-consumption

7.7 PV on ‘Dachgeschoss’

The integration of 40 m² as BAPV on the south inclined roof with an inclination of 60° (Mansardendach) is presented in Table 7.8.

Geometry	Length (x)	Width (y)	Height	N Floors	Area	South Inc	South area	East Inc	East area	North Inc	North area	West Inc	West area	Roof area	Floor area			
	10,00	10,00	3,00	1,00	100,00	90,00	30,00	90,00	73,50	90,00	30,00	90,00	73,50	100,00	100,00			
Components	01(90 0) O + W		Area	02(90 -90) O + W		Area	03(90 180) O + W + BI		Area	04(90 90) O + W		Area	05(60 0) O + W		Area	07(60 180) O + W		Area
	Opaque	0,80	24,00	0,80	58,80	0,80	24,00	0,80	58,80	0,80	24,00	0,80	58,80	0,40	40,00	0,80	80,00	
Window	0,20	6,00	0,20	14,70	0,20	6,00	0,20	14,70	0,20	6,00	0,20	14,70	0,20	20,00	0,20	20,00		
BIPV	0,00	0,00	0,00	0,00	0,00	0,00	0,00	0,00	0,00	0,00	0,00	0,00	0,00	0,00	0,00	0,00		
BAPV	0,00	0,00	0,00	0,00	0,00	0,00	0,00	0,00	0,00	0,00	0,00	0,00	0,40	40,00	0,00	0,00		
PVG	0,00	0,00	0,00	0,00	0,00	0,00	0,00	0,00	0,00	0,00	0,00	0,00	0,00	0,00	0,00	0,00		
	Wall area %		0,05		TFA		190		Total TFA		190							
Final performance (W/24 d) + Dimensions																		
	Generation + Demands	H demand	C demand	Flat rate	E for heating	E for cooling	Generated E	Covered demand	Self-sufficiency	Self-consumption								
	705632	240947	246240	235211	80316	447228	339261	0,60	0,76									

Tab. 7.8 Variant-07, 2 stories, sloping roof, 40 m² BAPV on south inclined roof, (Mansardendach-60°) Energy demands and electricity generation (W/24 days), Self-sufficiency and self-consumption

Allocating 40 m² as BAPV on the east and west inclined roofs with an inclination of 60° (Mansardendach) is presented in Table 7.9.

Geometry	Length (x)	Width (y)	Height	N Floors	Area	South Inc	South area	East Inc	East area	North Inc	North area	West Inc	West area	Roof area	Floor area			
	10,00	10,00	3,00	1,00	100,00	90,00	73,50	90,00	30,00	90,00	73,50	90,00	30,00	100,00	100,00			
Components	01(90 0) O + W		Area	02(90 -90) O + W		Area	03(90 180) O + W + BI		Area	04(90 90) O + W		Area	06(60 -90) O + W + BI		Area	08(60 90) O + W + BI		Area
	Opaque	0,80	58,80	0,80	24,00	0,80	58,80	0,80	24,00	0,80	24,00	0,80	24,00	0,60	60,00	0,60	60,00	
Window	0,20	14,70	0,20	6,00	0,20	6,00	0,20	14,70	0,20	6,00	0,20	6,00	0,20	20,00	0,20	20,00		
BIPV	0,00	0,00	0,00	0,00	0,00	0,00	0,00	0,00	0,00	0,00	0,00	0,00	0,00	0,00	0,00	0,00		
BAPV	0,00	0,00	0,00	0,00	0,00	0,00	0,00	0,00	0,00	0,00	0,00	0,00	0,20	20,00	0,20	20,00		
PVG	0,00	0,00	0,00	0,00	0,00	0,00	0,00	0,00	0,00	0,00	0,00	0,00	0,00	0,00	0,00	0,00		
	Wall area %		0,05		TFA		190		Total TFA		190							
Final performance (W/24 d) + Dimensions																		
	Generation + Demands	H demand	C demand	Flat rate	E for heating	E for cooling	Generated E	Covered demand	Self-sufficiency	Self-consumption								
	711912	262153	246240	237304	87384	342826	294592	0,52	0,86									

Tab. 7.9 Variant-08, 2 stories, sloping roof, 20 m² BAPV on east and west inclined roof (Mansardendach-60°) Energy demands and electricity generation (W/24 days), Self-sufficiency and self-consumption

7.8 PV on ‘Sloping roof’

The integration of 40 m² as BAPV on the south inclined roof with an inclination of 60°, where there is no heated space under the roof, has also been calculated. In this setup, two standard stories are used for living spaces, and the inclined roof solely holds PVs without any heated space beneath it (see Table 7.10).

Geometry	Length (x)	Width (y)	Height	N Floors	Area	South Inc	South area	East Inc	East area	North Inc	North area	West Inc	West area	Roof area	Floor area					
	10,00	10,00	6,00	2,00	200,00	90,00	60,00	90,00	60,00	90,00	60,00	90,00	60,00	100,00	100,00					
Components	01(90 0)		Area	02(90 -90)		Area	03(90 180)		Area	04(90 90)		Area	05(60 0)		Area	07(60 180)		Area		
	O + W			O + W			O + W + BI			O + W			0,40		40,00	0,00		0,00		
	Opaque	0,80	48,00	0,80	48,00	0,80	48,00	0,80	48,00	0,80	48,00	0,80	48,00							
	Window	0,20	12,00	0,20	12,00	0,20	12,00	0,20	12,00	0,20	12,00	0,20	12,00							
	BIPV	0,00	0,00	0,00	0,00	0,00	0,00	0,00	0,00	0,00	0,00	0,00	0,00							
BAPV	0,00	0,00	0,00	0,00	0,00	0,00	0,00	0,00	0,00	0,00	0,00	0,00								
PVG	0,00	0,00	0,00	0,00	0,00	0,00	0,00	0,00	0,00	0,00	0,00	0,00								
	<table border="1"> <tr> <td>Wall area %</td> <td>0,05</td> </tr> <tr> <td>TFA</td> <td>190</td> </tr> <tr> <td>Total TFA</td> <td>190</td> </tr> </table>														Wall area %	0,05	TFA	190	Total TFA	190
Wall area %	0,05																			
TFA	190																			
Total TFA	190																			
Final performance (W/24 d) + Dimensions																				
Generation + Demands	H demand	C demand	Flat rate	E for heating	E for cooling	Generated E	Covered demand	Self-sufficiency	Self-consumption											
	603475	120861	246240	201158	40287	447228	326134	0,67	0,73											

Tab. 7.10 Variant-09, 2 stories, sloping roof, 40 m² BAPV on south inclined roof (60°), without heated space under roof, Energy demands and electricity generation (W/24 days), Self-sufficiency and self-consumption

Allocating 40 m² as BAPV on the east and west inclined roofs (each 20 m²) with an inclination of 60°, where there is no heated space under the roof, is presented in Table 7.11.

Geometry	Length (x)	Width (y)	Height	N Floors	Area	South Inc	South area	East Inc	East area	North Inc	North area	West Inc	West area	Roof area	Floor area					
	10,00	10,00	6,00	2,00	200,00	90,00	60,00	90,00	60,00	90,00	60,00	90,00	60,00	100,00	100,00					
Components	01(90 0)		Area	02(90 -90)		Area	03(90 180)		Area	04(90 90)		Area	06(60 -90)		Area	08(60 90)		Area		
	O + W			O + W			O + W + BI			O + W			0,20		20,00	0,20		20,00		
	Opaque	0,80	48,00	0,80	48,00	0,80	48,00	0,80	48,00	0,80	48,00	0,80	48,00							
	Window	0,20	12,00	0,20	12,00	0,20	12,00	0,20	12,00	0,20	12,00	0,20	12,00							
	BIPV	0,00	0,00	0,00	0,00	0,00	0,00	0,00	0,00	0,00	0,00	0,00	0,00							
BAPV	0,00	0,00	0,00	0,00	0,00	0,00	0,00	0,00	0,00	0,00	0,00	0,00								
PVG	0,00	0,00	0,00	0,00	0,00	0,00	0,00	0,00	0,00	0,00	0,00	0,00								
	<table border="1"> <tr> <td>Wall area %</td> <td>0,05</td> </tr> <tr> <td>TFA</td> <td>190</td> </tr> <tr> <td>Total TFA</td> <td>190</td> </tr> </table>														Wall area %	0,05	TFA	190	Total TFA	190
Wall area %	0,05																			
TFA	190																			
Total TFA	190																			
Final performance (W/24 d) + Dimensions																				
Generation + Demands	H demand	C demand	Flat rate	E for heating	E for cooling	Generated E	Covered demand	Self-sufficiency	Self-consumption											
	603475	120861	246240	201158	40287	342826	286935	0,59	0,84											

Tab. 7.11 Variant-10, 2 stories, sloping roof, 20 m² BAPV on east and west inclined roof (60°), without heated space under roof, Energy demands and electricity generation (W/24 days), Self-sufficiency and self-consumption

The integration of 40 m² as BAPV on the south inclined roof with an inclination of 30°, where there is no heated space under the roof, is presented in Table 7.12.

Geometry	Length (x)	Width (y)	Height	N Floors	Area	South Inc	South area	East Inc	East area	North Inc	North area	West Inc	West area	Roof area	Floor area		
	10,00	10,00	6,00	2,00	200,00	90,00	60,00	90,00	60,00	90,00	60,00	90,00	60,00	100,00	100,00		
Components	01(90 0)		Area	02(90 -90)		Area	03(90 180)		Area	04(90 90)		Area	09(30 0)		Area	Wall area %	0,05
	O + W			O + W			O + W + Bi			O + W			0,69		40,00	TFA	190
	Opaque	0,80	48,00	0,80	48,00	0,80	48,00	0,80	48,00	0,80	48,00			Total TFA	190		
	Window	0,20	12,00	0,20	12,00	0,20	12,00	0,20	12,00	0,20	12,00						
	BIPV	0,00	0,00	0,00	0,00	0,00	0,00	0,00	0,00	0,00	0,00						
	BAPV	0,00	0,00	0,00	0,00	0,00	0,00	0,00	0,00	0,00	0,00						
PVG	0,00	0,00	0,00	0,00	0,00	0,00	0,00	0,00	0,00	0,00							
Final performance (W/24 d) + Dimensions																	
	Generation + Demands	H demand	C demand	Flat rate	E for heating	E for cooling	Generated E	Covered demand	Self-sufficiency	Self-consumption							
	603475	120861	246240	201158	40287	493983	335883	0,69	0,68								

Tab. 7.12 Variant-11, 2 stories, sloping roof, 40 m² BAPV on south inclined roof (30°), without heated space under roof, Energy demands and electricity generation (W/24 days), Self-sufficiency and self-consumption

Allocating 40 m² as BAPV on the east and west inclined roofs (each 20 m²) with an inclination of 30°, where there is no heated space under the roof, is presented in Table 7.13.

Geometry	Length (x)	Width (y)	Height	N Floors	Area	South Inc	South area	East Inc	East area	North Inc	North area	West Inc	West area	Roof area	Floor area		
	10,00	10,00	6,00	2,00	200,00	90,00	60,00	90,00	60,00	90,00	60,00	90,00	60,00	100,00	100,00		
Components	01(90 0)		Area	02(90 -90)		Area	03(90 180)		Area	04(90 90)		Area	10(30 -90)		Area	12(30 90)	Area
	O + W			O + W			O + W + Bi			O + W			0,35		20,00	0,35	20,00
	Opaque	0,80	48,00	0,80	48,00	0,80	48,00	0,80	48,00	0,80	48,00			Wall area %	0,05		
	Window	0,20	12,00	0,20	12,00	0,20	12,00	0,20	12,00	0,20	12,00			TFA	190		
	BIPV	0,00	0,00	0,00	0,00	0,00	0,00	0,00	0,00	0,00	0,00			Total TFA	190		
	BAPV	0,00	0,00	0,00	0,00	0,00	0,00	0,00	0,00	0,00	0,00						
PVG	0,00	0,00	0,00	0,00	0,00	0,00	0,00	0,00	0,00	0,00							
Final performance (W/24 d) + Dimensions																	
	Generation + Demands	H demand	C demand	Flat rate	E for heating	E for cooling	Generated E	Covered demand	Self-sufficiency	Self-consumption							
	603475	120861	246240	201158	40287	407366	305427	0,63	0,75								

Tab. 7.13 Variant-12, 2 stories, sloping roof, 20 m² BAPV on east and west inclined roof (30°), without heated space under roof, Energy demands and electricity generation (W/24 days), Self-sufficiency and self-consumption

7.9 PV on ‘Sloping wall’

Rotating the south face of the building (with 40 m²) of BAPV is presented in Table 7.14.

Geometry	Length (x) 10,00 Width (y) 10,87 Height 6,00 N Floors 2,00 Area 200,00 South Inc 60,00 South area 69,28 East Inc 90,00 East area 54,80 North Inc 90,00 North area 60,00 West Inc 90,00 West area 54,80 Roof area 74,02 Floor area 108,66															
	Components	02(90-90)	Area	03(90-180)	Area	04(90-90)	Area	05(60-0)	Area					13(0-0)	Area	
O + W			O + W + BI		O + W		O + W						O + BA		Wall area %	0,05
0,80		43,84	0,80	48,00	0,80	43,84	0,22	15,43					1,00	74,02	TFA	190,00
0,20		10,96	0,20	12,00	0,20	10,96	0,20	13,86					0,00	0,00	Total TFA	190,00
0,00		0,00	0,00	0,00	0,00	0,00	0,00	0,00					0,00	0,00		
0,00		0,00	0,00	0,00	0,00	0,00	0,58	40,00					0,00	0,00		
0,00		0,00	0,00	0,00	0,00	0,00	0,00	0,00					0,00	0,00		
Final performance (W/24 d) + Dimensions																
	Generation + Demands	H demand	C demand	Flat rate	E for heating	E for cooling	Generated E	Covered demand	Self-sufficiency	Self-consumption						
	570511	148104	246338	190170	49368	447228	325335	0,67	0,73							

Tab. 7.14 Variant-13, 2 stories, flat roof, 40 m² BAPV on south inclined wall (60°) Energy demands and electricity generation (W/24 days), Self-sufficiency and self-consumption

7.10 Domain of influence of geometry

In terms of the calculated 'indicative energy performance' of all 13 variants, the range of changes in the two indexes, self-sufficiency and self-consumption, is illustrated in Figure 7.1. It is evident that both indexes exhibit significant variations. For example, Variant-06, representing a building that distributes 40 m² of BAPVs across all four main facades, shows the lowest SS at 0.5 and the highest SC at 0.97. Also, Variant-11 offers the maximum SS at 0.69, while Variant-01 presents the minimum SC at 0.72.

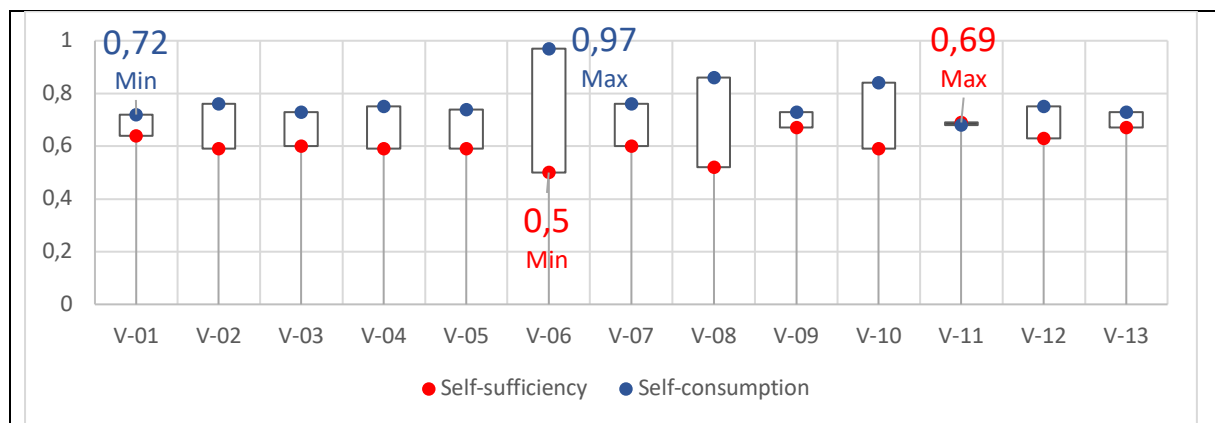


Fig. 7.1 Domain of changing two indexes of self-sufficiency and self-consumption in 13 geometrical setups

Among the 13 investigated geometrical setups, self-sufficiency varies by 19% (ranging from 0.5 to 0.69), while self-consumption varies by 15% (ranging from 0.72 to 0.97). It can be concluded that both indexes are significantly influenced by changes in geometrical parameters.

8. Geometry setups and indicative of energy efficiency

The developed method of this work indicates ‘self-sufficiency’ and ‘self-consumption’ as ‘energy efficiency indicative.’ Determining effects of different geometry setups of the building in changing quantities of the ‘energy efficiency indicative’ will illustrate the optimum geometry setup of the building that offers higher ‘energy efficiency indicative’. It should be noted that this optimum geometry setup is constantly dependent on the defined boundary condition, material combination properties, efficiency of PVs and parallel integrated devices (in this case, a heat pump with the certain defined efficiency). So, in a specific geographical location with certain materials, PVs, and parallel device combination, ‘energy efficiency indicative’ of different geometry setups can be compared if the constraint of ‘equal offered area of the building’ and ‘equal amount of integrated PV’ is constantly applied as well.

The upcoming discussion mainly compares effects of geometry setups on ‘energy efficiency indicative’ through different phases. In the first phase, the basic geometrical parameters of the building are considered, and their offered ‘self-sufficiency’ and ‘self-consumption’ are compared together to illustrate the optimum variant and effectiveness of each geometrical parameter.

In the first phase of discussion, geometrical proportions, orientation of the building, inclination of a specific component with or without PV with different WWRs, WWR of the envelope of the building, and roof type are initially discussed through the first phase of discussion. So, the elementary outcome of this section can recommend a specific setup of the building (regarding its basic geometrical parameters) that offers higher quantities of ‘energy efficiency indicative’. In this regard, two indexes of ‘self-sufficiency’ and ‘self-consumption’ are simultaneously calculated, and the specific variant (regarding its geometry setup) offering the highest ‘self-sufficiency’ is highlighted. ‘Self-consumption’ is additionally calculated and in the case of similar offered quantities of ‘self-sufficiency’ in some variants can be used to illustrate the more economical variant.

In the second phase of the discussion, architectural decisions resulting from specific ‘geometrical setups’ are employed, and the offered ‘energy efficiency indicatives’ are compared. For example, the roof type, with its inclination in different orientations of the building, is discussed. The roof, as a fundamental component of the building, is investigated concerning its two main applications: when it is used as a second covering roof applied to a flat roof, and when it is integrated with livable space underneath, featuring a sharp inclination. In this context, an inclination of 60°, which is close to the traditional type of roof in Germany known as ‘Dachgeschoss,’ is simulated and compared to the first variant, where there is an intermediate flat roof between the last livable place and the sloping roof.

The expansion of the building is also examined, considering constant quantities of ‘integrated PV per capita,’ which determines how energy efficiency changes when a medium-sized building expands vertically and horizontally. Given the scope of this work, focused on ‘medium-sized’ buildings, energy efficiency changes are simulated and compared for buildings ranging from one dwelling to five dwellings, all with a constant amount of ‘allocated PV per TFA.’

In this phase of the investigation, the distribution of PV on different sides of a sloping roof is simulated using two main configurations: symmetric and asymmetric installations. The aim is to determine which variant, among different inclinations and orientations of the roof,

results in higher energy efficiency when the limited quantities of PV are integrated on one side (asymmetric) or two sides (symmetric) of the sloping roof.

Furthermore, this phase explores the effects of changing 'more than one parameter' on the final 'energy efficiency indicative.' For example, two developed matrices are used to assess the effects of 'proportion + orientation + WWR' and 'inclination + orientation + WWR.' These matrices help determine if changes in the 'energy efficiency indicative' are consistent when multiple 'geometrical properties' are altered simultaneously. Additionally, they identify which parameter has the greatest influence and is more powerful in altering the final results. It's important to note that similar approaches can be applied to investigate the effects of each favorable parameter in combination with other parameters.

In the third phase of the discussion, the priority of integrating different components of the building during various phases of 'PV integration' is simulated and discussed. These discussions aim to determine whether the sequence of priority for 'PV integration' remains the same as the building is progressively integrated with 'constant quantities of PVs' at different intervals. This means that after each integration, new 'energy demands' result from the effects of the 'last applied PV integration.' The goal is to answer the question of how these newly calculated 'energy demand' and 'electricity generation' should be considered when determining changes in the 'sequence of priorities' for components in subsequent integrations.

This phase of discussion takes into account both flat roof and sloping roof setups, including different roof inclinations of 30° and 60°, and two orientations of 'south-north' and 'east-west.' Additionally, an additional configuration involving 'Dachgeschoss installation' is considered with orientations of 'south-north' and 'east-west.' The aim is to explore how the order of component integration might change during different phases of PV integration and how this impacts energy efficiency.

8.1. Proportions

The effects of different proportions in a one-storey building with a constant total area of 100 m² and the same height have been studied. The first variant represents a square building, and the next four variants transform it into rectangles with different proportions. Table 8.1 presents the transformation of the prototype and the recorded quantities of self-consumption (SC) and self-sufficiency (SS). The results are calculated at both high and low comfort temperatures.

CT	Index	Proportions									
		V-01		V-02		V-03		V-04		V-05	
		Length	Width	Length	Width	Length	Width	Length	Width	Length	Width
H	SC	10	10	12.5	8	16	6.25	8	12.5	6.25	16
	SS	0.77		0.77		0.77		0.77		0.78	
L	SC	10	10	12.5	8	16	6.25	8	12.5	6.25	16
	SS	0.58		0.57		0.57		0.58		0.57	
L	SC	10	10	12.5	8	16	6.25	8	12.5	6.25	16
	SS	0.88		0.88		0.89		0.88		0.89	
L	SC	10	10	12.5	8	16	6.25	8	12.5	6.25	16
	SS	0.62		0.62		0.61		0.61		0.59	

Tab. 8.1 Geometry setups - Calculations of SS and SC - One-storey building – 20 m² BAPV on flat roof – High and low CT

The fluctuations in self-sufficiency (SS) and self-consumption (SC) for the five different proportions of the one-storey building and the energy performance of V-01 are depicted in Figure 8.1. The results are presented for both high and low comfort temperatures (CT).

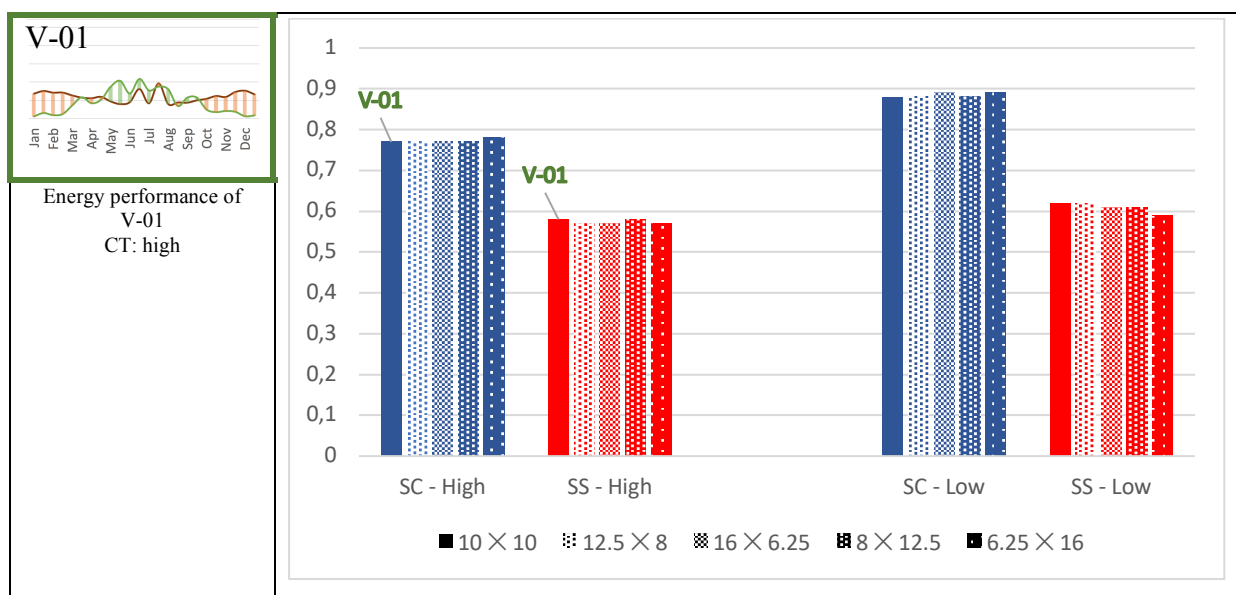


Fig. 8.1 SS and SC - Five Proportions of one-storey building – 20 m² BAPV on flat roof - High and low CT (right) + Energy performance of V-01 in high CT (left)

The results indicate that as the building proportion changes from a square shape to a rectangle, self-sufficiency (SS) gradually decreases, while self-consumption (SC) increases. The specific direction of changing the width and length of the building is not related to power generation since the electricity generation remains constant across all five variants, mainly through the integrated BAPV on the roof.

8.2. Orientation

8.2.1 BAPV on flat roof

The effects of different orientations in a square one-storey building with the same width and length and the same height ($10 \times 10 \times 3$ m) have been studied. The second and third variants involve rotating the prototype by 30° and 60° toward the west, respectively. Table 8.2 displays the rotations of the prototype and the corresponding SC and SS values.

CT	Index	Orientation		
		V-01	V-02	V-03
		Angle to south	Angle to south	Angle to south
		0°	-30°	-60°
H	SC	0.77	0.77	0.77
	SS	0.58	0.58	0.58
L	SC	0.88	0.88	0.88
	SS	0.62	0.62	0.62

Tab. 8.2 Geometry setups + Calculations of SS and SC - Orientation of one-storey building in square shape – 20 m^2 BAPV on flat roof - High and low CT

The fluctuation of SS and SC for the three orientations of the one-storey building and the energy performance of V-01 is displayed in Figure 8.2.

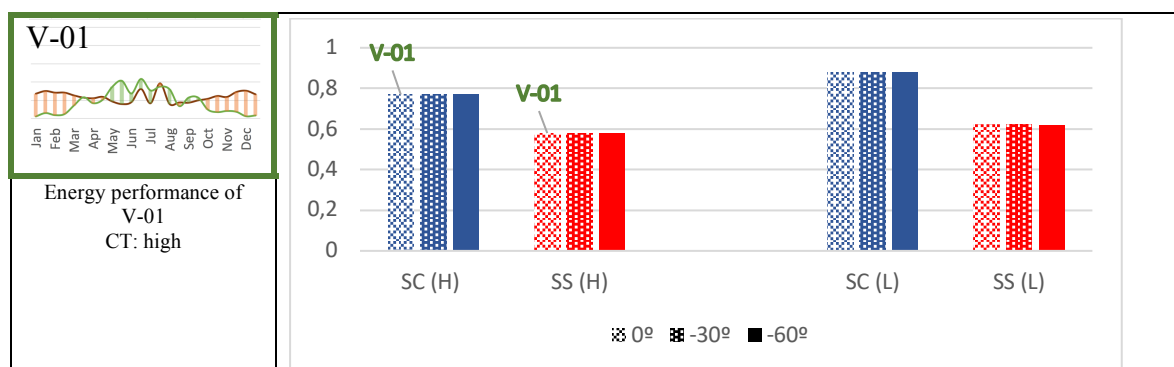


Fig. 8.2 SS and SC – Three orientations of one-storey building – 20 m^2 BAPV on flat roof - High and low CT (right) + Energy performance of V-01 in high CT (left)

The results indicate that both SS and SC remain constant at both high and low comfort temperatures when the prototype is rotated. It's important to note that the prototype is a square shape, and the on-roof integrated BAPV generates a constant amount of electricity, which is unaffected by the rotation of the building.

8.2.2 BAPV on sloping roof

The effects of different orientations of a square building with a symmetric sloping roof (60° inclination) are studied in this comparison. The integrated roof is an "extra sloping roof" that doesn't add additional living space to the entire building. The flat roof separates the building from the sloping roof, and external parameters of the boundary condition are applied only to the sloping roof, not to the internal flat roof of the building. Twelve variants represent the rotation of the building with 20m² of BAPV integrated on one side of the symmetric sloping roof. Table 8.3 shows the recorded quantities of SC and SS influenced by the rotation of the prototype at both high and low comfort temperatures.

CT	Index	Orientation – BAPV on sloping roof with inclination of 60°											
		1 st quarter			2 nd quarter			3 rd quarter			4 th quarter		
		V-01 0°	V-02 -30°	V-03 -60°	V-04 -90°	V-05 -120°	V-06 -150°	V-07 -180°	V-08 +150°	V-09 +120°	V-10 +90°	V-11 +60°	V-12 +30°
H	SC	0.78	0.81	0.86	0.91	0.96	0.99	0.99	0.97	0.91	0.86	0.80	0.78
	SS	0.61	0.59	0.56	0.51	0.45	0.39	0.37	0.41	0.47	0.55	0.58	0.61
L	SC	0.88	0.90	0.92	0.95	0.97	0.98	0.98	0.96	0.94	0.92	0.90	0.89
	SS	0.63	0.60	0.55	0.49	0.42	0.36	0.33	0.37	0.45	0.54	0.60	0.63

Tab. 8.3 Geometry setups + Calculations of SS and SC - Orientation of one-storey building in square shape – 20 m² BAPV on one side of sloping roof (Inc. 60°) - High and low CT

The fluctuation of SS and SC for the twelve orientations of the considered prototype and the energy performance of V-01, V-02, and V-03 are presented in Figure 8.3. Results are shown for both high and low comfort temperatures.

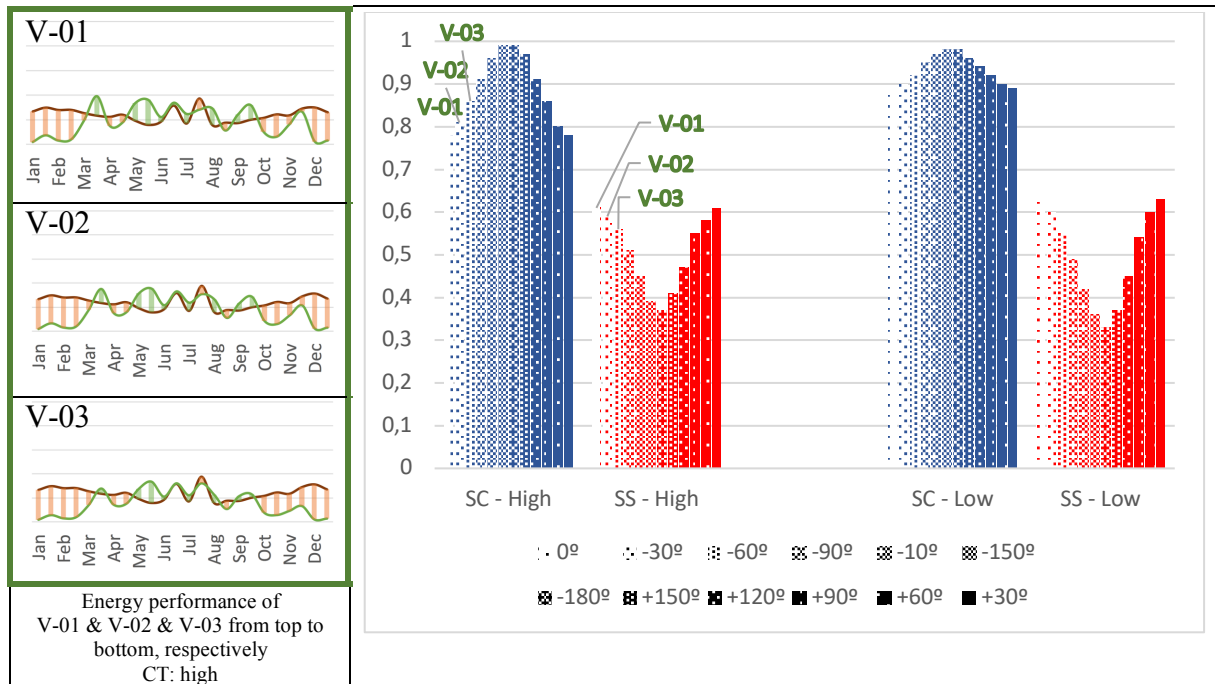


Fig. 8.3 SS and SC – Twelve orientations of one-storey building – 20 m² BAPV on one side of sloping roof - High and low CT (right) + Energy performances of V-01- V02 and V-03 in high CT (left)

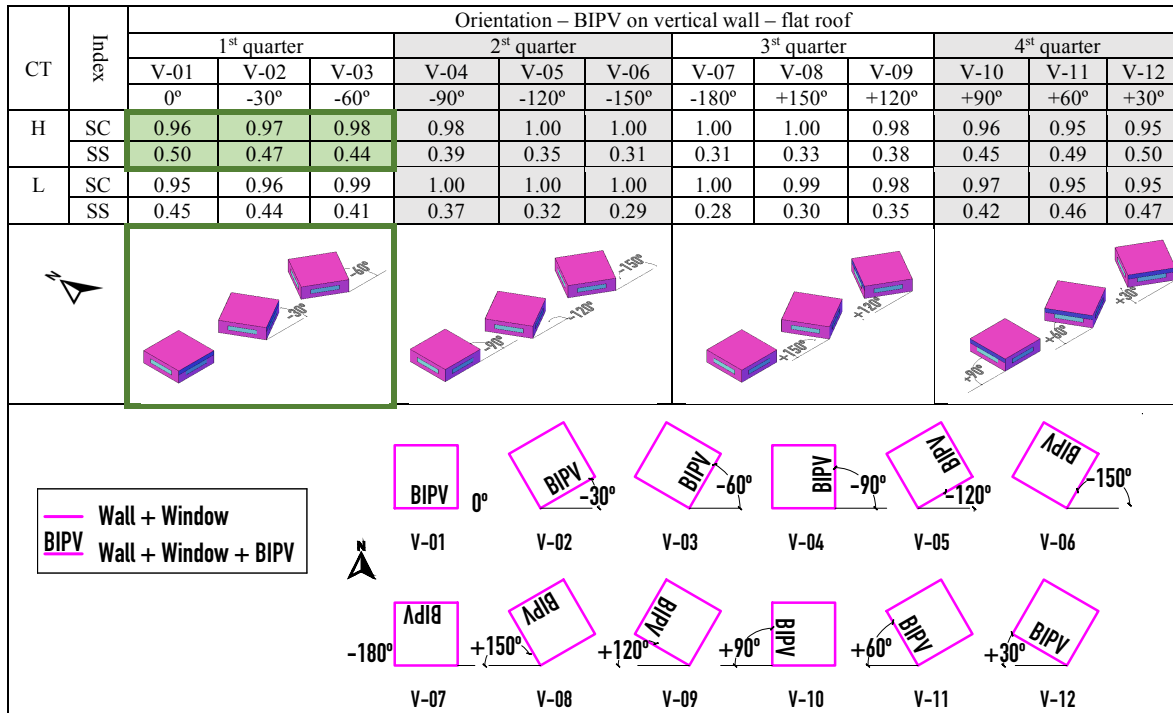
The results indicate that both SS and SC are significantly influenced by the rotation of the building, and this effect is more pronounced in low comfort temperatures. The changes in SS and SC are primarily driven by variations in electricity generation rather than the thermal performance of the building.

Additionally, it is observed that SS is more sensitive to the orientation of the building in low comfort temperatures compared to high comfort temperatures, as evidenced by a larger difference between the maximum and minimum SS values in low CT.

8.2.3 BIPV and BAPV on wall

The following text appears to be a description of a study or analysis that investigates the effects of different orientations of a square building with a flat roof that holds both Building-Integrated Photovoltaics (BIPV) and Building-Attached Photovoltaics (BAPV) on just one wall. The study records quantities of self-sufficiency (SS) and self-consumption (SC) for various orientations of the building, considering both high and low comfort temperature conditions.

However, the specific results of this analysis are not provided in the text you've provided. If you'd like more information or if you have any specific questions about this study, please let me know, and I'll do my best to assist you further.



Tab. 8.4 Geometry setups + Calculations of SS and SC - Orientation of one-storey building in square shape – 20 m² BIPV on one vertical wall - SS and SC – High and low CT

The figure illustrates the fluctuations in SS and SC for twelve different orientations of the prototype, which incorporates 10 square meters of BIPV on one face. Additionally, it provides the energy performance results for V-01, V-02, and V-03 (high and low CT).

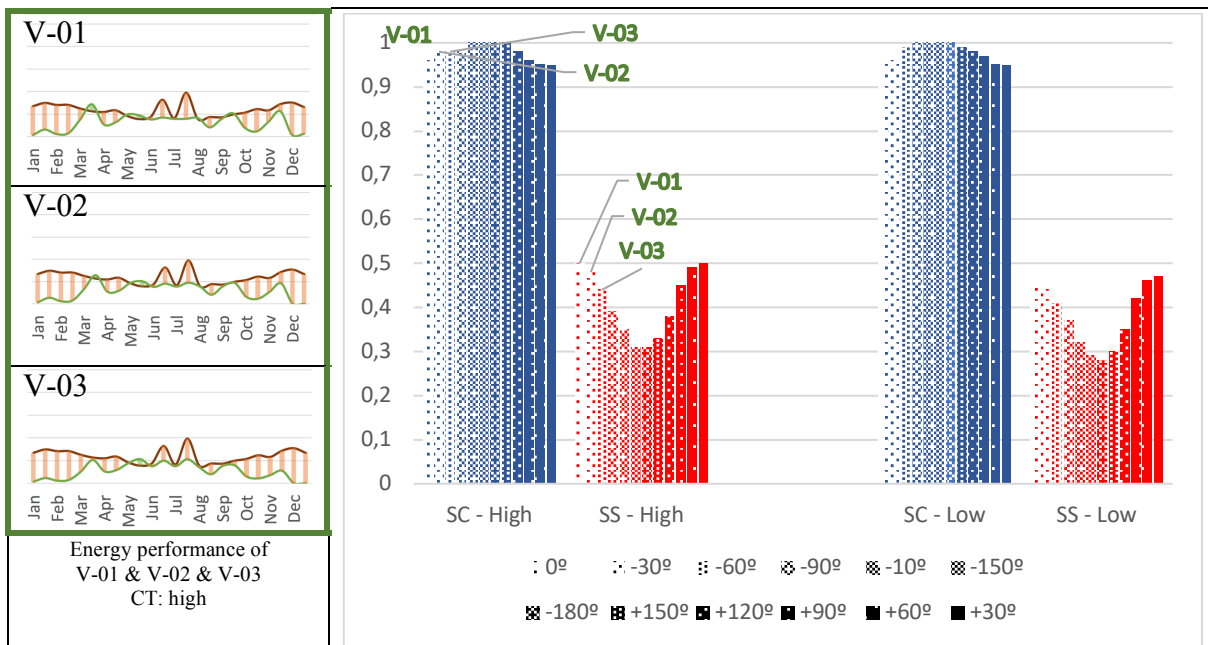
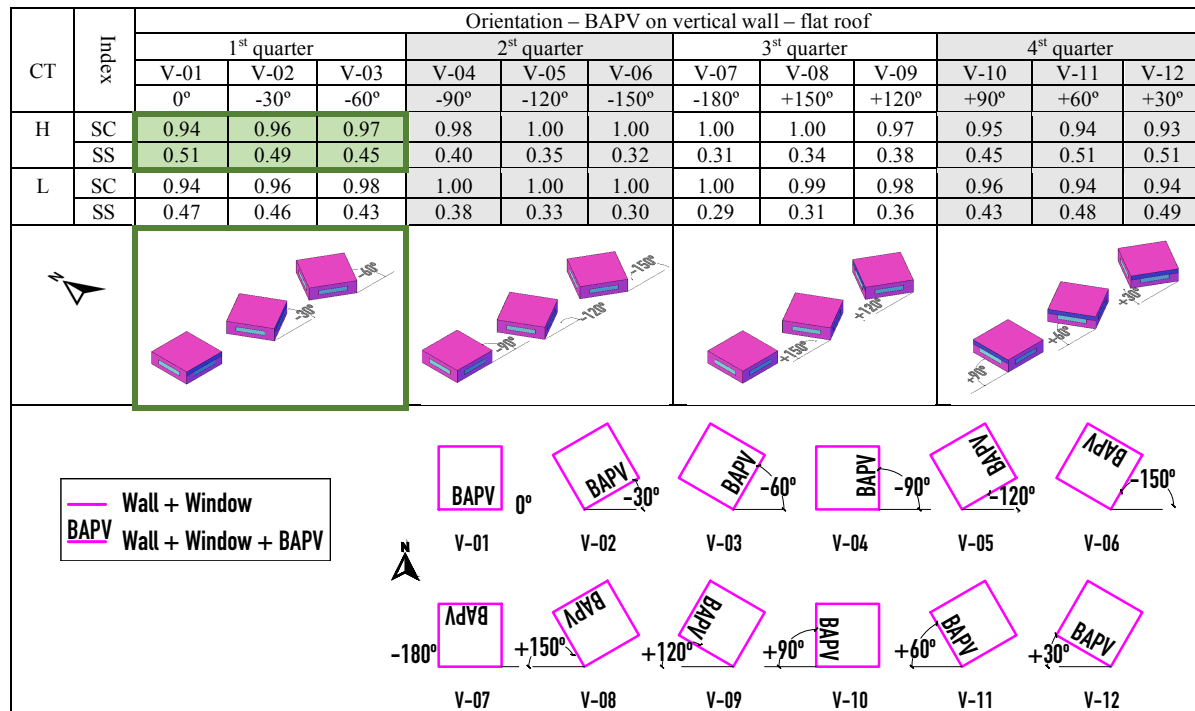


Fig. 8.4 SS and SC – Twelve orientations of one-storey building – 20 m² BIPV on one vertical wall - High and low CT (right) + Energy performances of V-01- V02 and V-03 in high CT (left)

Similar results are achieved when comparing the maximum and minimum energy performance of this prototype equipped with both BIPV and BAPV. There is only a marginal difference in energy performance between these two integration types. Notably, the sensitivity

of SS to rotation is significantly higher than that of SC, with SS decreasing from approximately 0.5 to 0.3, while SC changes from 0.95 to 1.00, in both BIPV and BAPV integrations. Additionally, it is evident that in high comfort temperature (CT) conditions, SS is more responsive to changes in the building's orientation compared to low CT, as the difference between the maximum and minimum SS values in high CT is larger than that in low CT. Table 8.5 provides recorded quantities of SC and SS influenced by the rotation of the building, which is equipped with BAPV on one vertical wall, under both high and low CT conditions.



Tab. 8.5 Geometry setups + Calculations of SS and SC - Orientation of one-storey building in square shape – 20 m² BAPV on one vertical wall - High and low CT

The fluctuations in SS and SC for twelve different orientations of the prototype, which incorporates a 10 m² BAPV installation on one face, are depicted in Figure 8.5.

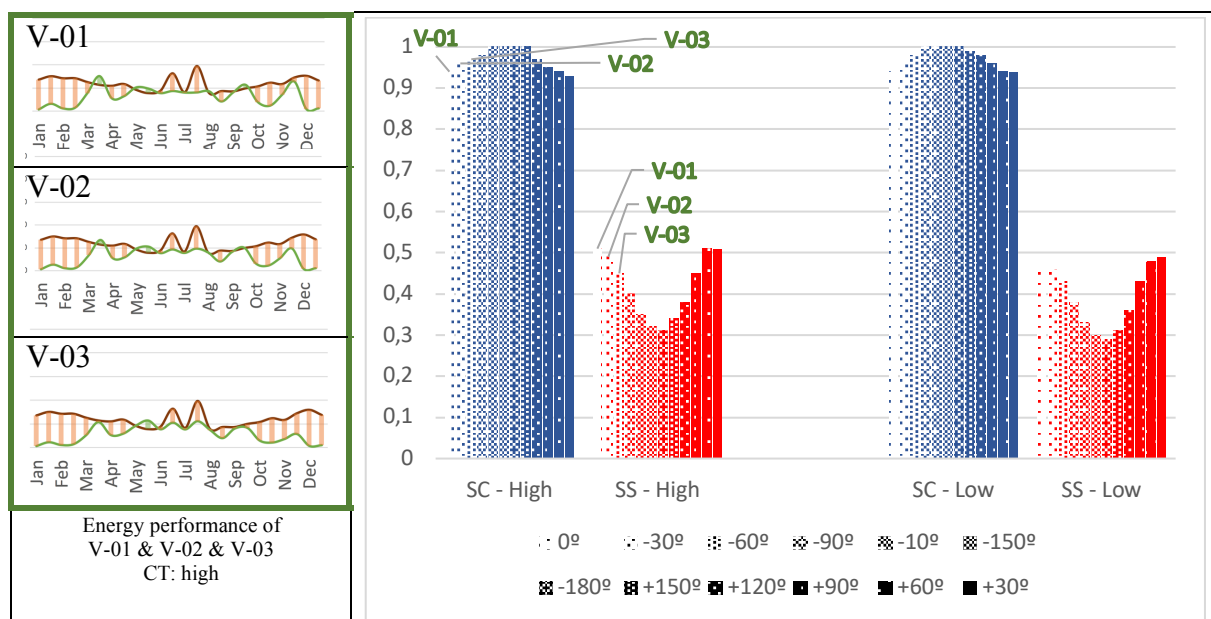


Fig. 8.5 SS and SC – Twelve orientations of one-storey building – 20 m² BAPV on one vertical wall - High and low CT (right) + Energy performance of V-01- V02 and V-03 at high CT (left)

Figure 8.5 illustrates that the sensitivity of SS to the orientation of the prototype is more pronounced in high CT compared to low CT. In high CT, the maximum SS is recorded at orientations of 0° and +30°, reaching 0.50. In contrast, in low CT, the maximum SS is achieved at an orientation of +30°, reaching 0.47, while an absolute south-facing building with an orientation of 0° exhibits a lower SS of 0.45.

8.2.4 PV glazing on wall

Effects of different orientations of a square building with a flat roof holding PV glazing on one vertical wall are presented in this comparison. The face holding PV glazing preserves its WWR as 0.2. Results are recorded in both high and low comfort temperatures (table 8.6).

CT	Index	Orientation – PVG on vertical wall (In addition to windows)			
		V-01 South	V-02 East	V-03 North	V-04 West
H	SC	1.00	1.00	1.00	0.99
	SS	0.36	0.28	0.22	0.32
L	SC	1.00	1.00	1.00	1.00
	SS	0.33	0.26	0.20	0.29

Legend:
 Wall + Window (Pink)
 Wall + Window + PVG (Magenta)

Orientation diagrams:
 V-01: South wall with PVG
 V-02: East wall with PVG
 V-03: North wall with PVG
 V-04: West wall with PVG

Tab. 8.6 Geometry setups + Calculations of SS and SC - Orientation of one-storey building in square shape – 20 m² PVglazing on one vertical wall – High and low CT

Fluctuations in SS and SC for four orientations of the prototype, as well as the energy performance of V-01, are presented in Figure 8.6. Results are provided for both high and low comfort temperatures.

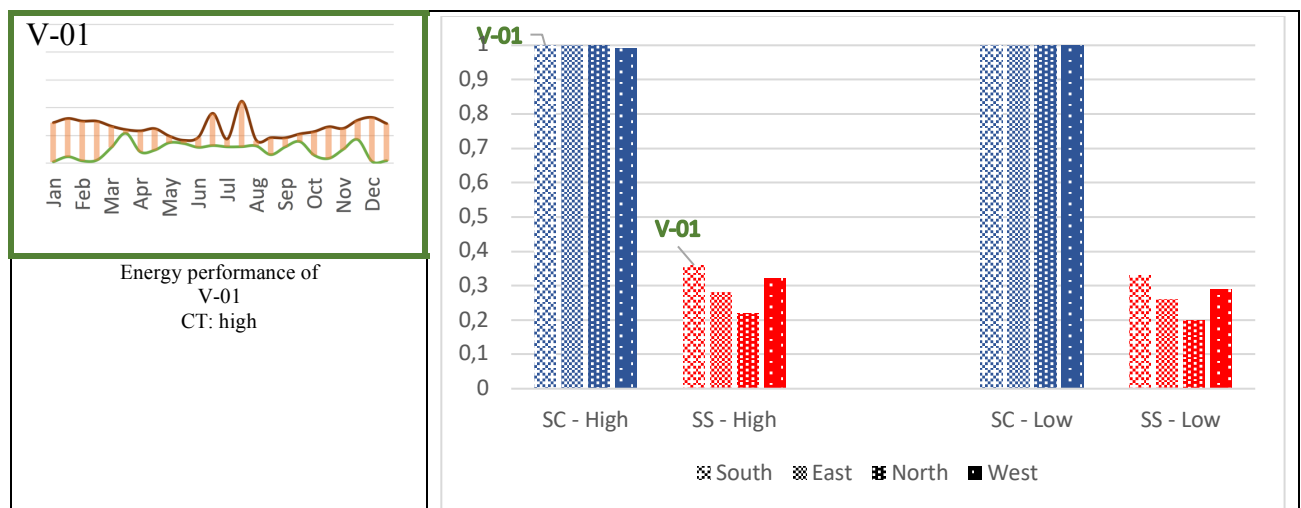


Fig. 8.6 SS and SC – Four orientations of one-storey building – 20 m² PV glazing on one vertical wall - High and low CT (right) + Energy performance of V-01 at high CT (left)

The results show that due to the low electricity generation by PV glazing compared to the energy demand of the prototype, SC remains around 1.00 in both high and low CT scenarios, as the entire electricity generation will be consumed by the prototype. The energy performance of V-01 indicates that throughout the year, electricity generation remains below the energy demand of the considered prototype. On average, the high setpoint of CT demonstrates higher SS compared to low CT.

8.3. Inclination

8.3.1 Wall with low WWR

The comparison presents the effects of different inclinations of one vertical wall in a square building with a flat roof holding 20 m² of BAPV on it. In all four variants, the four faces equally have a WWR of 0.2. The rotated face with a new inclination of 60° preserves its WWR as 0.2.

Additionally, the energy performance of a square building with completely vertical walls is presented for comparison with the four variants, each of which has one inclined face in one direction. The results are recorded at both high and low comfort temperatures (table 8.7).

CT	Index	Wall inclination				
		V-01	V-02	V-03	V-04	V-05
		All four walls 90°	South 60°	East 60°	North 60°	West 60°
H	SC	0.77	0.77	0.76	0.76	0.77
	SS	0.58	0.59	0.59	0.59	0.59
L	SC	0.88	0.88	0.88	0.88	0.88
	SS	0.62	0.60	0.62	0.62	0.61

Tab. 8.7 Geometry setups + Calculations of SS and SC - Inclination of one face of one-storey building in square shape with WWR of 0.2 – 20m² BAPV on flat roof – High and low CT

The figure presents the fluctuation of SS and SC for the prototype with absolute vertical walls and the four variants, each of which has one inclined face, along with the energy performance of V-01 (with absolute vertical walls). These results are provided for both high and low CT (figure 8.7).

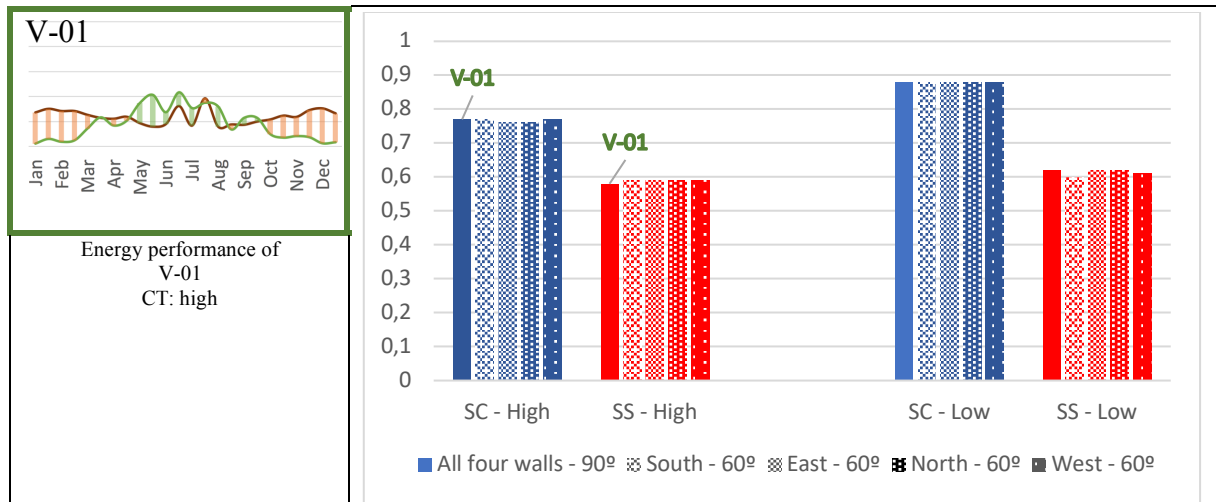


Fig. 8.7 SS and SC – Inclination of one face of one-storey building beside prototype with absolute vertical walls with WWR of 0.8 – 20m² BAPV on flat roof - High and low CT (right) + Energy performance of V-01 in high CT (left)

Considering the changes in SS, it becomes apparent that the energy performance of the prototype varies differently in different CT setpoints when one face is rotated. In a high CT setpoint, rotating a vertical wall into a new inclination of 60° in all four faces increases SS from 58% to 59%, while in a low CT setpoint, SS decreases from 62% to 61% and 60% with the same geometrical change. If only the SS index is to be considered, it can be concluded that in this boundary condition and material setup, the rotation of one wall from 90° to 60° is only beneficial when the comfort temperature is set to a high setpoint.

8.3.2 Wall with high WWR

Effects of different inclinations of one vertical wall in a square building with a flat roof holding 20 m² BAPV on it are presented in this comparison. All four faces equally have a WWR of 0.8, as the rotated face with a new inclination of 60° also preserves its WWR at 0.8. Energy performance of a square building with absolute vertical walls is compared to four variants, each with one inclined face in one direction. Results are recorded at both high and low comfort temperatures (table 8.8).

CT	Index	Wall inclination				
		V-01	V-02	V-03	V-04	V-05
		All four walls 90°	South 60°	East 60°	North 60°	West 60°
H	SC	0.83	0.81	0.81	0.81	0.81
	SS	0.46	0.49	0.49	0.49	0.50
L	SC	0.90	0.89	0.89	0.89	0.89
	SS	0.36	0.40	0.40	0.39	0.42

Tab. 8.8 Geometry setups + Calculations of SS and SC - Inclination of one face of one-storey building in square shape with WWR of 0.8 – 20m² BAPV on flat roof – High and low CT

Fluctuations in SS and SC of the prototype with absolute vertical walls and the four variants, each with one inclined face, along with the energy performance of V-01 (absolute vertical walls), are presented in figure 8.8. Results are shown for both high and low CT.

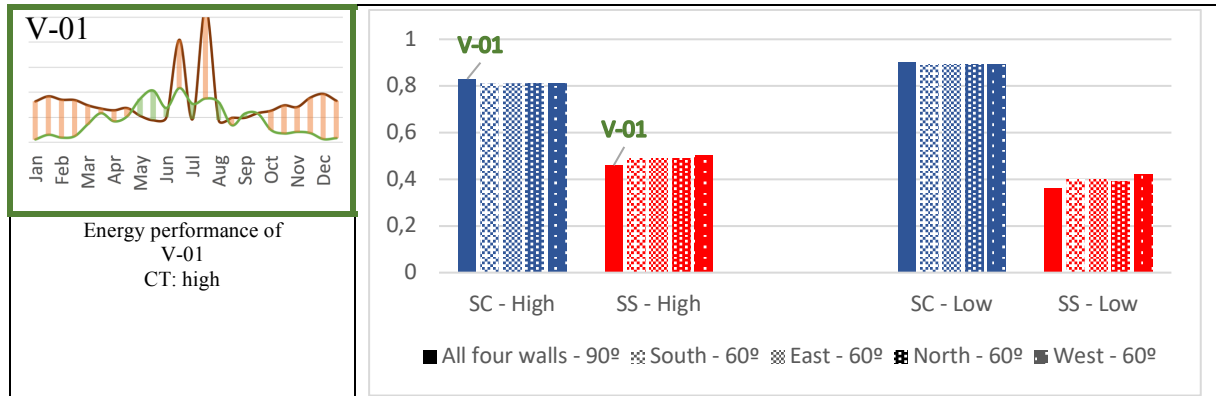


Fig. 8.8 SS and SC – Inclination of one face of one-storey building beside prototype with absolute vertical walls with WWR of 0.8 – 20m² BAPV on flat roof - High and low CT (right) + Energy performance of V-01 at high CT (left)

Figure 8.8 demonstrates that the face most sensitive to the change in inclination from 90° to 60°, both in high and low CT, is the west face, even when compared to the south face of the building. It's important to note that these changes in SS are solely influenced by alterations in the 'thermal performance' of the building, as BAPV is integrated on the flat roof, keeping electricity generation constant.

8.3.3 Wall holding BIPV

The effects of rotating one vertical wall, which holds 20 m² of BIPV, from 90° to 60° while maintaining a constant WWR of 0.2 in all four faces, are presented in this comparison. The new wall, with an inclination of 60°, retains its WWR as 0.2, and the total amount of BIPV remains at 20 m². In the transformation of one face holding BIPV, both of these aspects are altered. Each transformation is compared with the building before the rotation of the representative face (table 8.9).

CT	Index	Wall inclination							
		V-01 South		V-02 East		V-03 North		V-04 West	
		90°	60°	90°	60°	90°	60°	90°	60°
H	SC	0.96	0.81	0.98	0.92	1.00	0.99	0.96	0.87
	SS	0.50	0.59	0.39	0.50	0.31	0.38	0.45	0.53
L	SC	0.95	0.88	1.00	0.94	1.00	0.94	0.97	0.90
	SS	0.45	0.57	0.37	0.46	0.28	0.34	0.42	0.50

The figure shows 3D models of a building with one wall inclined at 90° or 60° for four different orientations (V-01 to V-04). Below the 3D models are 2D diagrams showing the wall and window configurations for each case, with dimensions of 10 units for the wall and window. A legend indicates: Wall + Window (pink), BIPV Wall + Window + BIPV (blue), and Sloping window & BIPV (light blue).

Tab. 8.9 Geometry setups + Calculations of SS and SC - Changing inclination of one face of one-storey building holding 20 m² BIPV – WWR: 0.2 in all four faces – High and low CT

The amounts of change in SS and SC of the prototype during the rotation of one face holding BIPV, in comparison to the same prototype with absolute vertical walls, and two different energy performances of the prototype with south wall inclinations of 90° and 60° (holding BIPV), are presented in figure 8.9. Results are shown for both high and low CT.

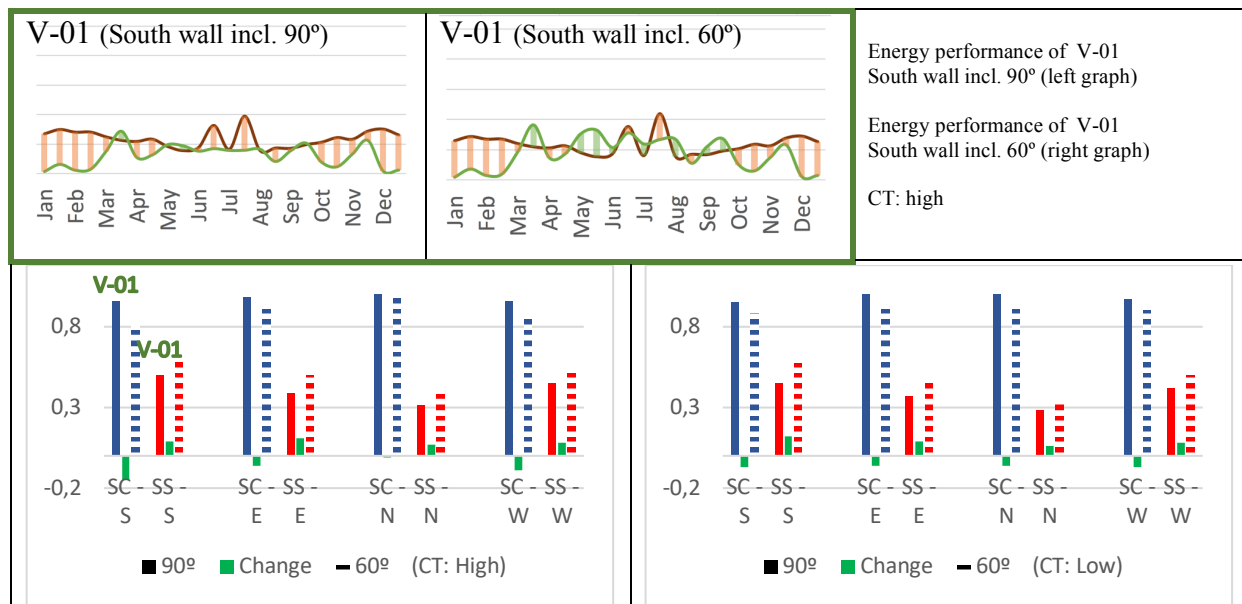


Fig. 8.9 SS and SC – Changing inclination of one face of one-storey building holding 20 m² BIPV compared to an absolute vertical wall – WWR: 0.2 - High and low CT (down) + Changing energy performance of V-01 at high CT (up)

The annual energy performance of V-01 in high CT has been shown with the south face as vertical or with an inclination of 60°. Comparing these two energy performances demonstrates that the annual thermal performance changes, as a south wall with an inclination of 60° results in higher cooling demand for the considered prototype. Conversely, the new south face with an inclination of 60° also generates more electricity in the middle of the year.

Comparing the four transformations for each face and their new SS and SC values demonstrates that the priority of rotating just one face from 90° to 60° to achieve higher SS depends on the comfort temperature setpoint as well. For instance, in high CT, eastward rotation increases the amount of SS (from 0.39 to 0.50) more effectively compared to the other three faces, whereas in low CT, southward rotation increases the amount of SS (from 0.45 to 0.57) more effectively compared to the other three faces. Considering SS changes in all four transformations reveals that in this prototype, changing the inclination of each face by 30° and putting it at a new inclination of 60° is always beneficial but results in different increases in energy performance.

8.3.4 Wall holding BAPV

The effects of rotating one vertical wall holding 20 m² BAPV from 90° to 60°, with a constant WWR of 0.2 in all four faces, are presented in this comparison. The new wall, with an inclination of 60°, preserves its WWR as 0.2 and the total amount of BAPV as 20 m². Each transformation has been compared with the building before the rotation of the representative face. Results are recorded at low comfort temperature (table 8.10).

CT	Index	Wall inclination							
		V-01		V-02		V-03		V-04	
		South		East		North		West	
		90°	60°	90°	60°	90°	60°	90°	60°
L	SC	0.94	0.87	1.00	0.94	1.00	0.96	0.96	0.90
	SS	0.47	0.61	0.38	0.49	0.29	0.34	0.43	0.53

Tab. 8.10 Geometry setups + Calculations of SS and SC - Changing inclination of one face of one-storey building holding 20 m² BAPV – WWR: 0.2 in all four faces – Low CT

Amounts of changing SS and SC of the prototype during rotation of one face holding BAPV in relation to the same prototype with absolute vertical walls and two different energy performances of prototype with south wall inclination of 90° and 60° (holding BIPV) is presented in figure 8.10. Results are at low CT.

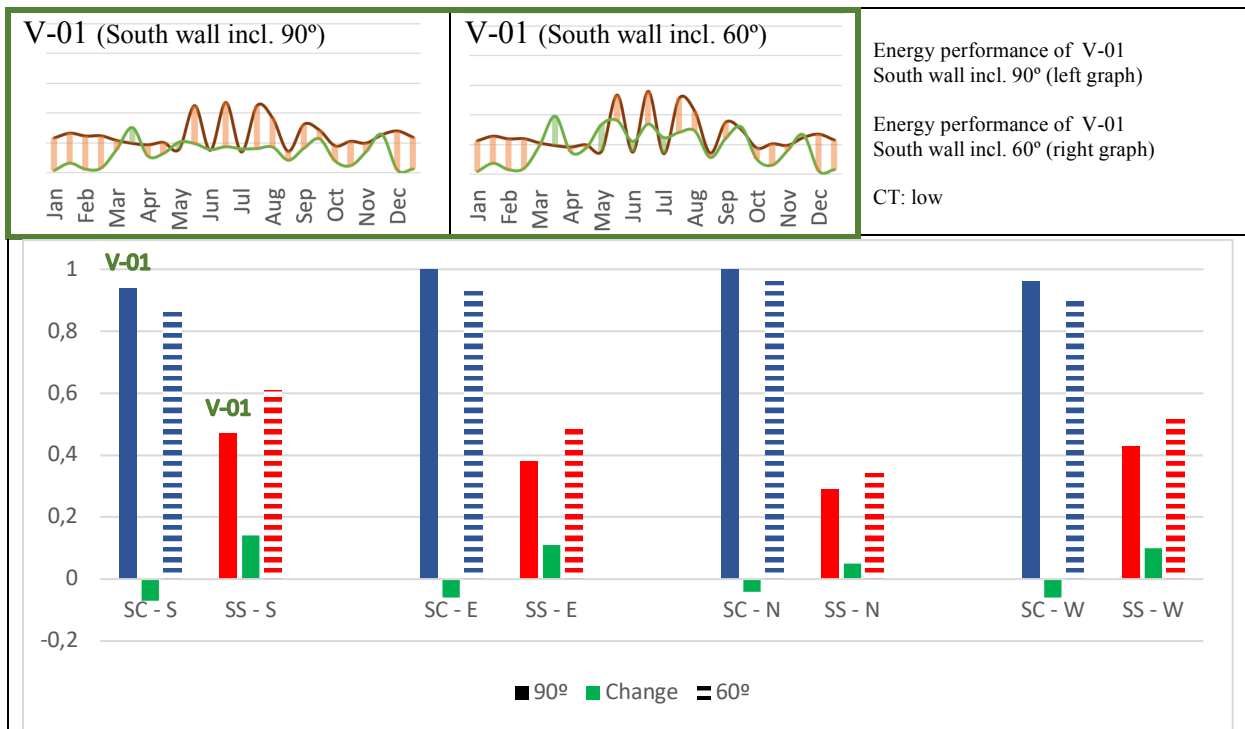


Fig. 8.10 SS and SC – Changing inclination of one face of one-storey building holding 20 m² BAPV compared to an absolute vertical wall – WWR: 0.2 - Low CT (down) + Changing energy performance of V-01 at low CT (up)

Comparing annual energy performance of this prototype with the same transformation holding BIPV (Figure 8.9) proves that comparative lower amounts of SS is achieved because of higher ‘energy demand’ of building when one face is integrated partly with BAPV (compared to BIPV) that obviously increases amounts of cooling demand (in mid-year). It also indicates that in this prototype rotation of one face of building (from 90° into 60°) that is partly covered by BAPV is beneficial and increases amount of SS but quantities of this increase are different in each face.

8.3.5 Sloping roof holding BAPV

The effects of integrating 20 m² of BAPV on one face of a symmetric sloping roof with different inclinations of 30° and 60° in both the south-north and east-west directions are presented in this comparison. WWR on all four faces is set to 0.2. The upcoming comparisons aim to answer the question of which face should be integrated with limited amounts of BAPV in the case of a symmetric sloping roof and what the amount of increase or decrease in SS is when the opposite side holds the same amounts of BAPV. Results are recorded at both high and low comfort temperatures (see table 8.11).

CT	Index	Roof type and inclination								
		V-01	V-02		V-03		V-04		V-05	
		Flat roof	S-N 30°		S-N 60°		E-W 30°		E-W 60°	
		S	N	S	N	E	W	E	W	
H	SC	0.77	0.72	0.90	0.78	0.99	0.82	0.78	0.91	0.86
	SS	0.58	0.62	0.48	0.61	0.37	0.56	0.58	0.51	0.55
L	SC	0.88	0.87	0.93	0.88	0.98	0.91	0.89	0.95	0.92
	SS	0.62	0.68	0.45	0.63	0.33	0.57	0.60	0.49	0.54

Tab. 8.11 Geometry setups + Calculations of SS and SC - Allocation of 20 m² BAPV to one face of sloping roof with inclination of 30° and 60° + sample building with flat roof - WWR: 0.2 all four faces – High & low CT

The changes in SS and SC of the prototype when bringing the same quantities of BAPV to the opposite side of the symmetric roof (at both high and low comfort temperatures) and the energy performance of the prototype with a sloping roof with an inclination of 30° when BAPV is applied on different sides (at high comfort temperatures) are presented in Figure 8.11.

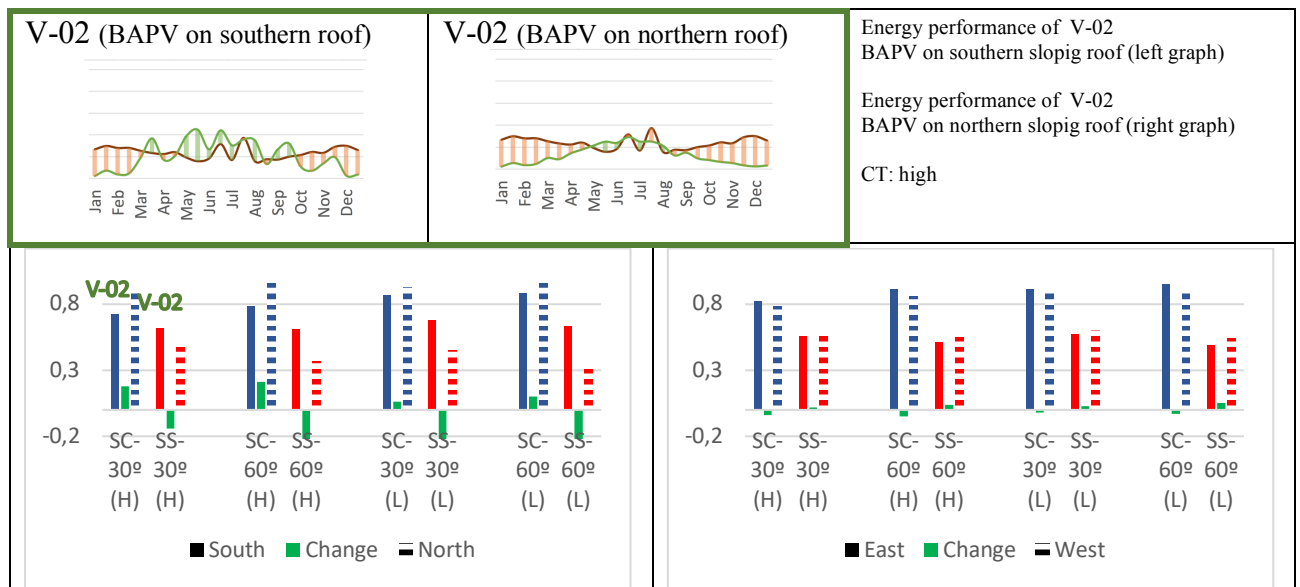
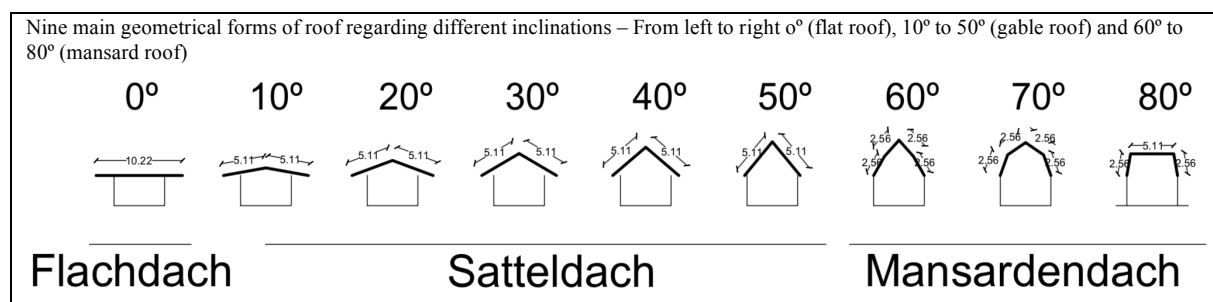


Fig. 8.11 SS and SC – Allocation of 20 m² BAPV to one face of sloping roof with inclination of 30° and 60° - WWR: 0.2 in all four faces – High and low CT (bottom) + Changing energy performance of V-02 in high CT (top)

Comparing the amounts of SS in the same building as the inclination of the sloping roof changes from 30° to 60° demonstrates that, in this prototype, a 60° inclination consistently offers less SS. However, this drop in efficiency is also related to the setpoint of the comfort temperature. For instance, this change in inclination decreases the efficiency of the prototype by just 1% (from 0.62 to 0.61) at high comfort temperatures, whereas the same change in inclination decreases the efficiency of the prototype by 5% (from 0.68 to 0.63) when the comfort temperature is set to a lower level. It should be noted that intermediate inclinations between 30° and 60° should also be simulated to identify the absolute optimum inclination among the calculated variants of this prototype.

8.3.5.1 Geometry of sloping roof

The availability of different inclinations in a limited area of the roof is initially presented in Table 8.12, which illustrates the transformation of a flat roof into a symmetric steep sloping roof with a maximum inclination of 80°. The primary constraint applied during this transformation is the requirement for the 'same total length' of the roof. Consequently, the offered area for PV integration remains constant, resulting in the use of 'the same amount of material' for each roof type. For example, a length of 10.22 m remains consistent across all upcoming sloping roof types. Comprehensive investigations of SS and SC calculations can be conducted using the matrix presented in Table 8.12 when the entire roof is covered by PVs. In this work, the 'energy performance' of just the flat roof (Flachdach) and two inclinations of 30° and 60° has been previously presented.



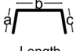














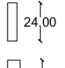











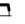

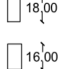



























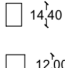
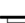












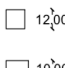


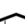








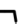
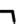
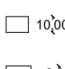













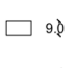













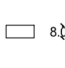













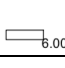
Tab. 8.12 Deformation of roofs with constraint of the same 'length' [64]

As the area of each rectangular roof is determined by multiplying its length by its width, the 'same area' constraint has been applied in the geometrical modeling of all roof types. Considering a seamless transition from a simple flat roof to steep sloping roofs, the following geometrical forms have been developed. These forms have been traditionally used for a long time in Germany and Central Europe, and there is still extensive use of these roof types in construction. They include the 'Flachdach,' a flat roof with an inclination of 0°, the 'Satteldach' with two symmetric slopes ranging from 10° to 50°, and the 'Mansardendach' with two symmetric slopes ranging from 60° to 80°.

By integrating the developed method of this work, which calculates the 'thermal performance' and 'electricity generation' of roofs with different inclinations, we can compare the offered 'self-sufficiency' and 'self-consumption' of all nine types of roofs presented in Table 8.12. To select the highest offered energy performance, these roofs should be compared in different orientations, as indicated in Table 8.3, which demonstrates that different orientations of symmetric sloping roofs (one-side integration) offer varying energy performances. To obtain more reliable results, the effect of shading on the roof due to side trails should also be

considered. As a result, in the development of the method in this work, the calculation of shadow from overhanging components may additionally be integrated.

The offered area of nine different roof types in table 8.12 can be geometrically more developed if different proportions of the building should also be taken into account. In this regard, a matrix of nine different proportions of the building with the constraint of offering a constant 'total area of roof' of 245 m² (as an instance) has been developed. All geometrical proportions (A, B, C, D, E, F, G, H, and I) with the same 'TFA' but different lengths result in the constant 'roof area.' Indeed, multiplying 'length of building' by 'length of roof' gives a constant amount of 245 m². Table 8.13 presents 'one-dwelling buildings' (D-01). The same proportional algorithm for multi-dwelling buildings has also been developed.

Left to right: deformation of roof types (constraint: the same length) – Top to bottom: geometrical proportions (constraint: the same area)															
R-01	R-02	R-03	R-04	R-05	R-06	R-07	R-08	R-09	R-10	R-11	R-12	R-13			Area
Flachdach	Satteldach				→ Nurdach		Mansardendach → Nurdach		Mansardendach → Nurdach		Mansardendach → Nurdach		Length of roof (a + b + c)	Length of building d	(a + b + c) × d
0°	10°	20°	30°	40°	50°	50°	60°	60°	70°	70°	80°	80°			
													10.22	24.00	245 A 
													13.63	18.00	245 B 
													15.33	16.00	245 C 
													17.04	14.40	245 D 
													20.44	12.00	245 E 
													24.53	10.00	245 F 
													27.26	9.00	245 G 
													30.67	8.00	245 H 
													40.89	6.00	245 I 

Tab. 8.13 Deformation of roofs and application in different geometrical proportions – Constraint: the same roof area

While the energy performance of each variant in the matrix presented in Table 8.13 is not included in this work, the aim is to demonstrate that with this type of developed matrix, predicting the energy performance of each variant will be feasible. This means that even in the very early phases of architectural design, the selection of a 'roof type' can be made with precision when estimating energy performance. In other words, during the initial phase of building design, the correct proportion of the building can also be determined based on the type of roof that will be integrated.

In the presented method of this work, partial or full coverage of the integrated roof by Building-Integrated Photovoltaics (BIPV) and Building-Attached Photovoltaics (BAPV) can be considered and applied in the process of estimating the 'energy performance indicator' of all prototypes. This approach takes into account the 'thermal performance' and 'energy generation' of the roof and the 'building envelope' simultaneously, providing a precise estimation of the 'energy performance' potential of each roof based on its integration proportion.

Taking into consideration upcoming geometrical parameters such as WWR and determining whether the roof is an additional layer applied on top of a flat roof or if it will be used as a 'Dachgeschoss' will result in a more realistic estimation of the energy performance of each geometrical variant.

8.4. WWR

8.4.1 Wall

The effects of changing the WWR of a square building (one storey) while integrating 20m² of BAPV on its flat roof are presented in this comparison. Each transformation involves altering WWRs to values of 0.2, 0.4, 0.6, and 0.8 on each face, while simultaneously maintaining a constant WWR of 0.2 on the other three faces. Annual energy performances of these transformations on the south face have also been presented to compare the overlap between 'electricity generation' and 'thermal performance' of this prototype. This demonstrates how changes in the thermal performance of the building (due to alterations in WWR) with a constant amount of 'electricity generation' (due to the consistent amount of BAPV on the flat roof) result in varying energy efficiency levels. Results are recorded at both high and low comfort temperatures (see table 8.14).

H T	Index	WWR in each face															
		V-01				V-02				V-03				V-04			
		South				East				North				West			
WWR	0.2	0.4	0.6	0.8	0.2	0.4	0.6	0.8	0.2	0.4	0.6	0.8	0.2	0.4	0.6	0.8	
H	SC	0.77	0.78	0.79	0.80	0.77	0.78	0.78	0.79	0.77	0.78	0.79	0.79	0.77	0.79	0.80	0.80
	SS	0.58	0.57	0.56	0.55	0.58	0.57	0.56	0.56	0.58	0.57	0.56	0.56	0.58	0.57	0.56	0.54
L	SC	0.88	0.88	0.89	0.89	0.88	0.88	0.89	0.89	0.88	0.88	0.89	0.89	0.88	0.88	0.89	0.89
	SS	0.62	0.58	0.55	0.52	0.62	0.59	0.56	0.54	0.62	0.60	0.57	0.55	0.62	0.58	0.53	0.50
						<p>The numbers on each wall are representative of the applied WWR. The bold numbers on each variant indicate procedure of changing WWR.</p>											

Tab. 8.14 Geometry setups + Calculations of SS and SC - Changing WWR of one vertical face from 0.2 to 0.8 – 20 m² BAPV on flat roof – High and low CT

Amounts of changing SS and SC of the prototype during changing WWR of one vertical face from 0.2 to 0.8 (in high and low CT) and energy performances of V-01 in all four WWR setups (at high CT) are presented in figure 8.12.

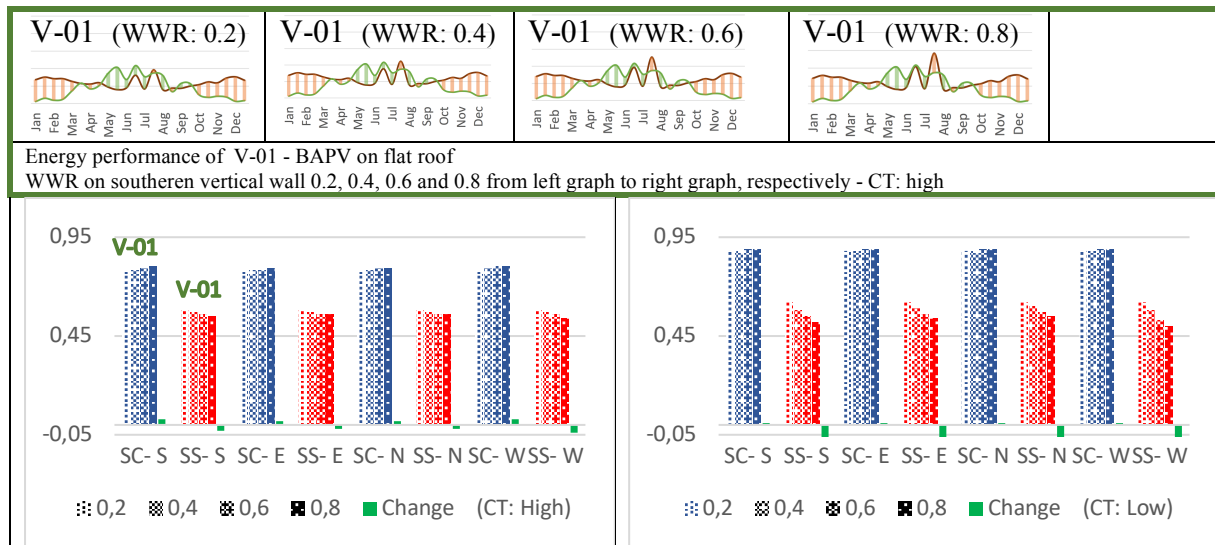


Fig. 8.12 SS and SC - Changing WWR of one vertical face from 0.2 to 0.8 – 20 m² BAPV on flat roof – High and low CT (down) + Changing energy performance of V-01 in high CT (up)

The results show that increasing the Window-to-Wall Ratio (WWR) in each face decreases the SS, but for different quantities. For instance, in high CT, this transformation in the north face decreases SS of this prototype by 2% (from 0.58 to 0.56), while the drop in SS in the west face is 4% (from 0.58 to 0.54). The fluctuation of SS demonstrates that the sensitivity of the prototype to changes in WWR in all four faces is significantly higher in low CT compared to high CT. For example, on the west face of the building, which is the most sensitive face to this transformation, the drop in SS is 8% in low CT (from 0.62 to 0.50), whereas in high CT, it's 4% (from 0.58 to 0.54). This fact is also demonstrated by comparing changes in SS in different faces, which indicate higher amounts of SS changes in all four faces when the comfort temperature is set to a low setpoint definition. Comparing the four annual energy performances of the south-face transformation indicates that the main reason for drops in SS is the increasing cooling demand of the prototype, primarily during the mid-year.

8.4.2 Sloping roof in 'Dachgeschoss'

As a tradition, constructing upper storeys of buildings with steep slopes is preferred in Germany and Europe for various architectural reasons. In this regard, the integration of specific windows into these sloping roofs and the resulting energy performance have been investigated through the defined prototype. An inclination of 60°, which is the most similar inclination of these roofs to 'Dachgeschoss,' has been intentionally selected.

The effects of changing the Window-to-Wall Ratio (WWR) in the upper sloping roof (Dachgeschoss) of a square building (two storeys + one 'Dachgeschoss') holding 40m² of BAPV on its south vertical wall are presented in this comparison. Thus, electricity generation remains at the same level, and changes in energy performance are solely due to changes in WWR. Three different WWR values of 0.0, 0.5, and 1.00 are compared, representing a pure opaque roof without windows, a 50% window roof, and a fully integrated window roof, respectively. Results are recorded at a high comfort temperature (see table 8.15).

Roof type and WWR in sloping roof (with top floor below)												
Index	V-01			V-02			V-03			V-04		
	S-N 60° + top floor South sloping face in TP			E-W 60° + top floor East sloping face in TP			S-N 60° + top floor North sloping face in TP			E-W 60° + top floor West sloping face in TP		
WWR	0	0.5	1	0	0.5	1	0	0.5	1	0	0.5	1
SC	0.99	0.99	1.00	0.99	0.99	1.00	0.99	0.99	1.00	0.99	0.99	0.99
SS	0.45	0.40	0.35	0.44	0.40	0.37	0.44	0.41	0.38	0.45	0.38	0.33
			The numbers on each sloping roof are representative of the applied WWR.									

Tab. 8.15 Geometry setups + Calculations of SS and SC - Changing WWR of sloping roof with inclination of 60° from 0.0 into 1.00 - 40 m² BAPV on southern face - WWR 0.2 in all four vertical faces – High CT

The changes in SS and SC of the prototype during changing WWR of the sloping roof with an inclination of 60° from 0.0 to 1.00 (in high CT) and the energy performances of V-01 in all three WWR setups (at high CT) are presented in Figure 8.13.

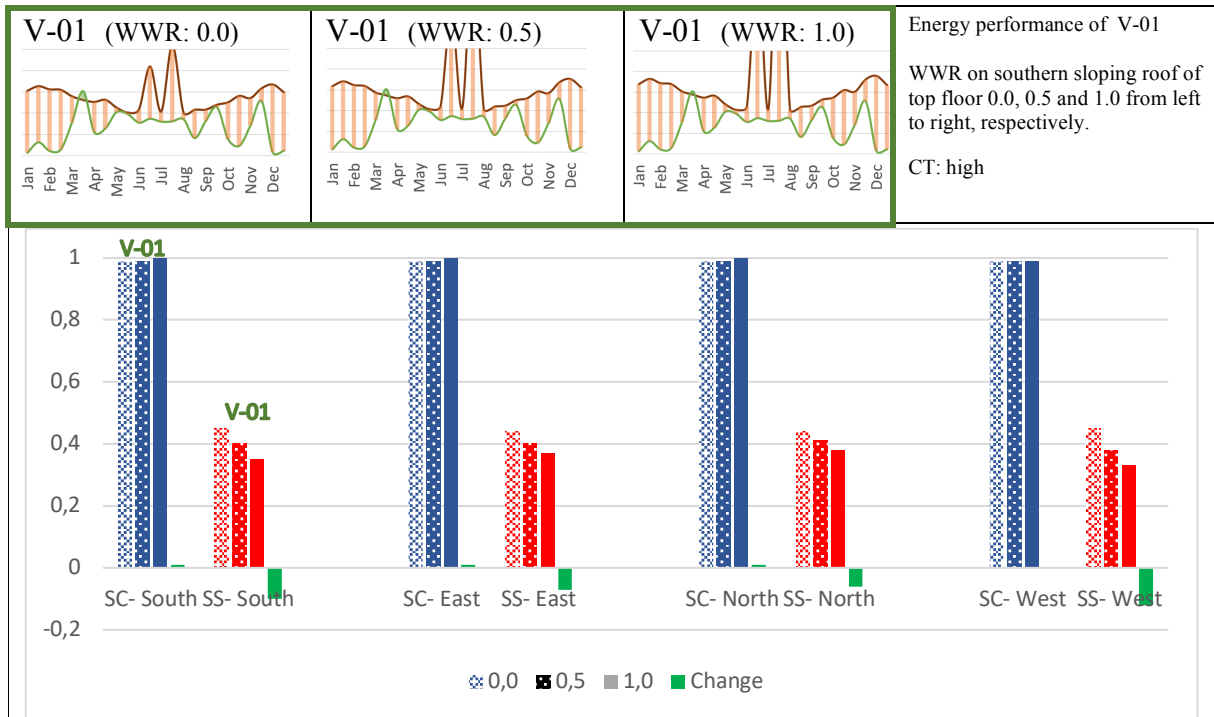


Fig. 8.13 SS and SC - Changing WWR of sloping roof with inclination of 60° from 0.0 into 1.00 - 40 m² BAPV on southern face - WWR 0.2 in all four vertical faces – CT: High (down) + Changing energy performance of V-01 in WWR of 0.0, 0.5 & 1.0 – CT: high (up)

The results indicate that increasing the WWR in each face of the sloping roof in the defined prototype effectively reduces the quantity of SS. The most sensitive face in this prototype to changes in WWR is the west face of an 'east-west' oriented 'Dachgeschoss,' as it shows a 12% drop in SS (from 0.45 to 0.33), whereas the north face of a 'south-north' orientation has only a 6% drop (from 0.44 to 0.38). Referring to the three presented energy performances of V-01 in three WWR values of 0.0, 0.5, and 1.0 on the southern sloping roof indicates that both 'heating demand' and 'cooling demand' of the prototype increase with higher WWR in the sloping roof, resulting in lower SS values.

8.5 Roof type

In the case of selecting a steep sloping roof (in this work, an inclination of 60°) for a two-story building, two different architectural roof concepts can be applied to the building. The first concept involves constructing two identical stories with the exact same vertical walls, covering the second floor with a flat roof, and finally integrating a symmetric sloping roof on the building. The second concept, which is also a traditional method in Germany, consists of constructing the first floor with vertical walls and using the sloping elements of the sloping roof as diagonal walls for the second floor ('Dachgeschoss'). As both concepts provide the exact same total 'living area,' their energy performances can be compared to determine which one offers a higher indication of energy efficiency. It should be noted that the total construction material used in the 'Dachgeschoss' is relatively less than in the 'building with an extra roof,' which can be considered in the process of selecting the concept, but is not a critical index of this work. Results are recorded at a high comfort temperature (see table 8.16).

	Index	Roof type – Dachgeschoss or extra sloping roof - inclination of 60°			
		V-01	V-02	V-03	V-04
		South	East	North	West
Dachgeschoss	SC	0.73	0.87	0.97	0.80
	SS	0.65	0.54	0.41	0.56
Extra roof	SC	0.73	0.87	0.97	0.79
	SS	0.67	0.57	0.43	0.60
			TF (Top floor) = Dachgeschoss Fl = Floor (storey) ER = Extra roof (extra sloping roof that covers the separate flat roof) 1Fl + 1 TF = 1 Storey + Dachgeschoss 2Fl + ER = 2 Storey + Sloping roof		

Tab. 8.16 Geometry setups + Calculations of SS and SC - Changing 'Dachgeschoss' to 'normal storey + sloping roof' in different orientations - 40 m² BAPV on representative sloping roof - WWR: 0.2 in all four faces (two-storeys building) - High CT

The changes in SS and SC of the prototype during the transformation from 'Dachgeschoss' to 'normal storey + sloping roof' in different orientations (at high CT), and the energy performances of V-01 in this transformation (at high CT), are presented in Figure 8.14.

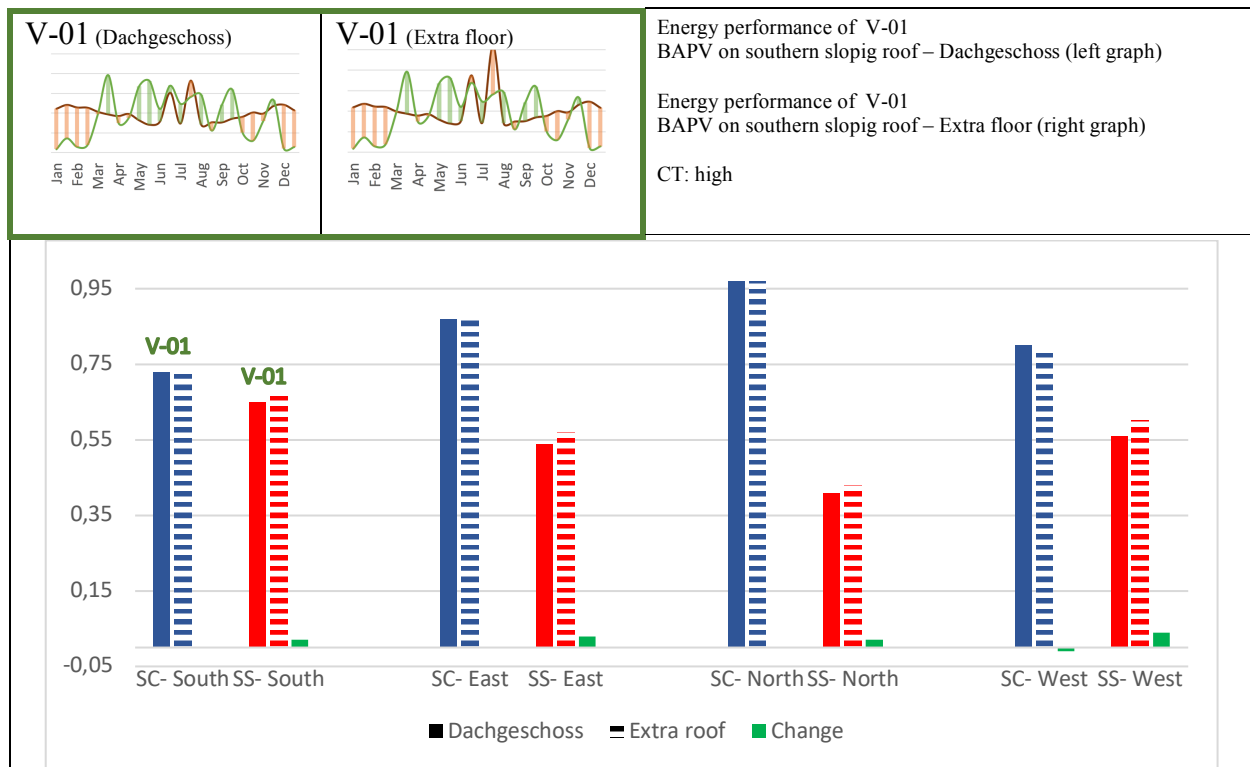


Fig. 8.14 SS and SC - Changing 'Dachgeschoss' to 'normal storey + sloping roof' in different orientations - 40 m² BAPV on representative sloping roof - WWR: 0.2 in all four faces (two-storeys building) – High CT (down) + Changing energy performance of V-01 in 'Dachgeschoss' and 'extra floor' – CT: high (up)

The results show that switching from 'Dachgeschoss' to 'extra roof' increases the SS of this prototype by 2% to 4% in different orientations. The west BAPV integration (V-04) is the most sensitive direction for this transformation, with a 4% increase in SS. Regarding the two presented energy performances of V-01, which compare these two concepts when 40 m² of BAPV is on the southern side, it is demonstrated that although the 'uncovered cooling demand' is relatively higher in the 'extra roof' concept, the lower heating demand offers a final more SS of 2% (comparing 0.65 m² with 0.67 m²).

8.6 Building expansion

Moving toward multi-dwelling houses to decrease material usage per capita can be achieved through both 'multi-storey construction' or 'flat expansion,' which offer 'vertical' and 'horizontal' expansion of the building, respectively. To compare the changes in energy performance resulting from the transformation of a 'single-family house' through 'vertical' or 'horizontal' expansion, the availability of the building's envelope for integrating PVs should also be considered. In both types of expansion, an equal amount of 'on-roof' BAPV is applied, demonstrating the changes in these two energy performances during the transformation from a 'single-family house' to a 'five-family house'.

8.6.1 Vertical expansion

The expansion of a 'one-storey' building through the construction of identical upper storeys is examined in this comparison. Five variants, labeled as 01 to 05, represent one-storey to 'five-storey buildings,' respectively. In all four faces of each variant, WWR is set to a constant

value of 0.2. During this expansion, 20 m² of BAPV on the flat roof is applied for each extra storey. Consequently, 0.2 m² of BAPV on the roof is allocated for each square meter of 'total area' throughout the entire expansion. To establish a fair energy performance comparison, 20 m², 40 m², 60 m², 80 m², and 100 m² of BAPV on the flat roof are allocated to v-01, v-02, v-03, v-04, and v-05, respectively. Results at both high and low comfort temperatures (table 8.17).

CT	Index	Vertical expansion – 20 m ² PV on roof for each 100 m ² area (BAPV)				
		V-01	V-02	V-03	V-04	V-05
		1 storey – 100 m ²	2 storey – 200 m ²	3 storey – 300 m ²	4 storey – 400 m ²	5 storey – 500 m ²
		20 m ²	40 m ²	60 m ²	80 m ²	100 m ²
H	SC	0.77	0.72	0.70	0.69	0.68
	SS	0.58	0.64	0.66	0.67	0.68
L	SC	0.88	0.86	0.85	0.84	0.84
	SS	0.62	0.68	0.70	0.71	0.72

Tab. 8.17 Geometry setups + Calculations of SS and SC - Vertical expansion of one-storey building - 20 m² BAPV on flat roof for each storey- WWR: 0.2 in all four faces (one-storey building into five-storeys building) – High and low CT

The changes in SS and SC of the prototype during the vertical expansion of a one-storey building (at both high and low CT), and the energy performances of V-01 and V-02 in this expansion (at high CT), are presented in Figure 8.15.

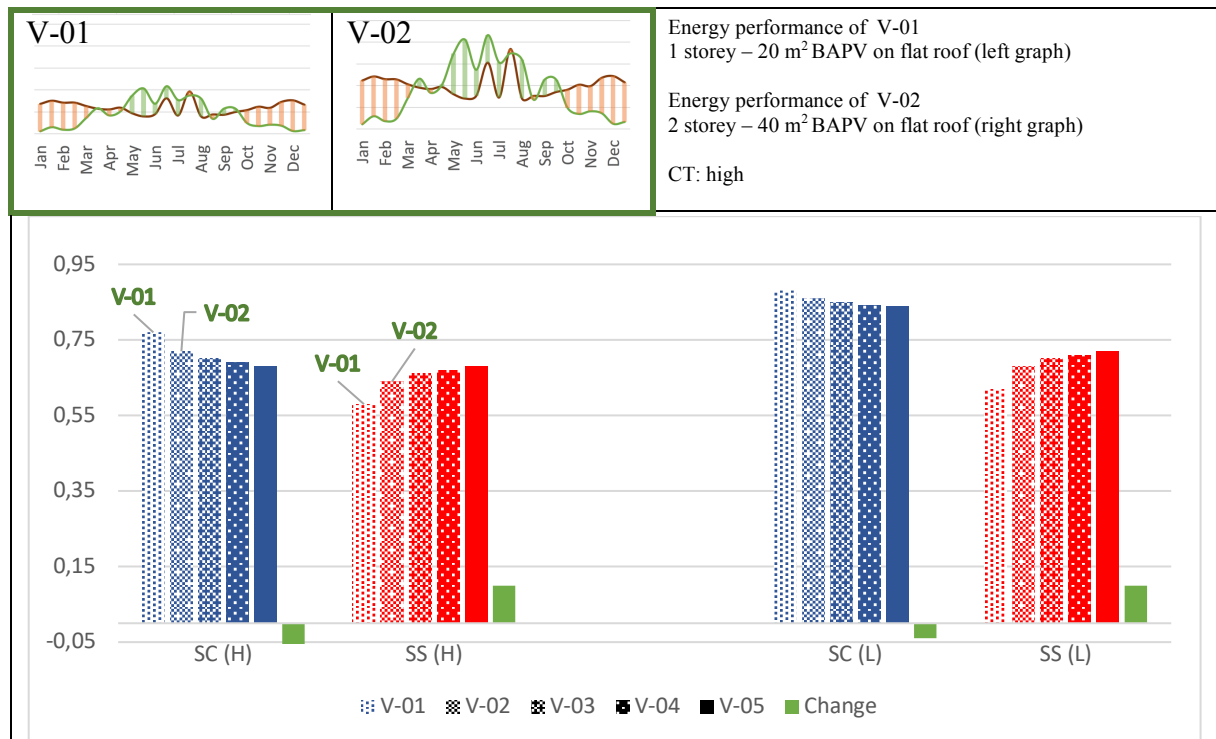


Fig. 8.15 SS and SC - Vertical expansion of one-storey building - 20 m² BAPV on flat roof for each storey- WWR: 0.2 in all four faces (one-storey building into five-storeys building) - High and low CT (down) + Changing energy performance of V-01 and V-02 – CT: high (up)

The results show that in both high and low setpoints for comfort temperature, the SS in this prototype increases by 10%. The decreases in SC vary, with reductions of 9% and 4% in high and low setpoints for CT, respectively. For example, the energy performance transformation from V-01 to V-02 (see Table x.32) indicates that as the annual energy demand of the building increases, a larger portion of the total energy demand is covered by self-generated electricity, leading to higher SS. Conversely, a smaller portion of self-generated electricity is consumed by the building, resulting in lower SC. The changing percentages of increased SS and decreased SC are moderated when moving toward higher prototypes.

8.6.2 Horizontal expansion

In this comparison, the expansion of a 'one-storey' building is achieved through an extension of its width and length. Five variants, labeled as 01 to 05, represent one-unit to five-unit buildings, with the constraint of remaining as 'one-storey' buildings and an equal allocation of PV per capita. Similar to vertical expansion, all four faces have a constant WWR of 0.2, and there is an allocation of 0.2 m² of BAPV on the roof for each one square meter of 'total area.'

Consequently, 20 m², 40 m², 60 m², 80 m², and 100 m² of BAPV on the flat roof are allocated to v-01, v-02, v-03, v-04, and v-05, respectively. Results are recorded at both high and low comfort temperatures (see table 8.18).

CT	Index	Horizontal expansion – 20 m ² PV on roof for each 100 m ² area (BAPV)				
		V-01	V-02	V-03	V-04	V-05
		1 storey – 100 m ² 20 m ²	1 storey – 200 m ² 40 m ²	1 storey – 300 m ² 60 m ²	1 storey – 400 m ² 80 m ²	1 storey – 500 m ² 100 m ²
H	SC	0.77	0.73	0.71	0.70	0.69
	SS	0.58	0.60	0.60	0.61	0.61
L	SC	0.88	0.84	0.80	0.78	0.76
	SS	0.62	0.67	0.68	0.68	0.68

Tab. 8.18 Geometry setups + Calculations of SS and SC - Horizontal expansion of one-storey building - 20 m² BAPV on flat roof for each storey- WWR: 0.2 in all four faces (Expansion of 100m² building into 500m² building in one storey) - High and low CT

The changes in SS and SC of the prototype during the horizontal expansion of a one-storey building (at both high and low CT), and the energy performances of V-01 and V-02 in this expansion (at high CT), are presented in Figure 8.16.

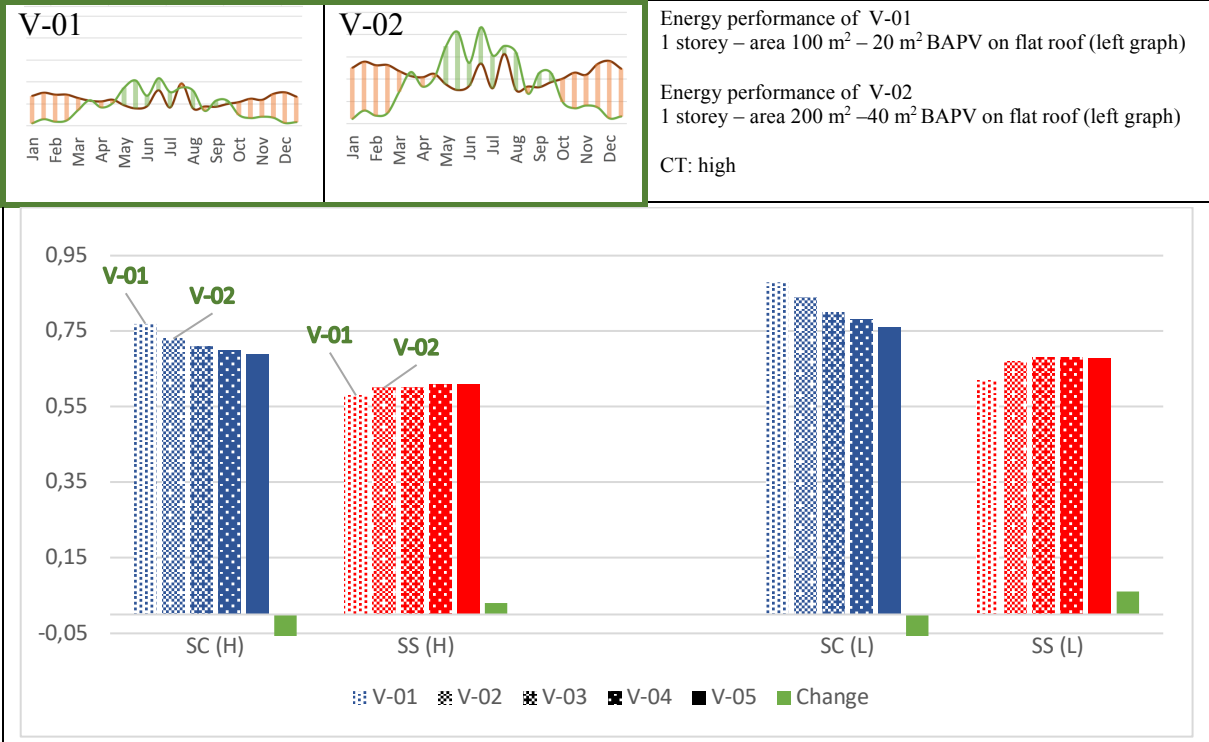


Fig. 8.16 SS and SC - Horizontal expansion of one-storey building - 20 m² BAPV on flat roof for each storey- WWR: 0.2 in all four faces (Expansion of 100m² building into 500m² building in one storey) – High and low CT (down) + Changing energy performance of V-01 and V-02 – CT: high (up)

The results indicate that in both high and low setpoints for comfort temperature, in this prototype, as we move towards more dwelling units in the building, SS increases. However, in the last three transformations (from V-02 to V-05), there is a less significant increase compared to vertical expansion. Additionally, horizontal expansion results in a lower increase in SS compared to vertical expansion. In vertical expansion, SS increases by 10% in both high and low CT, whereas horizontal expansion provides a 3% increase in high CT and a 6% increase in low CT, respectively.

8.7 Distribution of PV

8.7.1 BAPV on sloping roof with different inclinations

In buildings with symmetric sloping roofs, deciding whether to allocate all the PVs to one side or divide them into two equal portions on each side of the roof is a critical decision in the early planning stages. To address this, different orientations of buildings should be applied in the developed geometrical matrix to observe the changes in each type of allocation for specific building orientations. Table 8.19 displays the allocation of 40 m² of BAPV on one side of a sloping roof with inclinations of 30° and 60° in 12 different orientations, with intervals of 30°. When allocating PV to two sides of the sloping roof, only 6 different orientations of the prototype are considered, as the symmetric roof provides the exact same setup in the second set of 'six orientations' of the prototype.

Orientation – distribution of PV on roof												
Inc 30° - PV one side												
Orn.	0°	-30°	-60°	-90°	-120°	-150°	-180°	+150°	+120°	+90°	+60°	+30°
SC	0.44	0.46	0.49	0.52	0.57	0.62	0.63	0.60	0.54	0.49	0.57	0.68
SS	0.77	0.76	0.73	0.71	0.69	0.67	0.67	0.68	0.70	0.73	0.69	0.68
Inc 60° - PV one side												
SC	0.48	0.51	0.56	0.61	0.70	0.80	0.82	0.75	0.64	0.56	0.51	0.48
SS	0.75	0.74	0.72	0.68	0.66	0.63	0.61	0.63	0.67	0.72	0.75	0.75
			Top: 360° rotation of one-side allocation – Inc. 30° Bottom: 360° rotation of one-side allocation – Inc. 60°									

Tab. 8.19 Geometry setups + Calculations of SS and SC - Orientation of building with one-side allocation of 40 m² BAPV on sloping roof with inclination of 30° and 60° - WWR: 0.2 in all four faces – High CT

The changes in SS and SC of the prototype during its orientation with one-side allocation of 40 m² of BAPV on a sloping roof with inclinations of 30° and 60° are presented in Figure 8.17.

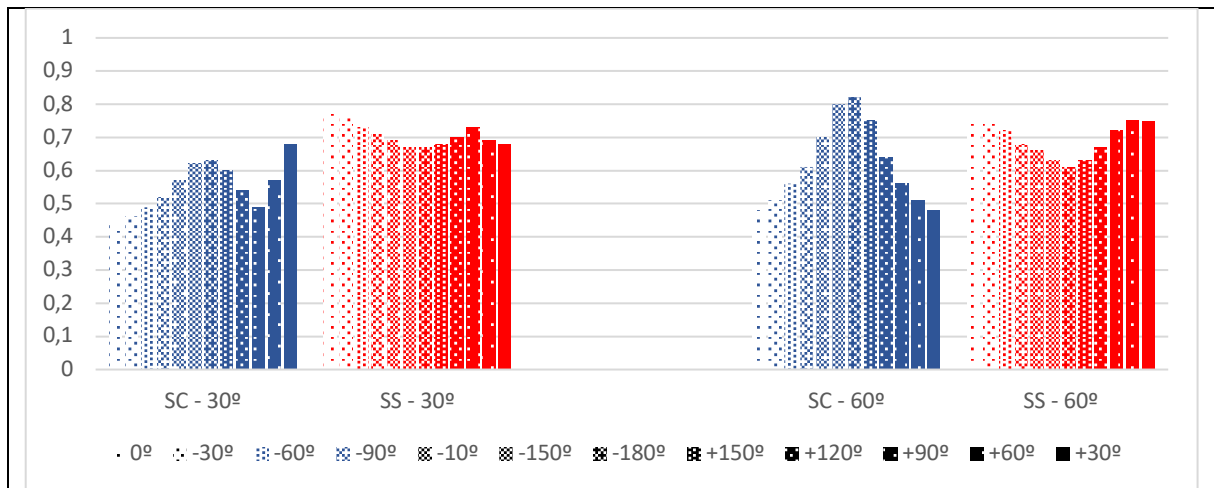


Fig. 8.17 SS and SC - Orientation of building with one-side allocation of 40 m² BAPV on sloping roof with inclination of 30° and 60° - WWR: 0.2 in all four faces – High CT

Table 8.20 displays equal allocation of 40 m² of BAPV on two sides of a sloping roof with inclinations of 30° and 60° in 6 different orientations of the prototype, with each rotation interval of 30°.

Inc 30° - PV two sides							Inc 60° - PV two sides					
SC	0.53	0.52	0.51	0.51	0.57	0.53	0.64	0.63	0.60	0.58	0.60	0.63
SS	0.74	0.73	0.72	0.72	0.69	0.74	0.74	0.72	0.70	0.70	0.72	0.74
			Left: 180° rotation of two-sides allocation – Inc. 30° Right: 180° rotation of two-sides allocation – Inc. 60°									

Tab. 8.20 Geometry setups + Calculations of SS and SC - Orientation of building with two-sides allocation of 40 m² BAPV on sloping roof with inclination of 30° and 60° - WWR: 0.2 in all four faces - High CT

The changes in SS and SC of the prototype during its orientation with two-sided allocation of 40 m² of BAPV on a sloping roof with inclinations of 30° and 60° are presented in Figure 8.18.

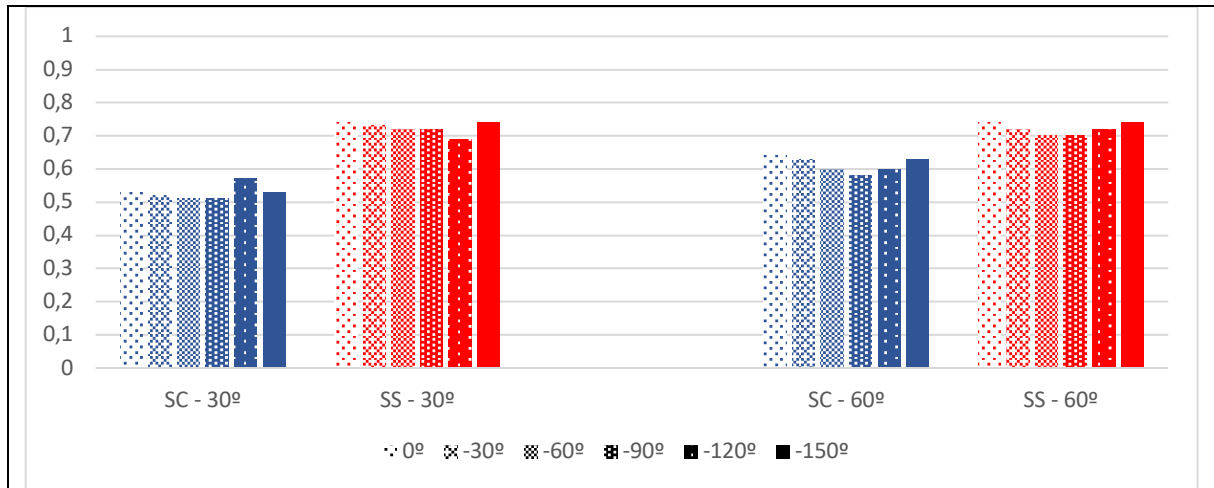


Fig. 8.18 SS and SC - Orientation of building with two-sides allocation of 40 m² BAPV on sloping roof with inclination of 30° and 60° - WWR: 0.2 in all four faces – High CT

Comparing the maximum SS of the prototype when 40 m² of BAPV is installed 'entirely on one side' or 'equally on two sides' of the sloping roof, it indicates that one-side installation of the entire BAPV offers a higher SS, resulting in an absolute south orientation. In this variant (one-side installation), the fluctuation of SS in all 12 orientations through two inclinations of 30° and 60° demonstrates different changes as the orientation of the building changes. In an inclination of 30°, instead of an absolute priority for south installation, a second peak is recorded in the absolute west (+90°) orientation. In an inclination of 60°, the minimum SS is offered by an absolute north orientation (180°), but the maximum SS is offered by the orientations of V-01, V-11, and V-12, which correspond to orientations of 0°, +60°, and +30°, respectively. So, in 'two-side distribution,' compared to 'one-side distribution,' this prototype is less sensitive to rotation (different orientations) and offers a lower 'maximum SS.' From another point of view, the minimum offered SS in 'one-side distribution' in an inclination of 60° is 0.61 (orientation 180°), whereas in 'two-side distribution,' SS will not drop below 0.70. So, it could be concluded that in this prototype and in a specific inclination of 60°, the minimum SS will be achieved in a less 'orientation-dependent' manner compared to 'one-side distribution' with the same inclination.

8.7.2 Symmetric and asymmetric distribution of BAPV

This section involves a comparison of the drop or increase in energy efficiency resulting from BAPV allocation on one side (asymmetric) versus dividing the same amount on two sides (symmetric) of a sloping roof with inclinations of 30° and 60°. The discussion and comparison are conducted for four main geographical orientations. In this scenario, 40 m² of BAPV is allocated on one side (asymmetric) of the sloping roof, and the results are compared to when 20 m² of BAPV is allocated on each side of the same sloping roof (symmetric). The comfort temperature is set to a high definition. Table 8.21 presents the asymmetric and symmetric distribution of BAPV on the roof with an inclination of 30°, along with recorded SS and SC at high comfort temperature.

Index	Distribution of PV on roof with inclination of 30°							
	V-01		V-02		V-03		V-04	
	South & south-north		East & east-west		North & north-south		West & west-east	
	40 m ² -S	20 m ² -S 20 m ² -N	40 m ² -E	20 m ² -E 20 m ² -W	40 m ² -N	20 m ² -N 20 m ² -S	40 m ² -W	20 m ² -W 20 m ² -E
SC	0.44	0.53	0.52	0.51	0.63	0.53	0.49	0.51
SS	0.77	0.74	0.71	0.72	0.67	0.74	0.73	0.72

Tab. 8.21 Geometry setups + Calculations of SS and SC - Asymmetric or symmetric allocation of 40 m² BAPV on sloping roof with inclination of 30° - All four main orientations - WWR: 0.2 in all four faces - High CT

The changes in SS and SC of the prototype during asymmetric or symmetric allocation of 40 m² of BAPV on a sloping roof with an inclination of 30° are presented in Figure 8.19.

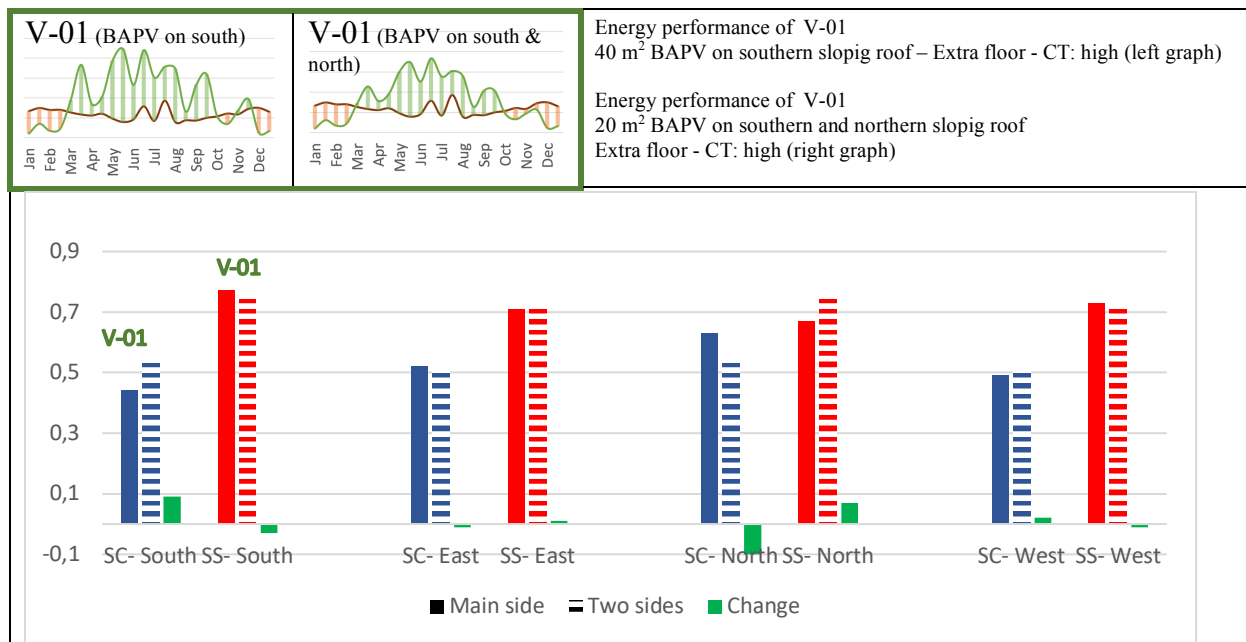


Fig. 8.19 SS and SC - Asymmetric or symmetric allocation of 40 m² BAPV on sloping roof with inclination of 30° - All four main orientations - WWR: 0.2 in all four faces - High CT (down) + Changing energy performance of V-01 in 'asymmetric' and 'symmetric' mode – CT: high (up)

The results demonstrate that in this prototype, the distribution of BAPV on both sides of a symmetric sloping roof with an inclination of 30° can increase or decrease SS depending on the building's orientation. For example, dividing the entire 40 m² of BAPV from a south-integrated system into south and north (each holding 20 m²) decreases SS by 3% (from 0.77 to 0.74). Similarly, switching from an absolute west integration to east-west integration decreases SS by 1% (from 0.73 to 0.72). However, dividing the entire 40 m² of BAPV from an east-integrated system into 20 m² in the east and 20 m² in the west increases SS by 1% (from 0.71 to 0.72). Similarly, switching from an absolute north integration to south-north integration increases SS by 7% (from 0.67 to 0.74). Table 8.22 presents the asymmetric and symmetric distribution of BAPV on the roof with an inclination of 60°, along with recorded SS and SC.

Index	Distribution of PV on roof with inclination of 60°							
	V-01		V-02		V-03		V-04	
	South & south-north		East & east-west		North & north-south		West & west-east	
	40 m ² -S	20 m ² -S 20 m ² -N	40 m ² -E	20 m ² -E 20 m ² -W	40 m ² -N	20 m ² -N 20 m ² -S	40 m ² -W	20 m ² -W 20 m ² -E
SC	0.48	0.64	0.61	0.58	0.82	0.64	0.56	0.58
SS	0.75	0.74	0.68	0.70	0.61	0.74	0.72	0.70

Tab. 8.22 Geometry setups + Calculations of SS and SC - Allocation of 40 m² BAPV asymmetric or symmetric on sloping roof with inclination of 60° - All four main orientations - WWR: 0.2 in all four faces - High CT

The changes in SS and SC of the prototype resulting from asymmetric or symmetric allocation of 40 m² of BAPV on a sloping roof (inclination of 60°) are presented in Figure 8.20.

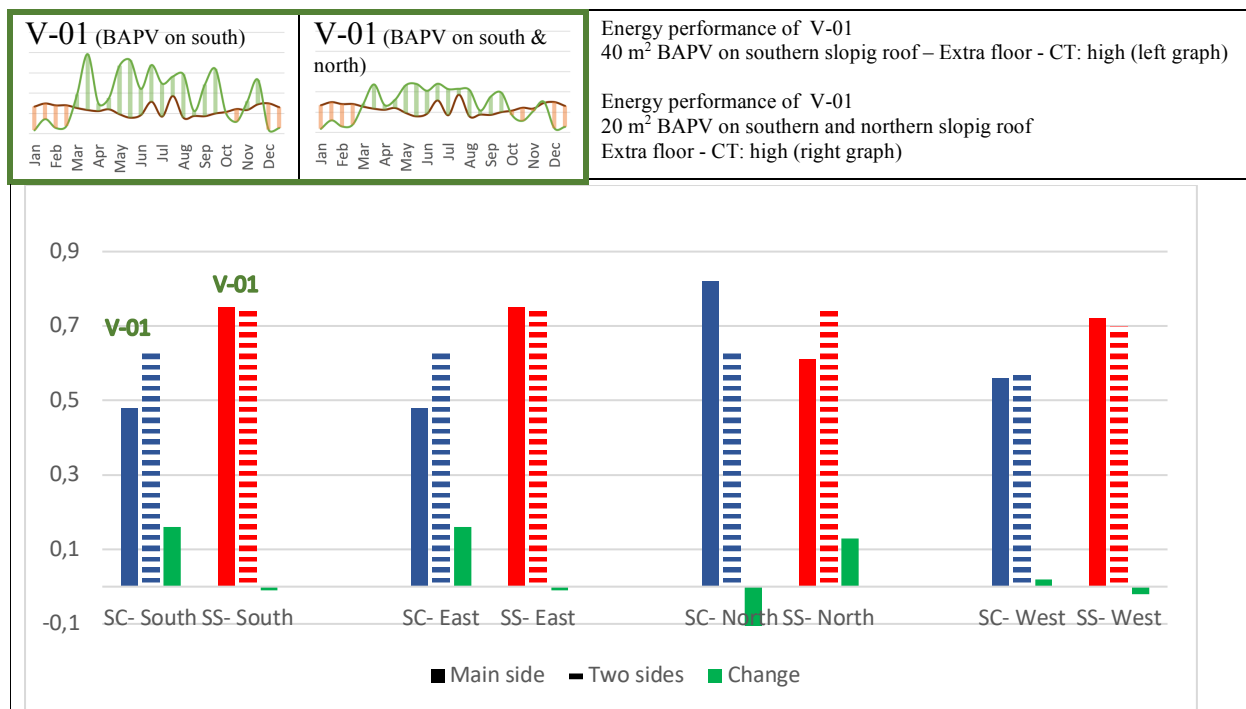


Fig. 8.20 SS and SC - Asymmetric or symmetric allocation of 40 m² BAPV on sloping roof with inclination of 60° - All four main orientations - WWR: 0.2 in all four faces - High CT (down) + Changing energy performance of V-01 in 'asymmetric' and 'symmetric' mode – CT: high (up)

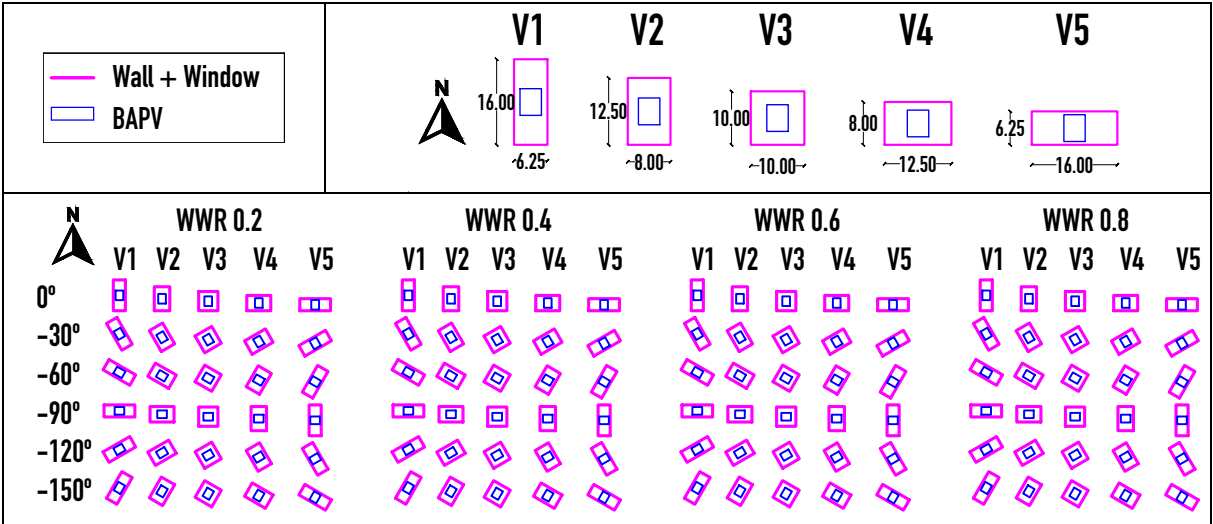
The results indicate that in this prototype, the distribution of BAPV on both sides of a symmetric sloping roof with an inclination of 60° (considering SS as the critical index) is mainly beneficial when the entire 40 m² of BAPV is integrated on one side of the roof. The most significant 'energy performance change' occurs in an absolute north integration, where SS increases by 13% (from 0.61 to 0.74) after shifting half of the PVs to the south roof.

Similarly, shifting half of the PVs from an east roof to a west roof increases SS by 2% (from 0.68 to 0.70).

8.8 Proportion + Orientation + WWR

To detect changes in the energy performance of a building when more than two geometrical parameters are altered, the effects of changing three parameters—orientation, proportion, and WWR—in a one-story building have been studied. The developed matrix presents five different proportions of the considered prototype, where four WWRs (0.2, 0.4, 0.6, and 0.8) and six orientations (0°, -30°, -60°, -90°, -120°, and -150°) are applied to all five proportions.

This matrix primarily aims to determine whether changing the values of orientation, proportion, and WWR affects the energy performance of the building in different configurations of each parameter. For example, it examines whether different energy performances resulting from different WWRs remain the same when the entire building rotates and to what extent these results differ in various proportions of the building. Table 8.23 presents the matrix of geometry setups for the considered proportions, orientations, and WWRs.



Tab. 8.23 Geometry setups – Algorithm of 5 proportions, 6 orientations and 4 WWRs - 20 m² BAPV on flat roof

Table 8.24 displays the changes in SS and SC of the prototype when altering three parameters: orientation, proportion, and WWR in a one-story building with 20 m² of BAPV on the flat roof (high CT).

		WWR 0.2					WWR 0.4					WWR 0.6					WWR 0.8				
		V-01	V-02	V-03	V-04	V-05	V-01	V-02	V-03	V-04	V-05	V-01	V-02	V-03	V-04	V-05	V-01	V-02	V-03	V-04	V-05
0°	SC	78	77	77	77	77	81	81	81	81	81	83	82	82	82	83	84	83	83	83	84
	SS	57	58	58	57	57	52	54	54	54	53	47	49	50	50	48	43	45	46	46	45
-30°	SC	78	77	77	77	77	81	81	81	81	81	83	82	82	82	83	84	83	83	83	84
	SS	57	57	58	57	57	52	53	54	54	53	47	49	49	49	48	43	45	46	45	44
-60°	SC	78	77	77	77	78	81	81	81	81	81	83	82	82	82	83	84	83	83	83	84
	SS	57	57	58	57	57	52	54	54	53	52	48	49	49	49	47	43	45	46	45	43
-90°	SC	77	77	77	77	77	81	81	81	81	81	83	82	82	82	83	84	83	83	83	84
	SS	57	57	58	58	58	53	54	54	54	52	48	50	50	49	47	45	46	46	45	43
-120°	SC	77	77	77	77	78	81	81	81	81	81	83	82	82	82	83	84	83	83	83	84
	SS	57	57	58	57	57	53	54	54	53	52	48	49	49	49	47	44	45	46	45	43
-150°	SC	78	77	77	77	78	81	81	81	81	81	83	82	82	82	83	84	83	83	83	84
	SS	57	57	58	57	57	52	53	54	54	52	47	49	49	49	48	43	45	46	45	43

The bar chart visualizes the data from Table 8.24. The y-axis represents the values for SC (0 to 0.9) and SS (0 to 0.9). The x-axis is divided into four sections for WWR values: 0.2, 0.4, 0.6, and 0.8. Each section contains five groups of bars for proportions V-01 to V-05. Within each group, there are two bars: a blue bar for SC and a red bar for SS. The legend indicates that the blue bars represent SC for orientations 0°, -30°, -60°, -90°, -120°, and -150°, while the red bars represent SS for the same orientations. The chart shows that SS values generally decrease as WWR increases, and SC values are consistently higher than SS values. The effect of orientation is more pronounced at higher WWR values.

Tab. 8.24 SS and SC – Matrix of combination of 5 proportions, 6 orientations and 4 WWRs - 20 m² BAPV on flat roof - CT: high

The results demonstrate that SS decreases as WWR increases in all five proportions and in each orientation. The effects of different orientations are more pronounced when the proportion of the prototype is closer to rectangular rather than a square proportion. Therefore, changes in SS in V-01 and V-05 exhibit more fluctuations compared to V-03, which represents a square building.

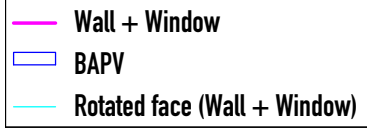
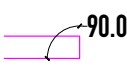
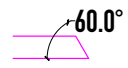
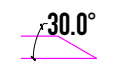

















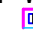







































































































































































































It can also be concluded that in this prototype, the variants with higher WWR (0.8 in this case) are more sensitive to changes in orientation because the thermal performance of windows changes more significantly compared to the opaque part of a wall due to the higher sensitivity of transparent components to changes in irradiation.

Additionally, it is revealed that for specific orientations and WWR in this prototype, certain 'rectangular' proportions can be competitive with an absolute square building when SS is considered the critical index. For example, this prototype with a fixed WWR of 0.6 and an absolute square form (V3) yields an SS of 0.49, while an absolute rectangular proportion (V5) with the same orientation and WWR has just a 1% lower SS, delivering a self-sufficiency of 0.48.

8.9 Inclination + Orientation + WWR

The effects of concurrent changes in three parameters—orientation, inclination, and WWR—in a one-story building have been studied. Table 8.25 presents a matrix that combines three inclinations (90°, 60°, and 30°) with six WWRs (0.0, 0.2, 0.4, 0.6, 0.8, and 1.0) across twelve orientations of the building (0°, -30°, -60°, -90°, -120°, -150°, 180°, +150°, +120°, +90°, +60°, and +30°). These three main defined inclinations are exclusively applied to just one face of the building in a representative orientation.

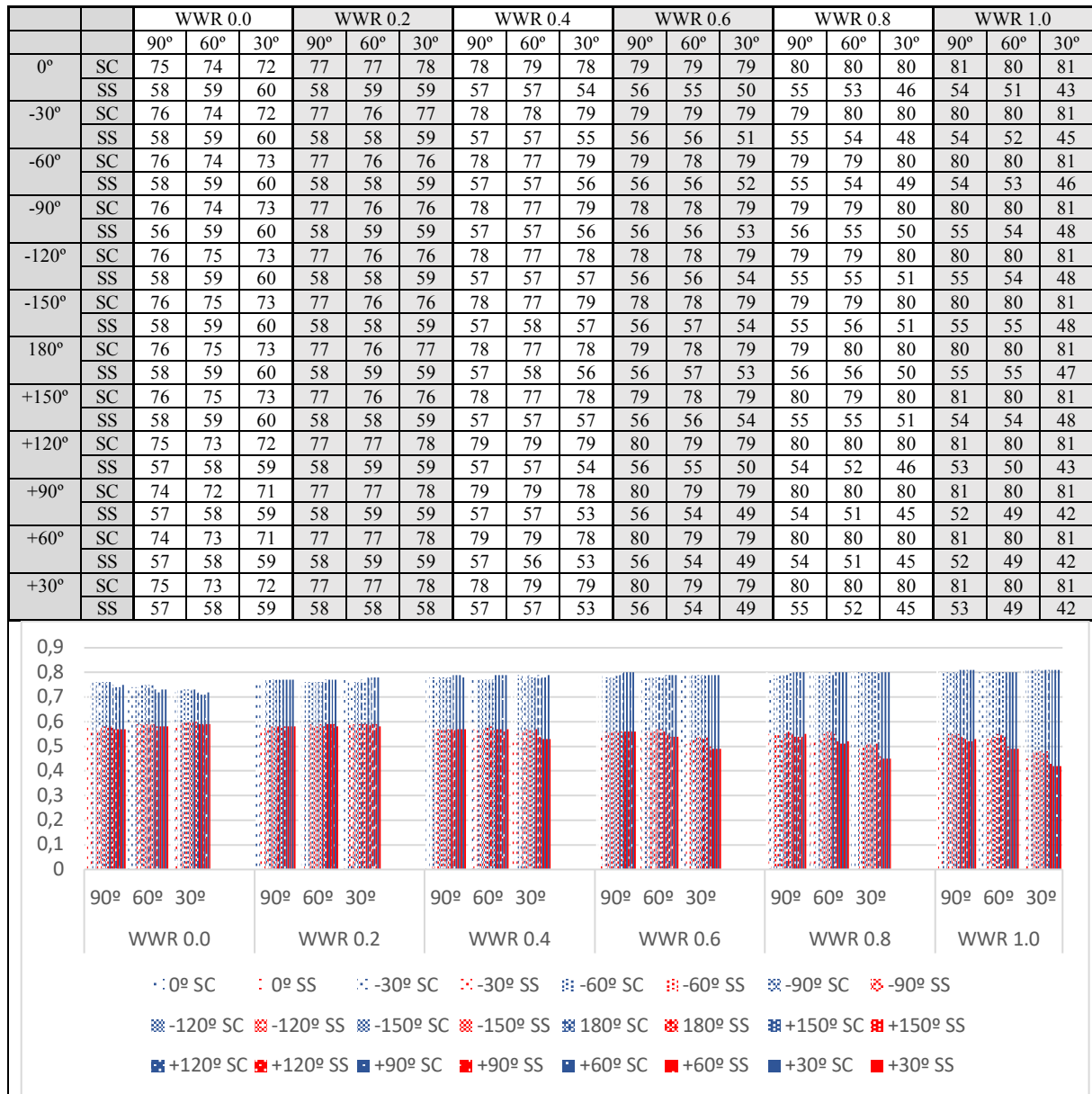
The developed matrix displays the geometry setups resulting from the combination of these three parameters in a one-story building with an absolute square proportion. A high setpoint of CT is applied.

		V1			V2			V3										
																		
N 	WWR 0.0			WWR 0.2			WWR 0.4			WWR 0.6			WWR 0.8			WWR 1.0		
	V1	V2	V3	V1	V2	V3	V1	V2	V3	V1	V2	V3	V1	V2	V3	V1	V2	V3
0°																		
-30°																		
-60°																		
-90°																		
-120°																		
-150°																		
180°																		
+150°																		
+120°																		
+90°																		
+60°																		
+30°																		

Tab. 8.25 Geometry setups – Matrix of 3 inclinations, 12 orientations and 6 WWRs - 20 m² BAPV on flat roof

The algorithm developed in Table 8.25 primarily aims to determine if changing quantitative parameters such as orientation, proportion, and WWR can alter the energy performance of a building across various combinations of these parameters. For example, it investigates whether different energy performances resulting from various WWRs remain consistent when the entire building rotates and the extent to which results differ in specific building proportions.

Table 8.26 displays the changes in SS and SC of the prototype when altering three parameters: orientation, inclination, and WWR in a one-story building with 20 m² of BAPV on a flat roof (high CT).



Tab. 8.26 SS and SC – Matrix of 3 inclinations, 12 orientations and 6 WWRs - 20 m² BAPV on flat roof - CT: high

The results in Table 8.26 demonstrate that the relationship between SS and the changing inclination of one face of the prototype is markedly different in variants with higher WWR values. On average, in all orientations of the considered prototype with fully opaque faces in all four walls (WWR 0.0), SS increases (from approximately 0.58 to 0.60) when one face changes. However, in variants with a high WWR, SS decreases (from approximately 0.55 to 0.50) when one face changes. Therefore, the benefit of converting the inclination of one face from vertical to inclinations of 60° and 30° can only increase SS in variants where the maximum WWR in all four faces is up to 0.2.

Similarly, the sensitivity of SS to the orientation of this prototype is much higher in higher WWR scenarios compared to lower WWR scenarios. For instance, in the prototype with a WWR of 0.2, changing the orientation of a face with an inclination of 60° delivers approximately constant SS of 0.58. In contrast, in the same prototype with a WWR of 0.8, SS exhibits a maximum and minimum of approximately 0.55 and 0.50, respectively.

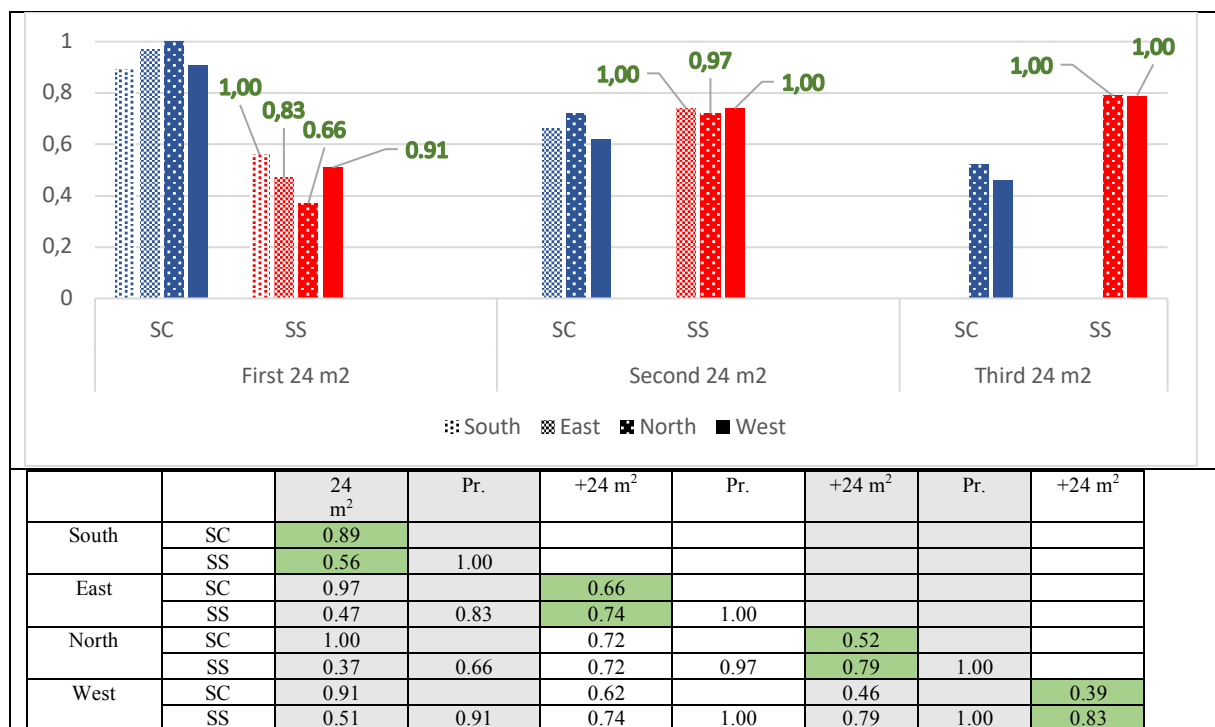
8.10 Priority of integration

In a building with various available components for PV integration, one critical decision is the priority of these components considering the offered SS. In this chapter, the main target of investigation is how the priority of components will change in a building that is going to be equipped with PVs multiple times, taking into account the new 'thermal performance' and 'coverage of demand' that should be considered in upcoming PV integrations. It's worth noting that this priority is a critical decision because, from an architectural standpoint, in the initial stages of design, illustrating the 'differences in energy efficiency' of a building through different 'areas of PV installation' is often overlooked. Therefore, it can be concluded that in cases where the priority of components for mounting PVs varies, different faces of the building should receive different quantities of PVs in different phases.

8.10.1 Flat roof

A very simple prototype representing a square building with a flat roof and constant WWR of 0.2 in all four faces has been considered. As each face of the building has 30 m², 6.0 m² is allocated to windows, and 24 m² will be available in each face for PV integration. Index of SS is selected to decide the priority of integration according to the highest offered quantity of SS by each component. After integration of the first 24 m² BAPV and applying the 'electricity generation' and changes of 'thermal performance,' the rest of the available components are compared regarding their offered 'self-sufficiency.' Following the procedure of priority of integration of the building by 24 m² BAPV illustrates deciding 'which component' should be integrated through 'which phase' of PV integration.

Table 8.27 shows different achievable SS and SC of the prototype through the installation of 24 m² BAPV on different components in different phases (high CT).



Tab. 8.27 Achievable SS and SC by installation of 24 m² BAPV on each component through 4 phases- One-storey building with flat roof – High CT

Figure 8.21 shows the priority of the four vertical walls of the defined prototype during three phases of 24 m² integration of BAPV regarding the offered SS (high CT).

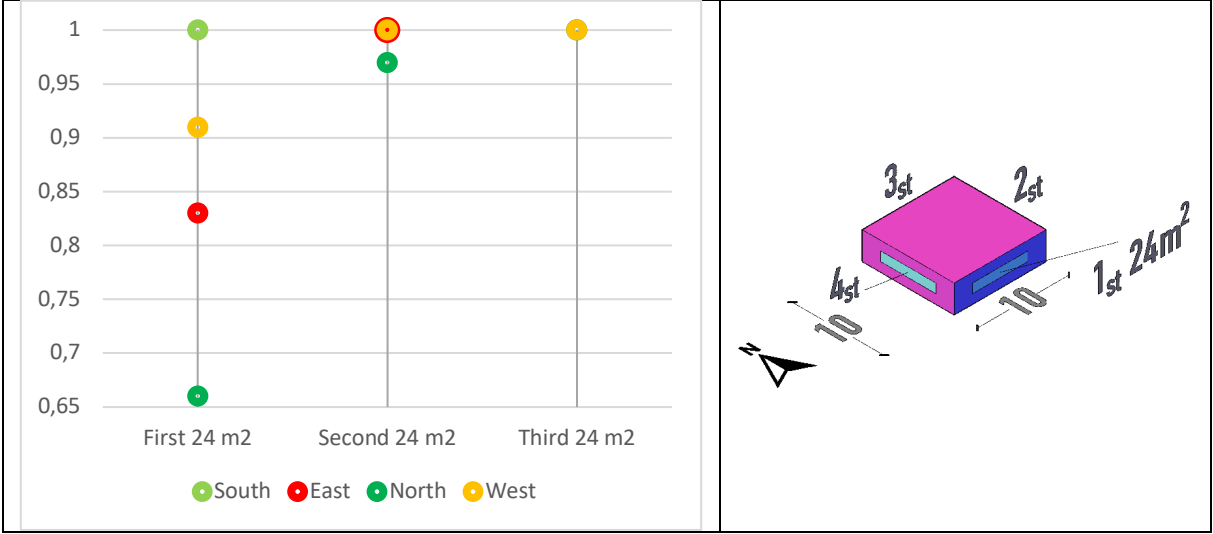


Fig. 8.21 Priority of integration based on offered SS - 24 m² BAPV (left) – Geometry and sequence of component’s priority (right) - One-storey building with flat roof - High CT

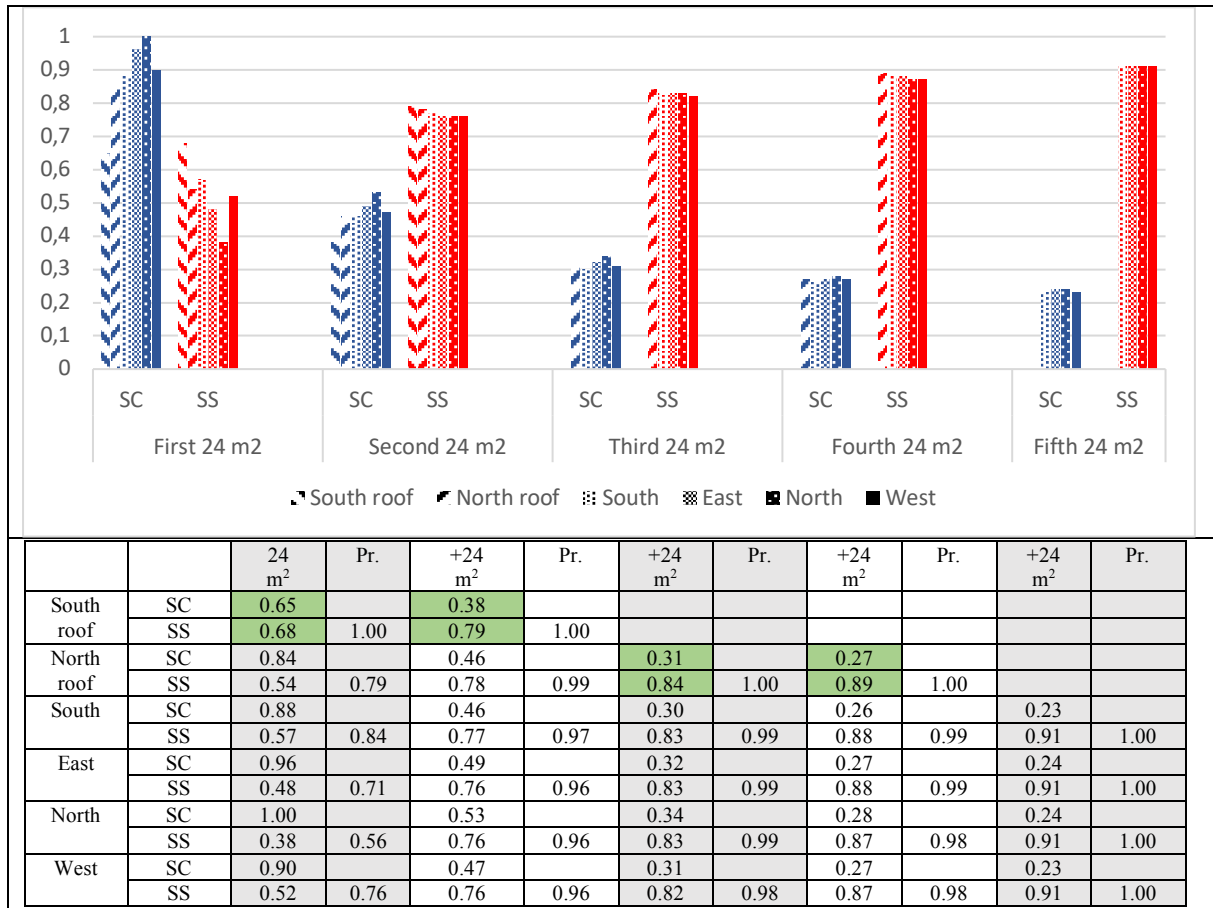
The results indicate that for the initial installation of 24 m² of BAPV on a building with four available components (vertical walls), the highest priority belongs to the south wall, offering an SS of 0.56, while the west, east, and north vertical walls follow in subsequent priority.

In the second installation of 24 m² of BAPV, the priority is determined by comparing the offered SS of the three components: east, north, and west vertical walls, as the south wall is already fully integrated with BAPV. In this context, the east and west walls offer the highest SS, with the north wall in the third position. So, when deciding between east and west integration, the choice becomes critical, especially if the entire 24 m² of BAPV is to be integrated in the first phase. Otherwise, in the second phase, both east and west walls offer nearly equal SS values of 0.74.

Considering a higher offered SC (Solar Conversion) by the east wall compared to the west wall (0.66 vs. 0.64), the east wall integration becomes preferable. In the third phase, both the north and west walls offer an equal SS of 0.79.

8.10.2 Sloping roof (Inc. 30° - south-north)

This prototype represents a square building equipped with a south-north symmetric sloping roof inclined at 30°. A constant WWR of 0.2 has been applied to all four faces. Since each face of the building is 30 m², 6.0 m² is allocated for windows, leaving 24 m² available for PV integration on each face. Similarly, each face of the roof offers 57 m² of available area for PV integration. Table 8.28 displays the different achievable SS and SC values for the prototype by installing 24 m² of BAPV on various components in different phases (high CT).



Tab. 8.28 Achievable SS and SC by installation of 24 m² BAPV on each component through 5 phases- One-storey building with sloping roof with inclination of 30° – High CT

Figure 8.22 shows the priority of the four vertical walls and the two faces of the sloping roof with a 30° inclination (south-north) in the defined prototype during five phases of 24 m² integration of BAPV regarding the offered SS (high CT).

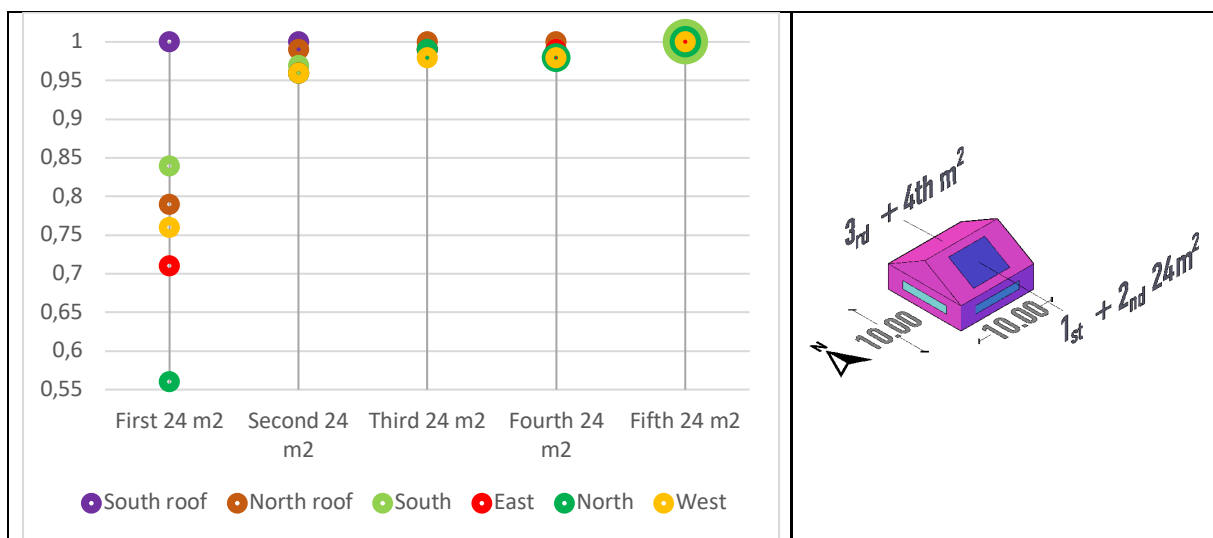


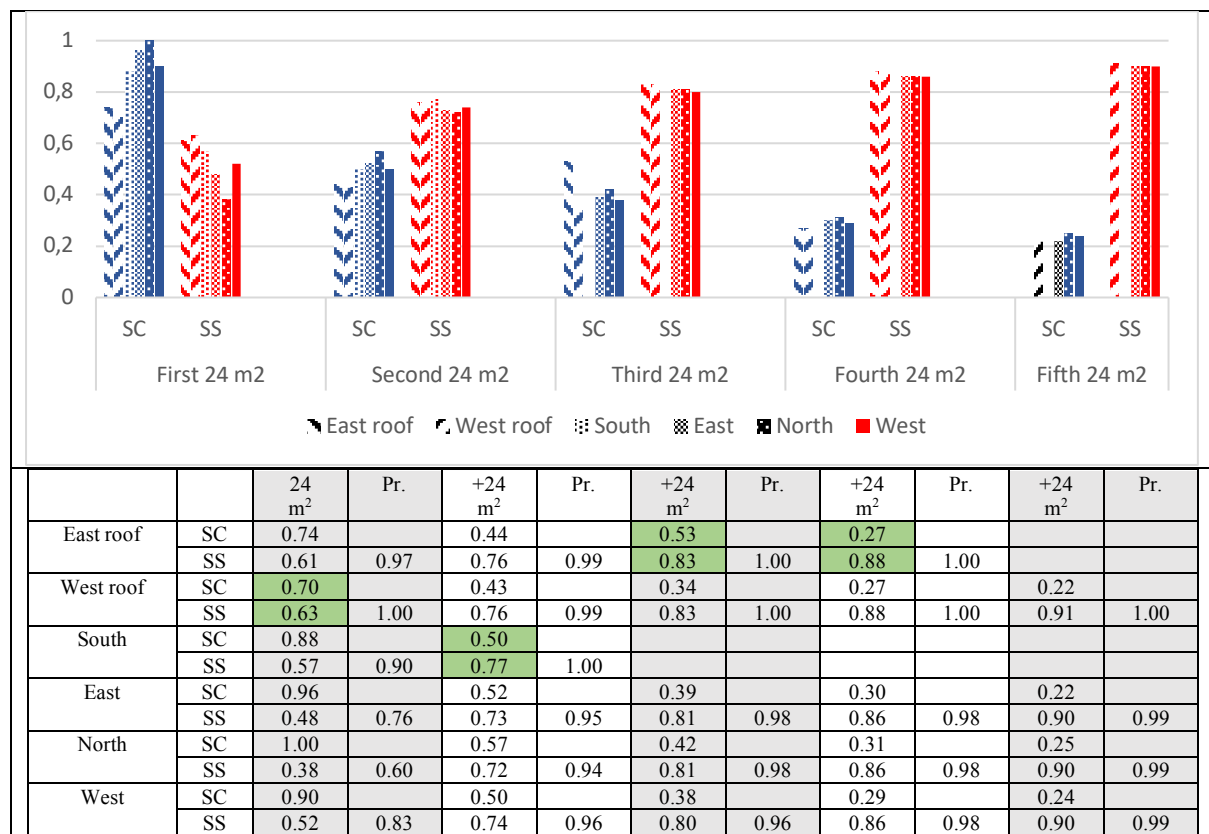
Fig. 8.22 Priority of integration based on offered SS - 24 m² BAPV (left) – Geometry and sequence of component's priority (right) – One-storey building with sloping roof (Inc.30° - south-north) - High CT

The graph presented in Figure 8.22 demonstrates that instead of merely moderating the differences in 'offered SS' among different components in various phases, their sequence of priority also changes. For instance, in the first integration, the south vertical wall and north roof are the second and third recommended components, respectively. However, in the second integration, the offered SS by the north roof exceeds that of the south vertical wall, even by 1%.

8.10.3 Sloping roof (Inc. 30° - east-west)

This prototype features a square building equipped with an east-west symmetric sloping roof inclined at 30°. A constant WWR of 0.2 has been applied to all four faces. Each wall of this prototype offers 24 m², and each face of the roof provides 57 m² of available area for PV integration.

Table 8.29 displays the different achievable SS and SC values for the prototype through the installation of 24 m² of BAPV on different components in different phases (high CT).



Tab. 8.29 Achievable SS and SC by installation of 24 m² BAPV on each component through 5 phases- One-storey building with sloping roof (Inc. 30° - east-west) – High CT

Figure 8.23 displays the priority of the four vertical walls and the two faces of the sloping roof, inclined at 30° (east-west), in the defined prototype during five phases of 24 m² integration of BAPV regarding the offered SS under high CT.

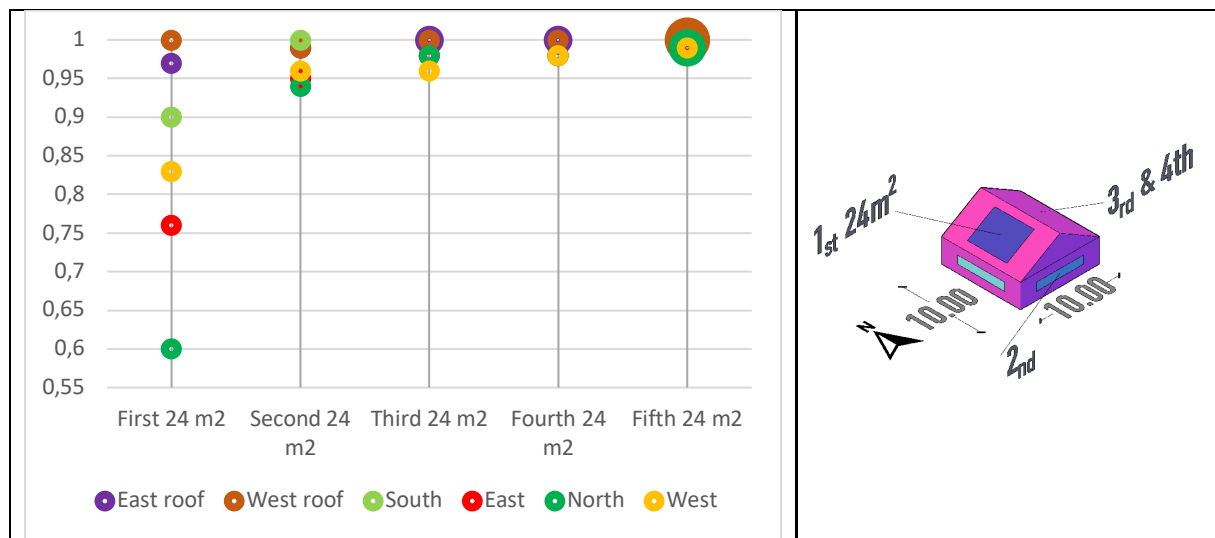


Fig. 8.23 Priority of integration based on offered SS - 24 m² BAPV (left) – Geometry and sequence of component's priority (right) – One-storey building with sloping roof (Inc.30° - east-west) - High CT

Figure 8.23 demonstrates that the sequence of priorities in this prototype changes during different phases of PV integration. For instance, in the first integration, the west roof takes absolute priority over the south wall, offering 6% more SS (0.63 compared to 0.57), while in the second integration, the south wall offers even 1% more SS (0.77 compared to 0.76).

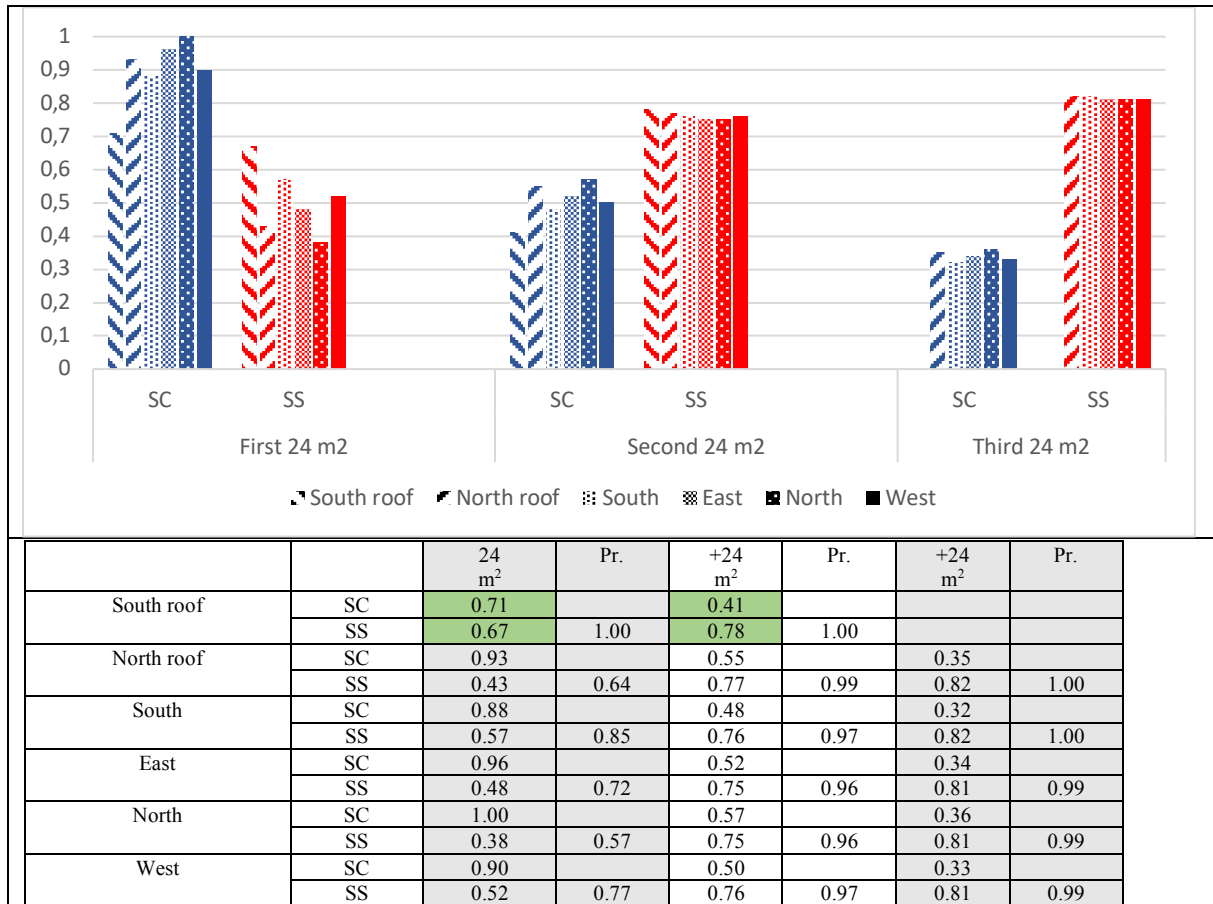
As another example, in the first integration, the west roof has a priority over the north wall with 14% more offered SS (0.52 compared to 0.38), but in the third integration, the north wall offers even 1% more SS (0.81 compared to 0.80).

In the fifth integration, the values for all remaining components are the same, with their offered SS indicating an approximate value of 0.90.

8.10.4 Sloping roof (Inc. 60° - south-north)

This prototype represents a square building equipped with a south-north symmetric sloping roof inclined at 60°. A constant WWR of 0.2 has been applied to all four faces. Each wall of this prototype offers 24 m², and each face of the roof provides 100 m² of available area for PV integration.

Table 8.30 displays the different achievable SS and SC values for the prototype through the installation of 24 m² of BAPV on different components in different phases (high CT).



Tab. 8.30 Achievable SS and SC by installation of 24 m² BAPV on each component through 3 phases- One-storey building with sloping roof (Inc. 60° - south-north) – High CT

Figure 8.24 displays the priority of the four vertical walls and the two faces of the sloping roof, inclined at 60° (south-north), in the defined prototype during five phases of 24 m² integration of BAPV regarding the offered SS under high CT.

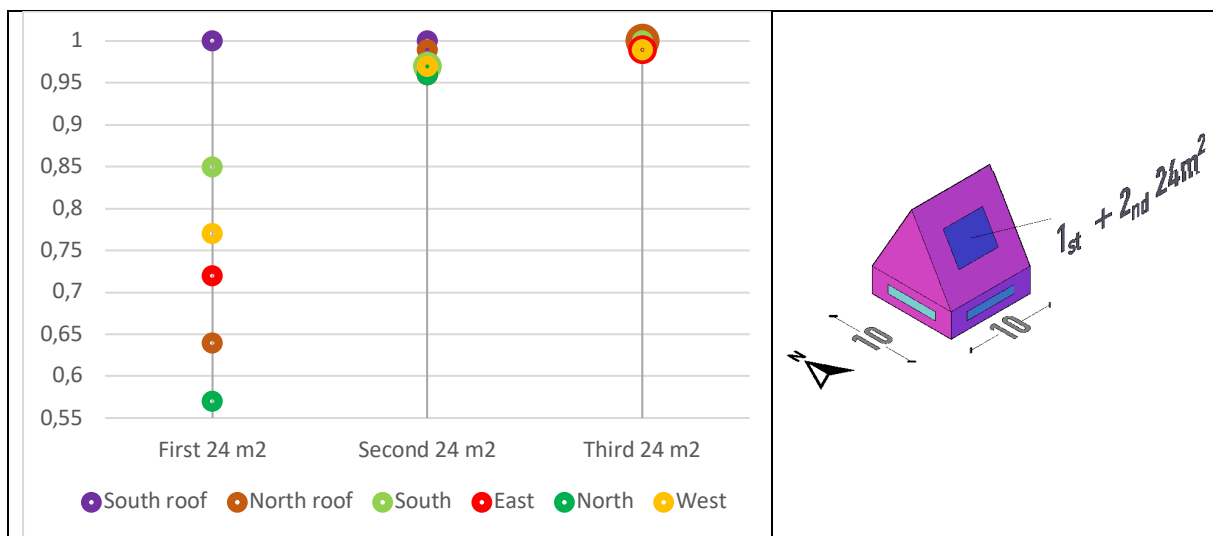


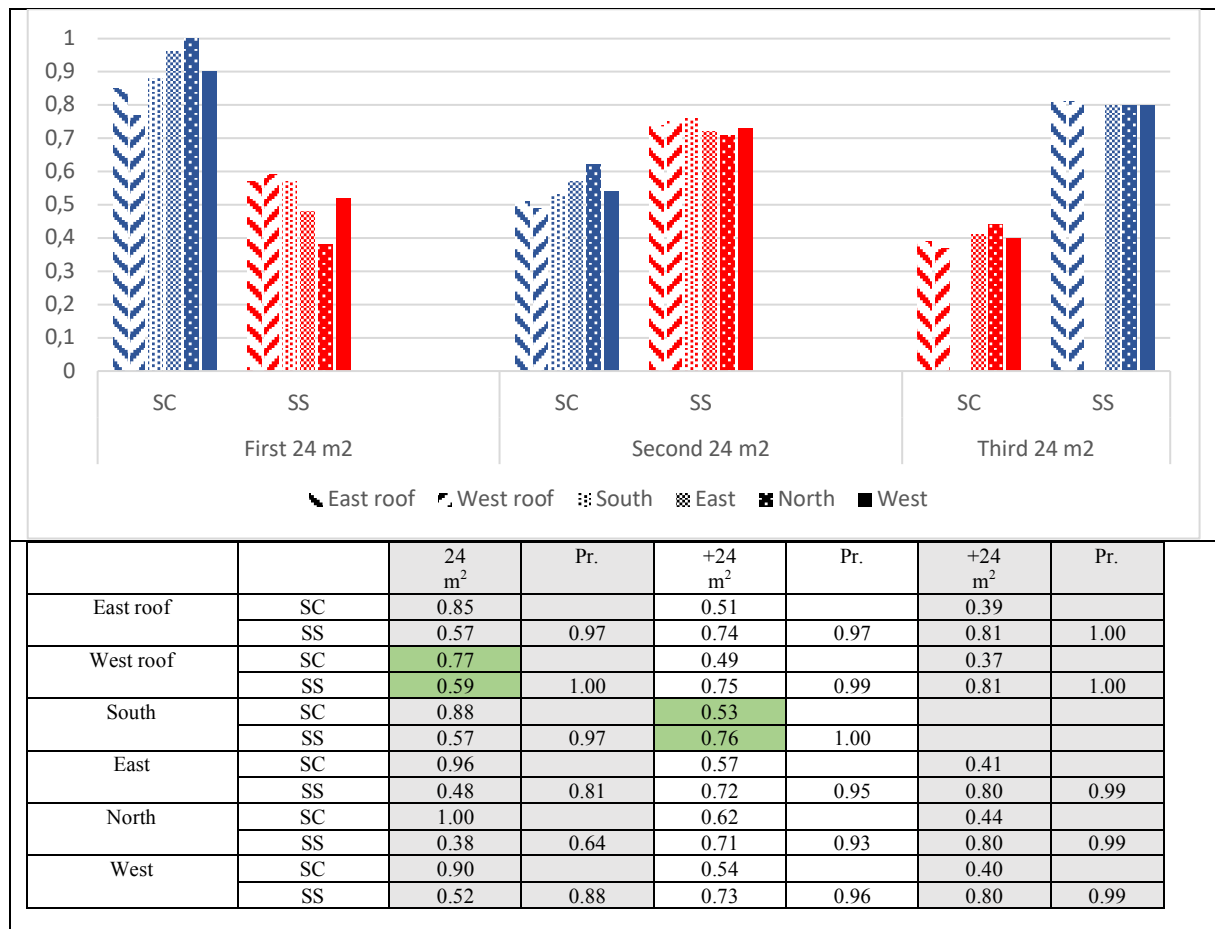
Fig. 8.24 Priority of integration based on offered SS - 24 m² BAPV (left) – Geometry and sequence of component's priority (right) – One-storey building with sloping roof (Inc.60° - south-north) - High CT

Figure 8.24 demonstrates that the sequence of priorities in this prototype significantly changes in the first two phases of PV integration. For instance, in the first integration, the north roof is in the fifth position due to its offered SS of 0.38, which falls behind the south roof, south wall, west roof, and east wall offering 0.67, 0.57, 0.52, and 0.48, respectively.

However, in the second integration, its priority rises to the second position as it offers an SS of 0.77, which is only 1% less than the offered SS of the south roof (0.78). In the third integration, the values for all remaining components are the same, with their offered SS indicating an equal amount of approximately 0.81.

8.10.5 Sloping roof (Inc. 60° - east-west)

This prototype represents a square building equipped with an east-west symmetric sloping roof inclined at 60°. A constant WWR of 0.2 has been applied to all four faces. Each wall of this prototype offers 24 m², and each face of the roof provides 100 m² of available area for PV integration. Table 8.31 displays the different achievable SS and SC values for the prototype through the installation of 24 m² of BAPV on different components in different phases (high CT).



Tab. 8.31 Achievable SS and SC by installation of 24 m² BAPV on each component through 3 phases- One-storey building with sloping roof (Inc. 60° - east-west) – High CT

Figure 8.25 displays the priority of the four vertical walls and the two faces of the sloping roof, inclined at 60° (east-west), in the defined prototype during five phases of 24 m² integration of BAPV regarding the offered SS under high CT.

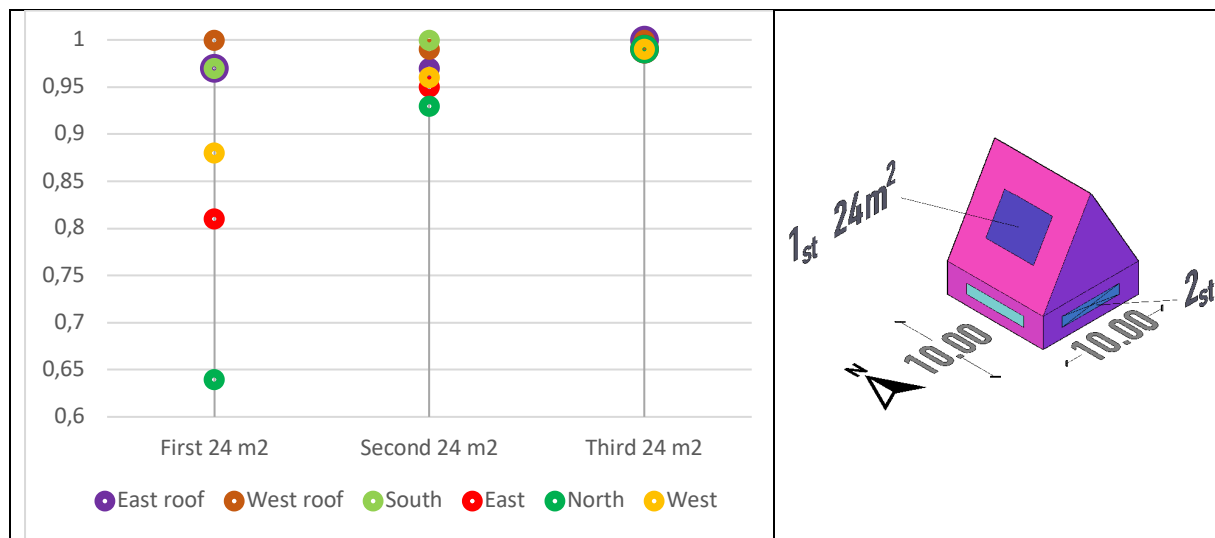


Fig. 8.25 Priority of integration based on offered SS - 24 m² BAPV (left) – Geometry and sequence of component's priority (right) – One-storey building with sloping roof (Inc.60° - east-west) - High CT

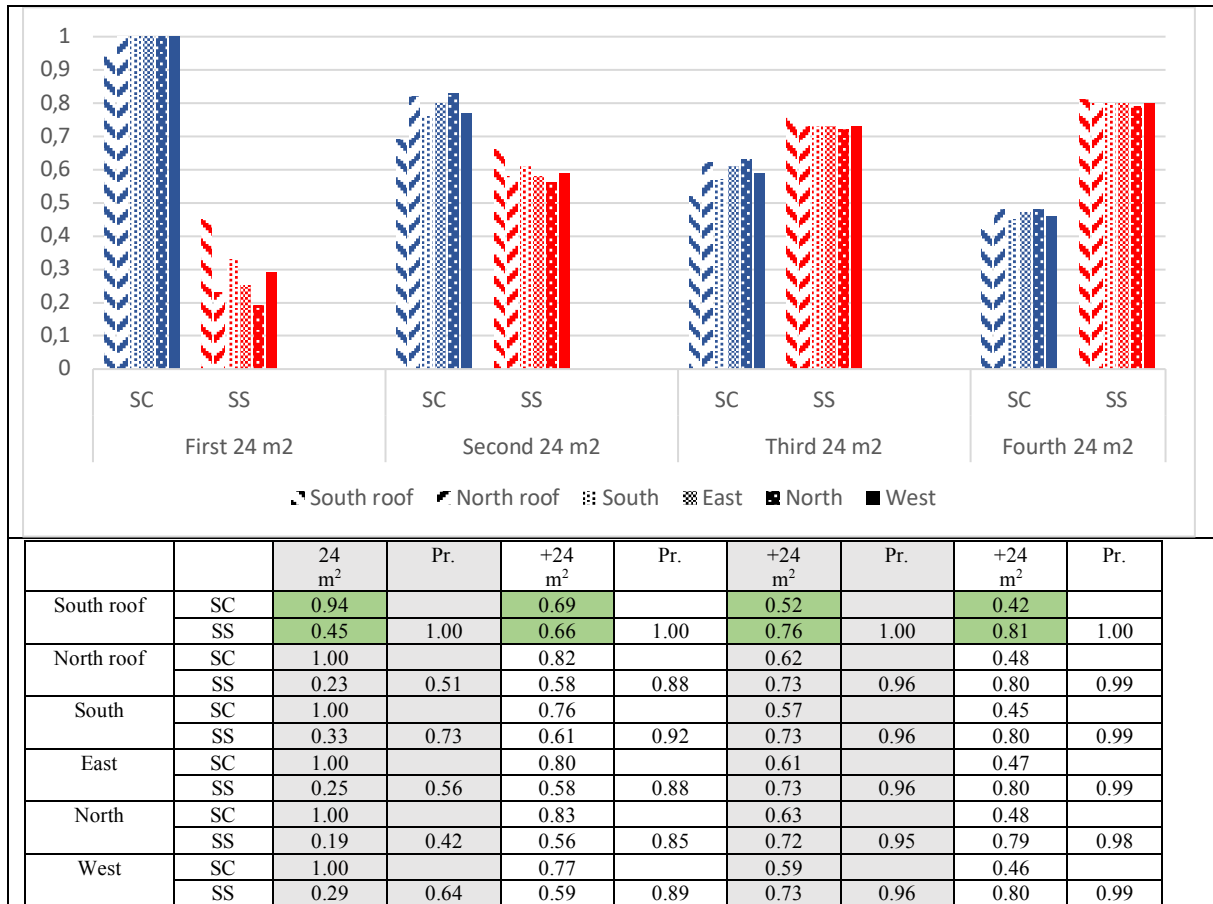
Figure 8.25 demonstrates that the sequence of priorities in this prototype changes, even in the case of the first position in the first two phases of PV integration. In the first integration, the west roof provides 0.02 more SS compared to the south wall (0.59 compared to 0.57). However, in the second integration, the offered SS of the west roof is even 1% less than the offered SS by the south roof (0.75 compared to 0.76).

So, considering SS as the critical index, the recommendation is that the first 24 m² integration should be on the west roof. Although the west roof still has an appropriate area for the second integration, the second integration should be on the south roof. In the third integration, the values for all remaining components are the same, with their offered SS indicating an equal amount of approximately 0.81.

8.10.6 Dachgeschoss (Inc. 60° - south-north)

This prototype presents a square building equipped with a south-north symmetric 'Dachgeschoss' with an inclination of 60°. The constant WWR of 0.2 in all four faces has been considered. Each wall of this prototype offers 24 m², and each face of the roof provides 100 m² available area for PV integration.

Table 8.32 shows different achievable SS and SC of the prototype through installation of 24 m² BAPV on different components in different phases (high CT).



Tab. 8.32 Achievable SS and SC by installation of 24 m² BAPV on each component through 4 phases - Two-storeys building with symmetric 'Dachgeschoss' (Inc. 60° - south-north) – High CT

Figure 8.26 displays the priority of the four vertical walls and the two faces of the symmetric 'Dachgeschoss' (attic) with an inclination of 60° (south-north) in the defined prototype during four phases of 24 m² integration of BAPV regarding the offered SS under high CT.

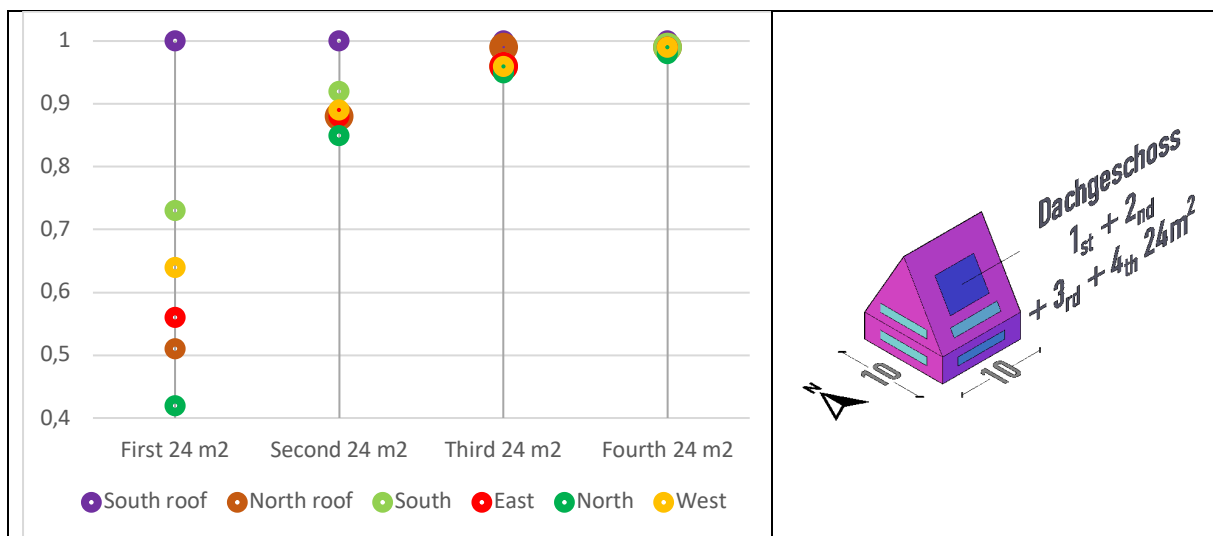


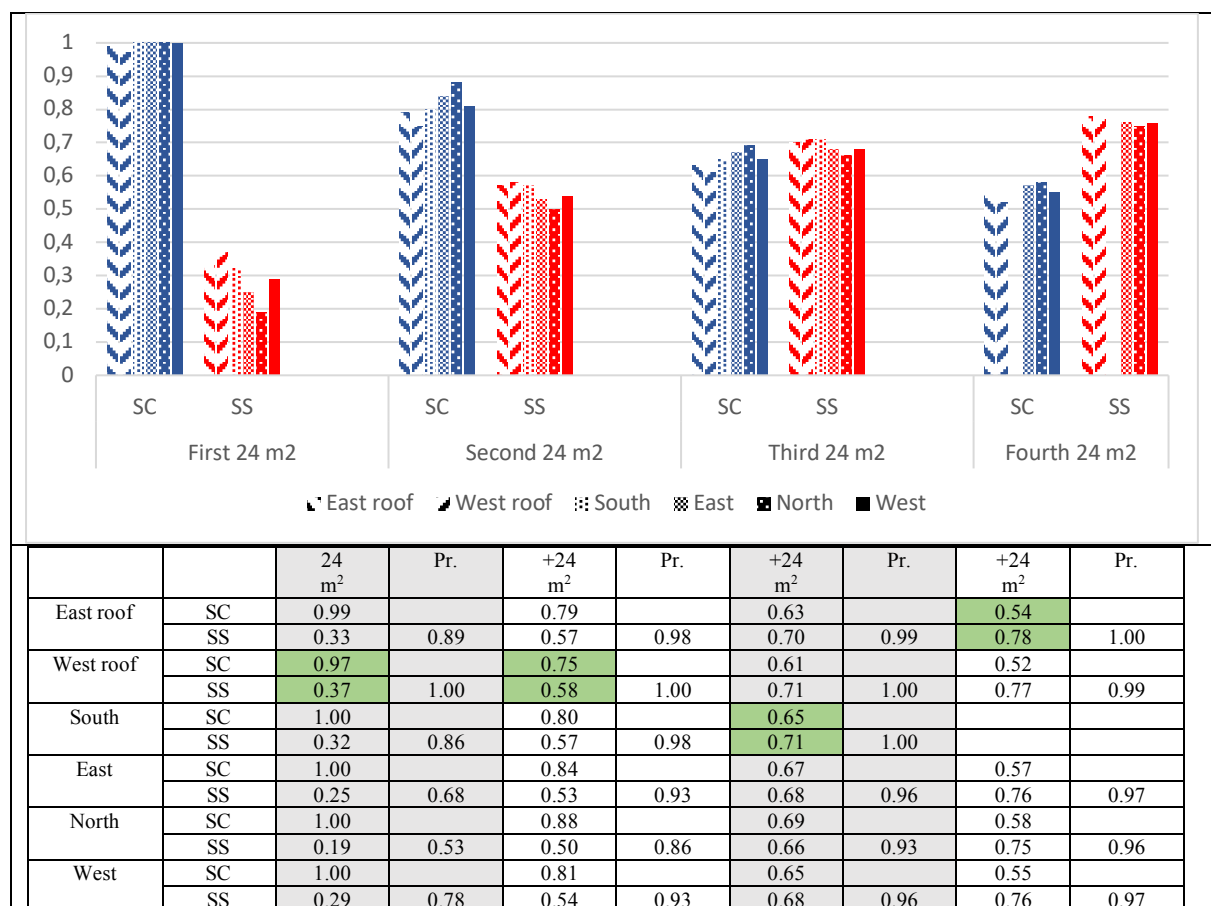
Fig. 8.26 Priority of integration based on offered SS - 24 m² BAPV (left) – Geometry and sequence of component's priority (right) – Two-storeys building with symmetric 'Dachgeschoss' (Inc.60° - south-north) - High CT

The results demonstrate that the sequence of priorities in this prototype mainly remains the same, which is entirely different from the same geometry of the 'non-Dachgeschoss' prototype presented in Figure 8.25. The primary reason for this difference is the distinct boundary conditions of the sloping roof in 'Dachgeschoss-mode' compared to a normal sloping roof. The inside temperature of the sloping roof is exactly at 'comfort temperature,' resulting in different SS when the building is equipped with the same roof geometry but without any living spaces beneath it.

Figure 8.26 indicates that the south roof offers the highest SS in the first, second, third, and fourth integrations compared to the other four components.

8.10.7 Dachgeschoss (Inc. 60° - east-west)

This prototype presents a square building equipped with an east-west symmetric 'Dachgeschoss' (attic) with an inclination of 60°. A constant WWR of 0.2 has been applied to all four faces. Each wall of this prototype offers 24 m², and each face of the roof provides 100 m² of available area for PV integration. Table 8.33 displays different achievable SS and SC values of the prototype through the installation of 24 m² BAPV on different components in different phases (high CT).



Tab. 8.33 Achievable SS and SC by installation of 24 m² BAPV on each component through 4 phases - Two-storeys building with symmetric 'Dachgeschoss' (Inc. 60° - east-west) – High CT

Figure 8.27 displays the priority of the four vertical walls and the two faces of the symmetric 'Dachgeschoss' (attic) with an inclination of 60° (east-west) in the defined prototype during four phases of 24 m² integration of BAPV regarding the offered SS under high CT.

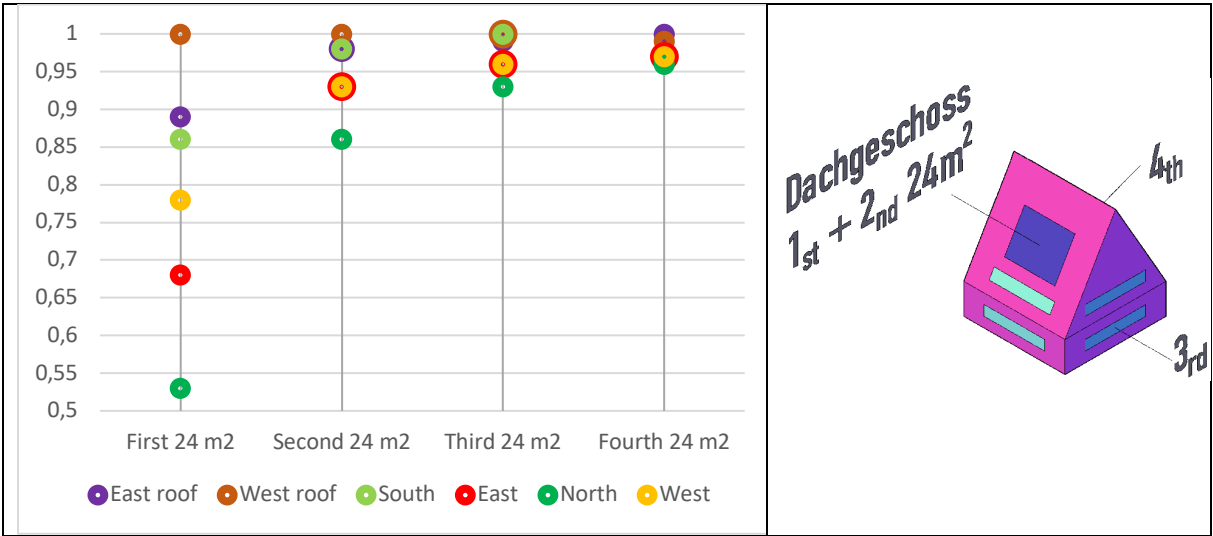


Fig. 8.27 Priority of integration based on offered SS - 24 m² BAPV (left) – Geometry and sequence of component's priority (right) – Two-storeys building with symmetric 'Dachgeschoss' (Inc.60° - south-north) - High CT

Figure 8.27 demonstrates that the sequence of priorities in this prototype varies. The results show that the west roof provides the highest SS in the first and second integration phases, whereas in the third and fourth integration phases, the south wall and east roof offer the highest SS.

When comparing this prototype to the one with an east-west sloping roof in Figure 8.26, which has the exact same geometry but a south-north orientation (with a constant priority of the south roof), it becomes evident that the integration priority in a two-storey building (with 'Dachgeschoss') depends on the main orientation of the building.

9. Conclusion

In relation to the four main hypotheses defined in this work, the calculated indexes, followed by relative comparisons, indicate the accuracy of the predicted targets as the scientific objectives of this work. Rather than limiting the application of this method and the derived results solely to these hypotheses, it is feasible to employ the same method and elementary parameters to establish new scientific objectives in parallel with the defined hypotheses. Therefore, further development of this work will either seek to achieve results within the framework of the defined hypotheses or use the same method and some of the calculated indexes to define higher-level scientific objectives.

The first hypothesis of this work involves integrating the basic phenomena of convection, conduction, emission, reflection, and transmission to calculate the energy balance of a building's component. Since the developed method primarily utilizes geometric parameters, thermal properties of materials, and the effects of these physical phenomena to calculate heat flow, the demonstrated results at the 'face level' are supposed to be applicable for deriving higher geometric levels of a house, namely the face and the entire building's geometry. Although, at this level, the focus is not on the energy efficiency of the building concerning its potential for electricity generation, the method has separately calculated the resulting thermal effects of covering a component with PVs through different installation configurations. Consequently, to establish an energy balance for a sample face at a desired level, the developed method can offer an optimized solution based on various principles.

1. Highlighting the relevance of thermal properties of a building's components to geometrical setups offers specific values of thermal resistance and heat flows. The initial integrated equations primarily incorporate both material properties and geometric configurations. Consequently, the relative comparisons not only indicate the resulting heat flow from each set of material properties within a particular geometric setup but also allow for the discussion of quantitative differences in the resulting heat flow from a specific 'material property' across different geometric setups.
2. Discussing the different quantities of resulting heat flows through various combinations of integrated components in a face is a central aspect of this work. Instead of limiting the analysis to two initial components, opaque and transparent, representative of walls and windows, the possibility of combining them with PVs to create BIPV, BAPV, and PV glazing has also been defined. Integrating any preferred component into the developed method is feasible, provided that the thermal properties and electrical efficiency of these new components (resulting in different thermal dissipations) are available. In this regard, any defined component, whether with or without PV, that can be used in future product development can be integrated into the procedure of developing the work undertaken.
3. Indicating the quantities of reflection, emission, and convection on the outside surface of a component is also possible with the integrated method by 'dividing diffraction of irradiation.' In this regard, considering any material sample with or without PV coverage through different setups reveals different proportions of reflection, emission, and convection. For example, two derived graphs in Figures 5.62 and 5.63 initially illustrate different proportions of outside convection and emission when an opaque component is covered by PV as BIPV, with the component having different orientations and inclinations. These two graphs are intentionally included in the final section of the simulation to demonstrate that varying geometrical setups, through different

orientations and inclinations, result in different amounts of final heat flows, primarily stemming from different proportions of outside convection and emission. Regarding the defined hypotheses of this work, further discussions of these graphs are omitted but could be valuable if the results of irradiation diffraction can be utilized in future research related to 'insulation types.' For example, it could be economically beneficial if differences in types of insulation materials can also be indicated in different geometrical setups. In cases where heat flow is primarily a result of emission, certain materials that obstruct the direct connection of the outer surface of the component may be more economically advantageous than larger quantities of insulating materials with higher U-values. For instance, the integration of simple foils or reflective coating materials (in combination with insulating materials) may be different recommendations for different geometrical setups. The elementary results of this work in this regard can be seen as an 'open question,' and further developments can specify the correlation between different proportions of outside convection and emission across different geometrical setups with various material combinations.

The core of the developed method in this work lies within the framework of the first defined hypothesis, which is a simplified logical definition aimed at indicating values for heat flow considering different boundary conditions related to the direction of heat flow and momentary temperature differences between the 'inside ambient temperature' and the 'outside ambient temperature' (as shown in Table 4.5). The use of the suggested definition of the 'value of heat flow,' rather than defining 'heating demand' and 'cooling demand,' specifies proportions of heat flow as 'heating auxiliary' and 'cooling auxiliary.' This means that dividing certain quantities of 'heat transfer' into 'heating demand + heating auxiliary' or 'cooling demand + cooling auxiliary' results in lower quantities of 'demands' when the consideration of 'auxiliaries' is taken into account. The accuracy of this decision can also be justified by the second calibration of this work, as the integration of the suggested 'definition of values of heat flow' in the tested building indicates an acceptable deviation of -5.9% in the 'calculated electricity demand,' which is directly related to the suggested method employed. In this regard, the monthly energy performance of windows in all four orientations of the assumed building (as shown in Figure 6.7) demonstrates that more than twice the calculated heat flow is subtracted and allocated to heating auxiliary. A similar subtraction has been applied to the four oriented walls (as shown in Figure 6.6), indicating that a certain quantity of calculated heat flow is considered as 'heating auxiliary' and does not increase the 'heating demand.' As a result, without subtracting these significant quantities of 'heat flow,' the final calculated 'electricity demand,' which is directly related to the energy demand of the building, would be much higher than the calculated amount of 5459 kWh/year (as shown in Table 6.16), and the deviation of the integrated method would not fall within an acceptable range.

Calibration of the initial calculation of heat flow in this step has been carried out using an east-oriented vertical opaque component, followed by a comparison of the results with those obtained from simulation software, specifically 'DesignBuilder.' Acceptable deviations of -0.537 °C in a temperature fluctuation of 6.33 °C during winter and -1.987 °C in a temperature fluctuation of 34.83 °C during summer justify the precise application of integrated equations under steady-state conditions. Referring to Figure 5.23 and Figure 5.24, which indicate the deviation of the calculated outside surface temperature on a winter day and a summer day, respectively, demonstrates that, when employing steady-state conditions and ignoring the 'storage capacities' of materials in the building's skin, fluctuations in outside surface temperature occur immediately after changes in weather data without any time lag. In this regard, two points should be considered:

1. In demonstrating the accuracy of the final derived heat flow compared to the results of the 'simulation software of 'DesignBuilder,' fluctuations over the entire 24-hour day should be taken into account. Therefore, the absolute mathematical values of temperatures in steady-state conditions are moderated, taking into consideration the higher recorded temperatures during mid-day and the lower recorded temperatures during the beginning and end of the day. The moderated absolute mathematical value indicates acceptable ranges of recorded values under steady-state conditions. These conditions employ much simpler equations compared to unsteady-state conditions, which, due to the dynamic consideration of parameters, require dealing with much more complex equations and procedures.

2. The developed method also has the potential to be used under unsteady-state conditions for dynamic heat transfer calculations. In this regard, thermal diffusivity of materials, taking into consideration 'thermal conductivity,' 'specific heat capacity,' and 'density' of the material, will be employed. The fluctuation of recorded outside temperatures will demonstrate a more real-time lag compared to intervals of outside temperature changes.

The second hypothesis of this work involves estimating the energy demand of a building by considering the interaction of all the faces that shape the building's envelope. In essence, it investigates the scaling up of calculated 'heating demand' and 'cooling demand' from the faces of the building to the entire geometry of the building through this hypothesis. Considering the final objective of this work, which is providing an indication of energy efficiency regarding the effectiveness of each 'geometrical parameter,' this level provides an opportunity to employ certain virtual geometrical properties, such as geometrical proportion, that do not have direct equivalent parameters. At a lower scale, a similar example of the possibilities for discussing virtual geometrical properties is the Window-to-Wall Ratio (WWR), as it considers components of a face when the two main components are opaque (wall) and transparent (window). At this level of geometrical discussion, instead of WWR as the 'window-to-wall ratio,' any preferred ratio of integrated components with or without PVs and the resulting heat flow can be defined and discussed. For instance, 'BIPV to wall ratio,' 'BAPV to wall ratio,' and combined variants like 'BIPV, wall, and window ratio' or 'BAPV, wall, and window ratio' are possible to be discussed using the current integrated method of this work. Regarding the initial geometrical discussions in this work, an exclusive discussion of suggested ratios can be pursued in upcoming developments.

To optimize favorable geometrical configurations regarding the delivered energy performance, initial angular differences are applied to define a three-dimensional matrix (as shown in Figure 4.17). Through this developed matrix, the energy performance of each component in various geometrical setups, in intervals of 30° , can be calculated and compared. The angular difference of 30° is applied to both orientation and inclination rotational variants, providing 37 different positions of the component (with the roof having an inclination and orientation of 0°). While these 37 different geometrical setups demand a significant amount of simulation time, for more precise geometrical optimization, it is recommended to consider angular differences of 15° or even 5° . This recommendation is primarily for a more accurate consideration of the effects of different wind directions (as shown in Figure 4.11) and the proportions of direct, diffuse, and reflected radiances (as shown in Figure 4.5) reaching the surface of a face with a specific geometrical setup. Between these two options, wind speed averages and their directions exhibit non-uniform changes and may also arise from weather

data with higher resolution to account for different quantities and directions in closer intervals, such as by the day, hour, or even minutes.

The third hypothesis of this work indicates that for a precise estimation of indicators of self-sufficiency and self-consumption, changes in the electrical and thermal performance of PVs in different configurations should also be taken into account. For this reason, in the calculation of Self-Sufficiency and Self-Consumption as two critical indexes in this work, the initial calculation principle explained in Figure 6.1, which is based on the proportion of 'uncovered demand,' 'unused and used electricity generation from on-site PV,' 'total electricity generation by on-site PV,' and 'total energy demand,' is employed. Additionally, further considerations beyond the explained principle have also been taken into account for more precise results:

1. Changes in the thermal performance of opaque components holding PVs in two setups, BIPV and BAPV, and the transparent component holding PVs in the PV glazing setup, are calculated. It should be noted that each PV panel has its own unique datasheet provided by its manufacturer, explaining the related electrical and thermal characteristics of the photovoltaic panel (as shown in Table 5.33). Consequently, applying the same rule for all types of products may not be feasible. Similarly, the material properties of constructional layers in BIPV and BAPV (as shown in Table 4.10) are exclusively related to a certain product, and as a result, the thermal resistance of each PV assembly will be calculated differently. The calculated example setup in the 'simulation' part of this work proves that there are significant differences in thermal performance when a component in the same geometrical setup holds PVs through the configuration of BIPV compared to BAPV (as shown in Figure 5.60). The calculated graphs demonstrate that the two configurations of BIPV and BAPV not only differ in the resulting quantities of 'heating demand,' but the resulting 'auxiliaries' could also be different. Regarding this presented setup (as shown in Figure 5.60), the calculated 'cooling auxiliary' in BAPV remains zero, while BIPV delivers considerable amounts of cooling auxiliary in mid-summer.

2. Changes in thermal performance in all five defined components—opaque, transparent, BIPV, BAPV, and PV glazing—are remarkably dependent on the 'inside air temperature,' which is the main parameter considered in the boundary condition applied from the inside of the component. This difference is calculated and presented for all five components in this work. For example, Figure 5.16 and Figure 5.39 demonstrate that the cumulative amounts of heating demand, heating auxiliary, cooling demand, and cooling auxiliary are entirely different at different defined inside temperatures for the opaque and transparent components, respectively (in this work, 'high' and 'low' inside temperatures). The same differences also apply to the combined components of BIPV, BAPV, and PV glazing, as these are combinations of opaque or transparent components with PVs. For this reason, in all calculations undertaken, the boundary conditions are explained using the term 'inside comfort temperature' as well.

3. Similarly, changes in 'electricity generation' of BIPV compared to BAPV, resulting from different material setups of constructional layers, are also calculated. It demonstrates a considerable difference that will be more remarkable in months with a higher average of irradiation. For example, the related monthly electricity generation (as shown in Figure 5.61) demonstrates that with the same integrated PV panels and in the same geometrical setup, the BAPV configuration generates a greater quantity of

electricity compared to BIPV. This difference could be justified by the lower operating temperature of BAPV resulting from backside ventilation.

4. In a specific setup of BAPV with certain amounts of backside air, different 'gap heat transfer coefficients' should also be applied, considering the different operating temperatures of PV modules and wall temperatures at different inclinations (as shown in Table 5.41) [55]. For the construction of BAPV considered in this work, an assumption of 12.00 to 12.70 W/m²K is applied to inclinations from 0° to 90°, respectively. In the case of any other construction layout of BAPV, these 'gap heat transfer coefficient changes' must be individually calculated.

Calibration of self-sufficiency and self-consumption for the selected building (as shown in Figure 6.2) demonstrates an acceptable deviation of -5.9% in 'calculated electricity demand' and +7.9% in 'calculated electricity generation.' Indeed, applying the exact same boundary conditions of the tested building to the 'calculations in this work' could result in more accurate outcomes if the exact weather data and inside comfort temperature were applied to the calculations.

The fourth hypothesis of this work indicates estimating the indicator of energy efficiency of a building regarding the balance of energy performance of all faces shaping the envelope of the building.' For this purpose, the effects of geometry have been initially investigated in Chapter 7 of this work. In this chapter, a simple geometry with the same amount of TFA, the total amount of PVs, and the configuration of PV installation (BAPV) has been considered and compared in 13 different variants resulting from geometrical modifications. Thus, the defined constraint of the fourth hypothesis, which is 'the same quantities of integrated PVs and TFA' or 'the same ratio of integrated PVs to TFA,' is applied to the developed geometries. The range of changes in two indexes, self-sufficiency and self-consumption, in these 13 geometrical setups demonstrates a 19% change in self-sufficiency and a 15% change in self-consumption, respectively. This initially proves that both indexes are influenced by altering geometrical parameters (as shown in Figure 7.1). Parts of the investigation also demonstrate that even a simple modification of the quantities of WWR in the exact same geometrical setup changes both the SS and SC indexes, which somehow depend on the orientation of the face whose WWR changes (as shown in Figure 7.3).

It should be noted that considering these 13 geometrical variants, even in variants with almost the same resulted SS and SC, referring to the 'energy demands and electricity generation' tables (from Table 7.1 to Table 7.14), quantities of heating demand, cooling demand, generated electricity, and as a result, electricity for heating and electricity for cooling are different. So, a deeper parametric comparison between the energy performance of different variants can be done regarding segments of correlation between the two indexes of self-sufficiency and self-consumption. That means, for instance, self-sufficiency can remain at the same level as long as both 'total energy demand' and 'electricity generation of on-site PV' change by a certain amount. Discussing the benefits of these variants would require employing economic parameters such as costs, payback period, Feed-in tariff, etc., which are not within the framework of the defined variables and integrated parameters. Therefore, further development of this work could alternatively be done by incorporating economic parameters in parallel with SS and SC.

After the elementary demonstration of the effects of geometry on the final energy performance of the building, Chapter 8 of this work aims to investigate two primary aspects. Firstly, it explores whether all geometrical modifications are effective in altering the final energy performance. Secondly, it estimates the quantities of these changes. Proportion,

orientation, inclination, and WWR are elementary geometrical parameters that primarily discuss changes in the 'indicative of energy performance' when PV is integrated as BIPV, BAPV, or PV glazing. Additionally, the effects of changing one geometrical parameter through different setups of other parameters have been calculated and compared. For instance, different inclinations of the wall with varying amounts of WWR or different orientations of the building when BAPV is on a flat roof, sloping roof, or a vertical wall. In this chapter, a special application of 'Dachgeschoss,' which represents a sloping roof with a steep inclination of 60°, has been considered, and its specific energy performance has been compared with other roof types.

A deeper consideration of geometrical parameters in Chapter 8 demonstrates that it is possible to quantitatively discuss new types of complex geometrical parameters that have been rarely introduced and considered thus far. A short list of these considered parameters and the importance of the related discussion is introduced:

1. 'Roof type' in steep sloping roofs (in this work, an inclination of 60°) is investigated through two different variants: when the sloping roof is applied above a flat roof (extra roof) or when it is used as diagonal walls in the last storey (Dachgeschoss). In the defined geometrical prototype (table 8.16), switching from an 'extra roof' to 'Dachgeschoss' results in a 2% to 4% drop in self-sufficiency, depending on the overall orientation of the building. However, it should be noted that in this case, the 'amount of integrated material' for constructing these two variants is different, and 'Dachgeschoss' requires less material. As a result, while the index of 'quantities of integrated materials' is not within the parameters of this work, in the process of further development, these 'economic parameters' may be additionally taken into account.

2. 'Building expansion' is a critical decision that can be clearly determined during the elementary stages of architectural design. This means that compacting a certain number of dwellings within the framework of one building can reduce the final total energy demand of the complex compared to the sum of the energy demand of individual buildings. Different types of expansion, considering possibilities of PV integration and the resulting energy demand, are initially defined and compared. For example, vertical and horizontal expansion of a 'one-storey' building with the same ratio of integrated PVs into TFA are considered. The results demonstrate that not only are the quantities of 'energy efficiency' different, but also the percentage of 'changing energy efficiency' through vertical and horizontal expansion of the building varies (Figure 8.15 and Figure 8.16). It should be noted that a more precise investigation of 'building expansion' should also take into consideration the 'availability of area' that a certain geometry can offer for further expansion. For example, in vertical expansion of a one-storey building (Table 8.17), adding more PV installations to the roof may not be feasible, while horizontal expansion (Table 8.18) can still offer available roof area for future expansions. Therefore, further development of this introduced geometrical parameter can be pursued regarding the entire area offered by the geometry for PV integration, which can be explored in upcoming research.

3. 'Distribution of PV' is also an initial decision that primarily involves allocating the entire PV system to one side of the roof or dividing it into two equal portions on each side of the roof. At the same time, different inclinations of a symmetric sloping roof through different orientations of the building should also be considered. The results demonstrate that a south orientation doesn't always have a constant priority for PV integration in all inclinations, and the outcomes vary when PVs are allocated entirely to one side of the sloping roof compared to splitting them between both sides. Similarly, dividing the total amount of PV between two sides of the sloping roof can be advantageous for achieving higher 'self-sufficiency' in certain

orientations, both in symmetric sloping roofs with inclinations of 30° and 60° (Table 8.21 and Table 8.22).

4. 'Proportion + Orientation + WWR' and 'Inclination + Orientation + WWR' are two examples of changes in the energy performance of a building when more than two geometrical parameters are altered. In this regard, Table 8.24 and Table 8.26 present changes in SS and SC, considering a geometrical matrix (Table 8.23 and Table 8.25) involving three geometrical parameter changes. For further development in this area, any favorable combination of geometrical parameters can also be applied to determine the effectiveness of each parameter, as long as other parameters are also adjusted. The orientation of the building in both of these two combinations is always a critical decision in the initial stages of architectural planning. Considering the quantities of 'energy efficiency changes' in each orientation can assist decision-makers in the early planning phases, determining whether achieving higher 'energy efficiency' is worthwhile or if a specific favorable building orientation (for various reasons) should be considered even if there is only a modest drop in energy efficiency. Thus, discussions between the planning team and users can be framed within the context of the 'energy efficiency index,' using estimated SS and SC values to guide decision-making in each geometrical setup.

5. 'Priority of integration,' another index introduced in this work, addresses the critical question of how to calculate the priority of PV integration when various components are available for installation, considering 'indicators of energy efficiency.' Furthermore, it explores whether this priority remains consistent. The innovative insight from this discussion highlights that as PVs are gradually added, the priorities of components undergo significant changes because initial PV integration impacts both the 'thermal performance' and 'electricity generation' of the building. In other words, it can be firmly concluded that the initial quantities of PVs should be allocated to the component that offers the highest SS. However, subsequent quantities of PVs may be allocated to other components, even if the first component still has available space for PV integration.

The concept of 'Priority of integration' has been explored across various building geometries, including those with flat roofs, sloping roofs with different inclinations, and different roof types. The results strongly advocate for the practical consideration of this index, as they unequivocally indicate that the priority of components largely shifts during subsequent phases of PV integration. Therefore, it would be advantageous to incorporate the possibility of integrating additional quantities of PVs in the early stages of building design. In some cases, due to financial constraints, a building may undergo further PV integration after a few years of operation. It's worth noting that for further development in this regard, smaller PV module sizes, such as '1 m² PV modules,' can be applied to define more precise intervals for determining when the remaining PV should be allocated to components that may offer higher 'self-sufficiency.'

Finally, it should be noted that the developed tool can be initially used to estimate the 'energy efficiency' of buildings by indicating the defined indexes. Since the entire set of results is based on 'steady heat transfer' to calculate temperatures and heating flow, it's also possible to integrate 'unsteady heat transfer' equations, which would provide information on the 'time lags' of heat flow due to the entropy of materials resulting from their mass properties. The primary application of this work can serve as an integrable and viable method for predicting changes in the efficiency of buildings based on geometric alterations. Further enhancements can be achieved through the integration of additional parameters, such as weather data, material properties, and the thermal and power characteristics of integrated PVs, leading to a more comprehensive and detailed parametric analysis for future developments.

10. Reference

- [01] R. Luthander, J. Widén, D. Nilsson, J. Palm, 2015, Photovoltaic self-consumption in buildings: A review, *Applied Energy* 142 (2015) 80–94
- [02] V. Bertsch, J. Geldermann, T. Lühn, 2017, What drives the profitability of household PV investments, self-consumption and self-sufficiency?, MPRA, Munich Personal RePEc Archive, <https://mpra.ub.uni-muenchen.de/78644/>
- [03] R. Luthander, B. Stridh, J. Widén, 2015, PV system layout for optimized self-consumption, 29th European Photovoltaic Solar Energy Conference and Exhibition
- [04] D. Bigot, F. Miranville, I. Ingar, A. Fekra, S. Guichart, H. Boyer, 2012, Thermal performance of photovoltaic systems integrated in buildings, *Solar collectors and panels*, Intech, pp. 405-411
- [05] E. Skoplaki, J.A. Palyvos, 2009, Operating temperature of photovoltaic modules: A survey of pertinent correlations, *Renewable Energy* 34 (2009) 23-29
- [06] P. Sánchez-Palencia, N. Martín-Chivelet, F. Chenlo, 2019, Modeling temperature and thermal transmittance of building integrated photovoltaic modules, *Solar Energy* 184 (2019) 153-161
- [07] T. Lang, D. Ammann, B. Girod, 2016, Profitability in absence of subsidies: A techno-economic analysis of rooftop photovoltaic self-consumption in residential and commercial buildings, *Renewable Energy* 87 (2016) 77e87
- [08] M. Hartner, A. Ortner, A. Hiesl, R. Haas, East to west – The optimal tilt angle and orientation of photovoltaic panels from an electricity system perspective, *Applied Energy* 160 (2015) 94–107
- [09] D. J. Gerber, S. Lin, Geometric complexity and energy simulation, *Evolving Performance Driven Architectural Form*, 2013, Proceedings of the 18th International Conference on Computer-Aided Architectural Design Research in Asia (CAADRIA 2013), 87–96. © 2013
- [10] A. Dhar, T. A. Reddy, D. E. Claridge, 1998, Modeling hourly energy use in commercial buildings with Fourier series functional forms, *Journal of Solar Energy Engineering*, August 1998, Vol. 120 / 223
- [11] R. Sullivan, S. Nozaki, R. Johnson, S. Selkowitz, 1983, Commercial building energy performance analysis using multiple regression procedures, Applied Science Division Lawrence Berkeley Laboratory University of California Berkeley CA 94720
- [12] R. Sullivan, S. Nozaki, 1983, Multiple regression techniques applied to fenestration effects on commercial building energy performance, ASHRAE Semi-Annual Meeting, Atlanta, GA, January 29 - February 2, 1984; <https://escholarship.org/uc/item/2fd9q96z>
- [13] D. M. Sander, S. Cornick, G. R. Newsham, 1990, Development of a simple model to relate heating and cooling energy to building envelope thermal characteristics, U.S. Environmental protection Agency

- [14] J. F. Kreider, D. E. Claridge, P. Curtiss, R. Dodier, J. S. Haberl, M. Krart, 1995, Building energy use prediction and system identification using recurrent neural networks, *Journal of Solar Energy Engineering*, August 1995, Vol. 117/161
- [15] H. Jedrzejuk, W. Marks, 2001, Optimization of shape and functional structure of buildings as well as heat source utilization. Basic theory, *Building and Environment* 37 (2002) 1379–1383
- [16] T. Catalina, J. Virgone, E. Blanco, 2008, Development and validation of regression models to predict monthly heating demand for residential buildings, *Energy and Buildings* 40 (2008) 1825–1832
- [17] I. Jaffal, C. Inard, C. Ghiaus, 2009, Fast method to predict building heating demand based on the design of experiments, *Energy and Buildings* 41 (2009) 669–677
- [18] V. Granadeiro, J. R. Correia, V. M.S. Leal, J. P. Duarte, 2013, Envelope-related energy demand: A design indicator of energy performance for residential buildings in early design stages, *Energy and Buildings* 61 (2013) 215–223
- [19] C. Koo, S. Park, T. Hong, H. S. Park, 2014, An estimation model for the heating and cooling demand of a residential building with a different envelope design using the finite element method, *Applied Energy* 115 (2014) 205–215
- [20] R. Ourghi, A. Al-Anzi, M. Krarti, 2007, A simplified analysis method to predict the impact of shape on annual energy use for office buildings, *Energy Conversion and Management* 48 (2007) 300–305
- [21] V. Granadeiro, J. P. Duarte, P. Palensky, 2011, Building envelope shape design using a shape grammar-based parametric design system integrating energy simulation, *IEEE Africon 2011 - The Falls Resort and Conference Centre, Livingstone, Zambia*
- [22] H. Koning, J. Eizenberg, 1981, The language of prairie; Frank Lloyd Wright's prairie houses, *Environment and Planning B*, 1981, volume 8, pages 295 – 323
- [23] C. Hachem, A. Athienitis, P. Fazio, 2011, Parametric investigation of geometric form effects on solar potential of housing units, *Solar Energy* 85 (2011) 1864–1877
- [24] C. Hachem, 2012, Investigation of design parameters for increased solar potential of dwellings and neighborhoods, PhD research in the department of building, civil, and environmental engineering, Concordia University, Montreal, Quebec, Canada
- [25] V. Granadeiro, J. P. Duarte, J. R. Correia, V. M.S. Leal, 2013, Building envelope shape design in early stages of the design process: Integrating architectural design systems and energy simulation, *Automation in Construction* 32 (2013) 196–209
- [26] M. Košir, T. Gostiša, Ž. Kristl, 2017, Influence of architectural building envelope characteristics on energy performance in Central European climatic conditions, *Journal of Building Engineering*, PII: S2352-7102(17)30494-1

- [27] Y. Wang, W. Tian, J. Ren, L. Zhu, Q. Wang, 2006, Influence of a buildings integrated-photovoltaics on heating and cooling loads, *Applied Energy* 83 (2006) 989–1003
- [28] S. Beringer, H. Schilke, I. Lohse, G. Seckmeyer, 2011, Case study showing that the tilt angle of photovoltaic plants is nearly irrelevant, *Solar Energy* 85 (2011) 470–476
- [29] S. Misara, N. Henze, A. Sidelev, 2012, Thermal Characteristics of BIPV (U-value and g-value), In the BMU research project "MULTIELEMENT, the Fraunhofer Institute for Wind Energy and Energy System Technology (IWES) together with 15 industrial partners
- [30] S. Misara, Doctoral research, Thermal Impacts on Building Integrated Photovoltaic (BIPV) (Electrical, Thermal and Mechanical Characteristics), 2014, Vorgelegt im Fachbereich Elektrotechnik/Informatik der Universität Kassel
- [31] M. Hartner, A. Ortner, A. Hiesl, R. Haas, 2015, East to west – The optimal tilt angle and orientation of photovoltaic panels from an electricity system perspective, *Applied Energy* 160 (2015) 94–107
- [32] E. Nyholm, J. Goop, M. Odenberger, F. Johnsson, 2016, Solar photovoltaic-battery systems in Swedish households – Self- consumption and self-sufficiency, *Applied Energy* 183 (2016) 148–159
- [33] A. Lahnaoui, P. Stenzel, J. Linssen, 2017, Tilt angle and orientation impact on the techno-economic performance of photovoltaic battery systems, *Energy Procedia* 105 (2017) 4312 – 4320
- [34] C. Toledo, R. López, J. Abad López, A. Urbina Yeregui, 2016, Building integrated photovoltaics (BIPV) vs. building attached photovoltaics (BAPV): Balance between energy production and architectural design, 20th International Congress on Project Management and Engineering Cartagena, 13-15th July 2016
- [35] P. Fokaides, K. Polycarpou, S. Kalogirou, 2017, The impact of the implementation of the European Energy Performance of Buildings Directive on the European building stock: The case of the Cyprus Land Development Corporation, *Energy Policy* 111 (2017) 1–8
- [36] DesignBuilder, DesignBuilder Software Ltd, <https://designbuilder.co.uk/simulation>,
- [37] Forschungsinitiative ‘Zukunft Bau’, www.forschungsinitiative.de, <https://www.zukunftbau.de/projekte/modellvorhaben/modellvorhaben-effizienzhaus-plus/schwabach>
- [38] F. Ishola¹, F. Oyawale¹, A. Inegbenebor, H. Boyo, S. Akinlabi, O. Oyetunji, 2020, Mathematical Analysis and Thermal Modelling of a Pilot-Scale Pyrolysis Gas Furnace, *Journal of Advanced Research in Fluid Mechanics and Thermal Sciences* 65, Issue 1 (2020) 81-93
- [39] R. de Dear, 2014, Adaptive comfort applications in Australia and impacts on building energy consumption, <https://www.researchgate.net/publication/228717629>

- [40] A. Dentel, U. Dietrich, 2007, Thermische Behaglichkeit – Komfort in Gebäuden, Dokumentation primero – komfort, HCU, HafenCity Universität, Hamburg
- [41] M. G. Emmel, M. O. Abadie, N. Mendes, 2007, New external convective heat transfer coefficient correlations for isolated low-rise buildings, *Energy and Buildings* 39 (2007) 335–342
- [42] C. A. Gueymard, 2009, Direct and indirect uncertainties in the prediction of tilted irradiance for solar engineering applications, *Solar Energy* 83 (2009) 432–444
- [43] C. Stanciu, D. Stanciu, 2014, Optimum tilt angle for flat plate collectors all over the World – A declination dependence formula and comparisons of three solar radiation models, *Energy Conversion and Management* 81 (2014) 133–143
- [44] B. P. Jelle, 2012, Solar Radiation Glazing Factors for Window Panes, Glass Structures and Electrochromic Windows in Buildings - Measurement and Calculation, *Solar Energy Materials and Solar Cells*, 2012
- [45] A. Pech, C. Pöhn, 2018, Bauphysik, zweite, aktualisierte Auflage, Die Deutsche Nationalbibliothek, E-Book (ISBN PDF 978-3-0356-0574-7)
- [46] windfinder.com, base model gfs, refresh rate 6h, coverage worldwide, resolution 22km–27km
- [47] A. Albatayneh, D. Alterman, A. Page, B. Moghtaderi, 2020, The Significance of Sky Temperature in the Assessment of the Thermal Performance of Buildings, *Licensee MDPI*, Basel, Switzerland
- [48] WeatherSpark.com, Cedar Lake Ventures, Inc. 2500 Shadywood Rd Ste 510 Excelsior, MN 55331-6203, United States
- [49] A. Karn, V. Chintala, S. Kumar, 2018, An investigation into sky temperature estimation, its variation, and significance in heat transfer calculations of solar cookers. *Heat Transfer—Asian Res.* 2019;48:1830–1856. <https://doi.org/10.1002/htj.21459>
- [50] E. Barreira, R. Almeida, M. L. Simões, 2021, Emissivity of Building Materials for Infrared Measurements, *Sensors* 2021, 21, 1961. <https://doi.org/10.3390/s21061961>
- [51] K.J. Kontoleon, D.K. Bikas, 2007, The effect of south wall’s outdoor absorption coefficient on time lag, decrement factor and temperature variations, *Energy and Buildings* 39 (2007) 1011–1018
- [52] I. Atmaca, O. Kaynakli, A. Yigit, 2007, Effects of radiant temperature on thermal comfort, *Building and Environment* 42 (2007) 3210–3220
- [53] O. Gliah, B. Kruczek, S. G. Etemad, J. Thibault, 2011, The effective sky temperature: an enigmatic concept, *Heat Mass Transfer* (2011) 47:1171–1180, DOI 10.1007/s00231-011-0780-1

- [54] H. Erhorn, A. Bergmann, 2015, Energieeffizienter Neubau von Wohngebäuden - Begleitforschung und Querauswertung von Modellvorhaben (Phase 2), IBP-Bericht WB 175/2015
- [55] S. Misara, 2014, Thermal Impacts on Building Integrated Photovoltaic (BIPV) (Electrical, Thermal and Mechanical Characteristics), Dissertation zur Erlangung des akademischen Grades Doktor der Ingenieurwissenschaften (Dr.-Ing.)
- [56] S. Misara, N. Henze, A. Sidelev, 2014, thermal characteristics of BIPV (U-value and g-value), Fraunhofer Institute for Wind Energy and Energy System Technology IWES, Kassel (Germany)
- [57] <https://energyplus.net/weather>, Department of Energy's (DOE) Building Technologies Office (BTO), and managed by the National Renewable Energy Laboratory (NREL)
- [58] "Dew Point". Glossary – NOAA's National Weather Service. 25 June 2009, <https://w1.weather.gov/glossary/index.php?word=dew+point>
- [59] NOAA Solar Calculations, U.S. Department of Commerce, National Oceanic & Atmospheric Administration, NOAA Research, <https://gml.noaa.gov/grad/solcalc/>
- [60] <https://www.wetteronline.de/klima-sonne>, WetterOnline Meteorologische Dienstleistungen GmbH
- [61] Hanwha Q CELLS GmbH, <https://www.q-cells.de/solar.html>
- [62] Forschungsinitiative 'Zukunft Bau', www.forschungsinitiative.de, <https://www.zukunftbau.de/projekte/modellvorhaben/modellvorhaben-effizienzhaus-plus/schwabach>
- [63] A. S. Anna, R. Bass, 2014, A new two-degree-of-freedom space heating model for demand response, SMARTGREENS 2014 - 3rd International Conference on Smart Grids and Green IT Systems
- [64] G. Graumann, 1988, Geometrie im Alltag – Konzeption, Themenübersicht, Praxisberichte, Mathematik lehren, 1988, Heft 29

Appendix 1

Extended explanation of sol-air temperature

PhD research:

Determining effects of geometry on energy efficiency of medium-sized solar
buildings

Abbas Rahmani

Supervisor: Prof. Dr.-Ing. R. Wagner

Second consultant: Prof. Dr.-Ing. M. Pfeifer

Institut Entwerfen und Bautechnik (IEB)
Fachgebiet Bautechnologie (FGB)

(2023)

Content

	Introduction	184
1.	Sol-air temperature and similar definitions	184
	1.1 D. G. Stephenson. 1957	184
	1.1.1 Derivation	185
	1.2 G.D. Chesser Jr et al. 2018	187
	1.2.1 Derivation	187
2	Summary	188
3	References	188

Introduction

Regarding the official presentation of this work hold on 12.01.2023 and considering the asked questions by jury committees, a short illustration of the work has been prepared to highlight and justify the content of the work.

In this part of illustration, sol-air temperature has been reintroduced regarding the very first attempts of its definitions and integration in previous researches. Simplification of the basic equations defining sol-air temperature has been presented to demonstrate the logic derivation of sol-air temperature integrated in the core equations of this work. It should be noted that these calculations are based on the reference equations of sol-air temperature that are also initially introduced in reference list of submitted dissertation. The upcoming references are additionally introduced to illustrate accuracy of integrated equations regarding the similarity of employed parameters to calculate sol-air temperature in two further references that are published in reliable journals as well.

1. Sol-air temperature and similar definitions

The sol-air temperature represents the equivalent outdoor air temperature that gives the same rate of heat flow to a surface as would the combination of incident solar radiation and convection/radiation with the environment. Indeed, the main equations of this work that are entirely in framework of steady-state method purposefully employ sol-air temperature to deliver more accurate results compared to simpler equations that just integrate outside air temperature and external convections that could cause inaccuracy in absence of equivalence of outside emission.

1.1 D. G. Stephenson. 1957

As the very first registered attempts, D. G. Stephenson [01] introduced sol-air temperature in 1957 as a simplified derivation in his work and compared two other expressions of sol-air temperature in previous researches. He meant that ‘the dominant weather elements which affect this energy exchange are sunshine, air temperature and wind’. Furthermore, regarding demand of integrating a meteorological parameter containing combination of some parameters he meant; ‘the normal meteorological readings which are taken do not adequately describe the weather for purposes of calculating its effect upon the surface energy exchange, particularly when sunshine is involved. Even if all the individual factors are measured there remains the problem of recombining these multiple streams of variables in the calculation’. Additionally, he pointed that it is absolutely necessary to develop equations that can employ characteristics of building’s skin in relation to light as he meant; ‘In addition, the shape and orientation of the building and its relationship to the ground and surrounding objects, as well as the absorptivity and emissivity characteristics of the surfaces will influence the results’. His particular suggestion to define a parameter holding outcome of these meteorological parameters is; ‘there is, fortunately, a way of achieving some simplification; a combined factor called sol-air temperature can be used so that it becomes necessary only to deal with a single stream of data’.

1.1.1 Derivation

D. G. Stephenson pointed to expression of sol-air temperature defined by ‘Parmelee and Aubele’ and meant that it appears to be the most satisfactory:

$$t'_{sa} = t_a + \frac{\alpha \cdot I_s - (\varepsilon \cdot \Delta I_L)}{h_c + h_r} \quad [01]$$

Where:

t_a	Temperature of the ambient air
α	Emissivity of surface for shortwave radiation
I_s	intensity of shortwave radiation, direct and diffuse combined
ε	Emissivity of surface for longwave radiation
I_L	Intensity of long wave radiation
h_c	Surface coefficient of heat transfer by convection
h_r	Radiation coefficient of heat transfer

The heat exchange at the surface of a building using the defined sol-air temperature can be calculated as:

$$q = (h_c + h_r) \cdot (t'_{sa} - t_s) \quad [01]$$

Where:

t_s	Surface temperature
-------	---------------------

Following this research, a second assumption of calculation sol-air temperature has been introduced by ‘Mackey and Wright’. ‘Mackey and Wright’ assumed that Surface coefficient of heat transfer can be united if radiation and convection heat transfer coefficient can be mathematically added together that means if:

$$h = h_c + h_r \quad [01]$$

Then sol-air temperature equation will be simplified to:

$$t_{sa} = t_a + \alpha \cdot I_s / h \quad [01]$$

So, the difference between two equations delivered by ‘Parmelee and Aubele’ and ‘Mackey and Wright’ as t'_{sa} and t_{sa} is presented here:

$$t'_{sa} = t_{sa} - (\varepsilon \cdot \Delta I_L / h) \quad [01]$$

According to justification of ‘D. G. Stephenson’, the phrase $\varepsilon \cdot \Delta I_L / h$ justifies a black body at air temperature. He has pointed that for a surface seeing only a clear sky, $\varepsilon \cdot \Delta I_L$ has the value indicated by equation 10, while for a completely overcast sky, $\varepsilon \cdot \Delta I_L$ is zero.

Going back to the employed equation of sol-air temperature in this work, the parameter of sky temperature has been purposefully employed to integrate effects of cloudiness (in clear sky and overcast conditions), and is similar to the phrase of $\varepsilon \cdot \Delta I_L / h$ that results different sol-air temperatures in different emissions quantities resulted from different proportions of cloud in the sky. The employed equation of sol-air temperature in this work is:

$$T_{Sol-air} = \left(T + \frac{a_s \cdot Q_{Sol}}{h_c} \right) - \left(\frac{\varepsilon \cdot \sigma (T^4 - T_{Sky}^4)}{h_c} \right) \quad (4.12)$$

Where:

- T Dry-bulb temperature
- a_s Solar absorptivity
- Q_{Sol} Cumulative solar irradiation
- h_c Outside convective heat transfer coefficient
- ε Emissivity of component
- σ Stefan–Boltzmann constant = $5670400 \times 10^{-8} \text{ W/m}^2\text{K}^4$
- T_{Sky} Sky temperature

And in this equation, sky temperature is:

$$T_{Sky} = (\varepsilon_{sky})^{0.25} \times T \quad (4.11)$$

Where;

- ε = Sky emissivity
- T = Dry bulb temperature

And finally, in employed equation of sky emissivity, parameter N is defined to alter quantity of emission in different cloudiness conditions as:

$$Sky_{emissivity} = 0.787 + \left(0.767 \times \ln \left(\frac{T_{dewpoint}}{273} \right) \right) + 0.0224N - 0.0035N^2 + 0.00028N^3 \quad (4.10)$$

Where;

$T_{dewpoint}$ = The temperature to which the air would have to cool (at constant pressure and constant water vapor content) in order to reach saturation.

N = Opaque sky cover (tenths), the expected amount of opaque clouds covering the sky valid for the indicated hour where N equals 0 for clear sky and 10 for overcast sky.

So, it can be concluded that in this work, the first part of sol-air temperature is equivalent of equation of sol-air temperature given by Mackey and Wright as the table:

First part of equation in this work	Equation of Mackey and Wright
$T_{Sol-air} = \left(T + \frac{a_s \cdot Q_{Sol}}{h_c} \right)$	$t_{sa} = t_a + \alpha \cdot I_s / h$

Indeed, the only difference is in the case of possibility of uniting heat transfer coefficients of convection and radiation from Mackey and Wright as; $h = h_c + h_r$, where in this work heat transfer coefficient just refers to convection. To compare the employed equation of sol-air temperature with sol-air temperature defined by Parmelee and Aubele, the second part of equations should be compared together as:

First part of equation in this work	Second part of equation employed by Parmelee and Aubele
$\left(\frac{\varepsilon \cdot \sigma (T^4 - T_{sky}^4)}{h_c}\right)$	$(\varepsilon \cdot \Delta I_L / h)$

From mathematical point of view, in both equations moving from cloudy days toward clear sky days result higher quantity for second part of equation means lower sol-air temperatures in clear days that radiation is logically more effective.

1.2 G.D. Chesser Jr et al. 2018

As one of latest research in this field ‘G.D. Chesser Jr et al.’ [02] meant that; ‘Sol-air temperature is a simplified method of accounting for the combined effects of conductive, convective, and radiative heat exchange in structures. Specifically, sol-air temperature can be described as a proxy temperature of outdoor air which, in the absence of radiative heat exchanges, gives the same rate of heat transfer into the structure as the combined mechanism of radiant heat transfer from the sun and other surroundings and convective heat exchange with the outdoor air.’

He meant also that ignorance of combination of weather data results specific inaccuracies. He tried similarly to integrate exterior air temperature and solar radiation to calculate sol-air temperature. He reminded also that; ‘variable conditions that dominantly affect the exchange of heat energy include solar radiation, outside ambient air temperature, wind, and air infiltration. Building orientation, relationship to the ground and surrounding objects, and the emissivity and absorptivity of building exterior surfaces also affect heat energy exchange.’ He described also sol-air temperature as an assumption combining outcome of the main phenomena and points that; ‘These combined conditions drive heat exchange through various levels of conductive, convective, and radiative heat transfer.’ He has also noted that; ‘Sol-air temperature is a simplified method of accounting for the combined effects of conductive, convective, and radiative heat exchange in building surfaces.’

1.2.1 Derivation

Similar to the employed equation of sol-air temperature in this work, the simplified equation has been introduced as;

$$t_e = t_o + \alpha \cdot E_t / h_o - \varepsilon \cdot \Delta R / h_o \quad [02]$$

Where;

t_e sol-air temperature

t_o outdoor air temperature

α absorptance of surface for solar radiation

E_t total solar radiation incident on surface

h_o coefficient of heat transfer by long-wave radiation and convection at outer surface

ΔR difference between long-wave radiation incident on surface from sky and surroundings and radiation emitted by blackbody at outdoor air temperature

To compare the employed equation of sol-air temperature in this work with definition of ‘G.D. Chesser Jr et al.’, only the last part of equations should be compared together as:

Last part of equation in this work	Last part of equation employed by G.D. Chesser Jr et al.
$\left(\frac{\varepsilon \cdot \sigma (T^4 - T_{sky}^4)}{h_c}\right)$	$\varepsilon \cdot \Delta R / h_o$

It should be reminded that defining sol-air temperature without the second part of equation still will result acceptable estimation of this parameter if effects of different cloudiness resulting different quantities of emissions is not in the focus of interest. Comparing the last part of equation in this work with the last part of estimated equation suggested by ‘G.D. Chesser Jr et al.’ indicates that both simplifications indicate drops of sol-air temperatures resulting interaction of external emission results in different cloudiness of sky.

2. Summary

In this part of illustration two main targets have been in focus of demonstration. As one of the key parameters employed in core of calculations in this work, Sol-air temperature has been re-introduced regarding two additional reliable references. The old one from D. G. Stephenson (1957) goes back to 66 years ago and the second one from G.D. Chesser Jr et al. (2018) that points to almost state of the art of this assumption. Similarities of derivations of simplification of equations in both references have been discussed and compared with the simplified equation of sol-air temperature employed in this work. Additionally, the difference between the equations (in the second part of equations) that try to involve effects of different cloudiness situations to alter amount of emissions will alter quantity of sol-air temperature. Quantitatively, putting weather data in all two reference equations will results more or less the same quantities of the calculated sol-air temperature as the integrated equation in this work.

3. References

- [01] Stephenson, D. G., 1957, Thermal radiation and its effect on the heating and cooling of buildings, National research council of Canada
- [02] G.D. Chesser Jr et al., 2018, Comparison of Outside Air and Sol-air Design Temperatures for Estimating Insulation Needs, 10th International Livestock Environment Symposium (ILES X)

Appendix 2

Description of energy demands of the selected building

PhD research:

Determining effects of geometry on energy efficiency of medium-sized solar
buildings

Abbas Rahmani

Supervisor: Prof. Dr.-Ing. R. Wagner

Second consultant: Prof. Dr.-Ing. M. Pfeifer

Institut Entwerfen und Bautechnik (IEB)
Fachgebiet Bautechnologie (FGB)

(2023)

Content

	Introduction	191
1	The final calculated heating and cooling demands	191
2	Geometry of building and materials	192
3	Heating demand	193
4	Cooling demand	197
5	Summary	201

Introduction

Regarding the official presentation of this work hold on 12.01.2023 and considering the asked questions by jury committees, a short illustration of the work has been prepared to highlight and illustrate content work.

In this part of illustration, Justification and explanation of calculated heating and cooling demands have be explained to justify connection of weather data with the calculated demands through the explained equations. As two critical example days, a cold winter day and a hot summer day have been selected that are also previously discussed in the submitted dissertation.

1. The final calculated heating and cooling demands

In this part to illustrate the calculated heating demand and cooling demand of the selected building in Schwabach, Germany (chapter 6.2 of work), the procedure of the entire calculation has been reintroduced. The target is to quantitatively demonstrate the accuracy of integrated equations to highlight that the final calculated heating demand and cooling demand are mathematically connected to initial weather data. The calculated table and final energy demands are in upcoming table.

	Jan 11th	Jan 26th	Feb 11th	Feb 26th	Mar 11th	Mar 26th	Apr 11th	Apr 26th	May 11th	May 26th	Jun 11th	Jun 26th
H Demand	48896,37	55907,73	53055,40	52856,15	40685,75	34665,39	31100,41	35748,08	21103,03	13085,76	19009,56	11147,05
H Demand (HP)	16298,79	18635,91	17685,13	17618,72	13561,92	11555,13	10366,80	11916,03	7034,34	4361,92	6336,52	3715,68
Extra Demand	9835,00	9835,00	9835,00	9835,00	9835,00	9835,00	9835,00	9835,00	9835,00	9835,00	9835,00	9835,00
DHW	2085,00	2085,00	2085,00	2085,00	2085,00	2085,00	2085,00	2085,00	2085,00	2085,00	2085,00	2085,00
C Demand	0,00	0,00	0,00	0,00	0,00	0,00	0,00	0,00	0,00	35724,18	0,00	45306,57
C Demand (HP)	0,00	0,00	0,00	0,00	0,00	0,00	0,00	0,00	0,00	11908,06	0,00	15102,19
Sum Demand	28218,79	30555,91	29605,13	29538,72	25481,92	23475,13	22286,80	23836,03	18954,34	28189,98	18256,52	30737,87
Cov Demand C	3406,13	11726,25	5609,34	7436,23	25481,92	23475,13	22286,80	23836,03	18954,34	28189,98	18256,52	30737,87
Un-Cov Demand A	24812,66	18829,66	23995,79	22102,49	0,00	0,00	0,00	0,00	0,00	0,00	0,00	0,00
Un-used E B	0,00	0,00	0,00	0,00	7362,43	41698,01	5795,37	12562,14	51432,54	51196,21	26508,06	48363,03
S-C	1,00	1,00	1,00	1,00	0,78	0,36	0,79	0,65	0,27	0,36	0,41	0,39
S-S	0,12	0,38	0,19	0,25	1,00	1,00	1,00	1,00	1,00	1,00	1,00	1,00
Electricity	3406,13	11726,25	5609,34	7436,23	32844,35	65173,14	28082,17	36398,16	70386,88	79386,19	44764,58	79100,90

	Jul 11th	Jul 26th	Aug 11th	Aug 26th	Sep 11th	Sep 26th	Oct 11th	Oct 26th	Nov 11th	Nov 26th	Dec 11th	Dec 26th
H Demand	15753,04	7855,59	13287,53	18289,04	17998,10	25906,16	29288,03	38672,64	35037,39	52123,66	63046,17	48446,80
H Demand (HP)	5251,01	2618,53	4429,18	6096,35	5999,37	8635,39	9762,68	12890,88	11679,13	17374,55	21015,39	16148,93
Extra Demand	9835,00	9835,00	9835,00	9835,00	9835,00	9835,00	9835,00	9835,00	9835,00	9835,00	9835,00	9835,00
DHW	2085,00	2085,00	2085,00	2085,00	2085,00	2085,00	2085,00	2085,00	2085,00	2085,00	2085,00	2085,00
C Demand	0,00	52626,07	23683,03	0,00	6290,63	0,00	0,00	0,00	0,00	0,00	0,00	0,00
C Demand (HP)	0,00	17542,02	7894,34	0,00	2096,88	0,00	0,00	0,00	0,00	0,00	0,00	0,00
Sum Demand	17171,01	32080,55	24243,52	18016,35	20016,24	20555,39	21682,68	24810,88	23599,13	29294,55	32935,39	28068,93
Cov Demand C	17171,01	32080,55	24243,52	18016,35	20016,24	20555,39	19315,54	11341,67	23599,13	29294,55	3831,88	5365,90
Un-Cov Demand A	0,00	0,00	0,00	0,00	0,00	0,00	2367,14	13469,21	0,00	0,00	29103,51	22703,03
Un-used E B	36241,87	26221,36	38094,44	3799,92	26079,29	37317,22	0,00	0,00	984,14	5674,03	0,00	0,00
S-C	0,32	0,55	0,39	0,83	0,43	0,36	1,00	1,00	0,96	0,84	1,00	1,00
S-S	1,00	1,00	1,00	1,00	1,00	1,00	0,89	0,46	1,00	1,00	0,12	0,19
Electricity	53412,88	58301,91	62337,96	21816,26	46095,53	57872,60	19315,54	11341,67	24583,27	34968,58	3831,88	5365,90

Tab. 6.8 Energy demands and electricity generation – First six months (top), second six months (bottom) (W)

Two example days of 26th January for its calculated heating demand and 26th July for its calculated cooling demand have been selected and the calculated procedure pointing to the employed equations are presented. It should be noted that each calculated demand considers entire skin of building that are consisted of:

- South-west facade (Combination of 50.30 m² wall + 22.71 m² windows)
- North-west façade (Combination of 76.39 m² wall + 6.95 m² windows +3.90 m² door)
- South-east façade (Combination of 66.06 m² wall + 21.18 m² windows)
- North-east façade (Combination of 69.27 m² wall + 3.74 m² windows)
- Ceiling (113.25 m²)

- South-west roof (80.50 m²)
- North-east roof (65.96 m²)
- South-west (projection part) roof (in this case irrelevant, as it only generates electricity (18.50 m²))

So, 12 different components are calculated as the entire skin of this building. Additionally, for each component in each day, 24 points as representative of 24 hours of day, are individually calculated. So, considering the calculated components and the resolution of calculation (each hour);

$$12 \times 24 = 288 \quad (\text{Number of simulations})$$

That means the same simulation has been done (288 times) for each component to deliver the final calculated demand in a specific day. As, presenting all these 288 points would not be that possible, one random point from one component has been selected. The selected component is opaque portion of south-west façade (50.30 m² wall) and the selected point is 20:00 o'clock in January and 16:00 o'clock in July.

2. Geometry of building and materials

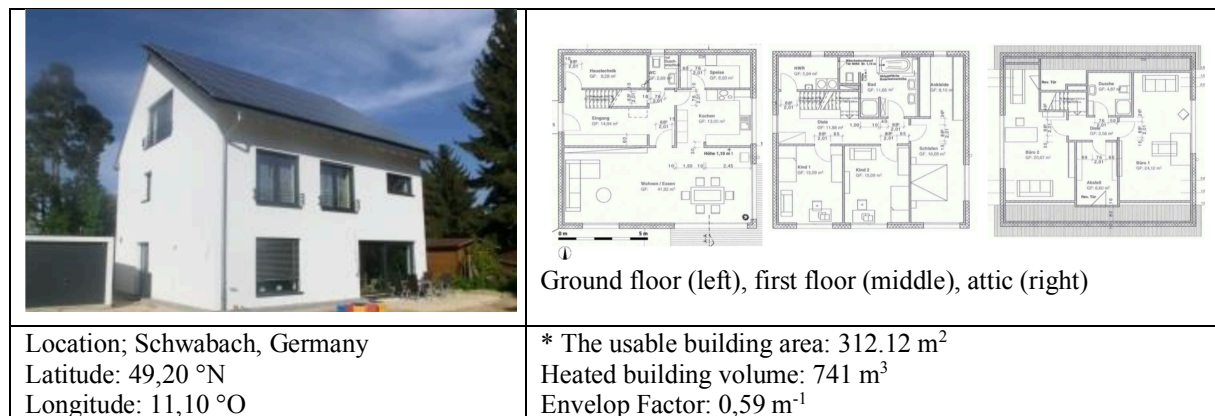


Fig. 7.1 Geographical location and geometrical setup of investigated building

	Base plate	Window N-E	Window S-E	Window N-W	Window S-W	Door-opaque N-W	Wall N-E	Wall S-E	Wall S-W	Wall N-W	Inclined roof S-W *	Inclined roof N-E
Area (m ²)	113,25	3,74	21,18	6,95	22,71	3,90	69,27	66,06	50,30	76,39	80,50	65,96
U-value (W/m ² .K)	0,14	0,80	0,80	0,80	0,80	1,00	0,14	0,14	0,14	0,14	0,12	0,12

Tab. 7.1 Components in selected building – area – U-value [51]

3. Heating demand

Here the elementary weather data on 26th January at 20:00 o'clock:

	Weather data at the beginning of year		The selected date
	Jan01:00	Jan02:00	Jan-m20:00
Direct Normal Solar (W/m2)	0	0	0
Diffuse Horizontal Solar (W/m2)	0	0	0
Outside Dry-Bulb Temperature (°C)	4,6	4,7	-3,3
Solar Altitude (°)	-61,13	-55,02	-31,63
Solar Azimuth (°)	25,84	49,73	277,4
Outside Dew-Point Temperature (°C)	2,6	2,7	-4,3
	11.01.02 01:00	11.01.02 02:00	26.01.02 20:00
Outside Dry-Bulb Temperature (°C)	4,6	4,7	-3,3
Outside Dew-Point Temperature (°C)	2,6	2,7	-4,3
Wind Speed (m/s)	6,2	4,6	1
Wind Direction (°)	220	220	290
Solar Altitude (°)	-61,13	-55,02	-31,63
Solar Azimuth (°)	25,84	49,73	277,4
Atmospheric Pressure (Pa)x10 ³	97000	97000	97300
Direct Normal Solar (W/m2)	0	0	0
Diffuse Horizontal Solar (W/m2)	0	0	0

The upcoming table shows elementary emerged weather data on 26th Jan at 20:00 and the calculated parameters for the representative component:

	Parameter & Symbol	Amount	Equation
01	Outside air temperature (T)	-3,30 °C 269,85 °K	Direct from weather data
02	dew-point temperature (T _{dewpoint})	-4,30 °C 268,85 °K	Direct from weather data
03	Inside air temperature (T _{in})	21,15 °C 294,30 °K	$T_{(in)} = 21.50 + (0.111 \times T_{(out)})$ (4.2)
04	Inside convective coefficient (h _i)	7,00 W/m ² .K	Average estimation
05	Outside convective coefficient (h _o)	13,80 W/m ² .K	Regarding Fig.4.9 Convective heat transfer coefficient for leeward and windward conditions
06	Wall thickness (d _{wal})	0,214 m	Assigned construction (Equivalence of U _{value} of 0,14)
07	Heat conductivity of wall (λ _{wal})	0,03 W/mK	Assigned construction (Equivalence of U _{value} of 0,14)
08	Thermal resistance of the wall excluding outside air film resistance (ΣR _I)	7,29 m ² k/W	$R = \sum_1^N \left(\frac{d_i}{\lambda_i}\right)$ (4.20) $\sum R_I = d_{wal} / \lambda_{wal} + 1/h_i$

09	Thermal resistance of the wall excluding inside and outside air film resistances (ΣR_{II})	7,14 m ² k/W	$R = \Sigma_1^N \left(\frac{d_i}{\lambda_i}\right)$ (4.20) $\Sigma R_{II} = d_{wal} / \lambda_{wal}$
10	Cumulative solar irradiation (Q_{sol})	0,00 W/m ²	$G_{Tt} = G_B + (G_D \frac{1+\cos\beta}{2}) + ((G_B + G_D)\rho \frac{1-\cos\beta}{2})$ (4.6)
11	Opaque sky cover (N)	6,60	Fig. 4.12 Monthly cloud cover categories– Stuttgart [36]
12	Sky emissivity (ϵ_{sky})	0,85	$Sky_{emissivity} = 0.787 + \left(0.767 \times \ln\left(\frac{T_{dewpoint}}{273}\right)\right) + 0.0224N - 0.0035N^2 + 0.00028N^3$ (4.10)
13	Sky temperature (T_{sky})	-13,96 °C 259,19 °K	$T_{sky} = (\epsilon_{sky})^{0.25} \times T$ (4.11)
14	Sol-air temperature ($T_{Sol-air}$)	-6,22 °C 266,93 °K	$T_{Sol-air} = \left(T + \frac{a_s \cdot Q_{Sol}}{h_c}\right) - \left(\frac{\epsilon \cdot \sigma (T^4 - T_{Sky}^4)}{h_c}\right)$ (4.12)

$a_s = 0,50$ (Solar absorptivity)
 $\sigma = 5670400 \times 10^{-8} \text{ W/m}^2\text{K}^4$

	Parameter & Symbol	Amount	Equation
15	Outside surface temperature (T_{s-out})	-5,95 °C 267,20 °K	$T_{s-out} = \frac{h_o \cdot T_{sol-air} + \left(\frac{T_{in}}{\Sigma R_I}\right)}{\left(\frac{1}{\Sigma R_I}\right) + h_o}$
16	Inside surface temperature (T_{s-in})	20,62 °C 293,77 °K	$T_{s-in} = T_{s-out} + (h_o \cdot \Sigma R_{II} \cdot (T_{s-out} - T_{sol-air}))$ (4.14)
17	Heat transfer (q)	-3,72 W/m ²	$q = h_o \cdot (T_{sol-air} - T_{s-out})$ (4.15)

According to definition in chapter 4.6;

1. The direction of heat flow is from inside into outside
2. $t_{out} < t_{in}$

So, the entire heat flow is marked as heating demand. Considering area of this component as 50,30 m², heating demand of opaque portion of South-west façade will be:

$$50,30 \text{ (m}^2\text{)} \times -3,72 \text{ (W/m}^2\text{)} = 187,12 \text{ W (Heating demand).}$$

At this time and date (at 20:00 on 26th Jan), heating demand of the rest of components in building have been similarly calculated:

Building's face	At 20:00 for each component	Sum (Excel)
South-west façade (F-01)	Wall: $50,30 \text{ (m}^2) \times -3,72 \text{ (W/m}^2) = -187,12 \text{ W}$	-611,20 W
	Windows: $22,71 \text{ (m}^2) \times -18,68 \text{ (W/m}^2) = -424,22 \text{ W}$	
North-west façade (F-02)	Wall: $76,39 \text{ (m}^2) \times -3,80 \text{ (W/m}^2) = -290,28 \text{ W}$ Windows: $6,95 \text{ (m}^2) \times -18,91 \text{ (W/m}^2) = -131,42 \text{ W}$ Door: $3,90 \text{ (m}^2) \times -22,75 \text{ (W/m}^2) = -88,73 \text{ W}$	-510,32 W
South-east façade (F-03)	Wall: $66,06 \text{ (m}^2) \times -3,80 \text{ (W/m}^2) = -251,02 \text{ W}$ Windows: $21,18 \text{ (m}^2) \times -18,91 \text{ (W/m}^2) = -400,51 \text{ W}$	-651,44 W
North-east façade (F-04)	Wall: $69,27 \text{ (m}^2) \times -3,92 \text{ (W/m}^2) = -271,54 \text{ W}$ Windows: $3,74 \text{ (m}^2) \times -19,27 \text{ (W/m}^2) = -72,07 \text{ W}$	-343,59 W
Ceiling (F-05)	$113,25 \text{ (m}^2) \times -3,36 \text{ (W/m}^2) = -380,52 \text{ W}$	-380,02 W
South-west roof (F-06)	$80,50 \text{ (m}^2) \times -2,86 \text{ (W/m}^2) = -230,23 \text{ W}$	-229,99 W
North-east roof (F-07)	$65,96 \text{ (m}^2) \times -3,38 \text{ (W/m}^2) = -222,94 \text{ W}$	-222,87 W
Sum	-2949,43 W	-2949,43 W

Based on seven main facades of building (including ceiling), shaping external face of building, individual calculation of heating demand of all seven facades on an hourly basis are presented here:

Time	F-01	F-02	F-03	F-04	F-05	F-06	F-07	Sum
01:00	562,49	470,80	600,99	318,16	345,31	208,99	206,35	2713,09
02:00	566,90	474,11	605,22	319,94	349,48	211,51	207,56	2734,72
03:00	565,90	473,48	604,41	319,89	348,09	210,67	207,41	2729,85
04:00	571,34	477,81	609,95	322,54	352,25	213,19	209,17	2756,25
05:00	584,00	488,27	623,29	329,53	360,58	218,23	213,66	2817,56
06:00	586,03	489,93	625,41	330,45	361,97	219,07	214,37	2827,23
07:00	594,25	496,68	634,03	334,85	367,52	222,43	217,24	2867,00
08:00	588,18	491,71	627,68	332,09	363,36	219,91	215,14	2838,07
09:00	486,17	454,03	530,12	308,69	364,75	220,75	206,52	2571,03
10:00	0,00	346,68	0,00	243,51	367,52	222,43	188,69	1368,83
11:00	0,00	279,57	52,49	202,00	353,64	214,03	164,68	1266,41
12:00	0,00	214,50	0,00	162,07	352,25	213,19	149,40	1091,41
13:00	0,00	184,65	0,00	143,61	346,70	209,83	141,25	1026,04
14:00	0,00	153,07	0,00	124,92	359,19	217,39	143,59	998,16
15:00	0,00	182,62	0,00	159,52	350,86	212,35	155,07	1060,42
16:00	0,00	271,72	176,62	221,60	357,81	216,55	175,58	1419,88
17:00	495,46	453,39	538,30	307,91	357,81	216,55	204,98	2574,40
18:00	587,80	491,33	627,20	331,33	363,36	219,91	214,93	2835,86
19:00	593,49	495,92	633,06	334,71	367,52	222,43	216,83	2863,96
20:00	611,20	510,32	651,44	343,59	380,02	229,99	222,87	2949,43
21:00	613,22	511,98	653,56	344,51	381,40	230,83	223,57	2959,07
22:00	612,85	511,60	653,08	344,45	381,40	230,83	223,37	2957,58
23:00	619,04	516,69	659,58	347,92	385,57	233,35	225,54	2987,69
24:00	558,44	467,48	596,76	316,32	342,54	207,31	204,95	2693,80
Sum	9796,77	9908,34	10703,18	6844,12	8660,90	5241,65	4752,76	55907,72

Calculation of heating demand (W) of selected building in a winter day on hourly basis. 26th January

4. Cooling demand

To select a random hour at peak calculated cooling demand, 16:00 o'clock on 26th July has been selected. Here the elementary weather data on 26th July:

Weather data at the beginning of year			The selected date
	Jan01:00	Jan02:00	Jul-m16:00
Direct Normal Solar (W/m2)	0	0	582
Diffuse Horizontal Solar (W/m2)	0	0	213
Outside Dry-Bulb Temperature (°C)	4,6	4,7	32,3
Solar Altitude (°)	-61,13	-55,02	35,25
Solar Azimuth (°)	25,84	49,73	259,42
Outside Dew-Point Temperature (°C)	2,6	2,7	12,6
	11.01.02 01:00	11.01.02 02:00	26.07.02 16:00
Outside Dry-Bulb Temperature (°C)	4,6	4,7	32,3
Outside Dew-Point Temperature (°C)	2,6	2,7	12,6
Wind Speed (m/s)	6,2	4,6	1,5
Wind Direction (°)	220	220	100
Solar Altitude (°)	-61,13	-55,02	35,25
Solar Azimuth (°)	25,84	49,73	259,42
Atmospheric Pressure (Pa)x10 ³	97000	97000	95800
Direct Normal Solar (W/m2)	0	0	582
Diffuse Horizontal Solar (W/m2)	0	0	213

The upcoming table shows elementary emerged weather data on 26th Jul at 16:00 and the calculated parameters for the representative component:

	Parameter & Symbol	Amount	Equation
01	Outside air temperature (T)	32,30 °C 305,45 °K	Direct from weather data
02	dew-point temperature (T _{dewpoint})	12,60 °C 285,75 °K	Direct from weather data
03	Inside air temperature (T _{in})	24,96 °C 298,11 °K	$T_{(in)} = 21.50 + (0.111 \times T_{(out)})$ (4.2)
04	Inside convective coefficient (h _i)	7,00 W/m ² .K	Average estimation
05	Outside convective coefficient (h _o)	13,80 W/m ² .K	Regarding Fig.4.9 Convective heat transfer coefficient for leeward and windward conditions
06	Wall thickness (d _{wal})	0,214 m	Assigned construction (Equivalence of U _{value} of 0,14)
07	Heat conductivity of wall (λ _{wal})	0,03 W/mK	Assigned construction (Equivalence of U _{value} of 0,14)
08	thermal resistance of the wall excluding outside air film resistance (ΣR _I)	7,29 m ² k/W	$R = \sum_1^N \left(\frac{d_i}{\lambda_i}\right)$ (4.20) $\sum R_I = d_{wal} / \lambda_{wal} + 1/h_i$
09	thermal resistance of the wall excluding inside and outside air film resistances (ΣR _{II})	7,14 m ² k/W	$R = \sum_1^N \left(\frac{d_i}{\lambda_i}\right)$ (4.20) $\sum R_{II} = d_{wal} / \lambda_{wal}$
10	Cumulative solar irradiation (Q _{sol})	451,67 W/m ²	$G_{Tt} = G_B + (G_D \frac{1+\cos\beta}{2}) + ((G_B + G_D)\rho \frac{1-\cos\beta}{2})$ (4.6)
11	Opaque sky cover (N)	4,00	Fig. 4.12 Monthly cloud cover categories– Stuttgart [36]
12	Sky emissivity (ε _{sky})	0,87	$Sky_{emissivity} = 0.787 + \left(0.767 \times \ln\left(\frac{T_{dewpoint}}{273}\right)\right) + 0.0224N - 0.0035N^2 + 0.00028N^3$ (4.10)
13	Sky temperature (T _{sky})	22,15 °C 295,30 °K	$T_{Sky} = (\varepsilon_{sky})^{0.25} \times T$ (4.11)
14	Sol-air temperature (T _{Sol-air})	44,59 °C 317,74 °K	$T_{Sol-air} = \left(T + \frac{a_s \cdot Q_{Sol}}{h_c}\right) - \left(\frac{\varepsilon \cdot \sigma (T^4 - T_{Sky}^4)}{h_c}\right)$ (4.12)

a_s = 0,50 (Solar absorptivity)

σ = 5670400 × 10⁻⁸ W/m²K⁴

	Parameter & Symbol	Amount	Equation
15	Outside surface temperature (T_{s-out})	44,40 °C 317,55 °K	$T_{s-out} = \frac{h_o \cdot T_{sol-air} + \left(\frac{T_{in}}{\sum R_I}\right)}{\left(\frac{1}{\sum R_I}\right) + h_o}$
16	Inside surface temperature (T_{s-in})	25,34 °C 298,49 °K	$T_{s-in} = T_{s-out} + (h_o \cdot \sum R_{II} \cdot (T_{s-out} - T_{sol-air})) \quad (4.14)$
17	Heat transfer (q)	+2,67 W/m ²	$q = h_o \cdot (T_{sol-air} - T_{s-out}) \quad (4.15)$

According to definition in chapter 4.6;

1. The direction of heat flow is from outside into inside
2. $t_{out} > t_{in}$

So, the entire heat flow is marked as cooling demand. Considering area of this component as 50,30 m², heating demand of opaque portion of South-west façade will be:

$50,30 \text{ (m}^2\text{)} \times 2,67 \text{ (W/m}^2\text{)} = 134,30 \text{ W}$ (Cooling demand). At this time and date (at 16:00 on 26th Jul), cooling demand of the rest of components in building have been similarly calculated:

Building's face	At 16:00 for each component	Sum (Excel)
South-west façade (F-01)	Wall: $50,30 \text{ (m}^2\text{)} \times 2,67 \text{ (W/m}^2\text{)} = 134,30 \text{ W}$	2670,16 W
	Windows: $22,71 \text{ (m}^2\text{)} \times 111,66 \text{ (W/m}^2\text{)} = 2535,80 \text{ W}$	
North-west façade (F-02)	Wall: $76,39 \text{ (m}^2\text{)} \times 3,57 \text{ (W/m}^2\text{)} = 272,71 \text{ W}$ Windows: $6,95 \text{ (m}^2\text{)} \times 156,08 \text{ (W/m}^2\text{)} = 1084,76 \text{ W}$	1440,89 W
South-east façade (F-03)	Wall: $66,06 \text{ (m}^2\text{)} \times 1,44 \text{ (W/m}^2\text{)} = 95,13 \text{ W}$ Windows: $21,18 \text{ (m}^2\text{)} \times 63,79 \text{ (W/m}^2\text{)} = 1351,07 \text{ W}$	1446,09 W
North-east façade (F-04)	Wall: $69,27 \text{ (m}^2\text{)} \times 1,56 \text{ (W/m}^2\text{)} = 108,06 \text{ W}$ Windows: $3,74 \text{ (m}^2\text{)} \times 63,05 \text{ (W/m}^2\text{)} = 235,81 \text{ W}$	343,85 W
Ceiling (F-05)	$113,25 \text{ (m}^2\text{)} \times 0,32 \text{ (W/m}^2\text{)} = 36,24 \text{ W}$	36,43 W
South-west roof (F-06)	$80,50 \text{ (m}^2\text{)} \times 0,86 \text{ (W/m}^2\text{)} = 69,23 \text{ W}$	69,09 W
North-east roof (F-07)	$65,96 \text{ (m}^2\text{)} \times 2,52 \text{ (W/m}^2\text{)} = 166,22 \text{ W}$	166,28 W
Sum	6172,79 W	6172,79 W

* The exact calculations are directly from excel file emerged and put in Sum results

And finally, based on seven main facades of building (including ceiling), shaping external face of building, individual calculation of cooling demand of all seven facades on an hourly basis are presented here:

Time	F-01	F-02	F-03	F-04	F-05	F-06	F-07	Sum
01:00	0,00	0,00	0,00	0,00	0,00	0,00	0,00	0,00
02:00	0,00	0,00	0,00	0,00	0,00	0,00	0,00	0,00
03:00	0,00	0,00	0,00	0,00	0,00	0,00	0,00	0,00
04:00	0,00	0,00	0,00	0,00	0,00	0,00	0,00	0,00
05:00	0,00	0,00	0,00	0,00	0,00	0,00	0,00	0,00
06:00	0,00	0,00	0,00	0,00	0,00	0,00	0,00	0,00
07:00	0,00	0,00	0,00	0,00	0,00	0,00	0,00	0,00
08:00	0,00	0,00	0,00	0,00	0,00	0,00	0,00	0,00
09:00	0,00	0,00	0,00	0,00	0,00	0,00	0,00	0,00
10:00	1264,42	425,73	3982,52	243,68	0,00	16,16	217,67	6150,18
11:00	1685,65	465,73	2876,76	269,33	10,05	29,60	234,95	5572,07
12:00	2487,53	611,70	2054,59	358,38	30,88	42,21	239,16	5824,45
13:00	2828,46	814,53	2092,98	482,64	39,20	47,25	222,88	6527,94
14:00	1873,09	648,43	1598,62	372,57	17,00	57,33	148,36	4715,40
15:00	3073,87	1059,01	2018,04	475,59	23,94	61,53	212,58	6924,56
16:00	2670,16	1440,89	1446,09	343,85	36,43	69,09	166,28	6172,79
17:00	1705,03	1153,85	1345,74	319,63	32,27	66,57	131,59	4754,68
18:00	1098,59	1012,66	967,43	229,39	28,11	64,05	91,43	3491,66
19:00	581,00	887,94	533,53	114,54	43,37	49,77	39,94	2250,09
20:00	69,70	17,19	52,40	0,00	16,99	33,80	0,00	190,08
21:00	0,00	0,00	0,00	0,00	11,44	30,44	0,00	41,88
22:00	0,00	0,00	0,00	0,00	0,00	10,28	0,00	10,28
23:00	0,00	0,00	0,00	0,00	0,00	0,00	0,00	6150,18
24:00	0,00	0,00	0,00	0,00	0,00	0,00	0,00	5572,07
Sum	19337,50	8537,67	18968,70	3209,60	289,70	578,08	1704,83	52626,07

Calculation of cooling demand of selected building in a summer day on hourly basis. 26th July

It should be noted that justifying the calculation of the cooling demand in above table, local wind is a strong parameter to affect the results. For this reason, to justify accuracy of the calculated demands, rather than quantities of irradiation, quantities of wind velocities regarding the angle to the selected component must continuously be taken into account as well. In other word, any calculated energy demand in this work, is outcome of interaction of outcome of temperature and irradiation and different quantities of external convection that will always is changed regarding different velocities of wind an any time.

5. Summary

In this part of illustration two critical days of 26th of January and 26th of July as peak recorded demands of heating and cooling have been selected respectively regarding the asked question by honorable Jury. The point of all represented tables and charts is to demonstrate accuracy of employment of equations to show the logic connection between the initial weather data and the resulted heating and cooling demands. It should be reminded that these two days are representatives of extreme cold and hot days. For instance, 26th of January with -3,30 °C and 26th of July with +32,30 °C present the coldest and hottest day of year, respectively that result the calculated heating and cooling demands. The calculated cooling demand of 52kW on 26th of July, has been supposed if the comfort temperature is going to remain about 24 °C and will be compensated by direct electricity. Any more moderated initial weather data, will quantitatively result more moderated energy demands.

Additionally, it should firmly be noted, that the selected building is not equipped with any kind of shading systems. Indeed, in the entire simulations the geometry of building is a simplified combination of external wall, windows and doors, ceiling and roof. Consequently, in absence of any manual or automatic devices to block or reflect entrance of light in periods of cooling demand, unnecessary quantities of light (coming in through windows as transmission) is additionally added to entire cooling demand of the calculations. That is a remarkable reason that average of cooling demand of the selected building in this work is remarkably higher than similar building with the same geometry. As, normally all buildings are either equipped by simple external shading components as shading louvers that work manually or automatic devices that decide to block the light in peaks time of cooling demands.

As possibilities of further development of this work, to achieve to more moderate quantities of cooling demand, adding external shading devices in this work is absolutely possible by adding simple scheduling time. As a result, in cooling demand periods, unnecessary quantities of light will be blocked and will result more moderate calculated quantities of cooling demands.

Appendix 3

Numerical calculation of energy demands

PhD research:

Determining effects of geometry on energy efficiency of medium-sized solar buildings

Abbas Rahmani

Supervisor: Prof. Dr.-Ing. R. Wagner

Second consultant: Prof. Dr.-Ing. M. Pfeifer

Institut Entwerfen und Bautechnik (IEB)
Fachgebiet Bautechnologie (FGB)

(2023)

As appendix of the work and in relation to this illustration the excel files are additionally delivered to assess accuracy of work. Here a short description of content of these submitted data:

No	Name of file	Explanation
01	01-SW (O)	South-west opaque wall
02	02-NW (O)	North-west opaque wall
03	03-SE (O)	South-east opaque wall
04	04-NE (O)	North-east opaque wall
05	05-SW (W)	South-west window
06	06-NW (W)	North-west window
07	07-SE (W)	South-east window
08	08-NE (W)	North-east window
09	09-SW (BAPV)	South-west sloping roof with BAPV
10	10-SW (BAPV-extension)	(Extension of) South-west sloping roof (with BAPV)
11	11-NE (R)	North-east sloping roof (without BAPV)
12	12-NW (D)	North-west door
13	13- (ceiling)	Ceiling
14	14-result-02	Rendered data and final result